IONOSPHERIC EFFECTS IN THE SOUTHERN RADIATION ANOMALY

A thesis submitted for the degree of Doctor of Philosophy

at Rhodes University

by

Douglas G. Torr

November, 1966.

Except where it is clear from the text that I am describing the work of others, the work described in this thesis is my own.

ACKNOWLEDGEMENTS

I am most grateful to Professor Gledhill for the expert guidance and training that I have received under his supervision. I express deep gratitude to my wife, Marsha Torr, for unfailing support, encouragement and help throughout the course of this research. My thanks to the Director of the National Institute for Telecommunications Research of the South African Council for Scientific and Industrial Research for facilities made available for the completion of this research in Johannesburg and to the South African Department of Transport for facilities in the Antarctic. I thank Mrs. B. Longmore and Miss. N. Papendorf for valuable assistance in plotting graphs and in calculating some of the frequencies of ionospheric disturbance.

CONTENTS.

INTRODUCTION

As ionospherici st on the 4th South African National Antarctic Expedition, I spent twelve months at Sanae ($70^{\circ}18'S$, $2^{\circ}21'W$, L = 4) in 1963. In the course of routine vertical incidence soundings, it was noticed with some surprise that the frequency of occurrence of ionospheric blackouts was unexpectedly high. Initially this aroused considerable concern about the reliability of the equipment. In fact it has been observed that some stations lying in and near the Southern Radiation Anomaly report such occasions as records lost due to non-ionospheric reasons. Coincidently, however, Gledhill and van Rooyen (1963), also of Rhodes University, predicted ionospheric irregularities and other geophysical phenomena in a region around Sanae where Ginsburg et al. (1962) observed high intensities of charged particles with Sputniks 5 and 6.

Figure 1 is a typical example of the unusual ionograms obtained at Sanae, which on my return to South Africa, led to a detailed investigation into a possible relationship between electron flux in the outer radiation belt and disturbances in the ionosphere. Dr. McDiarmid of the Division of Pure Physics, National Research Council in Canada, supplied electron flux data observed by the satellite Alouette. I then examined the various ionospheric parameters at times when Alouette observed large increases in the intensity of the precipitated electron

2/.....

FIGURE 1.

A typical ionogram observed at Sanae which led to the investigation of the electron flux and ionosphere data. The first frequency and height markers represent 1 Mc/s and 100 km respectively. The markers are shown at intervals of 100km and 1 Mc/s.

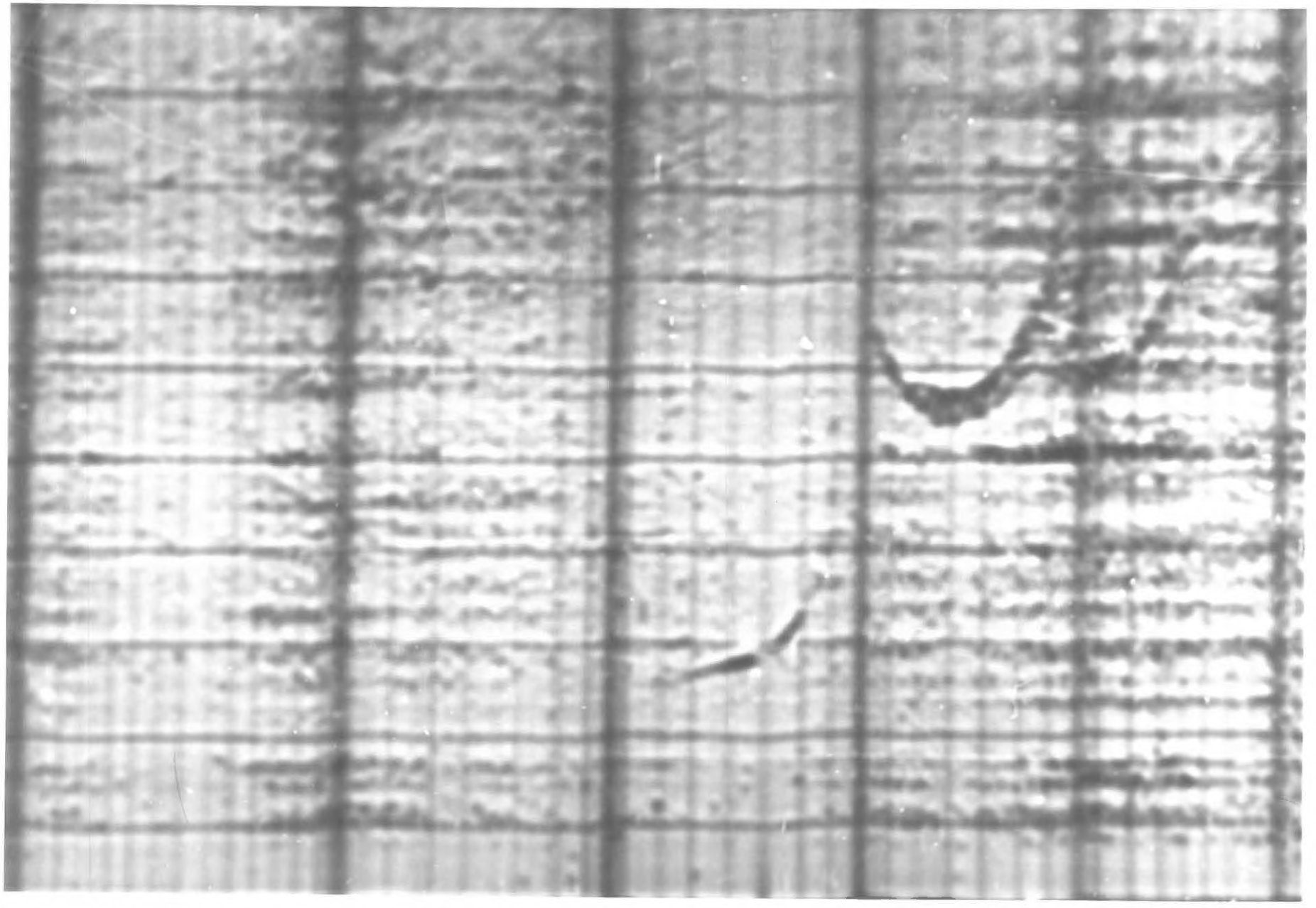

flux (p.e.f.).

Part 1 of this thesis describes this analysis and the exciting results which established the first real one to one relationship between high values of p.e.f. and ionospheric disturbances (i.d.'s) at a station lying outside the auroral zone. While this work was being presented in a paper (Gledhill and Torr, 1965) at the Sixth Cospar Conference in Buenos Aires, M.R.Torr and I extended the research considerably by the discovery of a critical value of flux, above which an ionospheric disturbance invariably occurs. It was further shown that the percentage of time for which the critical flux is exceeded at each station examined near the magnetic shell L =4, is almost exactly the same as the percentage time for which the ionosphere is disturbed. These results were reported in a paper by Gledhill, Torr and Torr, (1967). An extension of this work to other L-shells indicated that electron bombardment may well be a major cause of all the i.d.'s of the type studied here.

The nature of these disturbances is consistent with heating of the ionosphere and since there is no good method at present to find the temperature in the upper atmosphere from ionograms, I decided to try to develope one to confirm these preliminary deductions. This aspect of the work is dealt with in Part 2 of this thesis, where it is shown that a hyperbolic temperature profile gives a much better fit to actual conditions in the upper atmosphere than the more commonly used linear temperature gradient. The ionospheric continuity equation

3/.....

is solved under these conditions and it is shown that temperature changes do produce a remarkable effect on the behaviour of the ionosphere and that the i.d.'s observed can be accounted for in terms of increased heating of the upper atmosphere.

Note: No attempt has been made to define terms which are now considered to be well known, such as the radiation belts, precipitated and trapped electron flux, L-values, invariant latitude, pitch angle and dumping cone.

PART 1

IONOSPHERIC DISTURBANCE AND ELECTRON PRECIPITATION FROM THE OUTER RADIATION BELT

CHAPTER 1.

THE EARLY WORK.

1.1 Introduction.

It had been suspected that the relatively low values of the total magnetic intensity in the southern Atlantic region, south of Cape Town, should have a profound effect on particles trapped in the outer Van Allen radiation belt. Whether or not these would interact sufficiently with the atmosphere to produce observable geophysical effects had been, until 1961, a matter of speculation. Cladis and Dessler (1961) suggested that balloons carrying X-ray detecting equipment should be launched south of Cape Town to detect bremsstrahlung produced by bombarding electrons. The observations by Russian (Ginsburg et al ., 1962) and American (Seward and Kornblum , 1963) satellites of high charged particle fluxes at altitudes as low as 200 km. in the southern Atlantic also suggested strongly that geophysical effects would be most marked there.

With the prospect of discovering new phenomena on our own 'door step', Gledhill and van Rooyen initiated South African research in this field by theoretically investigating these possibilities. The results of their researches suggested that the low scalar values of the geomagnetic field results in the formation of a 'sink' for particles in the outer radiation belt in a region centered approximately on the most southern boundary of the Indian and Atlantic Oceans. They predicted that there should be observable airglow, enhanced heating, X-ray and ionization effects in this

5/.....

FIGURE 2.

Region of high counting rate observed by Ginsburg et al. using Sputniks 5 and 6 (relative counting rate) and Seward and Kornblum using Discoverer 31 (absolute counting rate in electrons/ cm^2/sec/ster.).

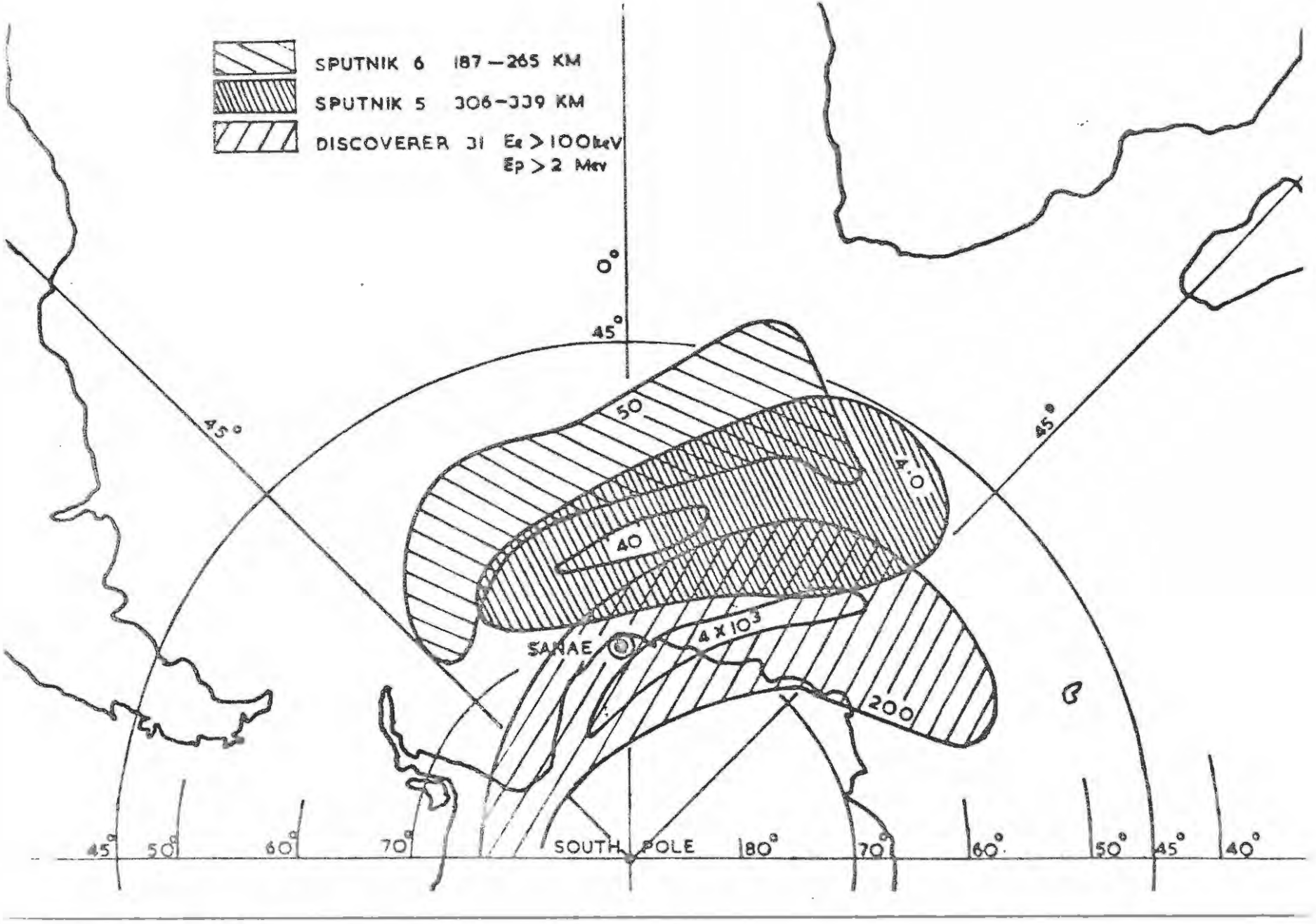
SPUTNIK 6 187 — 265 KM
SPUTNIK 5 306 — 339 KM
DISCOVERER 31 Ee > 100 keV
Ep > 2 Mev
0°
45°
45°
45°
50
40
4·0
4 X 10³
200
SANAE
45°
50°
60°
70°
SOUTH POLE
180°
70°
60°
50°
45°
40°

region.

At this stage of the work there were sufficient pieces in place in the puzzle to arouse considerable enthusiasm and interest in this work. Therefore, in view of the clues the South African Antarctic ionosphere project had provided, I decided to use our experimental observations to confirm these predictions.

1.2 The Initial Stage Of The Project.

Figure 2 shows areas of high counting rate observed by Ginsburg et al., (1962) using Sputniks 5 and 6, and Seward and Kornblum, (1963), with Discoverer 31. The position of Sanae is also shown. It is evident that Sanae lies in the region where the effects of particle bombardment could be expected to be most pronounced. Sanae also lies on the magnetic shell characterised by L = 4, which passes through the heart of the outer radiation belt. Therefore we decided to compare measurements of electron flux made in the outer belt with ionospheric observations made at Sanae.

We were faced with one major difficulty viz. that of obtaining the electron flux data essential to the investigation. While waiting for replies to our requests for data we decided to compare the variation of certain ionospheric parameters at stations in or near the 'high count region' (named the Southern Radiation Anomaly by the Russians) with the variations at stations nearest their respective conjugate points. We reasoned that if particles impinging on the atmosphere were the cause of the i.d.'s

6/.....

observed at Sanae, it might well be true that similar events occur at other stations near the Anomaly and also at their conjugate points. These investigations were carried out by M.R.Torr (1964), but we were unable to draw any conclusions from the results obtained at that stage. At the time these investigations were performed we could only suggest intuitively that conditions outside the Anomaly differed vastly from those within. This we can now show quantitatively and these results will be discussed later.

The results of Gledhill and van Rooyen (1963) and Rees (1963) indicated that high energy electrons ($E \gg 40$kev) would affect the D-region, and the low energy electrons ($E \ll 40$kev), the F-region of the ionosphere. Therefore, if the electron flux energy spectrum contained both high and low energy particles, when a large deviation in f_{min} occurred, one could expect to find an accompanying variation in $h'F_2$ and/or f_oF_2. A correlation analysis between high values of f_{min} (using arbitrary criteria) and the magnitude of the deviation of $h'F_2$ and f_oF_2 from their respective medians resulted in a correlation coefficient of about 0.1. Qualitatively it seemed that variations in f_{min} were accompanied by random variations in f_oF_2 and $h'F_2$ both in phase and amplitude. On some occasions f_{min} increased without any significant change in the other two parameters. Although we felt that we could hypothetically account for this apparent lack of correlation in terms of variations in the electron flux energy spectrum, the results were most discouraging. Had we been more observant and more objective in selecting our criteria we may have

7/.....

accompanied by deviations of $h'F_2$ and f_oF_2 from their respective medians. Figure 3 shows a typical disturbance of this type.

1.4 The Correlation of Ionospheric Disturbances at Sanae with P.E.F. Measured by Alouette.

1.4.1 Introduction.

In the preliminary analysis we correlated obviously high values of p.e.f. with large variations in the ionosphere at Sanae. The satellite Alouette only telemetered data while in the northern hemisphere. Therefore we used measurements of p.e.f. that had been made closest to the conjugate point to Sanae. Having discovered this correlation we could then set about defining objective criteria with which to conduct a detailed analysis. These involved definitions of 'high' and 'low' flux, an 'ionospheric disturbance' and 'the conjugate area'. The latter involved a definition of an area which could be regarded as conjugate to Sanae. All observations made by Alouette in this area would then be used in the analysis.

1.4.2 The Available Data.

The relevant data available from Alouette consisted of values of p.e.f. measured at a height of approximately 1000 km. together with invariant latitude Λ, geographic longitude and time of observation. The counter on the satellite responded to electrons with energies greater than 40 kev.,

9/.....

FIGURE 3.

A typical disturbance of the type observed at Sanae. (The frequency scale should read 2.5 and 5 instead of 5 and 10 Mc/s.)

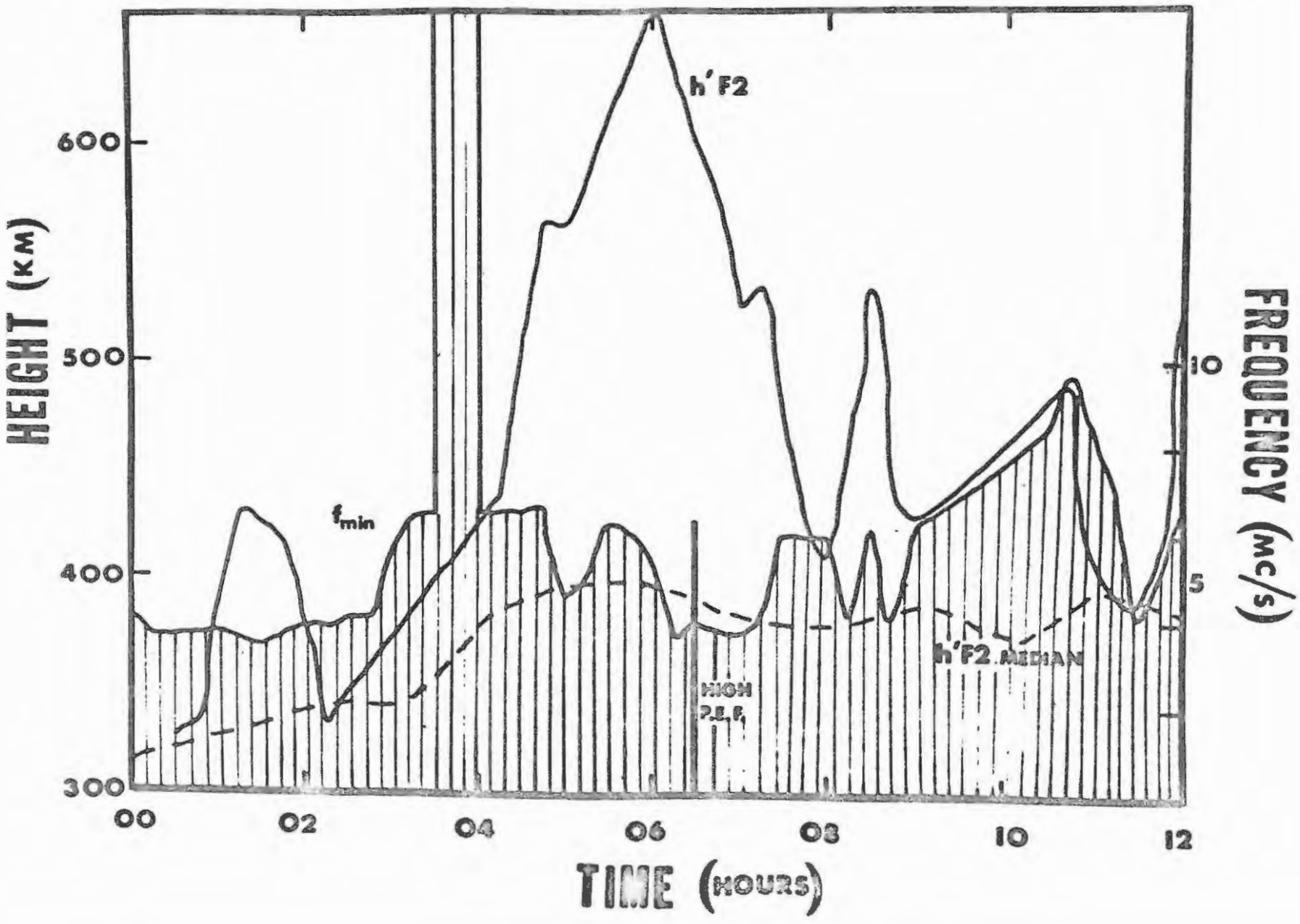
HEIGHT (KM)
600
500
400
300
h'F2
f_{min}
HIGH P.E.F.
h'F2 MEDIAN
00
02
04
06
08
10
12
TIME (HOURS)
FREQUENCY (mc/s)
10
5

if their pitch angles placed them in the dumping cone. Telemetry was recorded for positions in the northern hemisphere approximately between longitudes 170°E to 330°E. The tables of data covered the period September, 1962 to August, 1963. Vertical incidence ionograms taken at Sanae were available for the whole of this period. Values of $h'F_2$, f_oF_2 and f_{min} were read from these.

1.4.3 The High-Low Flux Boundary.

The precipitated flux measurements were divided into two classes of 'high' or 'low' according as to whether the observed value was greater or less than 1.4×10^4 electrons/cm^2/sec. This value was selected on the basis of the information given by McDiarmid (private communication) that this was the lowest precipitated flux which could be reliably detected by the instruments on the satellite. It was found that the adoption of this value did not impair the correlation reported below.

1.4.4 The Conjugate Area to Sanae.

The geographic coordinates of the conjugate point to Sanae are 325°E, 54°N, the invariant latitude being 58°30'. The longitudinal limits were set by trial and error to be the widest limits which gave the good correlation reported later. It was found possible to set these at 290°E and 335°E. The maximum extent in latitude was determined by a characteristic of the satellite, viz. it recorded over certain bands of invariant latitude, 2°

10/.....

in width. Since Sanae lies on L = 4 ($58^{\circ}30'$ invariant latitude), the band between 58°-60° invariant latitude was used.

1.4.5 The Disturbance Criterion.

In drawing up an objective criterion for an ionospheric disturbance, data for $h'F_2$ and f_{min} for each of the 10 International Quiet Days (J.Virginia Lincoln, 1963a, b, c, d, e, f) were used to determine maximum undisturbed ranges for each month used in the analysis. These parameters were chosen because they exhibited the greatest variation at the times high values of p.e.f. were observed. Sometimes large fluctuations occurred in the values even on magnetically quiet days; in such cases the extreme values were discarded and the next biggest ones used as the limits of the range.

We were unable to determine the limits in this way for October, 1962, however, as the F-region at Sanae then becomes unstable in its behaviour. This type of phenomenon (which has also been observed by Piggott and Shapley, 1962) is a characteristic of Antarctic stations near the Weddell Sea, where the behaviour of the ionosphere changes over from a typical winter to a typical summer pattern. Therefore the quartile range as determined from all the days of the month was used instead.

11/.....

1.4.6 The Analysis.

The ionosphere was classified as disturbed if either f_{min} or $h'F_2$ fell outside the allowed maximum undisturbed range. In the final analysis we found that we could narrow down the time during which the i.d. must occur for it to be regarded as correlated with a high p.e.f. value, to a period of two hours centered on the time of the flux observation. The correlation was carried out for the period 2nd October, 1962 to 4th March, 1963 (which is the Antarctic summer). No data are available for the F-region at night during winter. Inclusion of this period may have introduced weighting in favour of the daytime.

1.5 The Results.

Alouette measured the p.e.f. in the conjugate area on 77 occasions for which times ionospheric data for Sanae were available. On 28 of these the flux was above the high-low boundary and without exception, the ionosphere was disturbed. The results of the analysis are given in Table 1 where H and L represent 'high' and 'low' p.e.f. and are defined as p.e.f. $\geq$ and $< 1.4 \times 10^4$ electrons/cm^2/sec respectively

Table 1.

	H	L
D	28	30
Q	0	19

12/.....

It is evident that the ionosphere was disturbed at Sanae on every occasion on which the p.e.f. was equal to or above 1.4 X 10^4 electrons/cm^2/sec, and in no case was there a high flux and a quiet ionosphere.

In order to estimate the probability that this correlation was due to chance alone a random sample of two hour periods of the ionospheric parameters $h'F_2$ and f_{min} for the 6 month period was taken. We found that the disturbance criterion was satisfied for approximately $65^{o}/_{o}$ of the total time. The probability that out of 28 periods taken at random, all would be disturbed and none quiet is less than 10^{-6}. We therefore concluded that the above correlation is highly significant. To the best of my knowledge, this was the first time that anyone had conclusively demonstrated that the precipitation of electrons from the outer radiation belts produces observable geophysical effects at sub-auroral latitudes.

We felt that we could account for the 30 cases where the ionosphere was disturbed but the precipitated flux low in three possible ways.

(1) Other causes of i.d.'s unrelated to electron influx may be responsible for some of these.

(2) The flux of electrons measured in the radiation belts is very variable (O'Brien, 1964). It is thus possible that some of the `low' flux measurements represent momentary low values in the vicinity of the satellite, while regions of `high' flux may exist in adjacent parts of the belt.

(3) Some of the 30 LD cases could be attributed to the fact that

13/.....

a value of 1.4 X 10^4 electrons/cm^2/sec may be too large a value for the high/low flux boundary.

These hypotheses are examined in Chapter 2 and will not be discussed further here.

1.6 Comparison with Other Stations.

By plotting the height of constant magnetic intensity over L = 4, Gledhill and van Rooyen,(1962) showed that electrons that mirror at 1000km over Iowa would mirror at 200km over the Sanae area. In a later publication (Gledhill and van Rooyen, 1963) they calculated that the decrease of the mirror heights would result in a much wider aperture of the dumping cone there than anywhere else. For example, their figures indicated that whereas particles with pitch angles less than 56° at 1000km would be precipitated over North America, particles with pitch angles up to 78° at 200km would be dumped over Sanae. The fairly sharp descent of the mirror heights over the Southern Radiation Anomaly shown in their paper (Gledhill and van Rooyen, 1962) implied that the precipitated flux near Sanae would be much larger than that measured in the North American sector,being enriched by some of the electrons regarded there as trapped. M.R.Torr and I (1967) have since extended their work considerably to a quantitative analysis of the behaviour of electrons in the outer radiation belt. This is discussed in Chapters 2 and 3 where other L-shells are examined.

The approach used to test this reasoning at the time this analysis

14/.....

was conducted, may seem rather unrefined by our present standard of knowledge. It nevertheless constituted an important phase of our research which served to guide our thinking into more important channels. To exclude it would leave this account chronologically incomplete.

In order to determine whether the ionospheric effects were less severe at stations lying outside the anomalous region, we examined the behaviour of the ionosphere at three other stations, at the times of the 28 electron-induced disturbances in Table 1. These were the only suitable stations for which we had ionospheric data at that time. The stations were:-

1) Campbell Island, which is on the same L-shell (4.0) as Sanae, but which lies in the Australian sector where the mirror points are more than 1000km higher.

2) St. Johns, which is near the same L-shell (3.5) and is the nearest station on this shell to the conjugate point to Sanae; the mirror heights are about 800km above those at Sanae.

3) Argentine Islands, which, although at a lower L value (2.5), lies in the drift path (Gledhill and van Rooyen, 1962) of the electrons observed by Ginsburg et al.,(1962) at low heights in the Southern Radiation Anomaly; the mirror heights are about 600km above those at Sanae.

The results of this analysis are shown in Table 2, which gives the maximum deviation of $h'F_2$ and f_{min} from the relevant monthly median for each station during a 12 hour period centered on the time of the satellite

15/.....

Table 2

Event			$\Delta h'F_2$ (km)			
No.	Date	U.T.	Sanae	Campbell Island	St. Johns	Argentine Islands
1	2/10/62	02.2	+80 B	+135	+45	+ 30
2	4/10/62	02.0	> +90 B	+40	+50	+ 60
3	7/10/62	23.2	> +75 B	+100	−80	+ 70
4	10/10/62	01.5	> +90 B	+105	− 20	+ 80
5	14/10/62	01.8	+115 B	+125	+25	< 20
6	23/10/62	22.7	−90 B	+115	−30	+ 20
7	24/10/62	23.7	> +130 B	+165	−20	+ 20
8	27/10/62	21.7	+110 B	+45	−30	+ 30
9	30/10/62	20.0	+80 B	+70	−40	+ 35
10	1/11/62	21.3	+110 B	+90	+20	< 20
11	3/11/62	20.7	+80 B	+40	< 20	+ 25
12	16/11/62	07.5	+260 B	+215	C	+ 60
13	21/11/62	07.0	+90	+50	−30	C
14	22/11/62	07.6	+185 B	+115 B	+35	C
15	23/11/62	06.5	+260 B	+60		C
16	8/1/63	12.6	+80 B	+20	− 20	+120
17	13/1/63	12.2	+280	+80	+40	− 30
18	31/1/63	09.2	BB	+235	B	C
19	31/1/63	16.2	BB	+235 B	+ 225 B	C
20	1/2/63	08.2	BB	+140	+35 B	< 20
21	1/2/63	10.0	BB	+140	+35 B	+ 40
22	2/2/63	08.8	+100 B	+60	−45	+ 30
23	16/2/63	18.9	−40	< 20	< 20	+ 25
24	18/2/63	20.2	+25 B	−40	< 20	+ 20
25	19/2/63	20.8	+40 B	−40	−40	< 20
26	22/2/63	19.2	−55 B	−35	< 20	+ 30
27	22/2/63	20.8	−55 B	−35	< 20	+ 30
28	26/2/63	18.2	+20 B	< 20	+ 20	< 20
Average $\Delta h'F_2$			105	70	30	35

B Blackout occurred sometime during the 12 hour period.

BB Total blackout during the whole 12 hour period.

C Records lost for non-ionospheric reasons.

Table 2 continued.

Event			$\triangle f_{min}$ (Mc/s)			
No.	Date	U.T.	Sanae	Campbell Island	St. Johns	Argentine Islands
1	2/10/62	02.2	0.2 B	1.5	0.6	0.1
2	4/10/62	02.0	2.0 B	0.9	0.2	0.2
3	7/10/62	23.2	1.5 B	1.6	0.2	0.5
4	10/10/62	01.5	2.6 B	0.1	0.2	0.1
5	14/10/63	01.8	2.3 B	1.3	0.1	0.1
6	23/10/62	22.7	3.7 B	0.4	0.3	0.6
7	24/10/62	23.7	2.1 B	1.1	0.2	0.1
8	27/10/62	21.7	2.3 B	0.7	0.6	0.1
9	30/10/62	20.0	2.2 B	0.7	0.8	1.0
10	1/11/62	21.3	2.4 B	0.4	0.8	0.6
11	3/11/62	20.7	3.0 B	1.7	0.4	0.7
12	16/11/62	07.5	3.0 B	1.6	0.1	0.3
13	21/11/62	07.0	3.0	0.5	0.2	C
14	22/11/62	07.6	1.8 B	2.0 B	0.3	C
15	23/11/62	06.5	2.8 B	0.8		C
16	8/1/63	12.6	1.5 B	0.1	0.9	0.1
17	13/1/63	12.2	1.5	0.5	0.1	0.2
18	31/1/63	09.2	BB	2.0	2.0 B	0.6
19	31/1/63	16.2	BB	2.0 B	1.0 B	C
20	1/2/63	08.2	BB	1.3	2.0 B	0.2
21	1/2/63	10.0	BB	1.3	2.0 B	0.1
22	2/2/63	08.8	1.8 B	0.7	B	1.0
23	16/2/63	18.9	0.9	0.1	0.8	0.4
24	18/2/63	20.2	2.3 B	0.1	0.2	0.7
25	19/2/63	20.8	1.7 B	0.1	0.3	0.9
26	22/2/63	19.2	1.4 B	0.2	0.5	0.2
27	22/2/63	20.8	1.4 B	0.2	0.5	0.2
28	26/2/63	18.2	2.3 B	0.4	0.1	0.2
Average $\triangle f_{min}$			2.0	0.7	0.4	0.4

B Blackout occurred sometime during the 12 hour period.
BB Total blackout during the whole 12 hour period.
C Records lost for non-ionospheric reasons.
$\triangle f_{min} = (f_{min})_{observed} - (f_{min})_{median}$

observation of the high p.e.f. for each of the 28 HD events in Table 1.

The averages at the foot of the table are taken excluding events 18 - 21, during which there was a total blackout over the whole 12 hour period at Sanae. Inclusion of the corresponding large deviations for other stations (but none for Sanae, where none could be obtained) would obviously have spoiled the comparison. This series of four events was evidently connected with a geomagnetic storm which occurred at that time (Lincoln, 1963d and e). Most other events show no such correlation (discussed in Chapter 5).

The figures for both $\Delta h'F_2$ and Δf_{min} show that the disturbances are much more pronounced at Sanae than at other stations, indicating that the precipitation of electrons on $L \doteq 4$ is controlled by their behaviour in the radiation belt, as suggested by Gledhill and van Rooyen's results(1962, 1963). It was clear at this stage that a continuation of their work was warranted. This was undertaken by M.R.Torr. Before deciding on what approach to adopt, she and I agreed that it was necessary to obtain more experimental data on the effect of electron precipitation outside the Anomaly. The very interesting results which emerged from our efforts are described in Chapter 2.

CHAPTER 2.

THE ANALYSIS OF IONOSPHERIC AND SATELLITE DATA AT OTHER STATIONS ON L = 4.

2.1 Introduction.

We decided to repeat the analysis of ionospheric and electron flux data for a station lying well outside the Anomaly. Campbell Island suited our purpose for this analysis very well; it was the nearest to L = 4 of all the stations for which both satellite and ionospheric data were available, and the mirror heights are about 1000km higher than at Sanae.

2.2 The Behaviour at Campbell Island.

The analysis was repeated for Campbell Island exactly as for Sanae. The criterion for an ionospheric disturbance was set up as before. The conjugate area could be set over bands of 2^{o} invariant latitude and 5^{o} geographic longitude, centered on the geographical coordinates of the conjugate point. The analysis was carried out for the same 6 month period as before. The satellite measured the p.e.f. in the conjugate area to Campbell Island on 38 occasions. Using 1.4×10^{4} electrons/cm^{2}/sec as the boundary between `high' and `low' flux again, Table 3 could be drawn up in the same way as Table 1 was drawn up for Sanae.

In this case there were 11 occasions on which the flux was high and the ionosphere quiet. It seemed that a correlation between ionospheric and p.e.f. data did not exist at Campbell Island. In Section 1.5 I mentioned

17/.....

Table 3.

	H	L
D	14	3
Q	11	10

that in the case of Sanae some of the 30 LD events could be attributed to the fact that a value of 1.4×10^4 electrons/cm^2/sec may be too large a value for the high/low flux boundary there. Until this stage we had not considered this point very seriously. Faced with these new results I decided to investigate what effect a higher boundary value would have on the results for Campbell Island. The analysis was therefore repeated, increasing the boundary value in small steps. As this was done, some of the HD and HQ cases moved over into the LD and LQ squares. Eventually, when the boundary value was 2.5×10^4 electrons/cm^2/sec. Table 3 had redistributed itself to become Table 4.

Table 4.

	H	L
D	8	9
Q	0	21

18/.....

Reasons why this result, while pleasing, was not entirely surprising, were given in our paper presented at the Inter Union Symposium on Solar-Terrestrial Physics in Belgrade in 1966:`.....the South Atlantic Geomagnetic Anomaly makes the circumstances very different at Sanae, which lies in the anomalous region, and at Campbell Island, which is well outside it. As a result a p.e.f. of 1.4 X 10^4 electrons/cm^2/sec in the conjugate area to Sanae corresponds to a considerably larger p.e.f. at Sanae itself, since the mirror points are so low in the region of the Anomaly. The same p.e.f. in the conjugate area of Campbell Island, on the other hand, corresponds to a smaller one over the Island itself, because at that longitude the mirror points are higher in the southern hemisphere than in the northern one.'

The fact that we were able to obtain a table for Campbell Island in which every `high' flux event was accompanied by an i.d. was regarded as proof that the precipitation of electrons causes disturbances at stations outside the Anomaly as well. That the electron flux had to exceed a critical value before an i.d. occurred, which was higher than that at Sanae, was taken as further evidence that these were Van Allen Belt electrons which are controlled by the geomagnetic field. The discovery of this critical value of flux hastened us to repeat the analysis for Sanae to find out whether 1.4 X 10^4electrons/cm^2/sec was the real critical value there.

19/.....

2.3 Re-evaluation of Sanae Data.

The high/low boundary for Sanae was decreased in small steps from 1.4 X 10^4 electrons/cm^2/sec to successively lower values. On doing this, some of the 30 LD cases moved into the HD square. The lowest critical value that could be obtained before the correlation began to collapse was found to be 8.2 X 10^3 electrons/cm^2/sec. Table 1 was then redistributed to give Table 5.

Table 5.

	H	L
D	38	20
Q	0	19

This meant that the critical p.e.f. lay in the region where the satellite data are questionable. However, the regular way in which some of the 30 LD cases moved into the HQ square each time the critical flux was decreased by a small amount, suggested that the measurements of p.e.f. were sufficiently reliable for this type of analysis.

We had certainly not expected to obtain results of such an indicative nature. The pattern that emerged was not only consistent with the current theory of that time, but also suggested that there was a regular or systematic feature to be found in the behaviour of electrons in the

20/.....

outer belt, despite the large variations in space and time that had been observed by O'Brien, (1964). We immediately set out to confirm these results by conducting a similar analysis for other ionosphere stations along L = 4.

2.4 Extension of the Analysis to Four Other Ionospheric Stations.

There were 4 other stations near L = 4 which lay within Alouette's telemetry range and for which ionosphere data were available. Three of these lay in the northern hemisphere where the satellite measured the p.e.f. directly over the station. In these cases we defined an area around the station itself, since the conjugate area was not involved. The results of these analyses are shown in Tables 6 to 9, together with the corresponding critical p.e.f. for each station.

The results shown in Tables 6 to 9 confirmed that a critical value of p.e.f. did exist at each of the stations examined along L = 4, above which the ionosphere was always disturbed. The fact that in no case was there a high flux and a quiet ionosphere meant that all the i.d.'s of the type we have studied here could be caused by precipitation of electrons.

The critical p.e.f.'s obtained in the conjugate areas of Campbell Island (2.5×10^4), Halley Bay (1.2×10^4) which lies on the western edge of the Southern Radiation Anomaly, and Sanae (8.2×10^3), show that it decreases progressively from the highest at Campbell Island, outside

21/.....

Table 6. Conjugate p.e.f. - ionospheric disturbance correlation for Halley Bay.

Critical flux = 1.2×10^4 electrons/cm^2/sec

	H	L
D	19	7
Q	0	10

Table 7. P.e.f. - ionospheric disturbance correlation for St. Johns.

Critical flux = 2.5×10^4 electrons/cm^2/sec

	H	L
D	8	4
Q	0	27

Table 8. P.e.f. - ionospheric disturbance correlation for Ottawa.

Critical flux = 2.2×10^4 electrons/cm^2/sec

	H	L
D	7	10
Q	0	23

Table 9. P.e.f. - ionospheric disturbance correlation for Winnipeg.

Critical flux = 2.1×10^4 electrons/cm^2/sec

	H	L
D	8	12
Q	0	11

22/.....

the Anomaly, to the lowest value at Sanae, near the heart of the Anomaly. This was consistent with the degree of severity with which the i.d.'s were found to occur at the three stations, and with our earlier reasoning. Our results had also shown that a definite conjugate relationship existed between the electron flux in the two hemispheres. Therefore we concluded that we had proved beyond doubt that the electrons involved were guided or controlled by the geomagnetic lines of force.

2.5 The Loss and Replenishment of Electrons in the Outer Radiation Belt.

These results led M.R.Torr (1965) to develop a model of the outer radiation belt and electron flux which considerably furthered our knowledge of the dynamics of charged particles in the belts and their effect on the ionosphere. Since we use this model in the work that follows, I shall summarise the main aspects here for convenience.

The regular way in which the critical flux decreased over the Anomaly with a corresponding increase in the severity of the i.d.'s, suggested that this was a direct consequence of the dynamics of trapped particles in a quiescent geomagnetic field. The results of Williams and Kohl (1965) provided additional information on the loss and replenishment of electrons upon passage through the South Atlantic Geomagnetic Anomaly. For trapped electrons with energies greater than 280kev as observed in the northern hemisphere, the trapped flux was 6×10^5 electrons/cm^2/sec, whereas after passage through the Anomaly at about 0°E the flux was

23/.....

well below the detector threshold of about 10^3 electrons/cm^2/sec. That the flux is replenished by a source mechanism was shown by the presence of a flux of 3×10^5 electrons/cm^2/sec at about 200°E. Therefore the depletion of particles in the Geomagnetic Anomaly must be counterbalanced by an injection into trapped orbits, so that a stable longitudinal dependence exists during magnetically quiet periods. The observations of Frank et al (1964) and Frank (1965) indicated that a violation of the third adiabatic invariant with conservation of the first two would provide a replenishment mechanism for electrons in the radiation belts. The total motion of a charged particle trapped in the geomagnetic field would then involve a gyration around and a translation along the field line, together with an azimuthal and inward radial drift with reflection at the mirror points.

Although a comprehensive treatment of charged particles in the geomagnetic field is highly complex (Roederer and Welch, 1965) M.R.Torr made a number of simplifying assumptions which we thought would severely limit her approach. However, the remarkable results she obtained justified her means, since the model successfully predicted the ratio of trapped to precipitated electron flux actually observed by Alouette along $L = 4$. It also accounted for the longitudinal variation of trapped flux observed by Williams and Kohl, (1965).

Essentially the model involved a continuous injection of electrons of isotropic angular distribution into the outer radiation belt. She

24/.....

restricted her attention to the L=4 shell, where the replenishment source was assumed to be operative along selected loci of constant B and L forming two rings in each hemisphere. The magnetic shell described by the lines of force connecting these rings was divided into sections longitudinally. The boundaries of each section were defined by lines of force spaced at intervals calculated to ensure that the azimuthal drift was less than one spacing during one bounce period. The injected flux was then divided into classes of trapped or precipitated according as to whether it would mirror above or below 100km altitude. Starting at the longitude of the lowest point on the B-L curve, account was kept of the trapped and precipitated flux for one complete drift cycle. The results of this procedure are shown in figures 7 and 8 in Chapter 3 where I have repeated the calculations for other L-shells. As I discuss the significance of these results comprehensively in Chapter 3, at this stage I will only refer to aspects relevant to the present analysis.

2.6 Minimum Disturbing Precipitated Electron Flux.

Figure 7 shows the longitudinal variation of p.e.f. for the two hemispheres. The sharp increase of precipitation over the Anomaly can be clearly seen in contrast to the small variation in the northern hemisphere. The emergence of the Anomaly from M.R.Torr's analysis was entirely consistent with the observations of satellites and quantit-

25/.....

atively demonstrates our earlier reasoning, enabling us to estimate the actual electron flux at a southern hemisphere station from that in the conjugate area.

To apply the theory to our case, all that is necessary is to find the longitude of the conjugate point and then to use Figure 7 to find the ratio of flux at the two conjugate points in question. For example, knowing that the critical p.e.f. in the conjugate area to Sanae is 8.2×10^3 electrons/cm^2sec, and using the ratio p.e.f. at Sanae/ p.e.f. at conjugate point (i.e. 2.15/0.67), we find that the actual p.e.f. at Sanae itself is $8.2 \times 10^3 \times 2.15/0.67 = 2.5 \times 10^4$ electrons/cm^2/sec. Table 10 shows the figures calculated in this way for each southern hemisphere station and the values determined directly for the northern hemisphere ones.

Table 10

Critical p.e.f.'s at the six stations.

Station	Critical p.e.f. in conjugate area, electrons/cm^2/sec.	Critical p.e.f. at station, electrons/cm^2/sec.
Sanae	8.2×10^3	2.5×10^4
Campbell Island	2.5×10^4	2.2×10^4
Halley Bay	1.2×10^4	2.5×10^4
St. Johns	-	2.5×10^4
Ottawa	-	2.2×10^4
Winnipeg	-	2.1×10^4

26/.....

These figures agree remarkably well and led us to believe that their mean value of 2.3×10^4 electrons/cm^2/sec, represents the minimum precipitated electron flux (or minimum disturbing flux, M.D.F.) which will produce an i.d.

2.7 The Frequency of Occurrence of Ionospheric Disturbances.

I mentioned earlier that the fact that every time the p.e.f. exceeded the critical value for a given station an ionospheric disturbance occurred, suggested that all i.d.'s defined by our criteria could be caused by precipitated electrons. If this were so, we would then expect the percentage total time for which the critical flux was exceeded at a given station to correspond closely to the percentage of total time for which the ionosphere was disturbed at that station. Until this stage we had not been able to test this reasoning, since the satellite did not record sufficiently large samples of data over each station to give statistically significant results. This is only too evident if we compare the number of high p.e.f. cases with disturbed ionosphere cases in Tables 4 to 9. However, Figure 7 shows that the p.e.f. in the northern hemisphere is independent of longitude to a first approximation. Therefore if M.R.Torr's replenishment mechanism is reasonably representative of the actual physical situation, we would expect to observe any one value of p.e.f. with approximately the same frequency of occurrence at all locations along L = 4 in the northern hemisphere.

27/.....

In Figure 4 we have therefore plotted the p.e.f. as abscissa and the percentage of the total number of satellite observations for which the p.e.f. was exceeded as ordinate. From this graph it was possible to read off the percentage time for which the p.e.f. exceeds the critical value at each station. Using large samples of ionospheric data we determined the percentage time for which our disturbance criterion was satisfied at these stations. A comparison of these figures is shown in Table 11.

Table 11.

Frequency of p.e.f. exceeding critical value and of ionospheric disturbance at six stations near L = 4.

Station	Lat.	Long.	L	% time p.e.f. $\geq$ critical value	% ionospheric disturbance
Sanae	70.3°S	2.4°W	3.99	67	65
Campbell Is.	52.55°S	169.15°E	4.02	29	31
Halley Bay	75.52°S	26.60°W	4.17	53	58
St. Johns	47.52°N	52.78°W	3.47	24	23
Ottawa	45.40°N	75.75°W	3.64	28	26
Winnipeg	49.90°N	97.40°W	4.22	30	31

The remarkable agreement between these figures led us to conclude that the precipitation of electrons from the outer radiation belt is responsible for all of the i.d.'s of the type discussed here on L = 4.

The discovery of the M.D.F. together with these results enabled

28/.....

FIGURE 4.

The % time for which given values of p.e.f. are exceeded at L = 4 in the Northern Hemisphere.

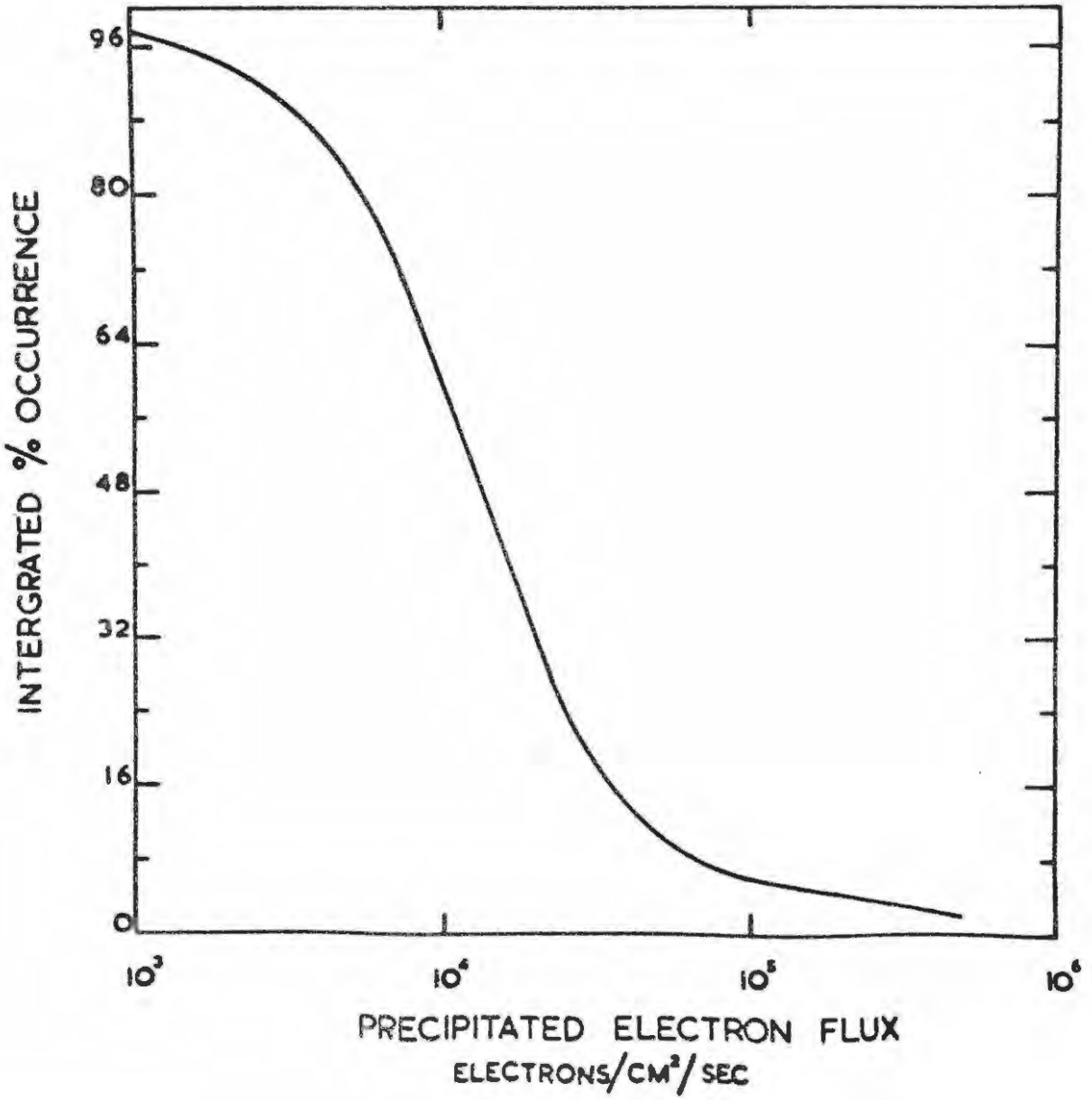
INTERGRATED % OCCURRENCE
96
80
64
48
32
16
0
10^3
10^4
10^5
10^6
PRECIPITATED ELECTRON FLUX
ELECTRONS/CM²/SEC

us to predict the percentage frequency of occurrence of i.d.'s at all locations on L ≃ 4. Knowing that the percentage time for which the M.D.F. is exceeded at a given station represents the percentage frequency of occurrence of i.d.'s, we calculated the corresponding values of critical flux at the conjugate points to locations lying in the southern hemisphere around L ≃ 4. The percentage time for which these values were exceeded was read from Figure 4 as before. The importance of these results, which are shown in Figure 5, lies in the application of this approach to other L-shells for which we were unable to obtain electron flux data.

FIGURE 5.

Calculated and observed percentage frequency of occurrence of ionospheric disturbances along L = 4. The circles and triangles represent southern and northern hemisphere observations respectively.

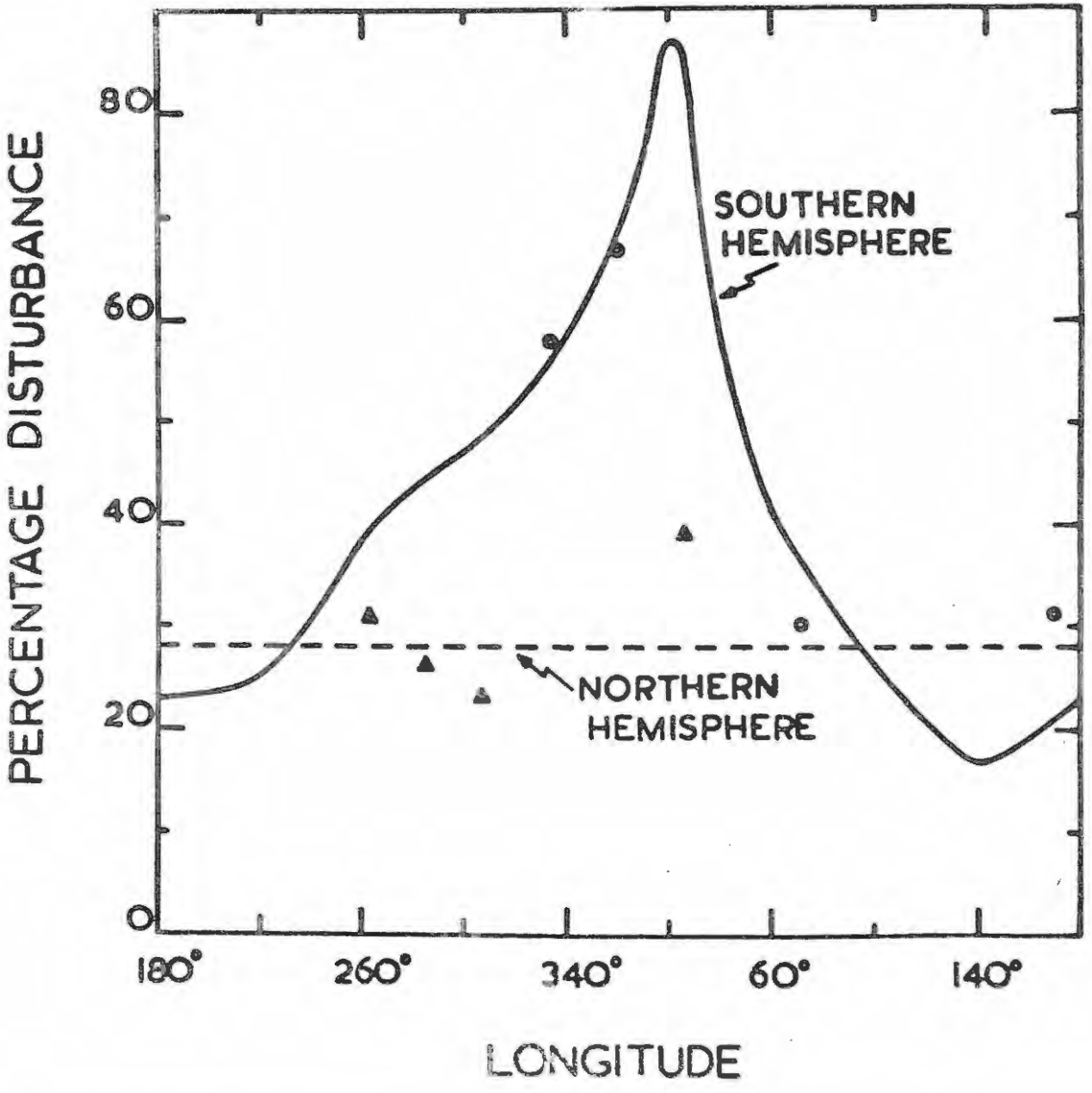
PERCENTAGE DISTURBANCE
80
60
40
20
0
SOUTHERN HEMISPHERE
NORTHERN HEMISPHERE
180°
260°
340°
60°
140°
LONGITUDE

CHAPTER 3.

EXPERIMENTAL AND THEORETICAL INVESTIGATIONS OF CHARGED PARTICLE FLUX AND IONOSPHERIC DISTURBANCES AT LOWER L SHELLS.

3.1 Introduction.

There appeared to be no reason why the effects discussed in Chapter 2 should be confined to the vicinity of the shell L = 4. It seemed probable that electron bombardment could be a major cause of i.d.'s at all sites which lie below the outer radiation belt. Our treatment has therefore been extended to lower L shells using a somewhat different approach.

3.2 Electron Flux Data.

The theory could not be tested directly using the approach described in the preceeding chapters as individual measurements of electron flux made at lower L shells could not be obtained. An intensive study of electron flux in the outer radiation belt has been made by Armstrong (1965). The data he presents were recorded in the northern hemisphere by the satellite Injun 3 during the period April to July 1963. His paper includes scatter plots of the directional intensity of both precipitated and trapped electrons with energies $>$ 40kev for the shells L = 2.2, 2.6, 3.5, and 4.5. The number of points shown in each of his diagrams varies from 244 for L = 2.2 to 413 for L = 4.5. These constitute large enough samples to estimate the integrated percentage frequency of occurrence of p.e.f. on each of these shells. This was done for each of the shells L = 2.2, 3.0 (by interpolation

30/.....

between 2.6 and 3.5) and 4.5. The resulting curves are shown in Figure 6. The profile shown in Figure 4 has also been included for purposes of comparison. The curve deduced from Injun 3 data (L = 4.5) is represented by a continuous line and that from Alouette (L = 4.4) by the broken line.

The absolute rms difference between the two curves is 5.5% for values of p.e.f. between 8×10^3 and 1×10^5 electrons/cm^2/sec. The frequency of p.e.f. which exceeds the critical p.e.f. for the 6 stations examined, as deduced from Injun 3 data, is shown in Table 12 compared with the Alouette results.

Table 12.

Station	Alouette % time p.e.f. ≥ critical value	Injun 3 % time p.e.f. ≥ critical value	% i.d.
Sanae	67	63	65
Campbell Is.	29	32	31
Halley Bay	53	54	58
St. Johns	24	32	23
Ottawa	28	35	26
Winnipeg	30	36	31

Considering that the accuracy of both the ionospheric and the satellite measurements is of the order of ±5%, the agreement of the Alouette and Injun 3 values with the percentage of i.d.'s is, on the whole, rather good, although the Injun 3 values do deviate in the cases of St. Johns,

31/.....

FIGURE 6.

The percentage time given values of p.e.f. are exceeded along various L shells.

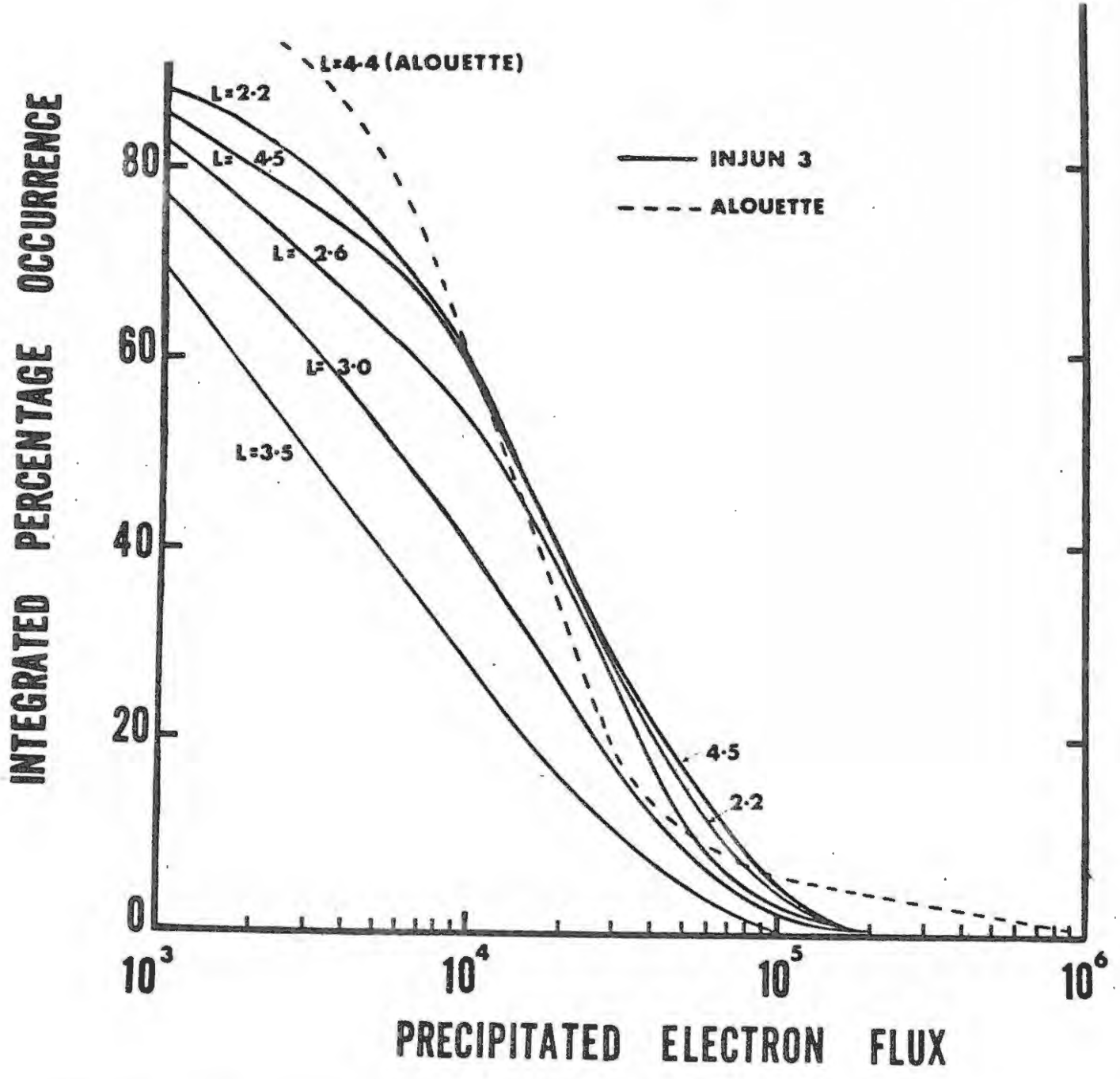
INTEGRATED PERCENTAGE OCCURRENCE
PRECIPITATED ELECTRON FLUX
L=4·4 (ALOUETTE)
L=2·2
L= 4·5
L= 2·6
L= 3·0
L=3·5
INJUN 3
ALOUETTE
4·5
2·2
0
20
40
60
80
10³
10⁴
10⁵
10⁶

Winnipeg and Ottawa.

This is to be expected from the shape of the Injun 3 curve for L = 4.5 in Figure 6, in the region of values of critical p.e.f. between about 2 X 10^4 and 7 X 10^4 electrons/cm^2/sec. The large difference in the Alouette and Injun 3 curves in the region below 1 X 10^4 electrons/cm^2/sec is probably due to the fact that the sensitivity limits of the counters in both satellites were of the order of 10^4 electrons/cm^2/sec.

Futhermore, differences between the two curves over the rest of their ranges may be due to a seasonal effect. Alouette observations were made during the period September, 1962 to August, 1963, which includes the northern hemisphere summer and winter, while Injun 3 data included only northern hemisphere summer observations. It therefore seems likely that the latter are weighted in favour of summer when it would not be unreasonable to expect a greater occurrence of larger p.e.f. values.

3.3 Frequency of Electron Precipitation and Ionospheric Disturbance at Lower L shells.

Also shown in Figure 6 are similar profiles for L = 2.2, 2.6, and 3 0. A significant feature is that the curves for L = 4.5 and 2.2 are very much the same. The question arises as to whether p.e.f. properties are the same on these two shells and in particular, whether the M.D.F. would be the same as for L = 4. If this were so, we would be able to estimate the longitudinal variation of the integrated percentage occurrence

32/.....

of flux at the lower L shells for purposes of comparison with ionospheric observations. In the absence of detailed p.e.f. data, it would be sufficient to show that the percentage frequency of i.d.'s increased towards longitudes where B is a minimum (at constant height and L) as this would be a convincing indication of particle induced effects.

The median values of p.e.f. can be estimated from Figure 6 by reading off the value of the flux that is exceeded for 50% of the time. The medians for the shells L=2.2, 4.4 and 4.5 were all found to be approximately 1.3×10^4 electrons/cm^2/sec.

Armstrong's results show that the integral energy spectrum of the electrons becomes soft towards L=3 and then harder again at L=2. The precipitated flux decreases by a factor of about 3 towards L=3.5 for electrons with energies > 40kev and by a factor of 100 for 230kev electrons. This effect is also observable in Figure 6, where the curves for L=3.0 and 3.5 lie well below those for 2.2 and 4.5. Williams and Kohl (1965) discuss a possible reason for the decrease in intensity towards L=3, but explanations of these effects will be sought in future research.

Lacking a better approach, I decided to use Armstrong's observations to repeat the type of analysis described in the last section of Chapter 2, on the assumptions that the electron flux properties are the same in the vicinity of the shells L=4 and 2, and consequently that the M.D.F. is the same.

A computer programme was written to repeat M. R. Torr's (1965)

33/.....

calculations for the shells L=3.0, 2.5, and 2.0. The Fortran listing is given in Appendix 1. (Since intense fluxes of protons have been observed toward the inner radiation belt, the calculations were also done for protons. The results are shown as a matter of interest and do not form part of the analysis.)

Figures 7 and 8 show the longitudinal variation of p.e.f. and trapped electron flux respectively for the various L shells. Figures 9 and 10 are the corresponding ones for protons. Tables of data for these shells have been included in Appendix 2. The profiles for protons show that precipitation could extend much further eastwards at times when the flux is high.

As in the case of L=4, the curves for the northern hemisphere show very little longitudinal variation. The procedure described in Section 2.7 was applied to data for L=3.0, 2.5, and 2.0. (Although this approach cannot be justified for the shell L=3, it is nevertheless included in the analysis.) The longitudinal variation of p.e.f. in the northern hemisphere was calculated for a corresponding southern hemisphere M.D.F. of 2.3 X 10^4 electrons/cm^2/sec. The percentages of total time for which these values of flux were exceeded were read from the corresponding curves in Figure 6. The results of this procedure are shown in Figure 11. For comparison the percentage frequency of occurrence of i.d.'s was determined as before for the same 6 month period and for as many ionosphere stations on these shells for which data were available.

34/.....

FIGURE 7.

The relative longitudinal variation of p.e.f. for various L shells. x is used to denote the intensity of the injected flux in electrons/ cm^2/sec. (see Torr, 1965). The longitude is in degrees east.

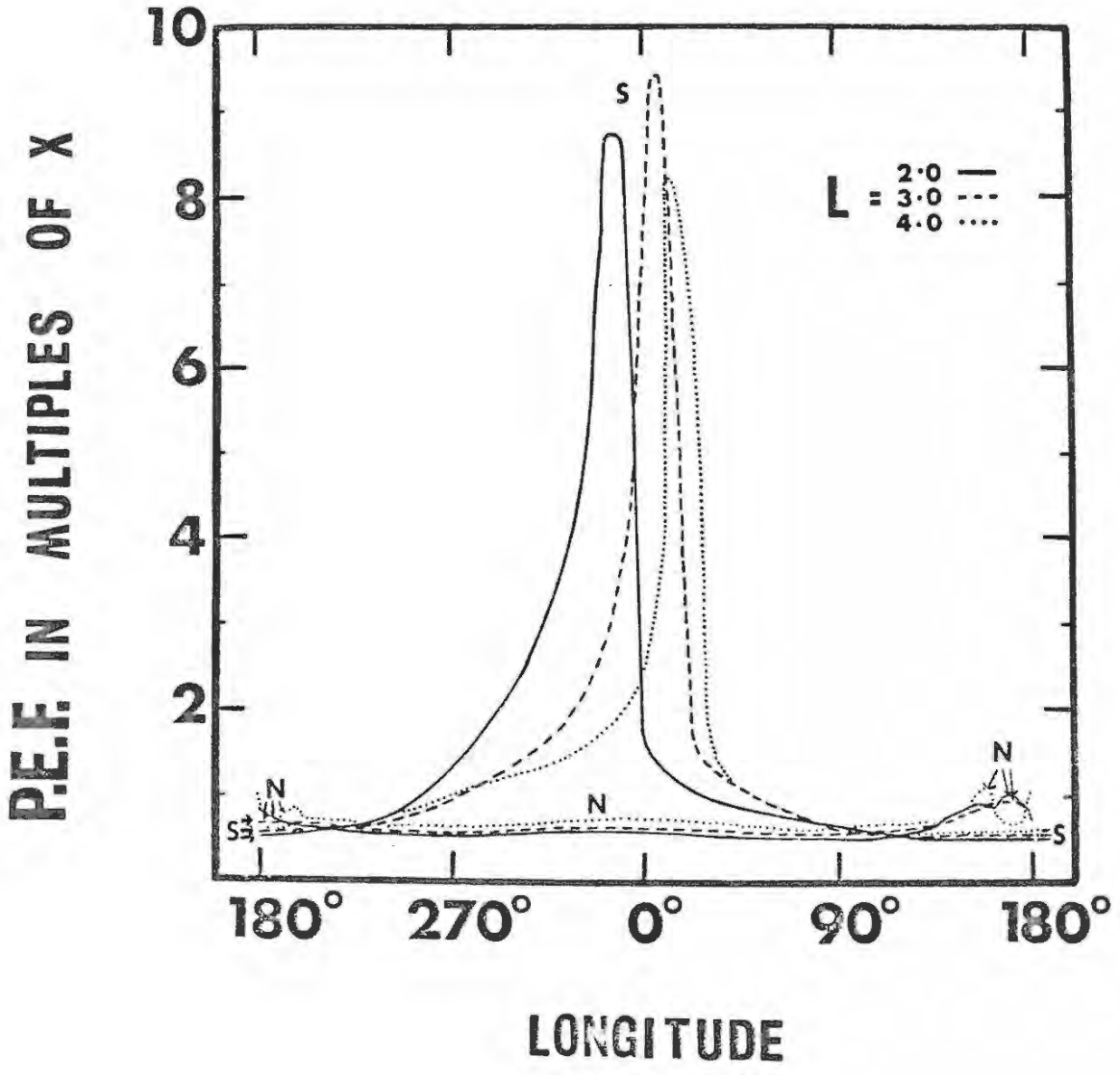
P.E.E. IN MULTIPLES OF X
10
8
6
4
2
S
N
N
N
S
S
L = 2·0
3·0
4·0
180°
270°
0°
90°
180°
LONGITUDE

FIGURE 8.

The relative longitudinal variation of trapped electron flux at various L shells. x is used to denote the intensity of the injected flux in electrons/cm^2/sec. (see Torr, 1965). The longitude is in degrees east.

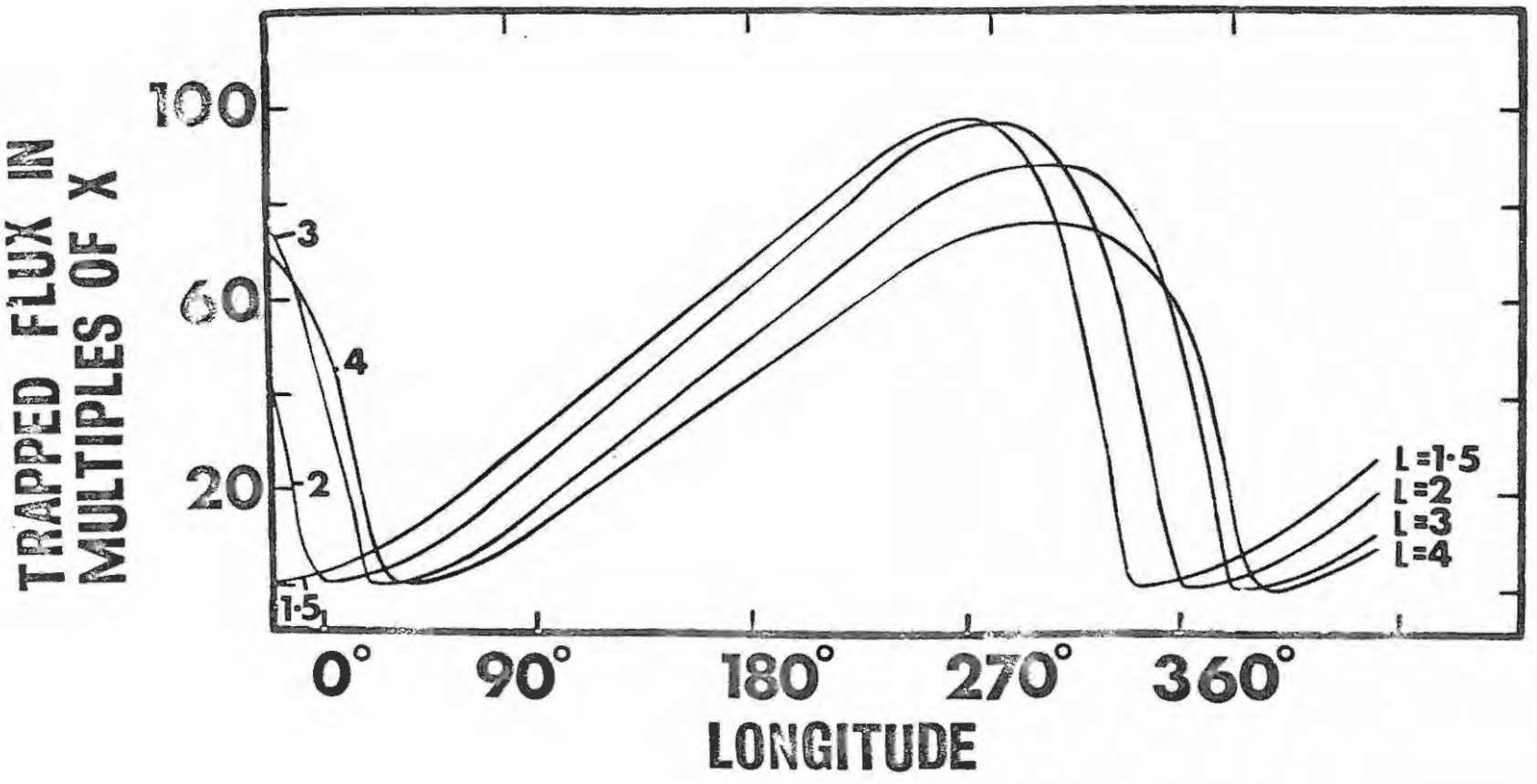
TRAPPED FLUX IN MULTIPLES OF X
100
60
20
3
4
2
1·5
L=1·5
L=2
L=3
L=4
0°
90°
180°
270°
360°
LONGITUDE

FIGURE 9.

The relative longitudinal variation of precipitated proton flux along various L shells in the southern hemisphere. x is used to denote the intensity of the injected flux in electrons/cm^2/sec. (see Torr, 1965). The longitude is in degrees east.

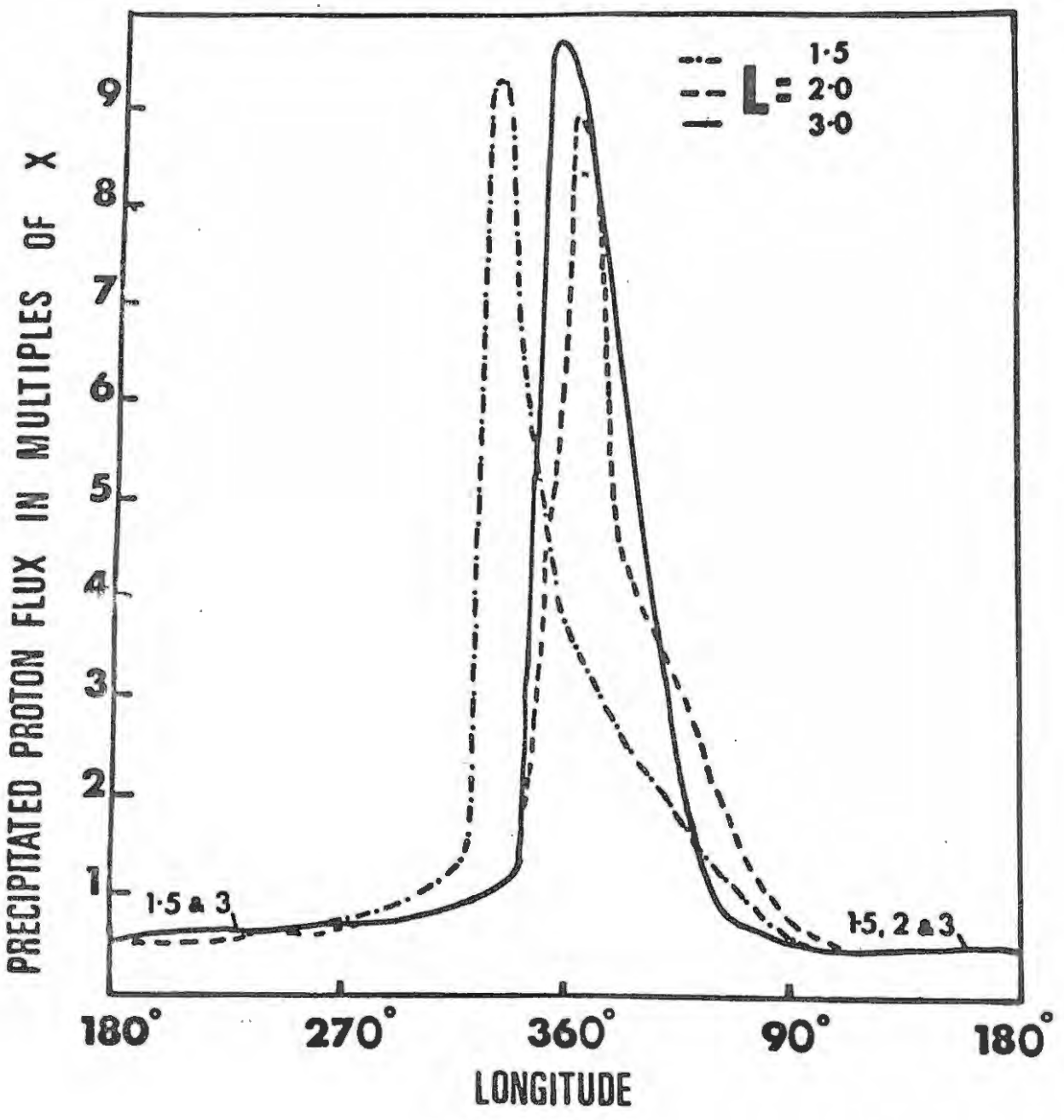
PRECIPITATED PROTON FLUX IN MULTIPLES OF X
9
8
7
6
5
4
3
2
1
L = 1·5
2·0
3·0
1·5 & 3
1·5, 2 & 3
180°
270°
360°
90°
180°
LONGITUDE

FIGURE 10.

The relative longitudinal variation of trapped proton flux along various L shells. The longitude is in degrees east.

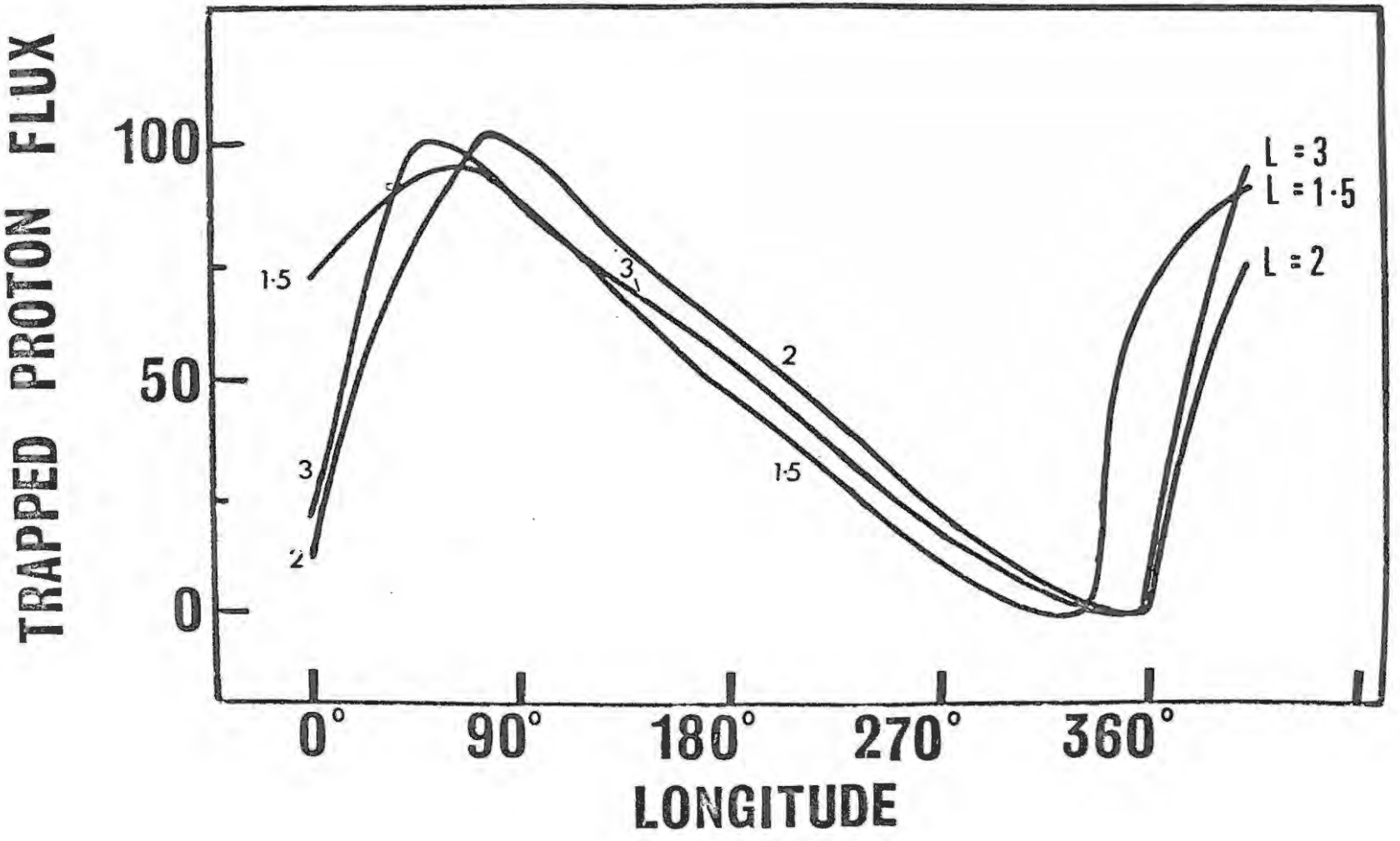
TRAPPED PROTON FLUX
100
50
0
0°
90°
180°
270°
360°
LONGITUDE
L = 3
L = 1·5
L = 2
1·5
3
2
3
2
1·5

FIGURE 11.

The calculated and observed percentage frequency of occurrence of ionospheric disturbances along various L shells. The numbers represent the following stations:

	L value		L value
1. Cape Town	1.83	9. Campbell Island	4.02
2. Canberra	2.08	10. Washington	2.73
3. Argentine Islands	2.50	11. Slough	2.53
4. Godley Head	2.52	12. Miedzeszun	2.37
5. Marion Island	2.81	13. Dourbes	2.31
6. Hobart	2.98	14. Juliusruh-Rugen	2.72
7. Halley Bay	4.17	15. Port Lockroy	2.30
8. Sanae	3.99		

The upper and lower dotted lines show the calculated percentage disturbance of the ionosphere for the shells L = 2 and 3 respectively for the northern hemisphere. The longitude is in degrees east.

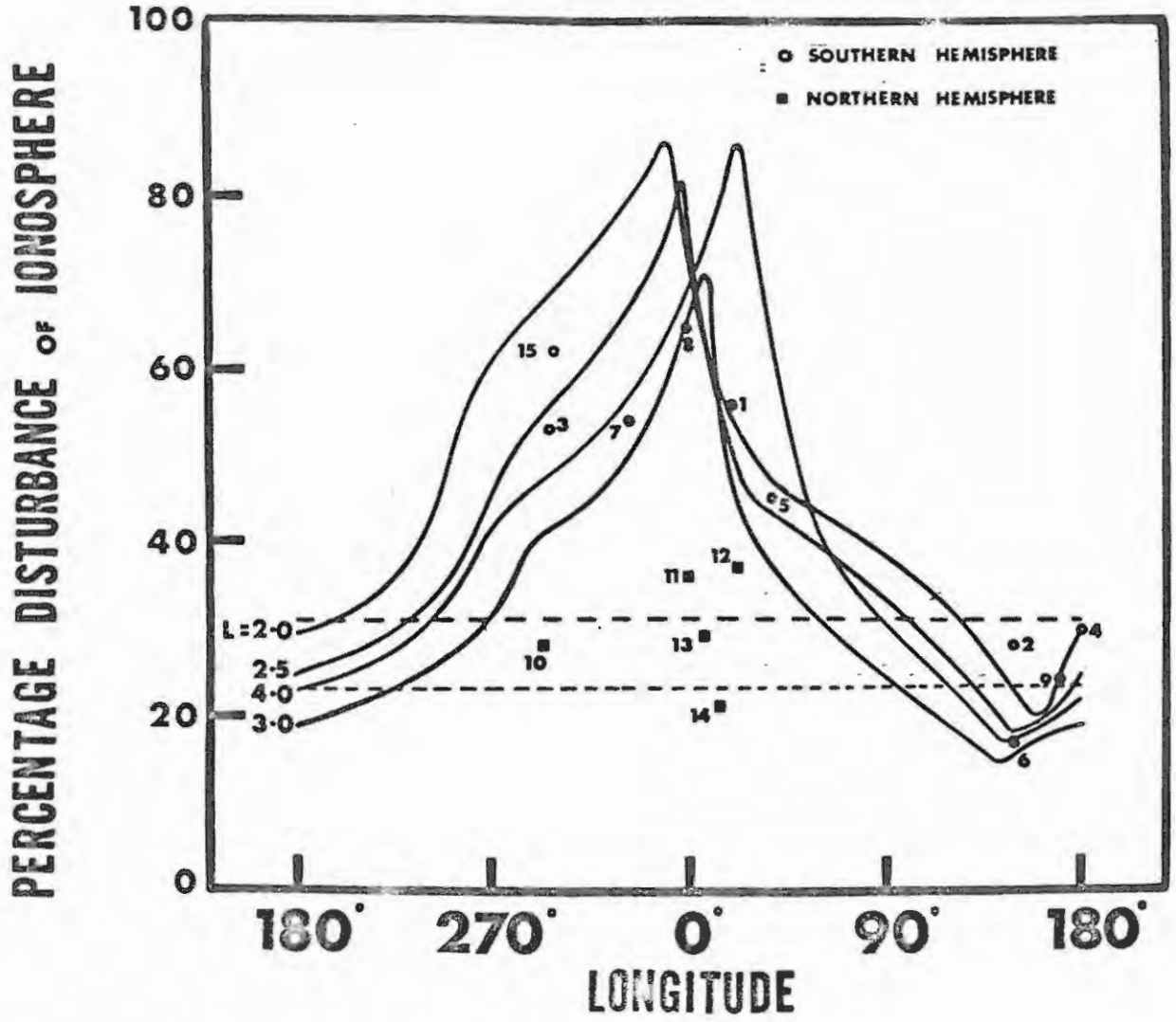
PERCENTAGE DISTURBANCE OF IONOSPHERE
100
80
60
40
20
0
o SOUTHERN HEMISPHERE
■ NORTHERN HEMISPHERE
15 o
8
o1
o3
7o
o5
12■
11■
L=2·0
2·5
4·0
3·0
10■
13■
14■
o2
o4
9o
6
180°
270°
0°
90°
180°
LONGITUDE

Although it would have been a better approach to do the analysis for April to July, 1963, (i.e. the period during which Injun 3 telemetered data) the ionosphere analysis had already been completed in anticipation of answers to our requests for satellite data by the time this approach was adopted. The results for the southern hemisphere are shown in Table 13.

Table 13.

Station	Lat.	Long	L value	Predicted % i.d.	Observed % i.d.
Cape Town	34.15°S	18.32°E	1.88	53	56
Canberra	35.32°S	149.00°E	2.08	23	28
Argentine Is.	65.25°S	64.27°W	2.50	57	53
Godley Head	43.57°S	172.80°E	2.52	25	30
Marion Is.	46.85°S	37.87°E	2.81	38	45
Hobart	42.92°S	147.17°E	2.98	15	17
Port Lockroy	64.83°S	63.51°W	2.30	62	62

The good agreement between these values show that there can be little doubt that the effects of electron precipitation from the radiation belts are readily observable at shells as low as L=2. It is also quite remarkable that fairly good agreement could be obtained for Marion Is. and Hobart near L=3, where the integral electron flux spectrum is different from that at both L=4 and 2. This suggests that very high

35/.....

energy electrons (>230kev) do not play an important part as a disturbing agent. As an ionosonde was only in operation on Marion Is. during the International Geophysical Year, data for the period October, 1957 to March, 1958 were used. Numerous data were lost due to faulty equipment and the value shown is only reliable to within ± 10%.

It was impossible to conduct an analysis for Deception Is. (L = 2.2, 60.6°W) where our results show that the ionosphere will be disturbed for 71% of the time. Large quantities of data were recorded as lost due to non-ionospheric reasons. It is possible that cases of strong non-deviative absorption have been mistaken for equipment failure. The same difficulty was experienced at Sanae where the ionosphere is about 5% less disturbed. Another example of misinterpretation of data is evident in the case of the Argentine Is. in Table 2 (events 18 and 19).

Table 14 shows the results for 5 northern hemisphere stations.

Table 14.

Station	Long.	Lat.	L value	% i.d.'s	Predicted % i.d.'s
Dourbes	4.6°E	50.10°N	2.31	29	34
Miedzeszun	21.2°E	52.17°N	2.37	37	34
Slough	0.57°W	51.48°N	2.53	31	33
Juliusruh-Rugen	13.38°E	54.63°N	2.72	21	32
Washington	77.13°W	38.73°N	2.73	28	32

The results shown here are entirely consistent with the observations made on L = 4.

36/.....

Since the frequency of occurrence of p.e.f. followed closely that of i.d.'s, I concluded that the M.D.F. must be approximately the same for all shells lying in the outer radiation belt and that whenever the p.e.f. exceeds this value, an i.d. occurs. I have shown that electron bombardment of the upper atmosphere is an important agent influencing the behaviour of the ionosphere over more than half the globe. As such, its importance in theories of layer formation should not be underestimated.

3.4 The Effect of Electron Precipitation on f_oF_2.

The next step was to investigate variations in the behaviour of the ionosphere which were typical of the i.d.'s studied. It seemed probable that the disturbance effects should produce observable changes in the monthly medians of the parameters $h'F_2$, f_oF_2 and f_{min}, which would be more marked over regions of intense precipitation. The parameters f_{min} and $h'F_2$ were unsuitable for direct comparison of values at various stations, since f_{min} is dependent on the instrument used and $h'F_2$ can lead to misleading results because it is not simply related to the real minimum height of the F_2 layer. Therefore f_oF_2 was the obvious parameter to examine.

Instead of using data supplied by individual ionospheric observatories, the task was made easier by using monthly world wide prediction charts issued by the Central Radio Propagation Laboratories (C.R.P.L.) of the U.S.A. These maps represent contours of predicted maximum usable

37/.....

frequency (MUF) for propagation at vertical incidence, MUF(0), and over distances of 4000km. Since MUF(0) is actually f_xF_2, the data supplied by C.R.P.L. represent $f_H/2$+ median values of f_oF_2, where f_H is the gyro-frequency. These maps are used in monthly ionospheric forecasting and the values have been found to be, on the whole, reliable. The predicted values, which are prepared three months in advance of the period to which they apply, are usually in good agreement with the results published in standard monthly ionosphere bulletins, although occasional descrepencies have been found. The charts available included data for the period May, 1963 to November, 1966. Values of MUF(0) were read from these.

From our theoretical analysis and from our observations of the longitudinal variation of electron flux and i.d.'s, I expected to find some variation of MUF(0) at southern hemisphere locations which would be more pronounced near regions of minimum geomagnetic intensity (B) on a given L shell. I also expected to observe very little corresponding variation in the northern hemisphere.

The disturbances in the F_2 region usually involved a decrease in f_oF_2 and an increase in $h'F_2$, although similar variations in opposite phase have also been observed. These were usually accompanied by increases in f_{min} which became less pronounced toward lower L shells. Because a decrease in f_oF_2 was the most usual variation that occurred during an i.d., I anticipated a decrease in MUF(0) toward minimum B in the southern hemisphere.

38/.....

Figure 12 shows the geographic coordinates of minimum B on all shells for $L \leqslant 5.0$. The circles indicate the locations of the various L shells. In Figure 13 MUF(0) at local midnight is plotted against longitude for various values of L. The full curves are for the southern hemisphere for May, 1963, and the dotted curves for the northern hemisphere for November, 1963 which is the corresponding seasonal period.

The southern hemisphere curves show unmistakably that MUF(0) does decrease with B, passing through a minimum, and then rising to a maximum to the west of lowest B. As was expected for the shells $2.0 \leqslant L \leqslant 5.0$, the northern hemisphere curves show very little longitudinal variation. The small peaks at 60°E and 30°E for L=5 and 4 respectively, are a little puzzling. It is difficult to say, however, how reliable the fine structure of these profiles is, as there are not many ionosphere stations at such high latitudes which supply C.R.P.L. with data for their predictions. Not knowing how they interpolate between stations, it is safest at this stage to disregard detailed variations. With the exception of L=3.0 and 2.5, the minima move westwards toward lower L as would be expected from Figure 12. These variations are observable at shells as low as L=1.5, whereafter it is likely that proton effects associated with the Brazilian Anomaly (Vernov et. al,1962) are dominant. There is also a peak in the northern hemisphere, which is approximately conjugate to the southern hemisphere valley. This peak becomes more and more pronounced at lower L shells and at L=1.2 the northern hemisphere variation

39/.....

FIGURE 12.

The geographic coordinates of minimum B for several L shells.

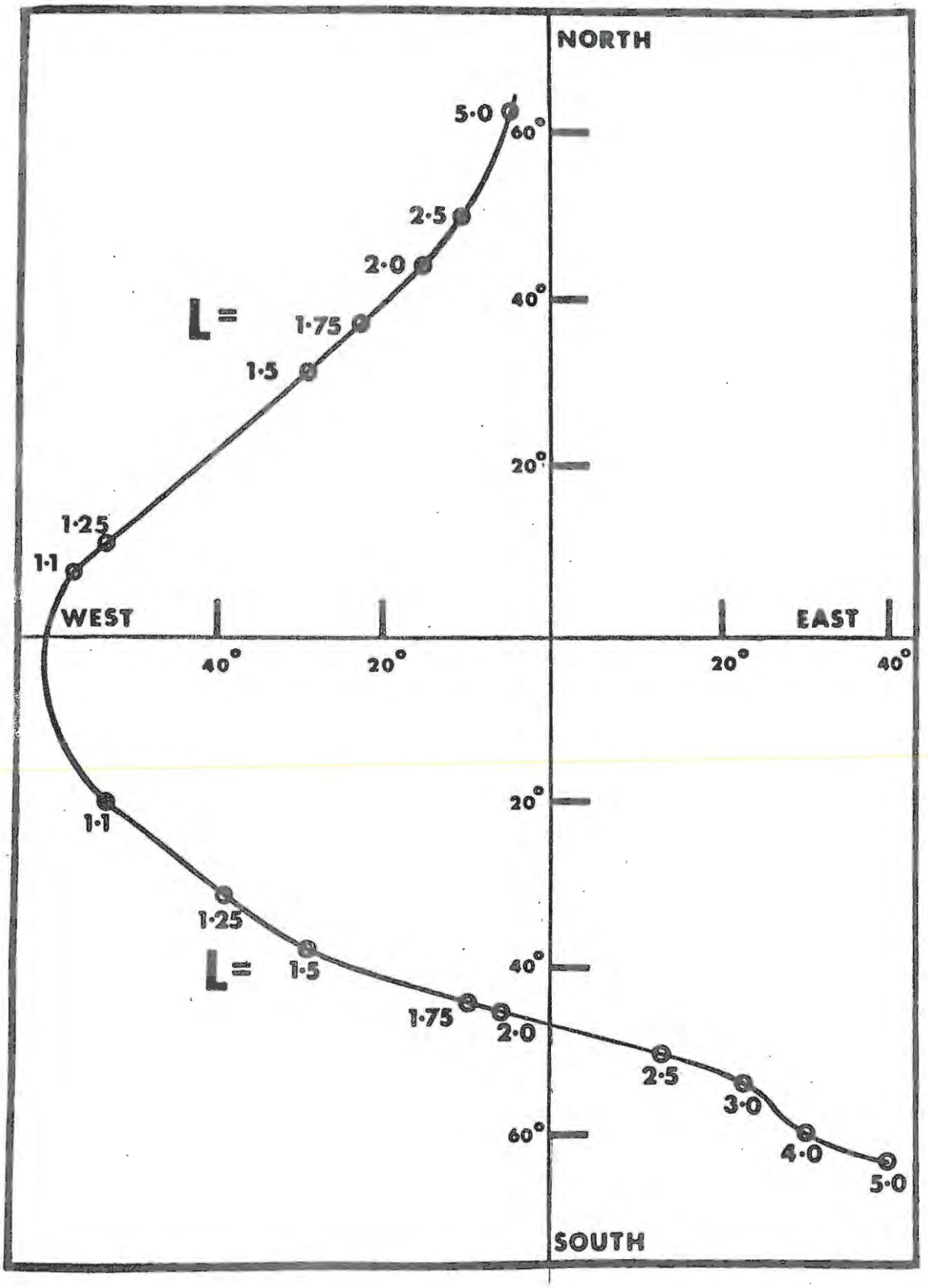
NORTH
5·0
60°
2·5
2·0
L=
1·75
1·5
40°
20°
1·25
1·1
WEST
EAST
40°
20°
20°
40°
20°
1·1
1·25
L=
1·5
40°
1·75
2·0
2·5
3·0
60°
4·0
5·0
SOUTH

FIGURE 13.

Longitudinal variation of MUF(0) along various L shells at local midnight.

The longitude is in degrees east.

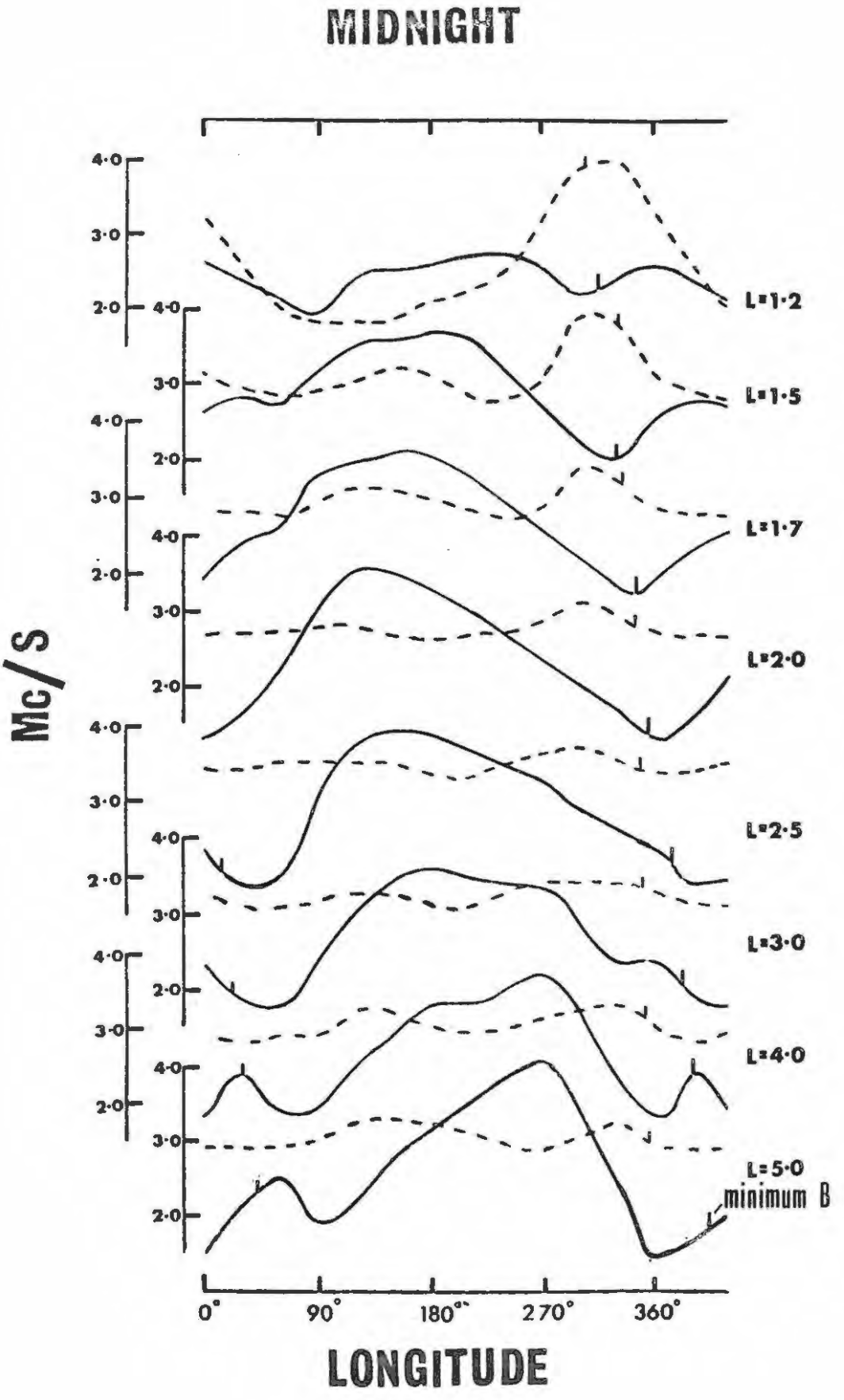
MIDNIGHT
Mc/S
4·0
3·0
2·0
L=1·2
L=1·5
L=1·7
L=2·0
L=2·5
L=3·0
L=4·0
L=5·0
minimum B
0°
90°
180°
270°
360°
LONGITUDE

is larger than that in the southern hemisphere. The northern hemisphere peak practically disappears at L=3, where the p.e.f. intensity decreases. Another peak is also discernable at about 150°E. This corresponds rather well to the small increase in precipitation (Figure 7) associated with the Russian Anomaly (Ginsburg et. al, 1962).

The magnitudes of the southern hemisphere variations are largest at L=5, becoming smaller toward L=3 and larger again at L=2 and then progressively smaller toward lower L values. This is entirely consistent with the variation of electron flux intensity across L space.

An unexpected phenomenon is the rapid westward shift of the peaks from 270°E at L=5 to 135°E at L=2, where the eastward decrease becomes correspondingly more gentle. These movements do not appear to be related to properties of the geomagnetic field. The question arises as to why these southern hemisphere peaks lie so far to the west and why they are higher than the corresponding values in the northern hemisphere when there is no other ion production source there at midnight. The peaks just to the west of minimum B in the southern hemisphere and conjugate to minimum B in the northern hemisphere, where there is a corresponding but smaller increase in precipitation, can be explained as follows.

It is thought that electrons bombarding the atmosphere lose their energy both in ionizing and in heating the air molecules. When the latter effect predominates, an increase in the total ion content may not be observable as an increase in f_oF_2, because the resulting expansion of

40/.....

atmospheric gas may redistribute the ionization to produce a decrease in f_oF_2. Since the energy input to the southern hemisphere atmosphere is far larger than that in the northern one, it is quite probable that heating predominates there, whereas an increase in ionization may be the most important effect in the northern hemisphere. Similarly, enhanced ionization would be expected to be the predominant effect to the west of the anomaly where the intensity of precipitation just begins to increase. Moving further east, this would be superseded by heating and expansion of the atmosphere resulting in the maximum ion density.

This led me to suspect that a critical value of flux may exist, above which heating would become the predominant effect. Moving west toward the anomaly, the p.e.f. begins to increase. The heating effect should begin to override the increase in ionization at the longitude at which the critical value is reached, and the increase in f_oF_2 should change over to a decrease. The longitude at which the critical value is reached should therefore correspond to the longitude at which the peak in MUF(0) occurs. The fact that the curve for L=2 in Figure 11 is much broader near the peak than that for L=4 suggests that the critical value should be reached much further to the west on L=2 than on L=4. To test this theory it is only necessary to compare absolute values of p.e.f. intensity at the longitudes at which the peaks in MUF(0) occur. If the theory is correct, the values of p.e.f. at these points should be the same. Furthermore, if electron flux is the sole agent responsible for

41/.....

the large variations in MUF(0) at midnight, it is logical to conclude that there must be an absolute relationship between these two parameters. Therefore, if the longitudinal variation of median (or average) values of actual p.e.f. were known, p.e.f. could be plotted against MUF(0) for one L shell to find this relationship. To verify this, values of MUF(0) on another L shell could be calculated from the values of p.e.f. on that shell and compared with observed values.

In order to estimate the absolute p.e.f. at locations in the southern hemisphere, median values were calculated for the shells L = 4, 3 and 2 from all Injun 3 northern hemisphere observations on each shell. Since the p.e.f. is practically constant over an L shell in the northern hemisphere, the same procedure described in Section 2.6 was used to calculate the actual p.e.f. in the southern hemisphere. (The calculations are described in detail in Appendix 3). The results are shown in Figure 14.

Values of p.e.f. and MUF(0) for L = 4 were read from Figures 14 and 13 respectively at the same longitudes. Only that part of the curve lying between 150°E and 0°E through 180°E was used as I doubted the reliability of the small peak at 30°E in Figure 13 which could not be checked against actual ionospheric observations. Along the rest of the curve, values were checked at the longitudes of Campbell Island (169°E), Halley Bay (333°E) and Sanae (358°E). The agreement was good. In Figure 15, values of p.e.f. have been plotted against MUF(0) (curve b). Values of p.e.f. for L = 2 were then read from

42/.....

FIGURE 14.

The longitudinal variation of median values of p.e.f. for the northern hemisphere summer and for the southern hemisphere winter. (The value of 10^5 on the right hand scale should read 10^3.) The longitude is in degrees east.

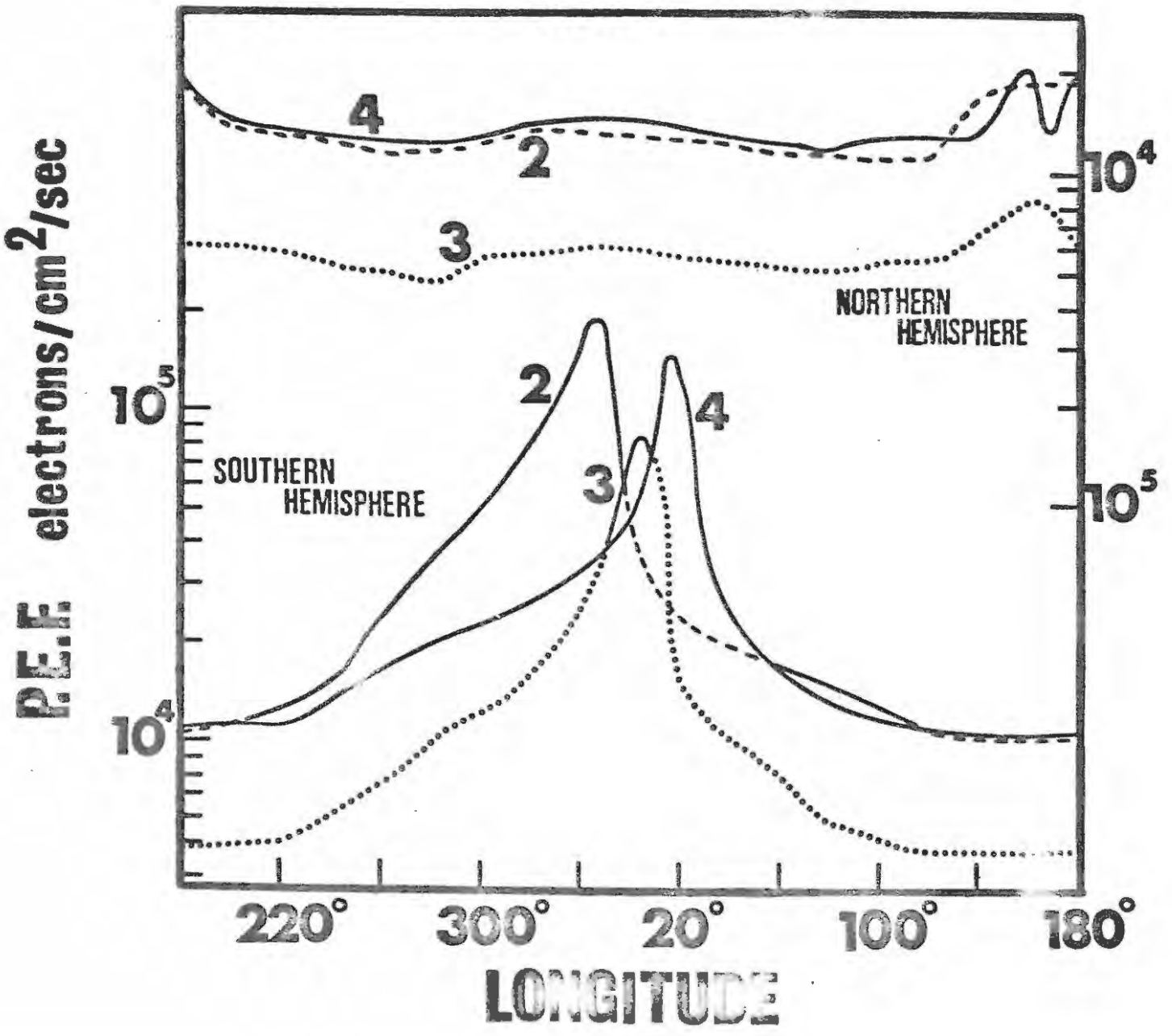
P.E.F. electrons/cm²/sec
10⁵
10⁴
4
2
3
NORTHERN HEMISPHERE
SOUTHERN HEMISPHERE
220°
300°
20°
100°
180°
LONGITUDE

FIGURE 15.

Plots of MUF(0) against p.e.f. for L = 4.

Curve (a) represents MUF(0) against midnight median values of p.e.f. and curve (b) daily median values of p.e.f. Curve (a) is directly proportional to curve (b) and so the points on the former have not been shown.

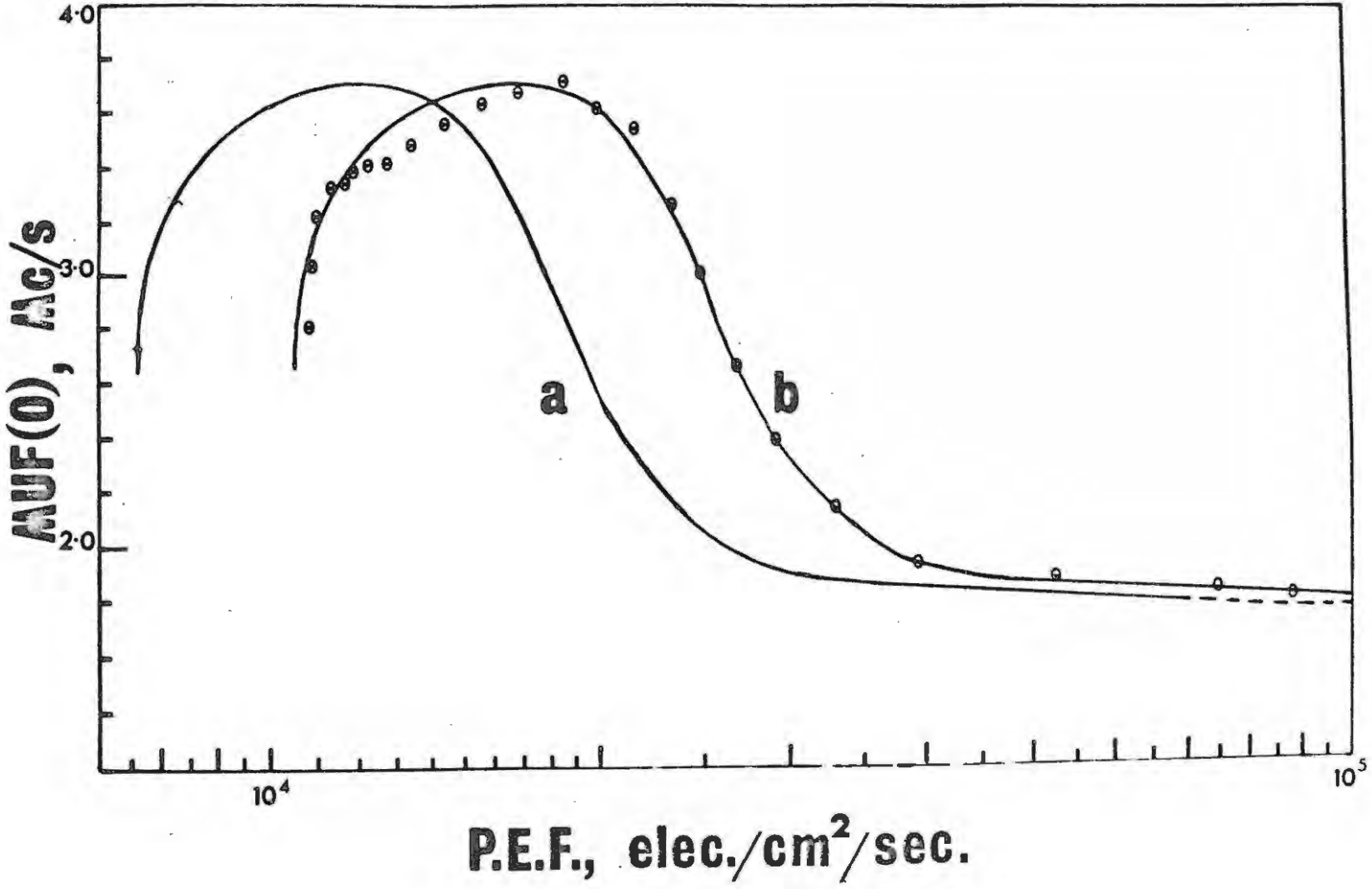
4·0
3·0
2·0
ΔUF(0), Δc/s
a
b
10⁴
10⁵
P.E.F., elec./cm²/sec.

Figure 14 and the corresponding longitude of each value noted. Corresponding values of MUF(0) were read from Figure 15 and plotted against the p.e.f. longitude. The results are shown in Figure 16 by the dashed curve/ labelled b. Also shown as the full line is the curve for L=2 from Figure 13.

The curves demonstrate that this theory can account for the westward shift of the peaks. The main valley is caused by the redistribution of ionization where the flux is highest. Moving eastward, away from the anomaly, the flux decreases with a corresponding decrease in heating and increase in enhanced ionization. The critical value is reached at 60°E and the enhanced ionization is the predominant effect. Moving further east again, the flux decreases even more and the additional ionization drops accordingly, reaching a minimum at 150°E, which is the longitude of minimum p.e.f. Further east the flux begins to increase again with a corresponding increase in ionization, until the critical value is reached at 240°E. Thereafter, heating begins to predominate again and MUF(0) decreases to a minimum at about 350°E where the flux is a maximum.

There are two things which may be responsible for the difference in shape of the two curves. The most obvious reason is that there are far too few stations on L=2 to expect to work out fine structure as complex as that which our calculations have revealed. The second possibility is that there may be other factors responsible for the observed variations.

43/.....

FIGURE 16.

Calculated and observed longitudinal variation of MUF(0) along L = 4 and 2 at midnight. Curve (a) represents values of MUF(0) calculated from midnight median values of p.e.f. and curve (b) from the daily median of p.e.f. for L = 2. The _._ curve for L = 4 shows the results calculated from the smoothed curve labelled (a) in Figure 15, compared with the experimental one from which the actual points shown in Figure 15 were obtained.

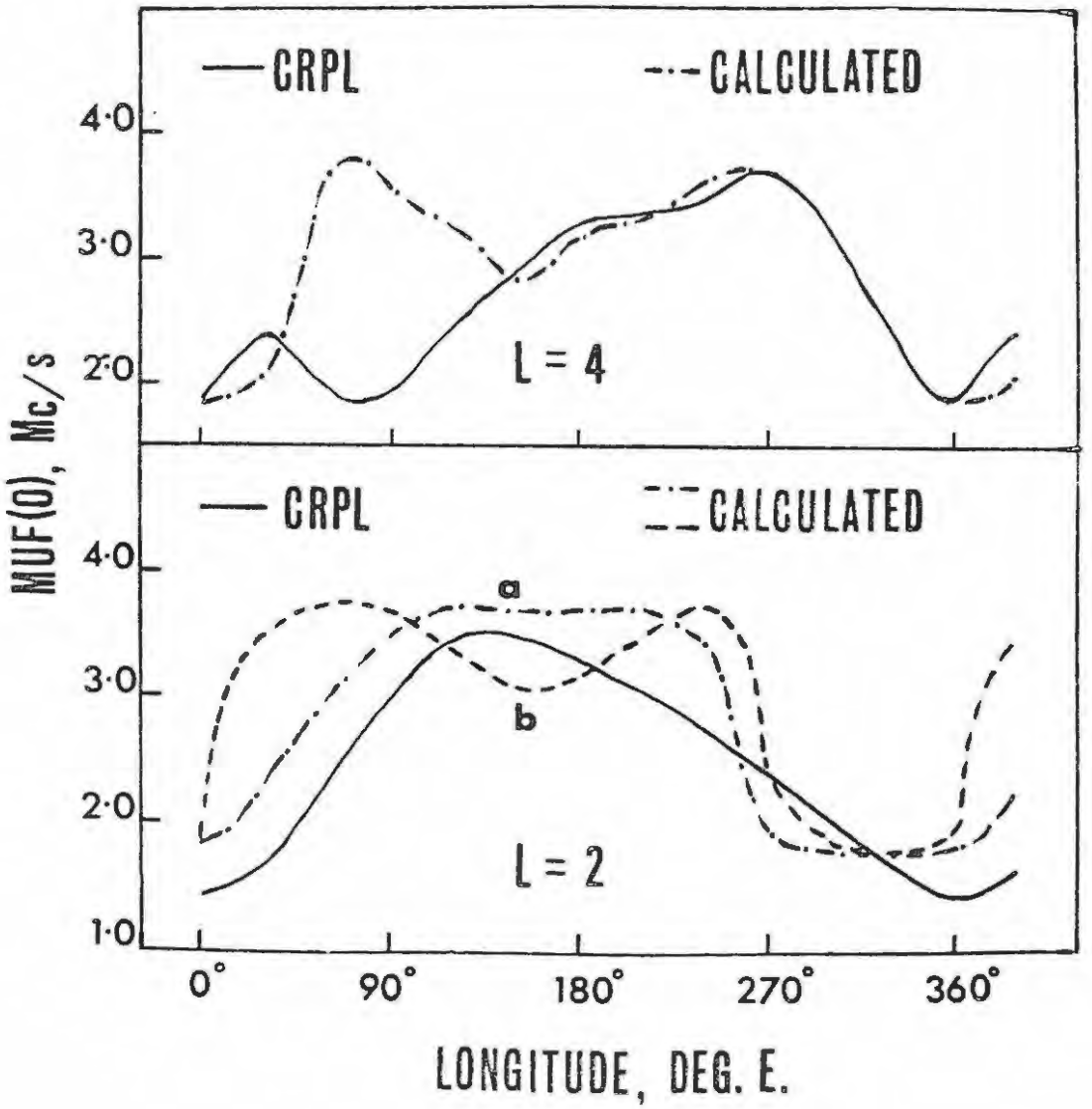
CRPL
CALCULATED
4·0
3·0
2·0
L = 4
CRPL
CALCULATED
4·0
3·0
2·0
1·0
a
b
L = 2
MUF(0), Mc/s
0°
90°
180°
270°
360°
LONGITUDE, DEG. E.

Considering the first possibility, available ionosphere data for L = 2 is limited to three ranges of longitude centered on Australasia (120°E - 170°E), South Africa (0° - 30°E) and the region around Graham Land in Antartica and the South Shetland Islands (65°W - 75°W) i.e. 285° - 295°E. The calculated curve agrees reasonably well with the Argentine Islands and Australasian observations, but not with those of Cape Town (15°E, L = 2.0), where the observed values are lower. Nothing can be said about the peak at 240°E until actual measurements are taken there.

The poor agreement of results around 30°E led me to investigate the second possibility. As Armstrong (1965) observed a diurnal variation during April to July, 1963, this seemed to be the obvious course of investigation to pursue. (It should be noted that we found no diurnal variation in p.e.f. from an analysis of Alouette data, while McDiarmid and Burrows (1964) found a variation only for L > 4.5)

Armstrong divided his measurements into 4 six hour periods centered on midday, evening, midnight and dawn. The p.e.f. medians that he obtained for these periods on L = 4.5 were 5.6×10^4, 8.5×10^3, 9.9×10^3 and 1.4×10^4 electrons/cm^2/sec. respectively. A smaller variation was found on L = 2.2 and the corresponding values are 1.4×10^4, 8.2×10^3, 1.2×10^4 and 1.2×10^4 electrons/cm^2/sec. respectively.

These effects will not be investigated in this thesis in detail, but the calculations will be redone using an appropriate diurnal variation in the injected flux in the near future.

44/.....

It is, however, possible to estimate to a first approximation, better p.e.f. values for the L = 4 shell. The p.e.f. medians for the northern hemisphere at midnight on the shells L = 2 and 4 are 1.2×10^4 and 9.9×10^3 electrons/cm^2/sec. respectively. In calculating absolute intensities along these shells, the median values used were 1.3×10^4 and 1.4×10^4 electrons/cm^2/sec. respectively. The flux on L = 4 should therefore, to a first approximation, be reduced by the factor $9.9 \times 10^3 / 1.4 \times 10^4$.

The procedure was therefore repeated using the corrected values of p.e.f. for L = 4. It was not necessary to do this for L = 2, because there is little difference between the overall median for the day and that for the night. The new curves (labelled a) are also shown in Figures 15 and 16 and this time the agreement is very much better. The critical value, which will be called the critical heating flux or CHF, corresponds to the peak value of MUF(0) in Figure 15. The CHF, as read at this point, is 1.3×10^4 electrons/cm^2/sec. as compared with a value of 2.3×10^4 electrons/cm^2/sec. for the MDF. This result confirms the suggestions in our paper (Gledhill, Torr and Torr, 1967) that smaller disturbances may occur which are not detectable by these methods of investigation. This would also account for even more of the LD cases found in Tables 6 to 9. These results suggest that the i.d.'s that accompany values of p.e.f. which lie below the currently accepted MDF should involve an increase in f_0F_2.

Similar calculations of MUF(0) were done for L = 4 for the part

45/.....

of the curve which was originally disregarded. The results are shown in Figure 16. The calculations show that a marked peak should exist at about 75°E. It is most remarkable that the CRPL data showed a peak at 30°E, which lies on the western edge of the sharp rise of the curve. One can only guess that this increase must have been observed at the Belgian Antarctic base, Roi Baudouin (70.5°S, 23.3°E, L=5.5), during the IGY.

The conclusions drawn at this stage are:

(1) that a critical value of p.e.f. exists above which the effect of electron bombardment becomes predominantly that of heating the atmosphere,

(2) that during the southern hemisphere winter there is a diurnal variation in the p.e.f. which, because of the CHF, results in a complicated longitudinal variation of f_oF_2 at constant L.

The results discussed deal with the night-time period which is best suited for a study of electron induced effects, because, as far as is known, there are no other causes of ionization effective then. The situation inevitably becomes more complex with the rising of the sun. Atmospheric heating and expansion occur and the ultra-violet light from the sun begins to ionize the air molecules. The latitudinal variation of loci of constant L would also be expected to introduce further variations in MUF(0), because of corresponding latitudinal changes in the solar zenith angle.

46/.....

Since the normal diurnal heating of the atmosphere will supplement the corpuscular energy, the CHF would be expected to be lower during the day than at night. This means that the MDF should also decrease during the day. In the absence of any other effects one would expect the peaks to follow the CHF and move closer together. However, until the influence of the additional ultra-violet ionization is investigated it is difficult to predict what is to be expected.

Figures 17, 18 and 19 show the longitudinal variation of MUF(0) at constant L for the times 0600, 1200 and 1800 hours. The same general pattern is observable at each of these times of day. At 0600 it seems as if the peak at L = 2 has moved to the east. A check of the CRPL data for L = 4 against median values of f_0F_2 at Halley Bay and Sanae for May, 1963 revealed an error in this data for dawn. The values of MUF(0) at these longitudes are approximately 1.0 Mc/s and 1.5 Mc/s too high for Sanae and Halley Bay respectively. This means that the valley on L = 4 should lie near Halley Bay (333°E), which by comparison with Figure 13, places the peak further to the west.

The variations at 0600 are less pronounced than expected. However, it is well known that the ionosphere undergoes rapid variations at sunrise and these may obscure the corpuscular effects. There is an increase in the peak of MUF(0) at midday which can be associated with the diurnal increase in UV ionization. The longitudinal variation in MUF(0) on the shells L = 2 at dawn and midday show additional

47/.....

FIGURE 17.

The longitudinal variation of MUF(0) at local dawn for various L shells. The longitude is in degrees east.

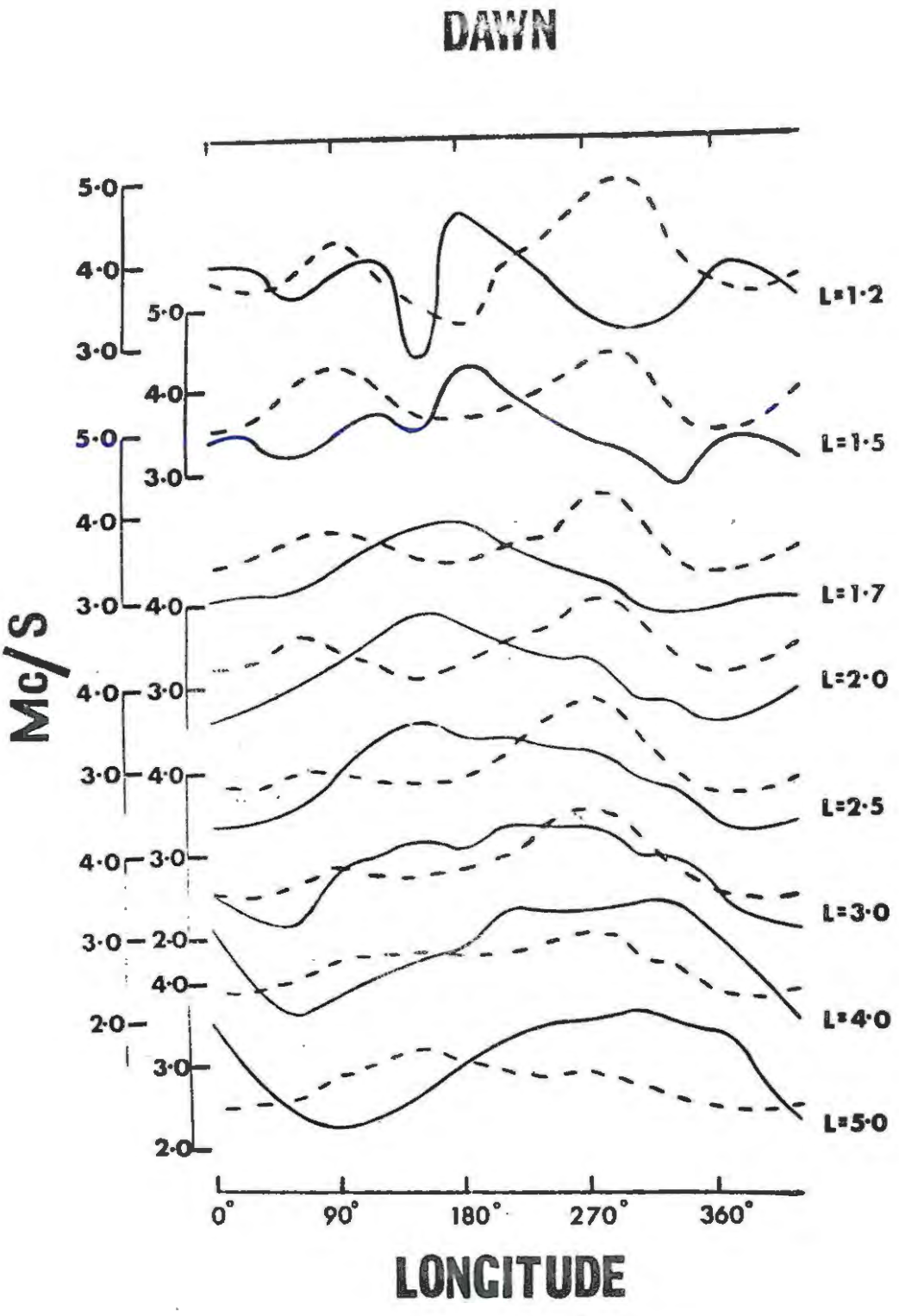
DAWN
Mc/S
5·0
4·0
3·0
5·0
4·0
3·0
4·0
3·0
4·0
3·0
4·0
3·0
4·0
3·0
4·0
3·0
2·0
4·0
2·0
3·0
2·0
L=1·2
L=1·5
L=1·7
L=2·0
L=2·5
L=3·0
L=4·0
L=5·0
0°
90°
180°
270°
360°
LONGITUDE

FIGURE 18.

The longitudinal variation of MUF(0) along various L shells at local midday. The longitude is in degrees east.

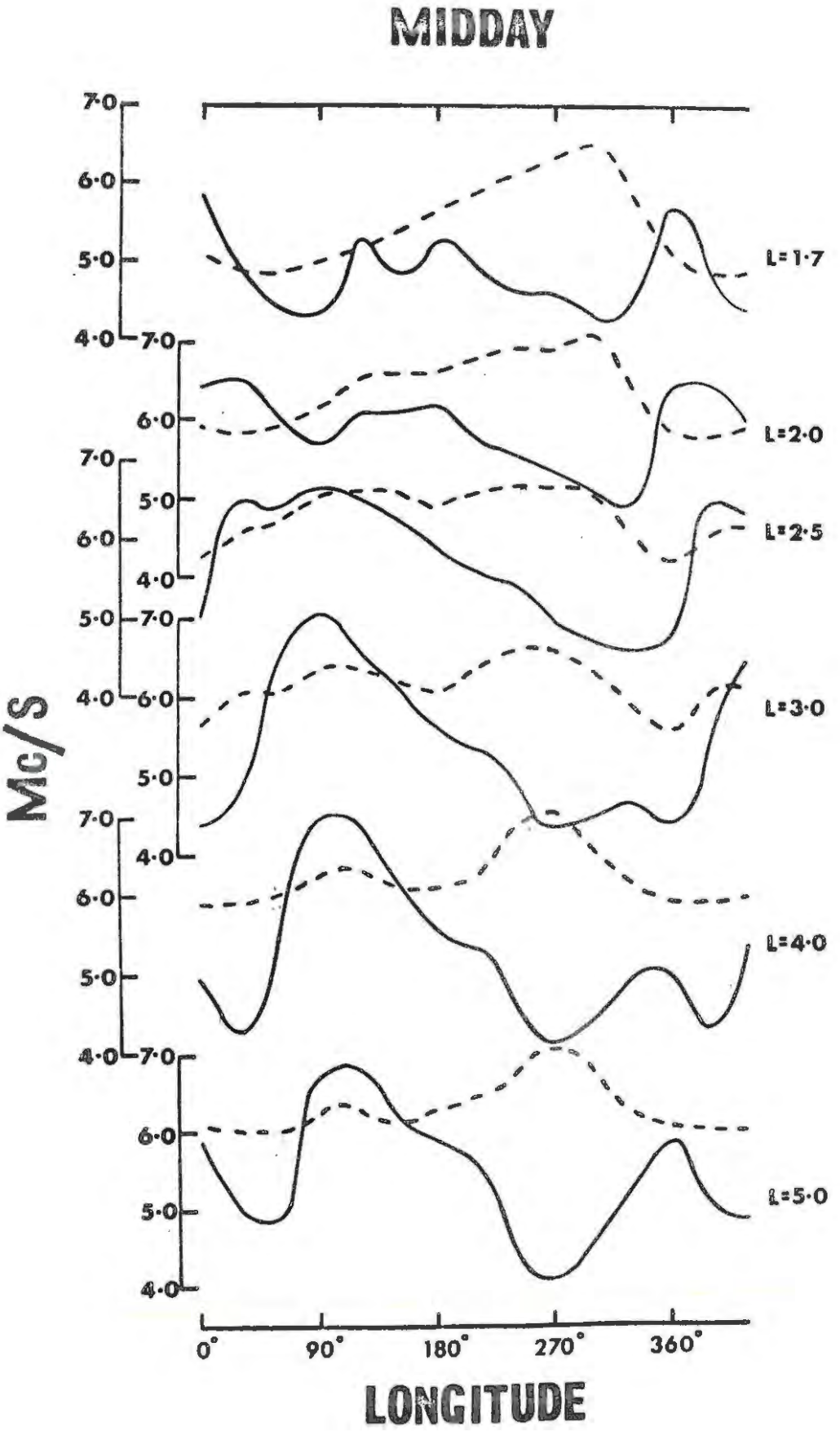
MIDDAY
Mc/S
7·0
6·0
5·0
4·0
L=1·7
L=2·0
L=2·5
L=3·0
L=4·0
L=5·0
0°
90°
180°
270°
360°
LONGITUDE

FIGURE 19.

Longitudinal variation of MUF(0) along various L shells at local evening. The longitude is in degrees east.

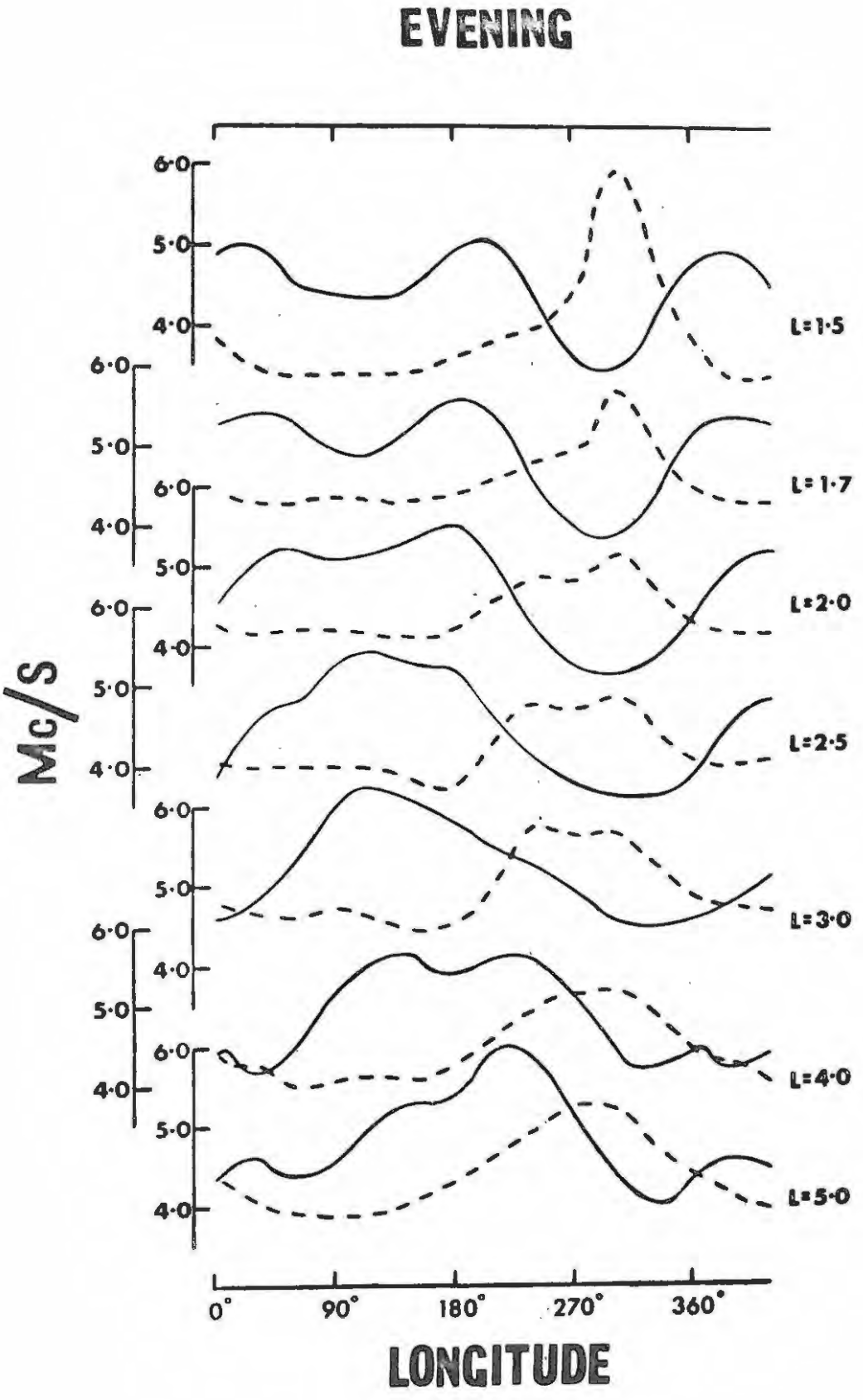
EVENING
Mc/S
6·0
5·0
4·0
L=1·5
L=1·7
L=2·0
L=2·5
L=3·0
L=4·0
L=5·0
0°
90°
180°
270°
360°
LONGITUDE

unexpected peaks and valleys.

There are many strange variations at all shells which I cannot explain at this stage. At midday the N.H. intensity on L = 4 rises to 5.6×10^4 electrons/cm^2/sec. as compared with 9.9×10^3 electrons/cm^2/sec. at midnight. Because of the complications introduced by solar ionization and heating, it was not possible to calculate values of MUF(0) for the day-time. It seemed likely that the left and right peaks would move toward the region of minimum flux around 180°E, where they may even merge to one peak, because of the increase in both the corpuscular and radiative energies (with a consequent decrease in the CHF). The curves for midday, however, do not show this behaviour at all. It is difficult to understand why the peaks lie at approximately 100°E for $5 \geq L \geq 3$, and around 0° to 30°E for $2 \leq L \leq 2.5$. That a peak does exist at approximately 0°E at L = 2 was confirmed by an examination of the ionosphere data for Cape Town. During the day-time, especially at midday, the entire phenomenon is probably too complex to be explained in terms of M.R. Torr's simple model of electron flux and this theory of a critical heating flux.

3.5 Conclusions and Discussion.

The first significant result which emerged from the analysis described in this chapter, was the discovery that the close relation

48/.....

between the frequency of occurrence of p.e.f. and i.d.'s found at L = 4, persists at all sites below the outer radiation belt. This in turn justified the initial assumption that electron flux properties are similar on the shells $2 \leqslant L \leqslant 4$.

The main conclusions drawn from the inspection of the MUF curves are:

(1) The variations in MUF(0) are caused by corpuscular bombardment of the atmosphere, because the southern hemisphere curves show a buildup of MUF(0) to a peak (or peaks) and then a decrease at or near to regions of minimum B.

(2) At midnight, when there are no other heating and ionizing agents present, the variations in MUF(0) can be explained simply in terms of corpuscular ionization and heating of the atmosphere.

(3) Broad longitudinal variations in f_0F_2 were predicted and found, but the approach used is too simple to explain the complex day-time variations. It seems probable that these are related to the diurnal variation in both p.e.f. and UV intensity.

(4) The effects of electron precipitation from the radiation belts are readily observable at shells as low as L = 1.5 and discernable at L = 1.2.

(5) The F_2 layer is notorious for its erratic behaviour. It was always this typically erratic behaviour that consistently satisfied the disturbance criterion. The fact that the frequency of

49/.....

occurrence of p.e.f. corresponded so well to that of i.d.'s, suggests very strongly that the key to the puzzle of the strange behaviour of the F_2 region has been found.

Unfortunately the investigation has been hampered to a certain extent, because satellite observations of p.e.f. are not available to us at present for lower L shells. The results obtained led to the conclusion that we are dealing with a global phenomenon which appears to form part of the regular behaviour of the ionosphere below the radiation belts. These results should lead to a better understanding, not only of the behaviour of the ionosphere, but also of charged particles in the radiation belts.

It is also evident that far more ionospheric and satellite observations are required for both hemispheres (in particular the southern one) to resolve the complicated daytime variations. This could possibly be achieved if interested countries could be persuaded to operate portable ionosondes to obtain more information over the large unmonitored regions.

In the absence of electron flux data, a promising alternative method seems to be a detailed correlation of 3914 Å auroral emission with ionospheric observations. South Africans could contribute substantially to a project of this nature by using the research ship, the RSA, to make ionospheric and airglow studies along lines of constant L in the Indian and South Atlantic Oceans.

50/.....

CHAPTER 4.

EXPLANATION OF F REGION PECULIARITIES.

4.1 Introduction.

It is obvious that the remarkable longitudinal variations found in f_oF_2 at constant L must be responsible for much of the strange behaviour of the F region. In the last chapter it was shown that these longitudinal variations at midnight were caused by corpuscular bombardment of the atmosphere. Superimposed on these during the day was a complex diurnal variation which could be related to the combined diurnal variations in p.e.f. and solar radiation. In this chapter, the effect of these variations on the diurnal behaviour of f_oF_2 at locations along constant L will be investigated. Seasonal changes in the pattern of the longitudinal variations are also investigated and it is shown that the summer behaviour is different from winter. This investigation supplied the answers to several previously unexplained F region phenomena.

4.2 An Unusual Decrease in f_oF_2 Over Rhodesia During The Evening in Winter, 1966.

The first problem solved in the light of this newly acquired knowledge involved the fading of 3.3 Mc/s signals of the Rhodesian Broadcasting Corporation. They reported that their 90 metre band transmission to Salisbury (17.8°S, 31.0°E, L=1.36) was disrupted in the evening for the period April to May, 1966. The transmitting station is

51/.....

situated at approximately 140 miles to the west of Salisbury. Fading of their 3396 kc/s transmission commenced at about 2100 hours and was followed soon after by their 3306 kc/s signal. On some occasions the fading lasted for periods of minutes and at other times until shutdown at 2300 hours.

It was discovered that this phenomenon could be explained in terms of an eastward shift of the MUF valley on L=1.3, together with the diurnal decrease of f_0F_2 with the approach of evening. Normally Salisbury lies to the east of the valley (see Figures 13 and 19). However, during April to May, 1966 the eastward shift was greater than for May, 1963.

Values of MUF (140 miles) were calculated for the region 330°E to 50°E at approximately L=1.3 using CRPL prediction charts. Ionosphere data recorded at Johannesburg were used to correct small errors in the predicted values. It was found that therewas a steady eastward shift of the valley toward evening. At about 2000 hours, MUF (140 miles) went below the Rhodesian transmission frequencies. About an hour later, the valley began to move westward again and MUF (140 miles) rose above the frequency of transmission.

This is one example of the successful application of these recent observations of corpuscular bombardment of the atmosphere to the explanation of what might otherwise have been a puzzling phenomenon.

52/.....

4.3 The Anomalous Morning Increase in f_0F_2 at Sanae and Halley Bay.

The success of the above reasoning led to the attempt of an explanation along similar lines of a peculiarity in the behaviour of f_0F_2 at some Antarctic stations. Workers have been baffled for some time by a striking anomalous summer morning increase in the peak electron density at several stations lying in and near the Southern Radiation Anomaly.

This type of behaviour was first noticed at Port Lockroy(67°S, 65°W) and at Deception Is. (63°S, 61°W) by Coroniti and Penndorf (1959). Later Knecht (1959) reported a similar phenomenon for the South Pole, Bellchambers and Piggott (1960) for Halley Bay (75.5°S, 27°W) and Baker and Gledhill (1964) for Sanae (70.3°S, 2°W). Among other stations, Falkland Is. (57.7°S, 57.8°W) also shows it. With the exception of the South Pole, all these stations lie within 0° to 70°W. Antarctic stations that do not show it include Terre Adelie(66.7°S, 140.6°E), MacQuarie Is.(54.3°S, 158.6°E) and Campbell Is.(52.5°S, 169.1°E), all lying east of the South Radiation Anomaly.

The object of this discussion is not to solve this problem in detail for all stations, but rather to show that the general solution has been found by explaining the typical cases of Halley Bay and Sanae.

In Figures 20 and 21, MUF(0) is plotted against longitude for L = 4 in the southern hemisphere for December and May,1963 and for the times 00 to 22, at 2-hourly intervals. As reasons for believing that the CRPL data may be unreliable at locations far removed from ionospheric observatories have previously

53/.....

FIGURE 20.

The summer longitudinal variation of MUF(0) on L = 4 at various times of day, in the southern hemisphere.

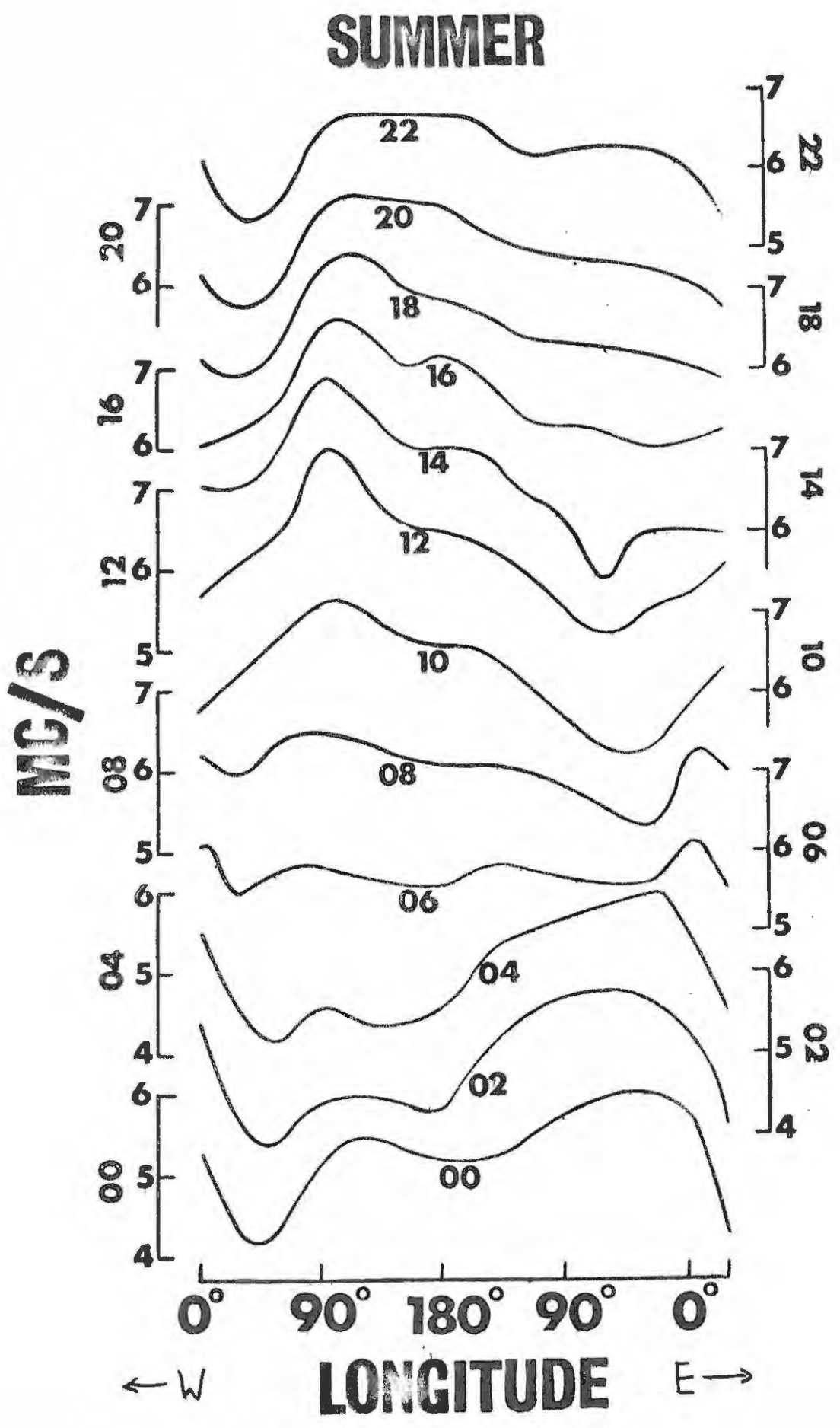
SUMMER
MG/S
22
20
18
16
14
12
10
08
06
04
02
00
0°
90°
180°
90°
0°
← W
LONGITUDE
E →

FIGURE 21.

Winter longitudinal variation of MUF(0) along

L = 4 at various times of day, in the southern hemisphere.

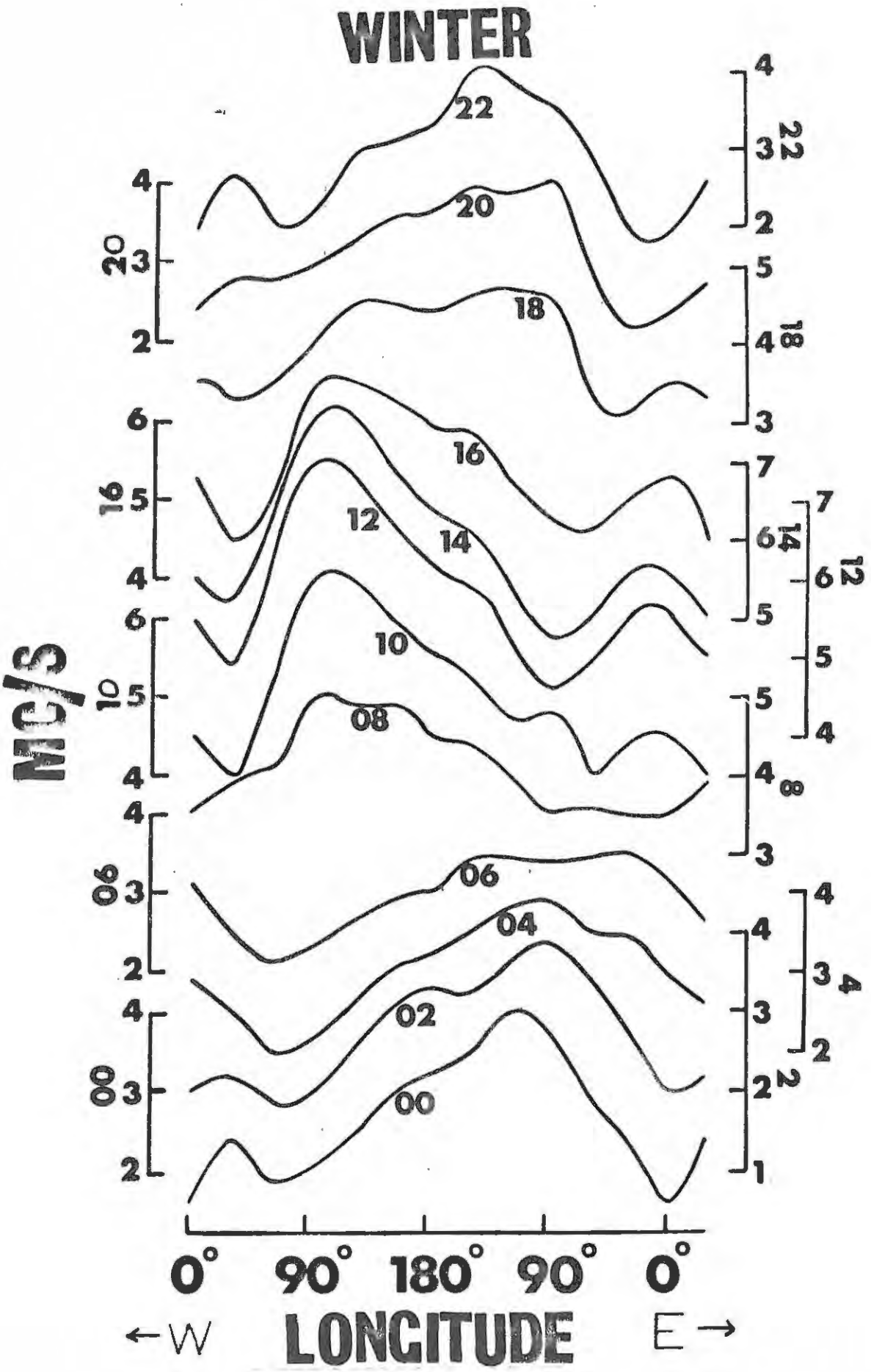
WINTER
MC/S
22
20
18
16
14
12
10
08
06
04
02
00
0°
90°
180°
90°
0°
←W
LONGITUDE
E→

been given, only conclusions based on CRPL data derived in the proximity of stations will be regarded as factual.

Comparing Figure 20 with 21, it can be seen that at midnight in summer the MUF(0) peak lies further to the east than in winter. This results in a midnight increase in ionization at Halley Bay ($27^{\circ}W$) and Sanae ($2^{\circ}W$). Unfortunately, Alouette did not record sufficiently large samples of data in December to calculate statistically significant median values of p.e.f. Therefore it was not possible to apply the CHF theory again. Furthermore, at the longitude of Sanae, the $L=4$ contour dips to the south and in summer the ionosphere is illuminated by the sun for 24 hours a day.

The combined effects of the radiative and corpuscular energies place the peak of MUF(0) at approximately $60^{\circ}W$ at midnight in December. Since the peak moves away from this position during the rest of the day, this causes f_oF_2 to attain a maximum value there at midnight. Although there are no stations at $60^{\circ}W$ on $L=4$, Coroniti and Penndorf (1959) observed a maximum at midnight at Port Lockroy on $L=2.3$. Similarly, Halley Bay and Sanae lie on the eastern slope of the peak, making f_oF_2 at these stations much higher than normal at midnight, even considering their geographic location. The value of f_oF_2 is correspondingly higher at Halley Bay than at Sanae, their respective MUF(0) values being 6.0 Mc/s and 5.8 Mc/s. At 0200 hours the peak moves further east, suggesting that the p.e.f. decreases in the early morning hours. A decrease in MUF(0)

54/.....

is therefore to be expected at about 150°E where the p.e.f. reaches a minimum. This is confirmed by the value for Campbell Island which decreases from 5.2 Mc/s at 0000 to 4.4 Mc/s at 0400 hours.

On the other hand the solar zenith angle is increasing with a corresponding increase in UV radiation. Together with the decrease in heating this results in an increase in MUF(0) from 5.7 Mc/s at 0200 to 6.0 Mc/s at 0400 at Halley Bay, whereas at Sanae the p.e.f. is still large enough to suppress an equal increase (in this case 5.4 Mc/s to 5.5 Mc/s) by heating the atmosphere. At 0600, however, the p.e.f. must become so small that it can only supplement the normal ionization at the point of maximum precipitation. In this case the curve resembles a typical northern hemisphere curve where corpuscular effects are very much less pronounced. This implies that the p.e.f. diurnal variation in summer must be different from that in winter. This causes an increase in f_oF_2 at Sanae at 0600, which then reaches a maximum at 0800. Halley Bay (27°W), on the other hand, lies a little too far to the west to experience this increase and f_oF_2 decreases at 0600. This entire phenomenon results in maxima at Halley Bay at midnight and 0400 hours and at approximately 0800 for Sanae. These observations are entirely in agreement with Bellchambers and Piggott (1960) and Baker and Gledhill (1964).

At 0800 hours the p.e.f. presumably begins to increase and the peak just to the east of the Anomaly begins to appear, as in the case of winter. The valley at Halley Bay is a little puzzling at this stage

55/.....

as it does not appear to fit the theory. However, it is possible that a strong diurnal variation in the injected flux may shift the region of maximum precipitation itself further to the west of minimum B. For example, if the extreme case is considered in which the injection of fresh electrons is restricted to that half of the globe lying opposite to Sanae - Halley Bay, it would be expected that most of the flux would be lost before minimum B is reached. Thus if a strong diurnal variation of this nature does exist, Halley Bay would experience greater precipitation than Sanae. According to M.R.Torr's model, the entire electron flux is wiped out by the time minimum B is reached. Since precipitation increases very rapidly from about 40°W, in the absence of replenishment, large quantities of flux would be wiped out to the west of minimum B. This would make the heating predominant to the west. What is left of the flux would then be lost within the last few degrees of longitude before minimum B. This would probably only be sufficient to enhance existing ionization. The point is that the change over from heating to enhanced ionization would be extremely sharp. The above is entirely consistent with the valley at Halley Bay and the sharp rise to a maximum at Sanae at 0800 hours.

At 1000 hours f_cF_2 decreases at both Halley Bay and Sanae and means that the p.e.f. is increasing again. It does not seem correct that the valley should start as far to the west as CRPL data indicate. A minimum at Halley Bay (27°W) with a sharper rise to the west would be more

56/.....

consistant with the CHF theory, It seems probable that in calculating these data CRPL must have interpolated across L space, which could be misleading because at lower L the minimum would occur further to the west. Once reliable ionospheric observations are available for locations along constant L, these problems will be much easier to solve.

The diurnal variation of MUF(0) was determined at locations lying 30° apart on L=4 by reading off the values at the times given in Figure 20. The results are shown in Figure 22. The morning maxima at Sanae and Halley Bay are clearly observable. At 60°W and 90°W the maxima occur at midnight, while at 120°W there are two peaks, one at 1000 and the other at 2000 hours. Further west the behaviour becomes the normal diurnal type. This happens because to the east of the Anomaly the movement of the peak in MUF(0) is roughly in phase with the diurnal variation. At midnight the peak lies close to the Anomaly and the eastern stations remain unaffected. With the approach of midday, the peak moves over to the eastern side to enhance normal ionization, working in phase with the sun.

This theory does not offer an explanation of similar phenomena at the South Pole. It is likely that the time of occurrence of maxima in f_0F_2 is directly related to diurnal variations in charged particle flux, being quite independent of the buildup caused by the radiation belts.

Figures 23 and 24 are similar plots of the longitudinal and

57/.....

FIGURE 22.

Summer diurnal variation of MUF(0) along L = 4 in the southern hemisphere.

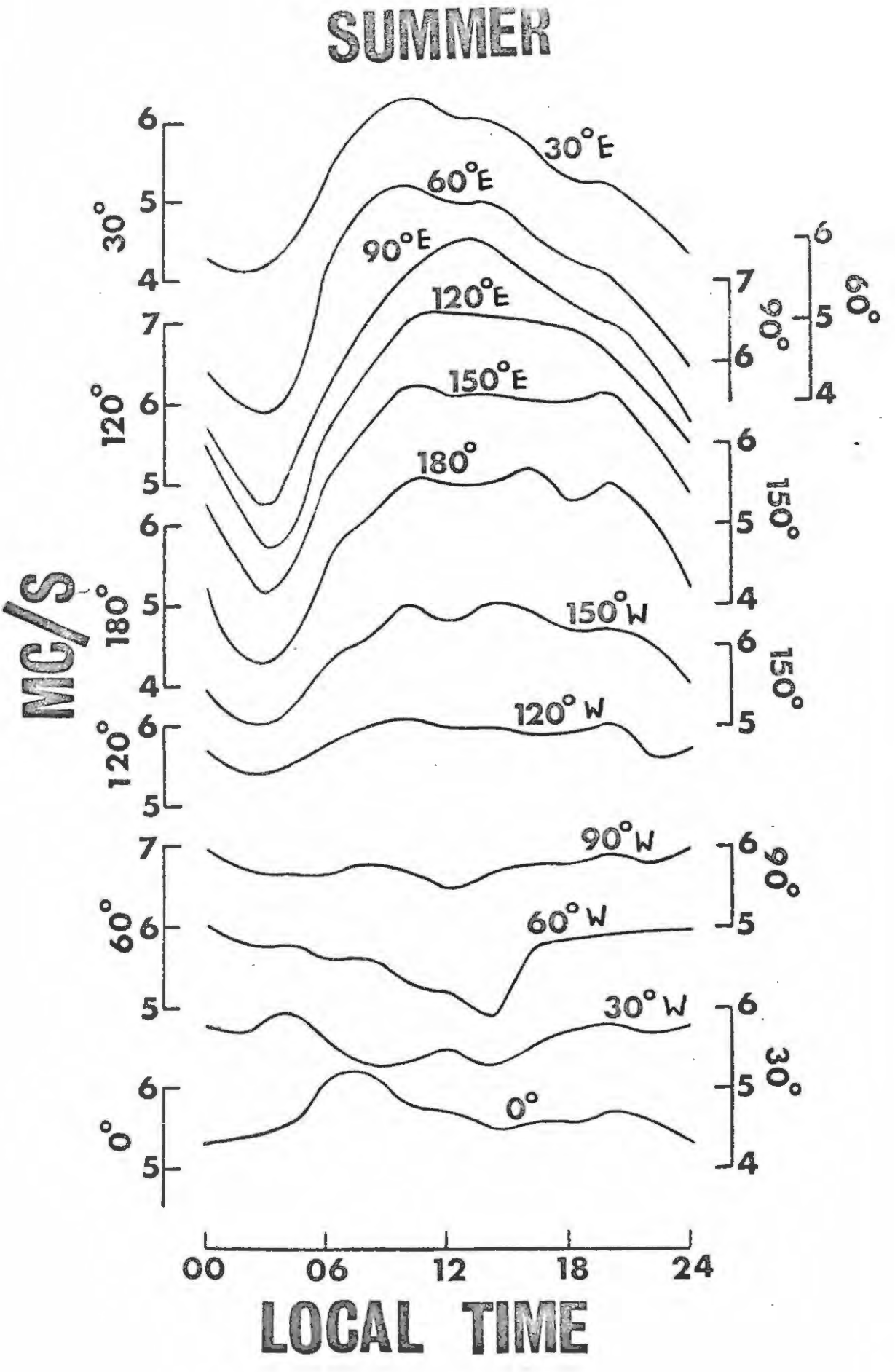
SUMMER
30°E
60°E
90°E
120°E
150°E
180°
150°W
120°W
90°W
60°W
30°W
0°
MC/S
LOCAL TIME
00
06
12
18
24

FIGURE 23.

Longitudinal variation of MUF(0) along L = 2 in summer in the southern hemisphere.

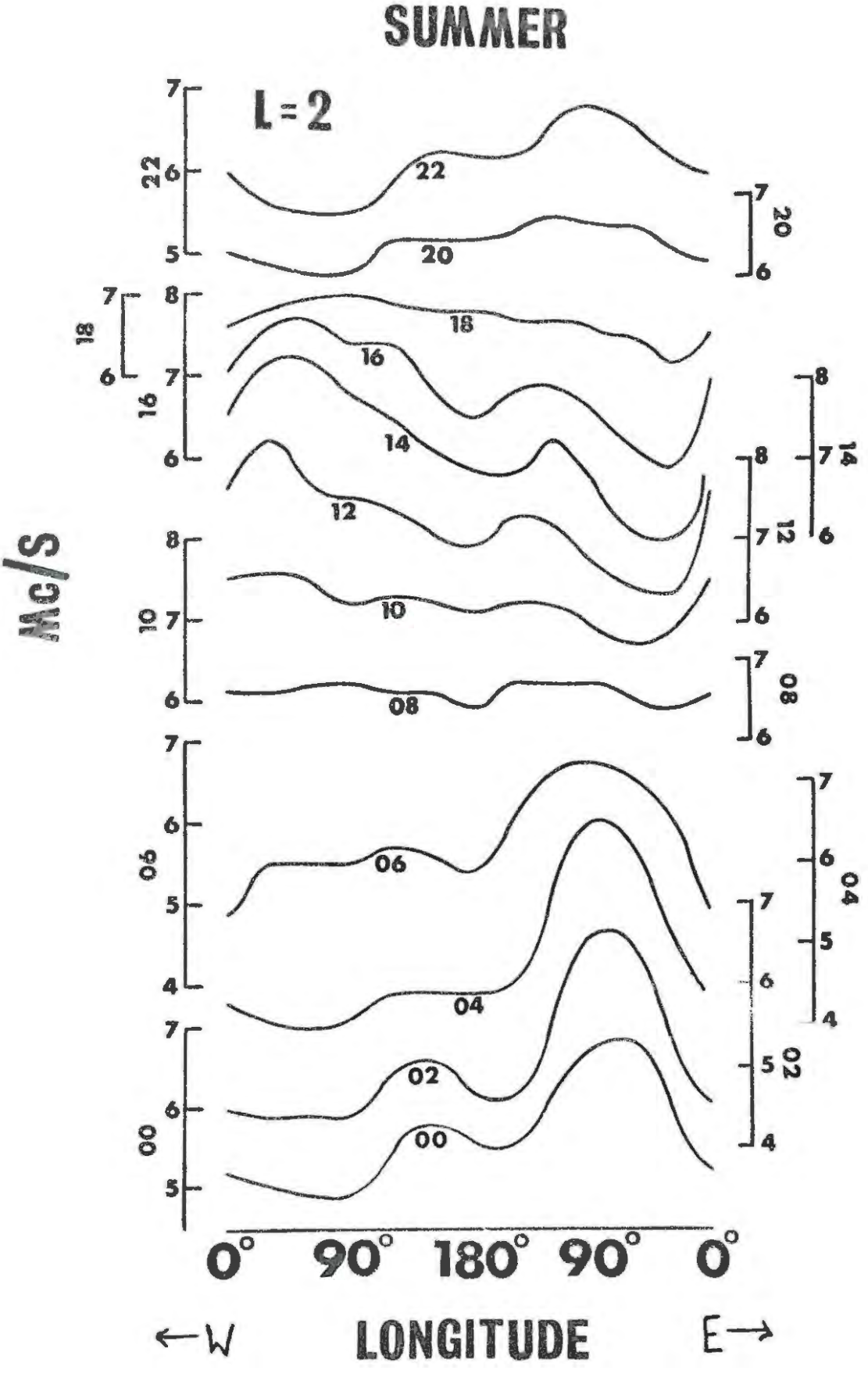
SUMMER
L = 2
22
20
18
16
14
12
10
08
06
04
02
00
Mc/S
0°
90°
180°
90°
0°
←W
LONGITUDE
E→

FIGURE 24.

Summer diurnal variation of MUF(0) along L = 2 in the southern hemisphere.

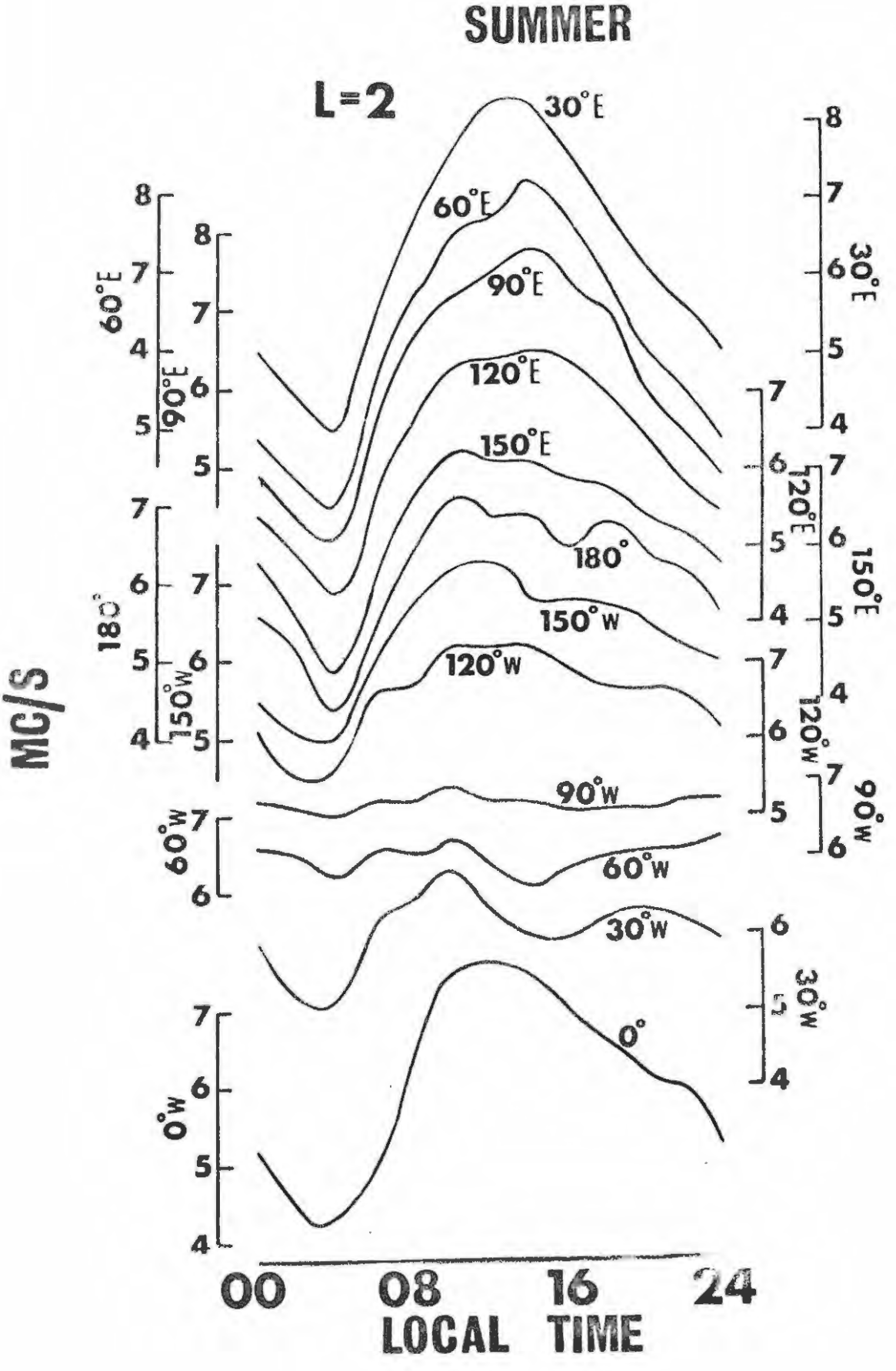
SUMMER
L=2
30°E
60°E
90°E
120°E
150°E
180°
150°W
120°W
90°W
60°W
30°W
0°
MC/S
00
08
16
24
LOCAL TIME

diurnal variations of MUF(0) at L = 2 for summer. These will not be discussed in detail, as the general features are so similar to the L = 4 case, indicating that the same explanation will apply there. In particular, the diurnal behaviour at Port Lockroy and Deception Island can now be understood.

It is most remarkable that the South African stations, Johannesburg (28°E), Grahamstown (26°E) and even Cape Town (18°E) to a certain degree, lie in the region where corpuscular effects work in phase with diurnal variations, (the behaviour at about L = 1.5 is similar to that at L = 2) whereas at a mere 45° to 60° further west, the behaviour is entirely different.

The next question is why is this phenomenon not observed in winter. The answer to this is that there are no ionosphere stations at locations where unusual behaviour of this type occurs during winter. Referring to Figures 21 and 20, it can be seen that the peak at 0000 hours lies at 60°W in summer, in comparison to 120°W in winter. In this case the peak is too far west to affect Sanae and Halley Bay. From the shift of the peaks in Figure 21, the region around 120°W would be expected to show the most unusual behaviour. At 120°E where the peak is directly in phase with the sun at midday, f_0F_2 reaches its highest value on the L = 4 shell.

Figure 25 represents the longitudinal variation of MUF(0) in winter for L = 2, and Figures 26 and 27, the winter diurnal variations for both L = 2 and 4 respectively. The latter two diagrams illustrate the conclusions drawn above.

58/.....

FIGURE 25.

Winter longitudinal variation of MUF(0) along L = 2 in the southern hemisphere.

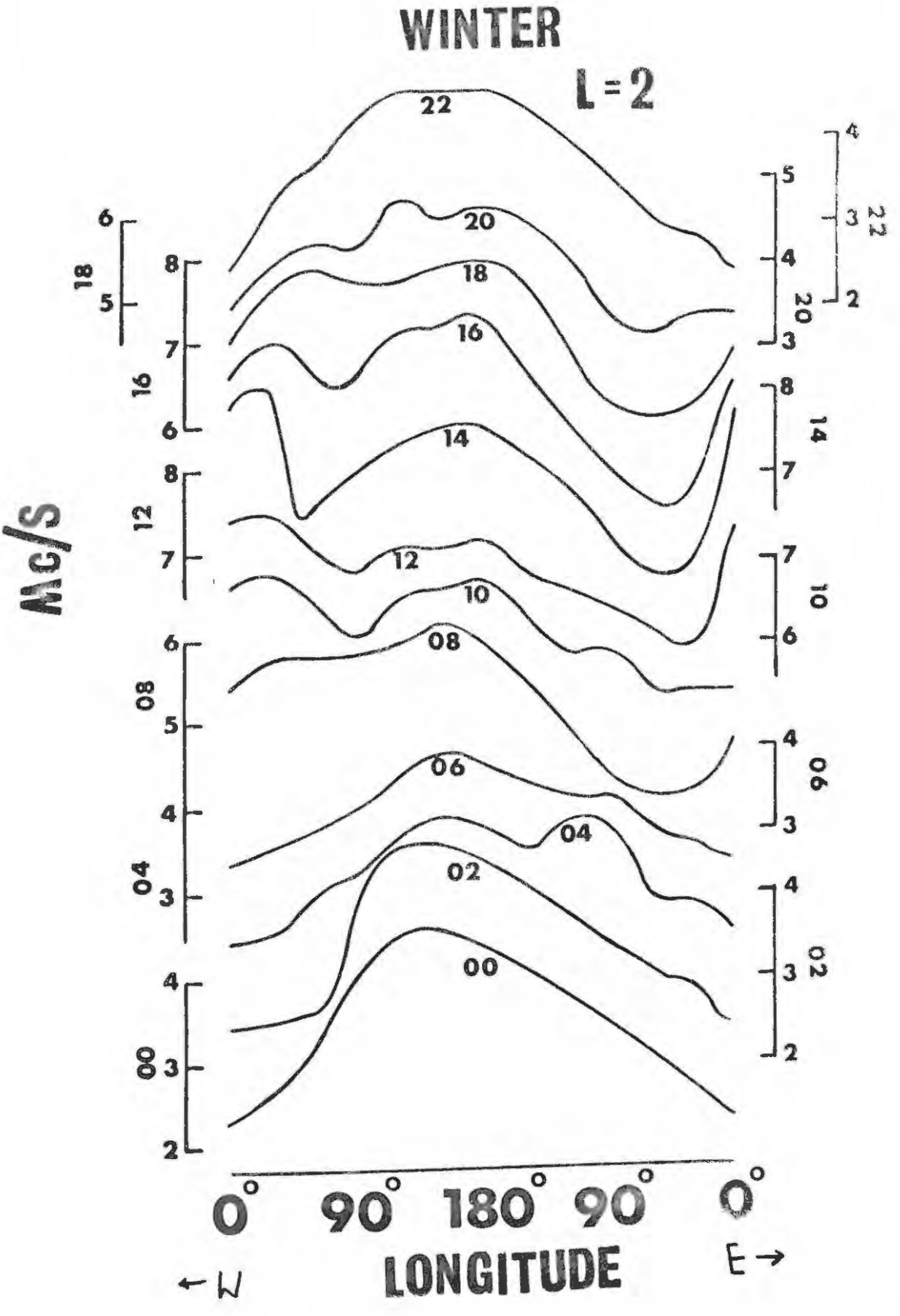
WINTER
L = 2
22
20
18
16
14
12
10
08
06
04
02
00
Mc/S
0° 90° 180° 90° 0°
← W
LONGITUDE
E →

FIGURE 26.

Winter diurnal variation of MUF(0) along L = 2 in the southern hemisphere.

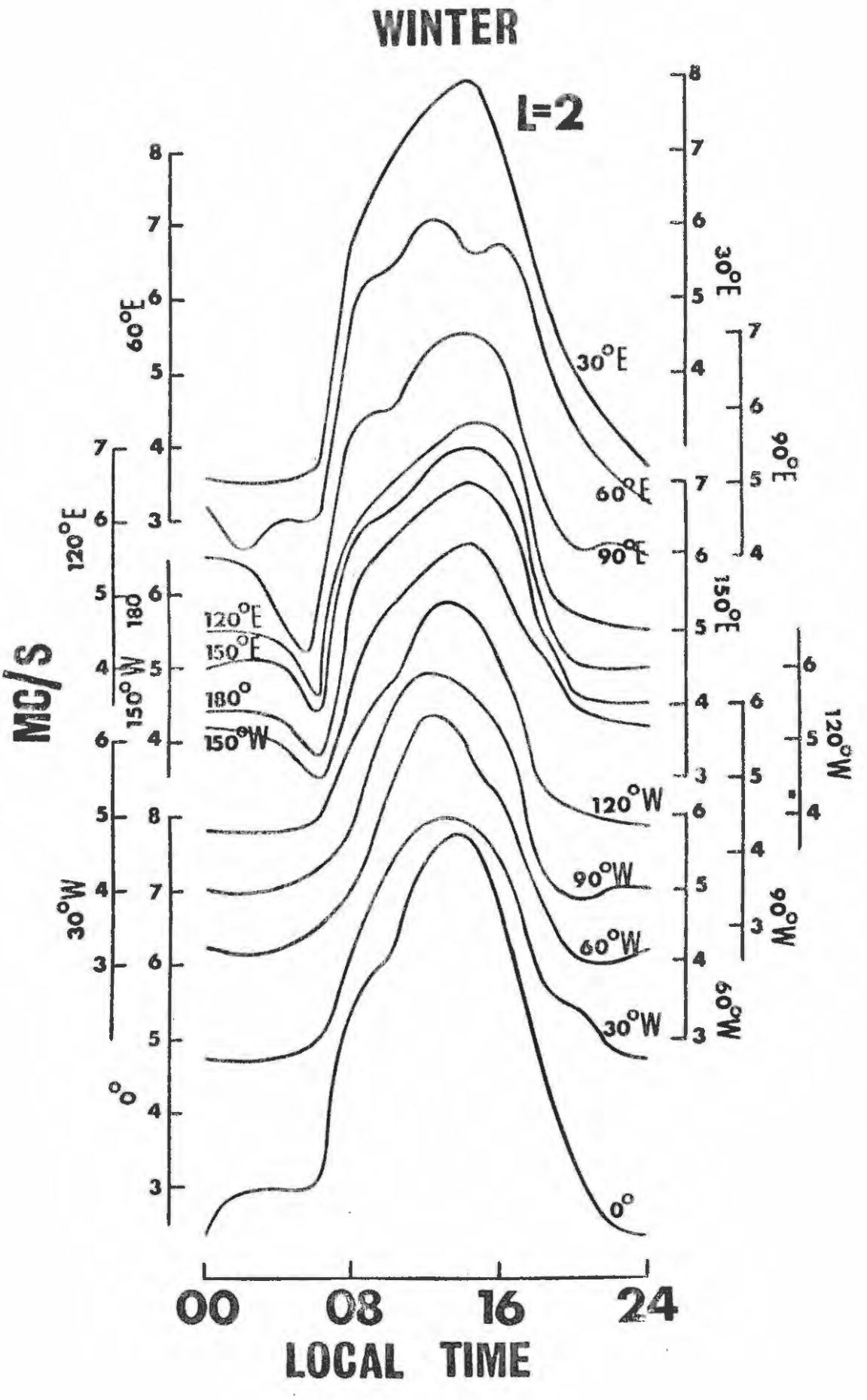
WINTER
L=2
MC/S
30°E
60°E
90°E
120°E
150°E
180°
150°W
120°W
90°W
60°W
30°W
0°
00
08
16
24
LOCAL TIME

FIGURE 27.

Winter diurnal variation of MUF(0) along L = 4 in the southern hemisphere.

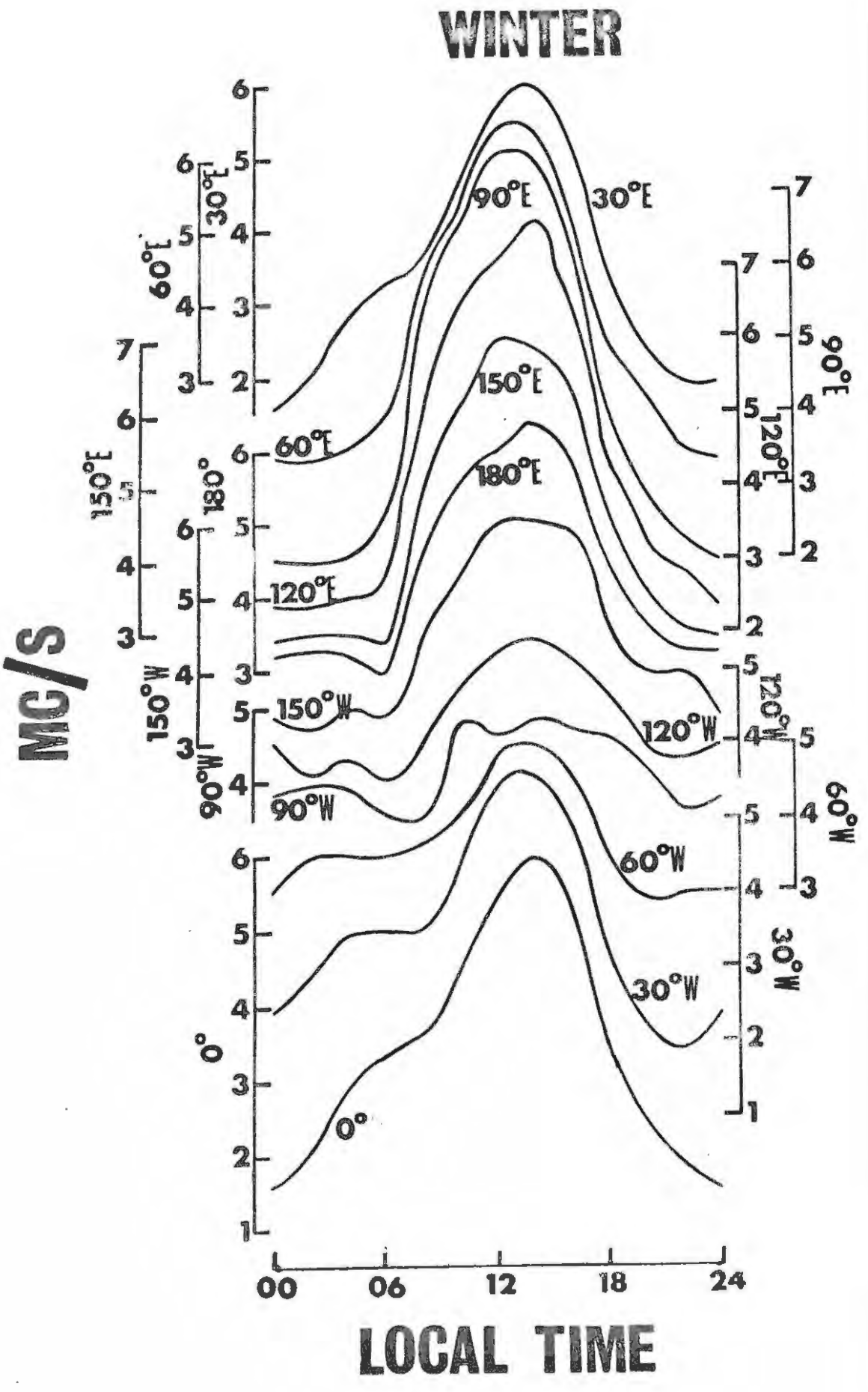
WINTER
MC/S
LOCAL TIME
00
06
12
18
24
0°
30°E
60°E
90°E
120°E
150°E
180°
150°W
120°W
90°W
60°W
30°W
0°

It therefore seems that the rapid change over from typical winter to typical summer behaviour at the equinoxes (Baker and Gledhill, 1964) is directly related to seasonal changes in both the dynamics of particles in the radiation belt and atmospheric properties.

The morning maximum in f_0F_2 at Antarctic stations near the Weddell Sea is a pronounced example of an effect that occurs to a lesser degree in other regions as well. According to present ionization theories, (Rishbeth and Garriott, 1964) the maxima in f_0F_2 should occur at a time $\frac{1}{\beta}$ later than noon, where β is the attachment coefficient. However, the times at which these maxima actually do occur show little systematic behaviour, varying from before to after noon. Variations of this nature have been reviewed by Wright(1962). The typical F_2 behaviour is illustrated in Figures 22, 24, 26 and 27. These effects can be explained using the arguments of this section and there can be little doubt at this stage that they are due to the bombardment of the upper atmosphere by electrons.

4.4 The F Region Winter Anomaly.

At most localities the F_2 ion density around midday is greatest in winter and least in summer, contrary to what would be expected from simple Chapman theory.

It has been hypothesized that the lower ion density in summer is due to accumulated heating and expansion of the F_2 layer, which

59/.....

causes the ions to be dispersed over greater height. Workers have estimated that the increased summer radiation, which is assumed to produce the higher temperatures, is insufficient to heat the atmosphere to this extent (Rishbeth, 1964)and remain puzzled as to why this increased radiation does not produce the expected higher ionization. Until 1963 there had been little basis for deciding whether the winter densities are anomalously high or whether the summer densities are anomalously low. Wright (1963) showed that the electron content (per cm^2 column) below the peak of the F_2 layer was larger in winter than in summer. He found that the electron content was practically independent of latitude in winter at zero solar zenith angle, whereas there was a noticeable decrease with latitude in summer. From this he concluded that summer was the anomalous season.

His explanation of this phenomenon involved an increase in the loss rate due to a seasonal change in atmospheric composition. He maintained that this could be achieved by an increase in the ratio of molecular nitrogen (N_2) to atomic oxygen (O). This would mean that

(1) more radiation would be absorbed from the incident flux without contributing to the electron content (see Part II)

(2) the partial loss rate depending on the reaction $O^+ + N_2 \rightarrow NO^+ + N$ would increase.

Although it is quite reasonable to suppose that Wright's theory is correct, it is possible that this is a secondary effect and that the

60/.....

primary cause of the anomalous behaviour is an enhancement of winter ionization and a redistribution of summer ionization due to electron bombardment of the atmosphere. In other words the winter values are anomalously high and the summer ones anomalously low. Some of the summer ionization would naturally be carried above the peak of the F_2 layer. This aspect will be examined in Part II.

Because the combined effects of corpuscular and solar radiation on the atmosphere are not understood at this stage, it is not possible to prove the above conclusively. A plausible theory can however, be developed to explain this phenomenon on the basis of the previous observations and deductions. Since the winter anomaly is easier to explain for the northern hemisphere, this will be discussed first.

4.4.1 The Northern Hemisphere.

Let us consider the case where the injection of fresh electrons into the radiation belts is independent of season. Seasonal and diurnal changes in the atmospheric properties would introduce corresponding variations in the trapped and precipitated flux which would be more pronounced over the anomaly. It is logical to expect a small increase in p.e.f. in the northern hemisphere in summer, because of increased atmospheric expansion (see Part II). Since the extent of precipitation over the anomaly is dependent on the buildup of trapped flux on passage through the northern hemisphere, the accumulated loss of flux in this

61/.....

hemisphere should produce a decrease in precipitation in the southern hemisphere in winter. The reverse effect would not be as pronounced for the northern hemisphere, as precipitation is practically independent of the buildup in trapped flux there.

Similarly, diurnal variations in p.e.f. should be expected over the anomaly (which is in agreement with Armstrong's observations, (1965)). This suggests that M.R.Torr's model could be improved by introducing a diurnal variation in the criterion defining trapped and precipitated flux.

It has been verified by an analysis of Alouette data that there is a small seasonal variation in p.e.f. in the northern hemisphere which makes precipitation greater in summer than in winter. The northern hemisphere values of p.e.f. for L=2 and 4 shown in Figure 14 lie very close to the winter midnight CHF (1.3×10^4 electrons/cm^2/sec.). Since Injun 3 observations were made during April to July, 1963, they represent northern hemisphere summer conditions. (The way in which these values were calculated is described in Appendix 3.)From Armstrong's observations, the overall midnight medians on the shells L=4 and 2 are 9.9×10^3 and 1.2×10^4 electrons/cm^2/sec. respectively, as compared with 5.6×10^4 and 1.4×10^4 respectively for midday. At midnight in summer the values lie below the winter CHF and the F region ionization should be enhanced. At midday the atmosphere is hotter, the CHF lower, and the flux is higher than the midnight CHF, indicating that heating

62/.....

should be the predominant effect. In winter not only is the flux lower, but the atmosphere is cooler and the CHF higher than in summer for both night and day. At night therefore, the p.e.f. will lie much further below the CHF, and the winter MUF(0) values should be much lower than the summer values. During the day the p.e.f. in winter should be close to the CHF and should enhance the day-time ionization, whereas in summer the midday p.e.f. is well above the CHF and redistribution of ionization should be predominant. It is also quite likely that the midday heating will bring about the change in atmospheric composition suggested by Wright (1963).

Figure 28 shows the northern hemisphere variation of MUF(0) at midday and midnight for both winter and summer for the shell L = 2, where the diurnal variation is even less pronounced than on L = 4. The curves show that at midnight the summer values are higher than the winter ones, whereas at midday the reverse occurs. It is interesting to note that in summer at midnight, there is a distinct increase in ionization at about 150°E which corresponds well with the maximum in p.e.f. in Figure 14. At midday on the other hand, there is a marked decrease over the same region which strongly supports the above theory. It is puzzling however, that in winter the maximum occurs at about 300°E and the increase in p.e.f. at 150°E to 180°E appears to have no effect at all.

63/.....

FIGURE 28.

Winter Anomaly: Northern Hemisphere longitudinal variation of MUF(0) for L = 2 at midnight and midday in summer and winter.

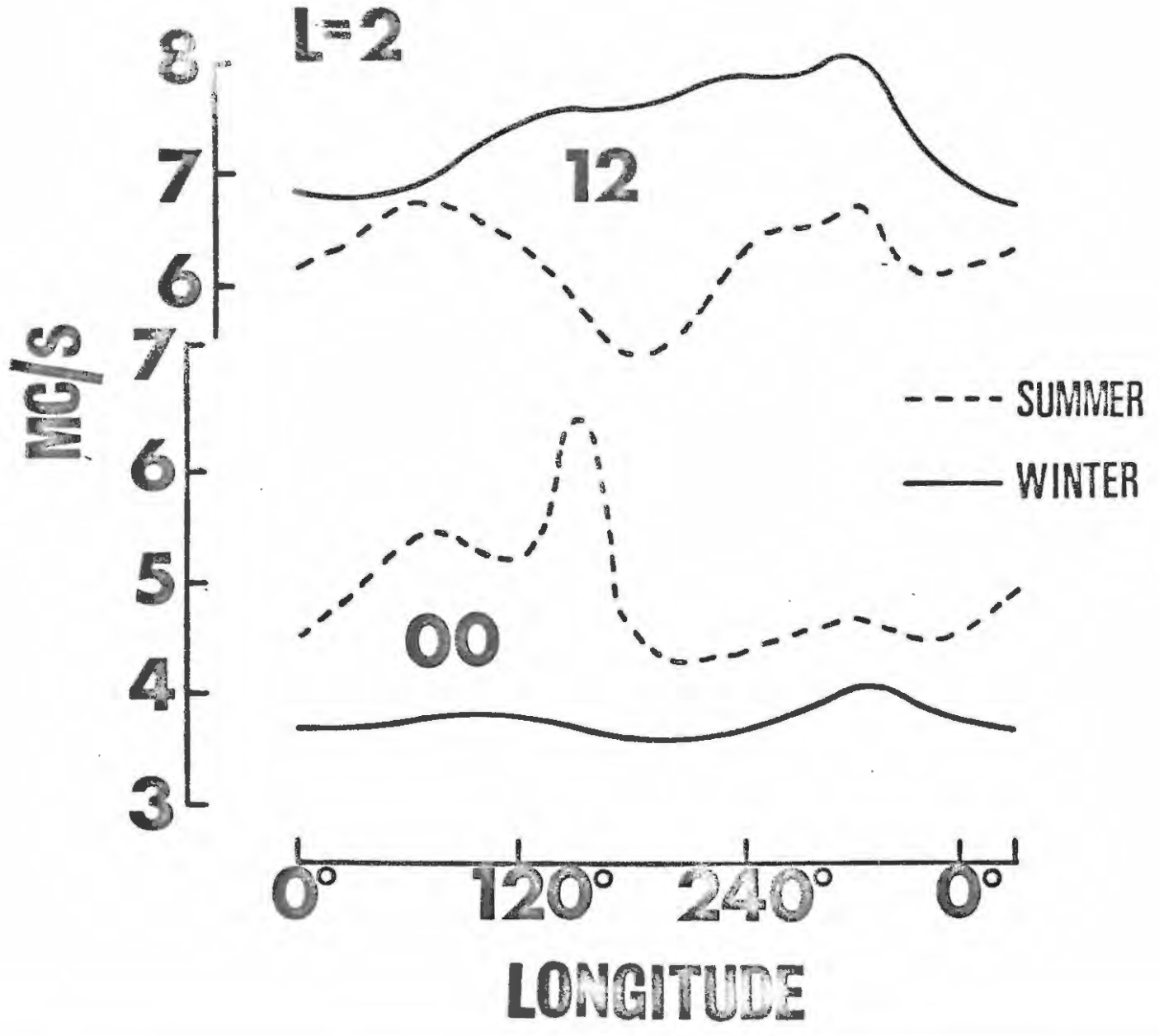
L=2
8
7
6
7
6
5
4
3
MC/S
12
00
SUMMER
WINTER
0°
120°
240°
0°
LONGITUDE

4.4.2 The Southern Hemisphere.

Figure 29 shows the longitudinal variation of MUF(0) in the southern hemisphere for both winter and summer. In this case the winter anomaly is very much less pronounced than in the case of the northern hemisphere. The reason for this is that the heating effect persists over a large range of longitude there, even in winter, due to the Southern Radiation Anomaly. In summer at midday the p.e.f. lies well above the midnight winter value of the CHF (1.3×10^4 electrons/cm^2/sec.) at all longitudes. For example the values shown in Figure 14 must be increased by the factor $5.5 \times 10^4 / 1.4 \times 10^4$ (see Section 4.3) to obtain midday values of p.e.f. The lowest value of p.e.f. on the L=4 shell at 150°E at midday, is 4.3×10^4 electrons/cm^2/sec. It therefore seems certain that the peaks in MUF(0) during the day in summer do not represent an increase in ionization due to electron influx, but rather a decrease in the redistribution of ionization where the p.e.f. is lowest.

The fact that both the winter and summer peaks lie at approximately the same longitude, indicates that even in winter , at midday, the p.e.f. does not go below the CHF anywhere on L=4. If, for example, the p.e.f. decreased by a factor of 3 from summer to winter, the lowest value of flux at 150°E would be approximately equal to the winter midnight value of the CHF. This should place both the winter and summer peaks in MUF(0) at the longitude of the lowest value of p.e.f. on L=4, viz.

64/.....

FIGURE 29.

Winter Anomaly: longitudinal variation of MUF(0) on L = 4 during winter and summer, for 1000, 1200, 1400 and 1600 hours.

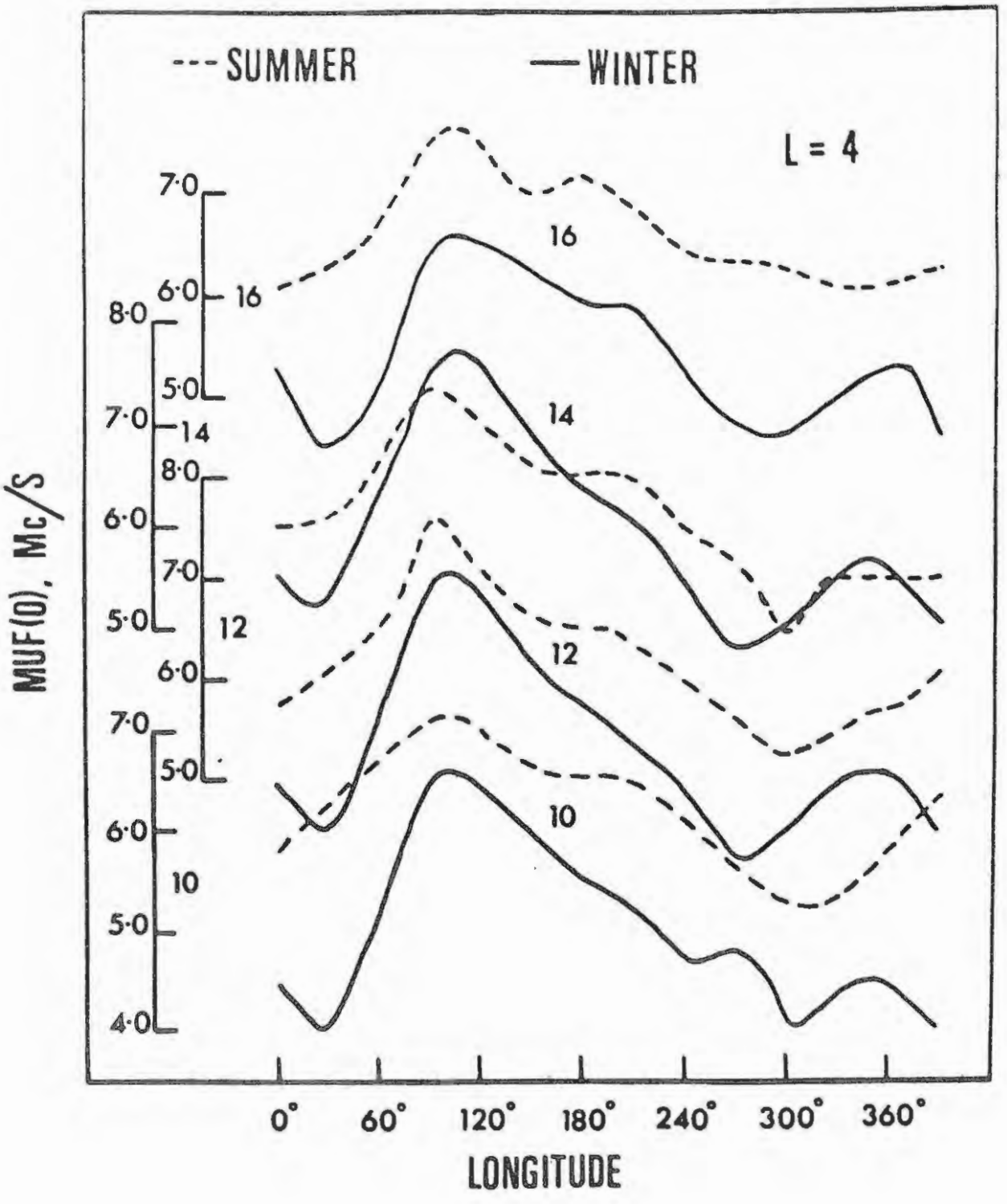
---SUMMER
—WINTER
L = 4
MUF(0), Mc/S
7·0
6·0
16
8·0
5·0
7·0
14
8·0
6·0
7·0
5·0
12
6·0
7·0
6·0
5·0
10
5·0
4·0
16
14
12
10
0°
60°
120°
180°
240°
300°
360°
LONGITUDE

between about 100°E and 220°E.

The actual peaks shown in Figure 29, however, lie between 90°E and 100°E. The only stations lying in the region in question are Kerguelen (70.27°E, L = 4.8) and Campbell Island (169.15°E, L = 4.0). The values of MUF(0) shown for these stations in Figure 29 for December, 1963 are 6.7 Mc/s and 6.5 Mc/s respectively. The actual median value of $f_0F_2 + f_H/2$ at Campbell Island was 6.2 Mc/s. Since there were no data available for Kerguelen in 1963, the values for December, 1959 were compared for the two stations to estimate the relative variation. In this case the median values of f_xF_2 at each of these station were 7.2 Mc/s and 7.0 Mc/S respectively.

There is, therefore, no experimental evidence for the sharp peaks shown in Figure 29 at 90°E to 100°E. Neither is there any experimental evidence to show that MUF(0) decreases before 200°E. In fact the actual values of f_xF_2 at Kerguelen and Campbell Island are more consistent with a broad peak from 70°E to at least 170°E.

Whether the winter values of MUF(0) are greater than the summer ones would depend on the extent to which the p.e.f. enhanced or redistributed the ionization in the southern hemisphere. A quantitative analysis of these phenomena has already been started and very much better estimates of the combined effects of p.e.f. and solar radiation will be available shortly.

65/.....

4.5 Discussion.

Since this study of the effects of corpuscular bombardment of the atmosphere over the Southern Radiation Anomaly began, several publications have appeared which support the conclusions drawn here. The theoretically deduced buildup and loss of electrons (M.R.Torr, 1965) on which many of the results depend, has been strongly supported by satellite measurements (Williams and Kohl, 1965). Sharp et al. (1965) presented results, obtained from satellites, of trapped and precipitated electron intensities and of the concentration of positive ions in the F region of the ionosphere. The results showed beyond doubt that electron bombardment makes a contribution to the ionization of the F region over the South Atlantic, both by day and night. This contribution is thought to be comparable in magnitude with that of X - rays and ultra - violet light from the sun. These results confirm our observations and lead one to believe that the missing factor in the theory of the ionosphere has been found.

The concept of the necessity of a corpuscular source of energy to explain unusual F region behaviour is not new. Several workers have suggested that such a mechanism could play an important part in governing the behaviour of the ionosphere. In particular, Bellchambers and Piggott (1960), Baker and Gledhill (1964) and Coroniti and Penndorf (1959) suggested that corpuscular bombardment of the atmosphere may be responsible for the unusual summer behaviour at Antarctic stations

66/.....

near the Weddell Sea.

Very convincing evidence supporting the results presented in the last two chapters are the deductions of Harris and Priester (1962a). They found that the absorption of solar extreme ultra - violet (EUV) could not explain the observed diurnal variation of atmospheric density and temperature, since it yielded a maximum of these properties at about 1700 hours local time instead of 1400 hours where it is observed. If the EUV is adjusted to give the observed average temperatures, the diurnal variation in density is too large compared with the observed amplitude. Also, comparison of the required EUV flux with the measurements made by Hinteregger (1962), showed that an extremely high efficiency of conversion of EUV to heat was required. Harris and Priester therefore concluded that it was necessary to have another source of heating which has a maximum at 0900 hours local time at a flux of 1 erg/cm^2/sec., and postulated the existence of a corpuscular source of energy.

All these observations and deductions are consistent. It is to be expected that the corpuscular energy source predicted by Harris and Priester should produce readily observable geophysical effects, which would vary with the corresponding diurnal and seasonal variations in flux.

In this thesis only the bare features indicating the link between particle influx and unsolved F region phenomena have been outlined. Very strong evidence has been presented, suggesting that the answer to

67/.....

the unusual summer behaviour of the F region in the South Atlantic has been found. This in turn led to the understanding of several F region peculiarities. In particular, a possible explanation of the well known ionosphere winter anomaly has been put forward. If the suggested longitudinal variations of f_oF_2 are confirmed, much improved charts for radio forecasting can be envisaged.

Requirements for future research involve extensive data on the diurnal, seasonal and solar cyclic variations of both the energy sources. It is possible that the diurnal variation of the corpuscular heat source may change in shape and position during the course of the solar cycle.

From the theoretical point of view, the most immediate requirement is the inclusion of the corpuscular source of energy in the theory of layer formation. As a first step in this field, I intend to investigate the effect of temperature changes on the behaviour of the ionosphere. This is dealt with in Part II. However, since no account has yet been given of the morphology of the disturbances we have studied, the first chapter in Part II is devoted to this important topic.

-oooOooo-

PART TWO

THE EFFECT OF TEMPERATURE CHANGES ON F-REGION ELECTRON DENSITY DISTRIBUTION OF THE IONOSPHERE

CHAPTER 5.

IONOSPHERIC DISTURBANCES.

5.1 Introduction.

In the early stages of the research, it was thought that the ionospheric disturbances dealt with in previous chapters were similar to the Sudden Ionospheric Disturbances or SID's, (Gledhill and Torr, 1965). In dealing with this newly discovered phenomenon, certain confusion arose in likening these events to known occurrences. For convenience, the type of disturbances studied here will be called 'Magneto - Ionospheric Disturbances' or MID's.

Ionospheric disturbances have been divided into two main classes:

(i) disturbances that take place in the lower ionosphere

(ii) F-region storms.

The main effect of (i) is enhancement of ionization, observable on ionograms as an increase in f_{min}. The effect of (ii) may be summarized as follows; at high latitudes there is a marked decrease in f_0F_2, while at low latitudes, an increase in electron density is very common and a decrease rather rare, occurring only during a severe storm. MID's would therefore fall into both these categories.

For purposes of clarification, some of the properties of MID's will be outlined and then the existing knowledge of i.d.'s and their causes will be briefly reviewed for comparison.

69/.....

5.2 Magneto - Ionospheric Disturbances.

A detailed study of latitudinal, longitudinal, seasonal and diurnal variations will be carried out in future research. Most of the available information has been obtained from the statistical analyses of the randomly chosen two hour periods used to estimate the frequency of occurrence of i.d.'s.

In the case of Sanae, the 28 12 hour plots centered on the times of a high electron influx were examined. A typical MID at Sanae involved an increase of about 2 Mc/s in f_{min} with corresponding deviations of about 100 km and 1.5 Mc/s from the respective medians of $h'F_2$ and f_oF_2. The most striking feature of a typical Sanae MID is intense enhancement of D region ionization. In 25 of the 28 cases examined, a blackout was observed to have occurred sometime during the 12 hour period. High values of f_{min} were observed in the remaining three. $h'F_2$ was disturbed in 20 cases and f_oF_2 in 17. In no case was there a disturbance in f_oF_2 without an accompanying one in $h'F_2$. The average duration of a MID is about 9 hours, although in one case the only variation observed was a single $\frac{1}{4}$ hourly record of a blackout. The vast majority of disturbances involved decreases in f_oF_2 and increases in $h'F_2$. With the exception of the 4 total blackouts, only 11 of the remaining 24 events were accompanied by local geomagnetic activity. The extent to which MID's are accompanied by related geophysical phenomena will be ascertained in future research.

70/.....

In order to obtain a rough idea of latitudinal effects, average features of MID's at Sanae were compared with those at Cape Town.

46 randomly chosen two-hour periods, which satisfied the disturbance criterion, were examined for Cape Town. In this case f_oF_2 was the most disturbed as opposed to f_{min} at Sanae. A typical disturbance involved about 0.4 Mc/s increase in f_{min} and/or deviations of about 1.3 Mc/s and 50 km from the respective medians of f_oF_2 and $h'F_2$. Unlike Sanae, simultaneous changes in the 3 parameters occurred very much less frequently. f_{min} was disturbed on 23 occasions and 16 of these were accompanied by disturbances in the F region. f_oF_2 and $h'F_2$ were disturbed in 28 and 21 cases respectively, of which only 10 occurred simultaneously. The most common variation in f_oF_2 was an increase which occurred in 16 of the 28 occasions. An increase was also most common in $h'F_2$, a decrease being observed in only 4 cases.

A fairly high correlation of MID's at Cape Town with geomagnetic activity can be expected, since the geomagnetic observatory at Hermanus (70 miles east of Cape Town) is well known for the unusually large number of magnetic bays observed there. This correlation will be performed in the near future.

MID's at Sanae are a very much more severe type of disturbance than those at Cape Town and the variations are more consistent.

Well outside the anomaly, there is very little difference in MID's at high and low latitudes. f_{min} is very much less affected and both

71/.....

f_oF_2 and $h'F_2$ usually increase. Out of 28 disturbed 2-hour periods at Dourbes, for example, f_{min} was affected on only 2 occasions. No decreases in $h'F_2$ were observed. Typical deviations of f_oF_2 and $h'F_2$ from the medians were of the order of 0.5 Mc/s and 35 km.

MID's were found to occur equally often both during the night and day. Geographically they occur at all sites lying below the outer radiation belt (and probably the inner one as well). Their effect on the ionosphere is readily observable in the monthly medians of f_oF_2 at all stations within this region. They therefore form part of the regular behaviour of the ionosphere and appear to be responsible for the unusual characteristics of the F_2 region.

The main characteristics of MID's are summerised in Table 15.

The question naturally arises whether the E-layer is also affected. Values of f_oE for Sanae were examined at the times of the 28 events listed in Chapter 1. It was found that on every occasion on which f_oE might have been observed, f_{min} lay above the expected frequency range of f_oE. Generally, f_oE was a very difficult parameter to read. Measurements were greatly influenced or made impossible by either deviative or non-deviative absorption. For this reason no detailed analysis of f_oE was attempted, although indications are that it must be affected by the disturbances. The height of the E-layer (when observable), however, does not show any unusual variations.

At Cape Town f_oE is readily observable and can be easily measured. A cursory inspection of ionosphere data for Cape Town showed a higher frequency of occurrence of stratifications, intermediate layers and night E during periods satisfying the D and F disturbance criterion. f_oF_1 at Sanae, on the other hand, appears to behave normally, even during the D and F region disturbances. These are aspects which will have to be investigated in future research as they may provide important information on the energy of the incoming particles.

72/.....

TABLE 15.

PHENOMENON	SID	PCA	AURORAL	MID
GEOMAGNETIC ACTIVITY	Independent of	Independent of	Nearly always accompanied by	Accompanied by for about 50% of the time
DURATION	From minutes to several hours	Days	Minutes to days	Minutes to several hours
DIURNAL VARIATIONS	Occurs only on the day-light side of the earth	Marked	Yes	According to this analysis - yes; according to past analyses - no
ASSOCIATED WITH SOLAR FLARES	Directly	Directly	Indirectly	Indirectly
GEOGRAPHICAL DISTRIBUTION	Global on daylight side	Polar cap regions	Auroral zone	At sites lying below the radiation belts
CAUSE	1 - 10 Å X-rays	Sub relativistic protons	'Fresh' high energy electrons	Electrons precipitated from the radiation belts
D REGION OR F REGION DISTURBANCE	D region	D region	Both, but mainly D region	Both

5.3 Lower Ionosphere Disturbances.

These have been divided into two types;

(i) the SID (ii) polar blackouts.

The discovery of a new type of polar blackout during the IGY (Bailey, 1957; 1959; Shapley and Knecht, 1958), led to the separation of (ii) into a further two classes, viz. auroral zone blackouts and polar cap absorption (PCA), (Obayashi, 1959; Reid and Collins, 1959).

5.3.1 The Sudden Ionospheric Disturbance.

The basic characteristic of a SID (discovered in 1930 by Mögel and rediscovered in 1935 by Dellinger) were described clearly for the first time by Dellinger in 1937. These involve the practically simultaneous beginning (within 1 to 3 minutes) of a geomagnetic crotchet, change in earth current potential and ionospheric fadeout. These last from a few minutes to several hours, with the occurrences of greater intensity producing effects of longer duration (Dellinger, 1937). SID's usually occur on a global scale on the daylight side. They are always associated with solar flares, although on most occasions the reverse does not hold (see, for example, Dodson et al, 1956).

All ionospheric effects were explainable by enhanced ionization in the D region. Numerous papers appeared at this time describing various ways of observing the enhanced ionization in the lower ionosphere and extensive surveys of the subject have been made by Warwick (1963) and Friedman (1963).

A distinct feature of the SID is that it is seldom accompanied by any appreciable effect in the F region. However, on a few occasions, marked increases in the electron density of the F_2 layer have been reported in the literature (Dieminger, 1950; Shapley and Knecht, 1959; Knecht and McDuffie, 1962). The solar flares in these cases were distinguished from others in that they were known to be associated with intense cosmic ray increases at sea level.

73/.....

As effects such as occurrence only on daylight side were inconsistent with theories of corpuscular ionization, it was generally believed that an excess of UV radiation (Lyman α) increased the ionization of the D region. However the real cause has since been found to be X - rays in the 1 - 10 Å range (Tousey et al, 1951; Byram et al, 1956; Friedman et al , 1958; Chubb et al, 1960 a, b). X -ray fluxes above a certain level were observed only in the presence of solar activity and above a certain higher level, only when ionospheric effects were observed.

5.3.2 Polar Blackouts: Polar Cap Absorption and Auroral Zone Blackouts.

The PCA is apparently associated neither with geomagnetic disturbances nor aurorae, but occurs after a large solar flare. This type of disturbance is clearly distinguishable from that of the SID, since it covers only the polar cap region and often continues for several days. It reveals a strong diurnal variation, being more intense during the day than during the night.

The general nature of the PCA event has been firmly established in the past few years (Hill, 1960; Chapman, 1960; Leinbach and Reid, 1960; Collins et al, 1961; Jelly, 1962; Hakura and Goh, 1961). It is now accepted that the PCA is caused by enhanced ionization in the lower ionosphere, due to incoming cosmic ray protons. The event usually precedes a geomagnetic storm, which is in turn accompanied by auroral

74/.....

zone blackouts and F region disturbances (Meek, 1953).

In the pre-SC period, the PCA is confined within geomagnetic latitudes of about 60^{o}(precipitation of solar protons confined by the geomagnetic field, Obayashi, 1959; 1961; Rothwell, 1959). During the geomagnetic storm the blackout extends toward lower latitudes, being enhanced by auroral type absorption, and decays gradually after two or three days, independently of the geomagnetic activity.

Auroral Zone Blackouts are due to a temporary formation of a strong absorbing region in the lower ionosphere, near the auroral zone. The occurrence is correlated with aurorae and local geomagnetic disturbances. Ionospheric absorption is very variable in time and may last for periods of minutes or hours.

Of the i.d.'s discussed, MID's are most similar to the auroral type of disturbance. Both involve variations in the D and F regions. The particles responsible for auroral disturbances are thought to be energetic electrons of 20 to 100 kev. (Winckler, 1962; Brown et al, 1961; McIlwain, 1960). O'Brien (1964) refuted the idea that these were dumped from the radiation belts, advocating strongly that they were fresh electrons having their origin in the solar wind.

Hence it seems likely that MID's result from the drift of these particles in L space, whereas auroral disturbances are caused by the initial influx near the trapping boundary. Thus one would expect auroral i.d.'s to correlate more closely with geomagnetic activity, (Campbell and Leinbach, 1961).

75/.....

5.4 F - Region Disturbances.

The most striking of the F region disturbances are those associated with geomagnetic storms and are called 'ionospheric storms'.

Many important systematic average features of ionospheric storms have been obtained from statistical studies (Appleton and Piggott, 1952; Martyn, 1953; Obayashi, 1952, 1954; Matsushita, 1953, 1959; Sinno, 1953, 1954, 1955; Lewis and McIntosh, 1953; Nagata, 1954; Sato, 1956, 1957).

Variations in the N(h) profile during geomagnetic storms occur above 180 km and seldom below this level. The variation of the sub-peak total electron content behaves in a way similar to the peak electron density in the F_2 layer i.e. during a storm it decreases at middle latitudes and increases at low latitudes. In summer and at the equinoxes the decrease of electron density occurs at levels higher than 180 km. In winter an increase is predominant above 300 km and a slight decrease below this level. The peak height and semi- thickness of the F layer during a storm generally increases both in summer and in winter, although an occasional decrease may appear in winter.

Satellite information on the total electron content up to 1000km appears to show a variation similar to that of the peak electron content during a storm (Garriott, 1960; Yeh and Swenson, 1961). Carpenter (1962) presented evidence from a whistler analysis to show that the depression in whistler delays during geomagnetic storms may be interpreted as a

76/.....

substantial loss in electron density in the magnetosphere. If these observations are correct, it means that ionospheric storm changes at middle and high latitudes represent real removal of ionization at all levels above 200 km to greater heights beyond the ionosphere. At lower latitudes evidence is reported by Bowles (1962), from incoherent scatter radio soundings at Lima, Peru, that the electron density at all levels above 400 km shows an increase during a geomagnetic storm.

It is generally believed that no appreciable simultaneous effect in the F_2 region is associated with most solar flares. Recently Thomas and Venables (1966) have shown that at middle latitudes, major F region disturbances are associated with the main phase of the magnetic storm and not with the sudden commencement. The start and initial form of the i.d. at any station is governed by the local time onset of the main phase. When this occurs during the night, an immediate depression of f_oF_2 occurs. When it happens during the day there is either an increase or no change in f_oF_2, followed by a decrease during the evening.

It is possible that whatever mechanism is responsible for these variations may also influence the behaviour of MID's.

5.5 Theories of Ionospheric Disturbances.

5.5.1 The Lower Ionosphere.

In the case of lower ionosphere disturbances, theoretical computations of electron density profiles have been made on the basis of

77/.....

data of the solar proton spectrum and of appropriate atmospheric models by Bailey (1959), Brown and Weir (1961) and Reid (1961). Rees (1963), Gledhill and van Rooyen (1963) and Maeda (1965) performed similar calculations for high energy electrons incident on the atmosphere. The results of these workers show that the radio absorption produced by the calculated ionization is in fair agreement with observation. An extension of this work to MID's will be done in future research.

5.5.2 The F Region.

Of greater interest at this stage, in view of the results discussed in the last two chapters, are theories of the cause of the decreases and increases in electron density and height that have been observed during F region storms. Although no completely satisfactory theory of F_2 ionospheric storms has yet appeared, there have been several promising attempts.

Two main theories have been proposed in the past. One is based on the electrodynamic drift motion of electrons and the other attributes the changes to electron loss rate enhanced by thermal effects in the F region. Martyn (1953) suggested that vertical drift motions of electrons would play an important role in the large diurnal part of the changes in the F_2 layer. This vertical drift would result from the interaction of the geomagnetic field and the electrostatic field associated with currents flowing in the ionosphere during a storm. This theory

78/.....

was later developed by Maeda (1955), Hirono (1955) and Sato (1957). The electric field in the dynamo region is estimated from the observed geomagnetic Ds variations, which in turn interact with the geomagnetic field and drive the drift motions of electrons in the F region. The ionospheric continuity equation is then solved using the estimated drift velocities and the assumed atmospheric model of electron production and loss rates. The results obtained by Sato and Maeda (1959) give reasonable agreement between the calculated and observed variations of Ds at middle and low latitudes, although the effect of diffusion is neglected in their computation. In support of this drift theory, an analysis made by Rishbeth (1963) indicates that, at middle latitude stations, geomagnetic storms which produce opposite changes of F region density variation also have different phases in local magnetic Ds variations.

Although the drift theory seems promising, it has some difficulties. The height distribution of electron loss rate assumed by Sato and Maeda is different from that which is now accepted from observations. Using the known decreasing electron loss rate with height, Yonezawa (1958), Rishbeth and Barron(1960) showed that the upward drift yields an increase in the peak electron density as well as its height and, conversely, the downward drift yields a decrease of density and of its height. This result suggests that the typical effect of storms, showing a decrease of the peak electron density accompanied by an increase in its height, cannot be explained by drift theory alone.

79/.....

In recent years it has become evident that the temperature in the F region increases considerably during geomagnetic storms. From observations of satellite drag, Jacchia (1961) and Groves (1961) inferred that there is a general heating of the atmosphere from 200 to 700 km during a geomagnetic storm. Yonezawa (1963) and Matuura (1963) have developed theories which explain storm variations in terms of an entire temperature change in the F_2 region. In his theory, Yonezawa has shown that the rate of chemical reactions in the charge exchange process is sensitive to temperature change. Thus the rate of electron loss is enhanced as the temperature increases and this results in the reduction of the peak electron density. Matuura showed that the main processes which control electron density variations during storms are predominantly those of loss and ambipolar diffusion. He calculated the temperature dependence of these terms, solving the continuity equation numerically and concluded that the electron loss and diffusion rates change appreciably and only small changes in temperature are required to account for the observed electron density variations.

Thus there are good reasons to believe that changes produced by geomagnetic storms in the F region are probably due to a combination of photochemical changes, heating of the atmosphere and electromagnetic movements. The main difference between the various types of ionospheric

80/.....

disturbances is the nature of the heat source. These would include

(1) heat conduction from the hot solar plasma surrounding the earth (Chapman, 1957);

(2) heating by hydromagnetic waves passing through the ionosphere (Dessler, 1959; Akasofu, 1960; Matuura, 1963)

(3) Joule heating dissipation of Ds currents (Cole, 1962)

and (4) the impinging of charged particles - protons and auroral and trapped electrons, the latter being responsible for MID's.

CHAPTER 6

THE THEORY OF LAYER FORMATION WITH A HYPERBOLIC TEMPERATURE FUNCTION

6.1 Introduction.

Throughout this thesis, reasons have been given for believing that the variations found in MID's can be explained by temperature changes in the ionosphere. Besides the work done on storm variations, several workers have investigated the effect of diurnal temperature changes on the electron density distribution in the F region of the ionosphere. Garriott and Rishbeth (1963) discussed the effect of temperature on the electron densities at fixed 'reduced heights' in the F_2 region. They introduced temperature dependencies of production, loss and diffusion into the continuity equation. By comparing the form of the modified continuity equation with the initial equation, they deduced that, for the assumptions made, the electron density at fixed reduced heights varies as $T^{-\frac{1}{2}}$. Their approach, however, does not readily predict the change in the height of maximum electron density, $h_m F_2$.

Several attempts have been made to solve the continuity equation. In most cases, however, the treatment is restricted to the isothermal case, or the case where the temperature is allowed to vary linearly with height. Yonezawa (1956, 1958) obtained analytical solutions for one particular case under daytime equilibrium conditions. Rishbeth and Barron (1960), Gliddon and Kendall (1960) and Rishbeth (1964) have investigated the time dependent variations in the ionosphere. Bowhill (1962) obtained explicit

82/.....

solutions of the continuity equation for various models. Recent work along similar lines has been done by Somayajulu (1964, 1966), Geisler and Bowhill (1965) and Chandra and Rangaswamy (1966).

With present day information on the actual temperature distribution in the atmosphere, it is possible to extend the work of these researchers by using a more realistic function to represent the temperature. In this analysis, the temperature dependence of the production, loss and diffusion terms in the continuity equation is investigated using a new temperature function. The main aim of the investigation is not to develop a new theory of layer formation, but merely to estimate whether the observed variations in MID's can be caused by temperature changes. An attempt is made to estimate actual temperature changes that take place at Halley Bay and Sanae during MID's from the ionograms recorded there.

6.2 The Continuity Equation.

The variation of electron density in the ionosphere is expressed by the continuity equation

$$\frac{\partial N}{\partial t} = q - L - \frac{\partial (NV)}{\partial h} \qquad (1)$$

where N is the electron density,

V is the effective velocity of the electron gas,

83/.....

q is the production rate, L is the loss rate. q and L may be determined by a suitable choice of solar ionizing radiation, atmospheric model, ionization and absorption cross-sections and rate coefficients of chemical processes. For the present it will be assumed that the main part of V comes from the velocity of ambipolar diffusion.

6.3 The Production Rate.

According to current ideas (Hinteregger and Watanabe, 1963) the production and ionization in the F region is believed to be due to the photoionization of atomic oxygen (O) by solar EUV radiation. Although the photoionization cross-sections for molecular nitrogen are large, (see Table 16), the removal process is so rapid that the contribution to the electron density is negligible. This fact was clearly shown by Nicolet and Swider in 1963. From Rishbeth and Garriott (1964), the production rate q is given by

$$q = \sum_{\lambda} I_{\infty\lambda}\, s'(o)_{\lambda}\, n(o) \mathrm{Exp}\left\{ -\left[\sum_{i} s_{\lambda i} \int_{h}^{\infty} n_i \, dh \right] \mathrm{Ch}\,\chi \right\} \quad (2)$$

where I_{∞} is the intensity (in photons/cm^2/sec.) beyond the atmosphere of the ionizing radiation of wavelength λ, n(o) is the concentration of atomic oxygen, n_i is the concentration of the i^{th} atmospheric constituent, h is the height, $s'(o)_{\lambda}$ is the ionization cross-section of O for radiation of wavelength λ, $s_{\lambda i}$ is the absorption cross-section of the i^{th} atmospheric constituent for radiation of wavelength λ.

84/.....

Ch χ is the Chapman function which, to a first approximation, can be replaced by sec χ for $\chi \leq 75^{\circ}$, where χ is the solar zenith angle.

Subscript i refers to summation over the absorption constituents and subscript λ refers to summation over the range of wavelengths which ionize the atmospheric constituents. Ionization due to corpuscular influx will be neglected at this stage.

6.3.1 Values of the Absorption and Photoionization Cross - sections.

Publications on absorption and photoionization cross - sections have been reviewed by Weissler, (1956) and Watanabe (1958). Theoretically deduced results have been published by Dalgarno and Parkinson (1960). Combining the results of these workers with their own, Watanabe and Hinteregger (1962) drew up a list of photoionization and absorption cross-sections for the range applicable to the E, F_1 and F_2 regions. Those applicable to the F_2 region have been selected from these which are shown in Table 16.

According to Rishbeth and Garriott (1964) the absorption of one photon of ionization produces one ion pair for most of the UV spectrum.

6.3.2 Solar Ultraviolet Intensities.

Recently major advances have been made in the measurement of solar UV intensities. Violet and Rense (1959), Hinteregger (1960), Tousey (1961) and Watanabe (1960) and their co-workers have closed the major observa-

85/.....

TABLE 16

SOLAR SPECTRAL INTENSITIES AT NORMAL INCIDENCE, (PHOTONS/CM^2/SEC) X 10^{-8}

AND ABSORPTION AND PHOTOIONIZATION CROSS-SECTIONS, (CM^2) X 10^{-18}

,A	s'(O)	$s(O_2)$	$s'(O_2)$	$s(N_2)$	$s'(N_2)$	I
1025.7		1.7	1.0			26
1000-1027		1.2, 1.8	0.9,1.1			15
989.8		2.2	1.8	0.4		5
977.0		3.7	3	0.8		30
972.5		30	25	280		10
949.7		5.6	5	1.9		5
911-1000		7.4	6	0.4 to 40		37
850-911	3	11	9	0.4 to 40		95
796-850	3.5	11	9	0.4 to 40		25
700-796	5	18	15	11, 19, 37	9, 15, 30	50
600-700	10	18	15	11, 19, 37	9, 15, 30	47
584.3	13	18	15	19	15	29
500-600	15	18	15	11, 19, 37	9, 15, 30	30
400-500	11	18	15	11, 19, 37	9, 15, 30	24
303.8	10	17	15	10	9	43
300-400	10	16	15	11, 19	9, 17	29
230-300	9	15	13	9	8	31
170-230	7	11	10	6	5	33
110-170	2.8	5	5	1.8	1.8	3.5
80-110	1.1	2	2	0.5	0.5	2.4
60-80	0.5	1	1	0.25	0.25	1.8
30-60	0.25	0.5	0.5	0.12	0.12	1.5
20-30	0.06	0.1	0.1	1.0	1.0	0.12
10-20	0.3	0.6	0.6	0.3	0.3	0.02

tional gap in the solar UV spectrum 100 - 1100 Å. The solar spectral intensities for a relatively quiet sun listed by these workers are used in the calculations that follow.

6.4 An Expression for the Number Densities of the Atmospheric Constituents.

From Rishbeth and Garriott (1964), the partial pressure of the i^{th} constituent at reduced height z_i for that constituent in an atmosphere which is in hydrostatic equilibrium, but which has an arbitrary temperature profile, is given by

$$p_i = p_{oi} e^{-z_i} \tag{3}$$

where p_o is the pressure at the reference level h_o and

$$z_i = \int_{h_o}^{h} \frac{dh}{H_i} \tag{4}$$

where H_i is the scale height of the i^{th} constituent, defined by

$$H_i = \frac{kT}{m_i g} \tag{5}$$

where T is the temperature,

m_i is the molecular mass of the i^{th} constituent,

g is the acceleration due to gravity, given by

$$g = g_o \left[\frac{h_o + R_E}{h + R_E} \right]^2$$

where g_o is the value of g at h_o and R_E is the earth's radius,

k is Boltzmann's constant.

These equations hold for the whole atmosphere if m_i is the mean

86/.....

molecular mass. They also apply to each constituent separately in a mixture in diffusive equilibrium, if p, p_o, z, H and m refer to this constituent only.

From the ideal gas law, the number density n_i of the i^{th} constituent in a mixture in diffusive equilibrium is given by

$$n_i = \frac{p_i}{kT} \qquad (6)$$

Substituting for p_i from equation (3),

$$n_i = \frac{p_{oi} e^{-z_i}}{kT} = \frac{T_o}{T} n_{oi} e^{-z_i} \qquad (7)$$

where we have used the fact that $n_{oi} = \frac{p_{oi}}{kT_o}$, where subscript o refers to conditions at h_o.

It now only remains to introduce a function for the temperature that will allow the expression for z (equation 4) to be integrated.

6.5 A Hyperbolic Temperature Function.

The actual temperature distribution in the upper atmosphere is determined by the absorption of solar energy and by heat transfer. The energy balance has been studied by Harris and Priester (1962a). They solved the relevant equations by numerical integration and compared the results with time dependent models derived from satellite density data. Their results are published (Harris and Priester, 1962b) in the form of

87/.....

tables of a number of atmospheric parameters including temperature at various heights. It is clear from these tables that the temperature is neither constant nor a linearly increasing function with height.

Temperature profiles drawn from Harris and Priester data show an obvious resemblance to rectangular hyperbolas and exponential curves of the form

$$T = A' - \frac{K'}{(h-B')} \qquad (8)$$

$$T = A - Ke^{-Bh} \qquad (9)$$

where A,A',B,B',K and K' are constants, different for each profile. An attempt was made to fit equations of this type to selected curves from the Harris and Priester data and also to various CIRA models (CIRA, 1965) which represent more recent data. A typical example is shown in Figure 30. Here the curve represents CIRA model 2 at 1200 hours and the constants in equations 8 and 9 have the values.

$A' = 1194^{\circ}K$ $\qquad$ $A = 1053^{\circ}K$

$B' = 77.5km$ $\qquad$ $B = 0.01535\ km^{-1}$

$K' = 42{,}125^{\circ}K\ km$ $\qquad$ $K = 4467^{\circ}K$

The rms error was $12.4^{\circ}K$ and $5.4^{\circ}K$ respectively. The fit is seen to be reasonably good in the case of both equations. It was found that equation 9 always yielded a better fit than equation 8. However, on substitution into equation 4, equation 8 yields an expression which can be explicitly integrated, whereas equation 9 does not.

88/.....

FIGURE 30.

A typical example of how exponential and hyperbolic functions can be used to represent the temperature in the atmosphere. The actual temperature distribution given here is taken from the CIRA model 2 atmosphere at 1200 hours.

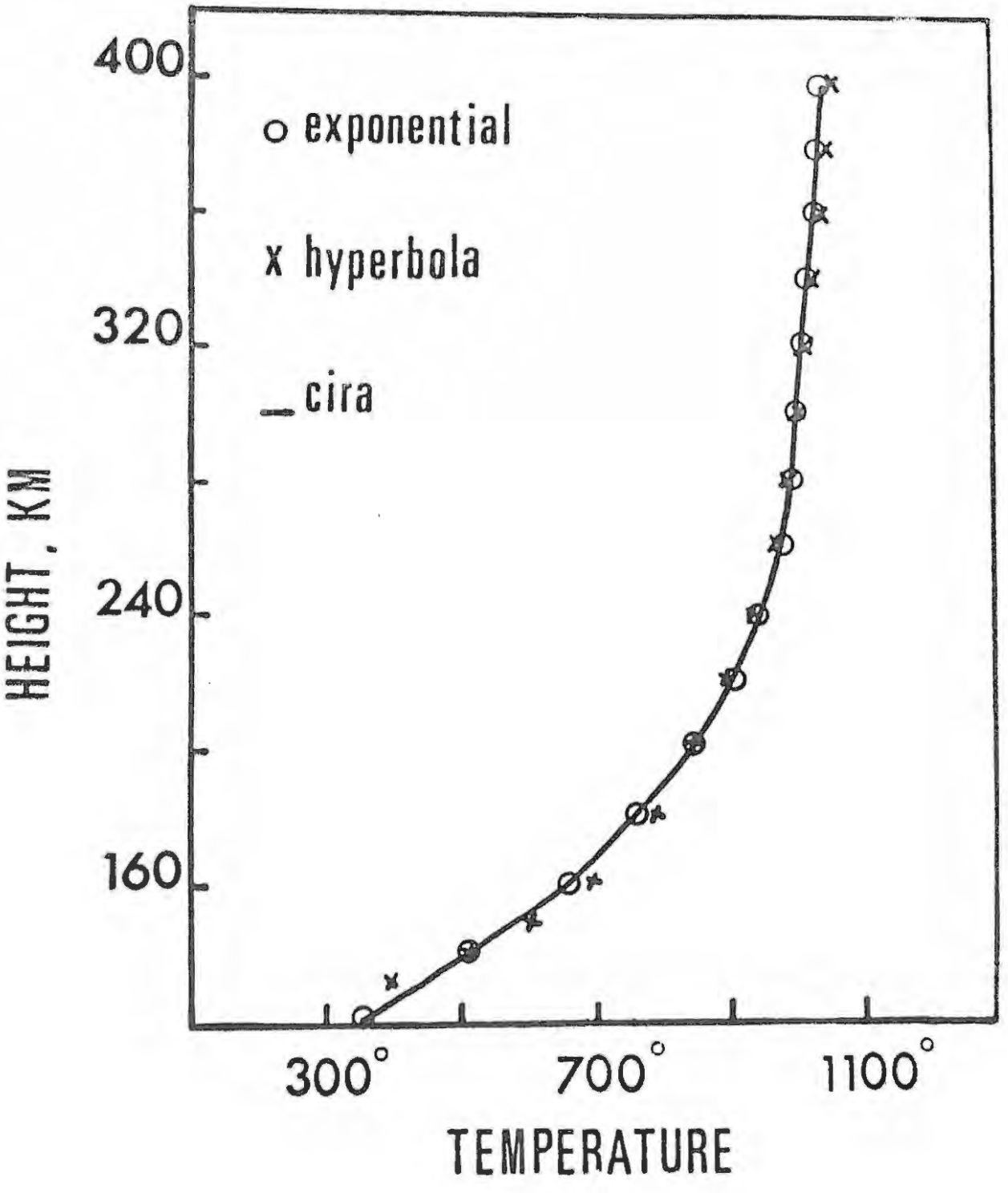
400
320
240
160
HEIGHT, KM
o exponential
x hyperbola
_ cira
300°
700°
1100°
TEMPERATURE

Therefore equation 8 was used in the work reported here.

The work of Kallman - Bijl and Sibley (1964) indicates that in the region of 100 km the number densities of O, O_2 and N_2 remain fairly constant throught the day. Since Harris and Priester assume a fixed temperature of $T_o = 355^oK$ at a datum level of $h_o = 120$ km, it is convenient to also adopt this as a fixed reference level in the present investigation. If these values are introduced, equation 8 becomes

$$T = T_\infty - \frac{(T_\infty - T_o)(h_o - b)}{(h - b)} \qquad (10)$$

where T_∞ is the asymtotic or exospheric temperature. This may be regarded as a two parameter equation which could give a much better fit to actual conditions in the upper atmosphere than the linear gradient which also has two parameters.

Substituting equations 5 and 10 into equation 4 and integrating (this is done in Appendix 4), an expression is obtained for z,

$$z = \frac{A}{h + R_E} + B \ln \frac{T_\infty h - d}{R_E + h} - C \qquad (11)$$

where A, B, C and d are constants given by

$$A = \frac{-a(b + R_E)}{(T_\infty R_E + d)} \qquad (12)$$

$$B = \frac{a(d - T_\infty b)}{(T_\infty R_E + d)^2} \qquad (13)$$

89/.....

$$C = \frac{A}{(h_o + R_E)} + B \ln \frac{T_\infty h_o - d}{h_o + R_E} \qquad (14)$$

$$\text{where } a = \frac{mg_o}{k}(h_o + R_E)^2 \qquad (15)$$

$$d = k' + T_\infty b \qquad (16)$$

$$\text{and} \qquad k' = (T_\infty - T_o)(h_o - b) \qquad (17)$$

6.6 The Loss Rate.

The principal loss of electrons in the F region is believed to be through a two stage process involving atomic oxygen ions. The O^+ ions are lost by a two stage process (Bates and Nicolet, 1960):

$$O^+ + XY \longrightarrow XY^+ + O \qquad \text{(Ion exchange)} \qquad (18)$$

$$XY^+ + e \longrightarrow X'' + Y'' \qquad \text{(Dissociative recombination)} \qquad (19)$$

In the upper part of the F region the loss rate is determined by process (18) which leads to the linear loss rate

$$L = \beta N \qquad (20)$$

$$\text{where} \quad \beta = \gamma\, n(XY) \qquad (21)$$

and γ is the reaction rate of (18).

Since in this region the neutral constituents are in diffusive equilibrium, from equation (7)

$$\beta = \gamma \frac{n_o(XY) T_o e^{-z(XY)}}{T} \qquad (22)$$

90/.....

The molecular species XY may be O_2 or N_2 (Bates and Nicolet, 1960). In general, when both are important, β may be written as

$$\beta = \gamma_1 n(N_2) + \gamma_2 n(O_2) \qquad (23)$$

where γ_1 and γ_2 are the ion-atom interchange reaction rates in the reactions

$$O^+ + O_2 \xrightarrow{\gamma_2} O_2^+ + O \qquad O_2^+ + e' \longrightarrow O + O \qquad (24)$$

and

$$O^+ + N_2 \xrightarrow{\gamma_1} NO^+ + O \qquad NO^+ + e' \longrightarrow N + O \qquad (25)$$

In the lower F region a non-linear loss function is more appropriate. This may be written as

$$L = \frac{\alpha \beta N^2}{\beta + \alpha N} \qquad (26)$$

where α is the recombination coefficient.

According to Swider (1965) and Donahue (1966), the ratio $\gamma_1/\gamma_2 \simeq 0.1$. At F region levels $n(N_2)/n(O_2) \simeq 10$, which suggests that the two terms on the right hand side of equation (23) are approximately equal. Since the scale heights of O_2 and N_2 are fairly close, some workers write β as

$$\beta = 2\gamma_2 n(O_2) = \gamma n(O_2) \qquad (27)$$

The temperature dependence of both γ_1 and γ_2 is subject to considerable uncertainty. Swider (1963, 1965) and Bates and Nicolet (1960) believe that γ is rather insensitive to temperature. Donahue (1966) has performed laboratory experiments on reaction rates and maintains that, if anything, both γ_1 and γ_2 must decrease with temperature. Somayajulu (1966), on the other hand, has performed calculations using equation (27), which show that when γ is independent of T, the observed

91/.....

decrease in $N_m F_2$ cannot be accounted for by typical increases in temperature that occur during storms (Jacchia, 1959, 1960, 1963; Groves, 1960; Jacchia and Slowey, 1962, 1963). In his treatment, Somayajulu allows the temperature to increase linearly to a height of about 200 km, whereafter T is kept constant. He points out that Swider's (1963, 1965) conclusions are based on the experimental determinations of β deduced by Nisbet and Quinn (1963) from ionospheric observations and warns that one has to be very cautious in using ionospheric determinations of β to estimate the temperature dependence of γ, as this may be contaminated by factors which are not accurately known.

He found that when γ was represented by

$$\gamma = \gamma_o T^{\frac{1}{2}} e^{-\frac{3000}{T}} \qquad (28)$$

(from theoretical considerations of Swider, (1963)) a decrease in $N_m F_2$ was obtained, although this was still not large enough to account for the observed variations.

There is experimental evidence, however, which strongly suggests that reactions (24) and (25) are each important over different height ranges. The products of reactions (24) and (25) are formed in an excited state and may subsequently emit radiation (Rishbeth and Garriott, 1964). Reaction (24) results in an emission of 5577Å green lines and reaction (25) in 6300/6364Å red lines. Night-time rocket experiments (Heppner and Meredith, 1958; Tousey, 1958) have shown that nearly all red emission originates above 150 km and green emission below this height. This was

92/.....

taken as evidence that reaction (25) is more important in the F region. Therefore, in this investigation, β will be given by

$$\beta = \gamma_1 n(N_2) \tag{29}$$

in which the temperature dependence of γ_1 will be examined. The method of approach is to formulate an expression for β based on the fact that reaction (25) appears to be bimolecular. From Hughes (1961), γ_1 can then be written as

$$\gamma_1 = \gamma_o T^{\frac{1}{2}} e^{\frac{-E}{kT}} \tag{30}$$

where γ_o is a constant, E is the activation energy (a constant), and k is Boltzmann's constant.

Fehsenfeld, Schmeltekopf and Ferguson (1965) have measured the reaction rate of (25) at 300°K and the value of γ_1 has been settled at $(3.0 \pm 1) \times 10^{-12} cm^3/sec$. Therefore, from equation (30)

$$\gamma_o = \frac{3.0 \times 10^{-12} e^{\frac{E}{300k}}}{\sqrt{300}} \tag{31}$$

substituting back into equation (30)

$$\gamma_1 = 1.7 \times 10^{-13} T^{\frac{1}{2}} e^{\frac{E}{k}\left(\frac{1}{300} - \frac{1}{T}\right)} \tag{32}$$

Although it would be a better approach to do the same thing for γ_2, this would involve yet another unknown (the activation energy for reaction (24)), which would make the situation even more speculative. In view of the experimental evidence given above, the first approach seems to be the most reasonable. The results obtained using this method will be compared with those obtained using equation (23) with γ_1 and

93/.....

γ_2 constants. In this case it is quite unnecessary to exclude reaction (24).

The currently accepted value for γ_2 (Donahue, 1966) is $4.0 \times 10^{-11} cm^3/sec$.

6.7 The Diffusion Term.

Shimazaki (1957) has shown that, if it is assumed that the electron, ion and neutral gas temperatures are the same, the velocity due to ambipolar diffusion can be given approximately as

$$V = -D \sin^2 I \left[\frac{1}{N} \frac{\partial N}{\partial h} + \frac{1}{T} \frac{\partial T}{\partial h} + \frac{\mu}{H} \right] \qquad (33)$$

where D is the diffusion coefficient given by Chapman and Cowling (1960) to a first approximation for a system of two gases consisting of rigid spheres of diameters σ_1 and σ_2, as

$$D = \frac{3}{8\sigma_{12}^2 n} \left[\frac{kT(m_1 + m_2)}{2\pi m_1 m_2} \right]^{\frac{1}{2}} \qquad (34)$$

where $n = n_1 + n_2$, the sum of the individual number densities of the two gases and σ_{12} is the collision diameter given by $\sigma_{12} = \frac{1}{2}(\sigma_1 + \sigma_2)$.

Case (1).

Dalgarno (1958a,b,1961,1964) has suggested that the diffusion of atomic oxygen ions (O^+) through the atomic oxygen gas (O) is appropriate for the F region.

94/.....

Under these conditions

$$m_1 \approx m_2 = m(0) \tag{35}$$

$$n = n(0) \tag{36}$$

$\sigma_{12} = 2 \times 10^{-8}$ cm.

Therefore, $$D = \frac{bT^{\frac{1}{2}}}{n} \tag{37}$$

where $$b = \frac{3}{8\sigma_{12}^2}\left(\frac{k}{\pi m(0)}\right)^{\frac{1}{2}} \tag{38}$$

and $$H = \frac{T}{C_a} \tag{39}$$

where $$C_a = \frac{m(0)g}{k} \tag{40}$$

and $$\mu = \tfrac{1}{2}m(0^+)/m(0) = \tfrac{1}{2} \tag{41}$$

The factor $\sin^2 I$ represents the fact that diffusion of electrons and ions can only take place parallel to magnetic lines of force.

Case (2).

There is also the possibility of D being the diffusion coefficient of O^+ in the neutral gas (Shimazaki, 1957). Although this should be dealt with as a system of four gases, for simplicity we shall write:

$$n = \sum_i n_i \tag{42}$$

$$m_1 = m(O^+)$$

$$m_2 = \sum_i \frac{m_i n_i}{n} \tag{43}$$

$$\sigma_{12} \approx 2.0 \times 10^{-8}\text{cm} \tag{44}$$

95/.....

$$C_a = \frac{m_2 g}{k} \tag{45}$$

$$\mu = \frac{m_1}{2m_2} \tag{46}$$

where subscript i refers to summation over the neutral atmospheric constituents. Both these possibilities will be considered in the numerical analysis that is conducted later.

Multiplying equation (33) by N and differentiating (Appendix 5), we get the divergence of the number flow,

$$\frac{\partial (NV)}{\partial h} = -D \sin^2 I \left[\frac{\partial^2 N}{\partial h^2} + \frac{R \partial N}{\partial h} + G'N \right] \tag{47}$$

where

$$R = \left[\frac{1}{T} \frac{\partial T}{\partial h} + \frac{\mu C_a}{T} + \frac{1}{D} \frac{\partial D}{\partial h} \right] \tag{48}$$

$$G' = \frac{1}{T} \left[-\frac{1}{T} \left(\frac{\partial T}{\partial h} \right)^2 + \frac{\partial^2 T}{\partial h^2} + \frac{T_d \mu}{H dh} - \frac{\mu T}{H^2} \frac{dH}{dh} + \frac{1}{D} \frac{\partial D}{\partial h} \left(\frac{\partial T}{\partial h} + \frac{\mu T}{H} \right) \right] \tag{49}$$

where

a) Case (1)

$$\frac{\partial D}{\partial h} = D \left[\frac{3}{2T} \frac{\partial T}{\partial h} + \frac{1}{H(O)} \right] \tag{50}$$

H(O) is the scale height of atomic oxygen.

$$\frac{\partial T}{\partial h} = \frac{(T_\infty - T_o)(h_o - b)}{(h - b)^2} \tag{51}$$

$$\frac{\partial^2 T}{\partial h^2} = \frac{-2(T_\infty - T_o)(h_o - b)}{(h - b)^3} \tag{52}$$

96/.....

$$\frac{\partial H}{\partial h} = \frac{k}{mg}\left(\frac{\partial T}{\partial h} - \frac{T}{g}\frac{\partial g}{\partial h}\right) \tag{53}$$

$$\frac{\partial g}{\partial h} = \frac{-2g}{(h + R_E)} \tag{54}$$

$$\mu = \tfrac{1}{2} \tag{55}$$

$$\frac{\partial \mu}{\partial h} = 0 \tag{56}$$

b) Case (2)

$$D = \frac{bT^{\frac{1}{2}}}{\sum n_i} \tag{57}$$

where

$$b = \frac{3}{8\sigma^2}\left(\frac{k}{2\pi}\right)^{\frac{1}{2}} m^{\frac{1}{2}} \tag{58}$$

$$m = \frac{\sum n_i}{\sum m_i n_i} + \frac{1}{m(0)} \tag{59}$$

$$\frac{\partial D}{\partial h} = \left\{ \frac{1}{2bm^{\frac{1}{2}}}\left[\sum n_i \frac{\sum m_i n_i / H_i}{(\sum m_i n_i)^2}\right] + \sum n_i / H_i \left(\frac{1}{\sum n_i} - \frac{1}{2bm^{\frac{1}{2}} \sum n_i m_i}\right) + \frac{3}{2}\frac{1}{T}\frac{\partial T}{\partial h}\right\} \tag{60}$$

$$H = \frac{kT}{m_a g} \tag{61}$$

$$m_a = \frac{\sum m_i n_i}{\sum n_i} \tag{62}$$

$$\frac{\partial H}{\partial h} = \frac{k}{m_a}\left[\frac{\partial}{\partial h}\left(\frac{T}{g}\right) - \frac{T}{m_a^2 g}\frac{\partial m_a}{\partial h}\right] \tag{63}$$

where

$$\frac{\partial m_a}{\partial h} = \frac{\sum m_i n_i \sum n_i / H_i}{(\sum n_i)^2} - \frac{\sum m_i n_i / H_i}{\sum n_i} \tag{64}$$

97/.....

$$\frac{\partial}{\partial h}\left(\frac{T}{g}\right) = \frac{1}{g}\left(\frac{\partial T}{\partial h} - \frac{T}{g}\frac{\partial g}{\partial h}\right) \qquad (65)$$

where $\frac{\partial T}{\partial h}$ and $\frac{\partial g}{\partial h}$ are given by equations (54) and (51).

6.8 The Continuity Equation in a New Form.

Substituting equation (47) into (1), we obtain

$$q - \beta N - D \sin^2 I \left[\frac{\partial^2 N}{\partial h^2} + R\frac{\partial N}{\partial h} + G'N\right] = \frac{\partial N}{\partial t} \qquad (66)$$

The time dependent solution of equation 66 is very complicated. However, the treatment can be simplified considerably by investigating the case where $\frac{\partial N}{\partial t} = 0$. Although this will restrict the analysis to daytime equilibrium conditions, we will still be able to assess the effect of temperature change on the F region electron density distribution. Under these conditions, equation 66 may be written as

$$\frac{\partial^2 N}{\partial h^2} + R\frac{\partial N}{\partial h} + GN - W = 0 \qquad (67)$$

where $G = G' + \frac{\beta}{D \sin^2 I}$ (68)

and $W = \frac{q}{D \sin^2 I}$. (69)

Equation 67 is a second order differential equation which can be solved numerically.

CHAPTER 7.

NUMERICAL SOLUTION OF THE CONTINUITY EQUATION

7.1 Outline of the Investigation.

Initially the main aim of this investigation was to find values of T_∞ and b in the temperature function which would yield N(h) profiles similar to those observed at Halley Bay and Sanae during both disturbed and quiet day conditions. However, in doing this the difficulty arose of assigning values to some of the quantities used in the expressions derived in the previous chapter. The true values of several of these are uncertain. The quantities in question include I_{∞} , $S(0)$, S_i', T_o, $n_o(O)$, $n_o(O_2)$, $n_o(N_2)$, β , and D.

Therefore in this investigation the treatment has been restricted to an assesment of the importance of temperature change on the F_2 region electron density distribution. The method of approach will be to solve the continuity equation numerically for a variety of values of T_∞ and b in the temperature function, to estimate the extent to which changes in temperature affect the electron density distribution.

With the exception of β and D, it appears unlikely that any of the remaining quantities can change sufficiently during MID's to account for the observed variations. Although it seems certain that the temperature and number densities at the datum level will change during MID's, this would not be expected to be as nearly pronounced as at higher levels (Kallman - Bijl and Sibley, 1964; Nicolet, 1961)

99/.....

It is reasonable to suppose that variations in I_∞ are due to solar cyclic changes and that these will be proportional to the 10cm flux which varies by a factor of about 3.5 over a solar cycle. The best available information to date on the absorption and ionization cross-sections are the data of Watanabe and Hinteregger (1962).

In the case of β, the calculations are performed with γ_1 and γ_2 initially independent of T, and then again for several values of E. The approximate temperature dependence of D, namely $D \propto T^{\frac{1}{2}}$, is regarded as reliable. In this case the constant of proportionality is varied. The values of the constants used in the calculation are given in Appendix 6.

7.2 Starting Conditions for the Calculation.

Equation (67) may now be used to compute the F_2 region electron density for specific values of the parameters involved. The Runge Kutta method (Romanelli, 1960) was chosen as a suitable means to perform the numerical integration. This method requires starting values for the calculation, in this case N_o and $\left(\frac{\partial N}{\partial h}\right)_o$, where the subscript o refers to a level at which these two quantities are known. During the trial calculations, the integration was started where N is given approximately by

100/.....

$$N = \frac{Q}{\beta} \tag{70}$$

i.e. at that height at which both loss due to the quadratic loss law (αN^2) and transport due to diffusion are unimportant. The starting height was chosen as 230 km. The calculations showed, however, that even at this height the loss rate cannot be given to within $\pm$ 10% by equation (20). Equation (67) must therefore be changed to

$$\frac{\partial^2 N}{\partial h^2} + R\frac{\partial N}{\partial h} + G'N + \frac{1}{D \sin^2 I}\left(\frac{\alpha \beta N^2}{\alpha N + \beta}\right) - W = 0 \tag{71}$$

which cannot be easily solved by known methods. The following approach was therefore developed. According to Hirsh (1959), if the ionosphere is in the steady state, the electron density may be given by

$$N = \frac{Q}{2\beta}\left[1 + \left(1 + \frac{4\beta^2}{\alpha Q}\right)^{\frac{1}{2}}\right] \tag{72}$$

at heights where diffusion is unimportant.

Equation (71) can be written as

$$\frac{\partial^2 N'}{\partial h^2} = -R\frac{\partial N'}{\partial h} - G'N' - \beta'N' + W \tag{73}$$

where β' is an effective value for the attachment coefficient in the region where the loss rate is not truly linear. Then β' is given by

$$\beta' = \frac{1}{D \sin^2 I}\left(\frac{\alpha \beta N''}{\alpha N'' + \beta}\right) \tag{74}$$

where initially N'' is given by equation (72). N' is the value of N

101/.....

that will be obtained solving equation (73) under these conditions.

At any particular height the actual electron density N would be given by

$$N = \frac{(q - A_1)}{2\beta}\left[1 \mp \left(1 \mp \frac{4\beta^2}{\alpha(q - A_1)}\right)^{\frac{1}{2}}\right] \qquad (75)$$

or $$N(h) = N'(h) \pm \Delta N(h) \qquad (76)$$

where A_1 represents the quantity $\frac{\partial(NV)}{\partial h}$.

Consider the two extreme cases where (1) $\alpha \ll \beta$ and (2) $\beta \ll \alpha$

In case (1) equations (72) and (75) respectively become

$$N'' = \sqrt{\frac{q}{\alpha}} \qquad N = \sqrt{\frac{q - A_1}{\alpha}} \qquad (77)$$

and in case (2) $$N'' = \frac{q}{\beta} \qquad N = \frac{q - A_1}{\beta} \qquad (78)$$

If A_1 is negative $N'' < N$ in both cases. (79)

If A_1 is positive $N'' > N$ in both cases. (80)

For cases (1) and (2) equation (74) reduces to $\beta' = \frac{\alpha N''}{D \sin^2 I}$ and $\beta' = \frac{\beta}{D \sin^2 I}$ respectively. In case (2) equation (67) is appropriate for the situation at hand, since N'' is not involved and $N \geq N'$. In case (1) if $N'' < N$, $\beta' < \frac{\alpha N}{D \sin^2 I}$, and if $N'' > N$, $\beta' > \frac{\alpha N}{D \sin^2 I}$.

The effect of this on the solution of equation (73) can be understood by examining the Runge Kutta method of integration.

The basic principle of the Runge Kutta integration can be outlined as follows, although the actual approach is more refined, being designed

102/.....

to approximate the Taylor series. Given the starting values of N_o and $\left(\frac{\partial N}{\partial h}\right)_o$, $\left(\frac{\partial^2 N}{\partial h^2}\right)_1$ can be calculated from equation (73), where the subscript refers to the step number in the integration.

$$\therefore \quad \left(\frac{\partial^2 N'}{\partial h^2}\right)_1 = -R_o\left(\frac{\partial N}{\partial h}\right)_o - G'_o N_o - \beta'_o N_o + W_o \qquad (81)$$

and

$$\left(\frac{\partial N'}{\partial h}\right)_1 = \left(\frac{\partial N}{\partial h}\right)_o + \Delta h\left(\frac{\partial^2 N'}{\partial h^2}\right)_1 \qquad (82)$$

and

$$N'_1 = N_o + \Delta h\left(\frac{\partial N'}{\partial h}\right)_1 \qquad (83)$$

If $\beta' < \frac{\alpha N}{D \sin^2 I}$, (84), $\left(\frac{\partial^2 N'}{\partial h^2}\right)_1 > \left(\frac{\partial^2 N}{\partial h^2}\right)_1$ (85)

$$\therefore \quad \left(\frac{\partial N'}{\partial h}\right)_1 > \left(\frac{\partial N}{\partial h}\right)_1 \qquad (86)$$

$$\therefore \quad N'_1 > N_1 \quad \text{as here } G'_o, R_o \text{ and } q \text{ are positive.} \qquad (87)$$

Similarly, if $\beta' > \frac{\alpha N}{D \sin^2 I}$, then $N'_1 < N_1$. (88)

Improved values for β' and N' can be obtained by using an iterative approach. For example, having calculated N'_1, a better value for β' can be obtained by replacing N'' by N' in equation (74) and repeating the calculation. If initially $N'_1 > N_1 > N''_1$, $\left[\beta' < \frac{\alpha\beta N_1}{D \sin^2 I(\alpha N_1 + \beta)}, \right]$ we make

$$\beta' = \frac{\alpha\beta N'_1}{D \sin^2 I(\alpha N'_1 + \beta)} \geq \frac{\alpha\beta N_1}{D \sin^2 I(\alpha N_1 + \beta)} \qquad (89)$$

103/.....

A new value can then be calculated for N_1' using the value of β' calculated from equation (89). Similarly β' is recalculated using the new value of N_1'. This time

$$N_1' \leq N_1$$

and $$\beta' \leq \frac{\alpha \beta N_1}{D \sin^2 I \left(\alpha N_1 + \beta\right)}$$

This process is continued until the value calculated for N_1' remains constant and is equal to N_1. In practice the starting values N_o and $\left(\frac{\partial N}{\partial h}\right)_o$ were calculated from equation (72) at a height where the contribution due to diffusion was small. (Appendix 7).

Since it is a straightforward matter to calculate N using equation (72), the computation was started at the datum level. As the production of electrons due to photoionization of O_2 has not been included in this treatment, the values of N only become realistic in the F_1 region. Should the necessity arise, it would be a simple matter to include this in the calculation. Exclusion of this factor does not affect the results for the F region, as values of N can be calculated exactly for any specific height from equation (72).

7.3 Presentation and Discussion of Results.

To illustrate the change in the electron density distribution, some sample N(h) profiles were calculated using equation (71) and the technique discussed previously. The computations were done on IBM 1620 and 704 computers for selected values of T_∞ and b and for three values

(Fortran listing given in Appendix 7)

104/.....

of χ . Values of I_{∞} applicable to the 6-month period under study were used. The calculations were done for γ both (1) independent of T and (2) dependent on T. In case (1), β was given by equation (23) using Donahue's values of γ_1 and γ_2, i.e. $\gamma_1 = 4 \times 10^{-12} cm^3/sec$ and $\gamma_2 = 4 \times 10^{-11} cm^3/sec$. α was taken to be $6 \times 10^{-8} cm^3/sec$. The results for case (1) are shown in Figure 31 where the three curves in each block represent $\chi = 0^\circ$, 60° and 80°. In cases where only 2 curves are shown, the one for $\chi = 80^\circ$ has been omitted. The values of T_∞ and b are shown.

The most striking effect noticeable is the obvious sensitivity of the shape of the profiles to temperature change. The curves are very sensitive to changes in T_∞, an increase of $400^\circ K$ decreasing N_{max} by a factor of 2 to 3. At low temperatures ($T_\infty = 800^\circ K$) the shapes of the curves are particularly sensitive to changes in the shape of the T(h) profile, the more rectangular the hyperbola, the greater the heating effect. For example, at $T_\infty = 800^\circ K$, a change in b from 50 km to 90 km, which increases T at 150 km by about $100^\circ K$, decreases N_{max} by a factor of 1.5 to 2. The actual values of the various quantities calculated are shown in Tables 17 to 20 for some values of T_∞ and b for $\chi = 0$. The effect of temperature change on the individual terms, production, loss and diffusion and their importance in governing the shape of the N(h) profile will be discussed later.

The temperature increase appears to have very little corresponding effect on the F_1 region, which is consistent with observation. These results are also consistent with those of Matuura (1963) who found that only small changes in T

105/.....

FIGURE 31.

Calculated N(h) profiles for γ independent of temperature for various values of T_∞ and b. The three curves in each block are for $\chi = 0^\circ$, 60° and 80°. In cases where only two curves are shown, the one for $\chi = 80^\circ$ has been omitted. The temperature profile is also shown. The upper horizontal scale should be labelled ELECTRON DENSITY X 10^{-5}, ELECTRONS/CM^3.

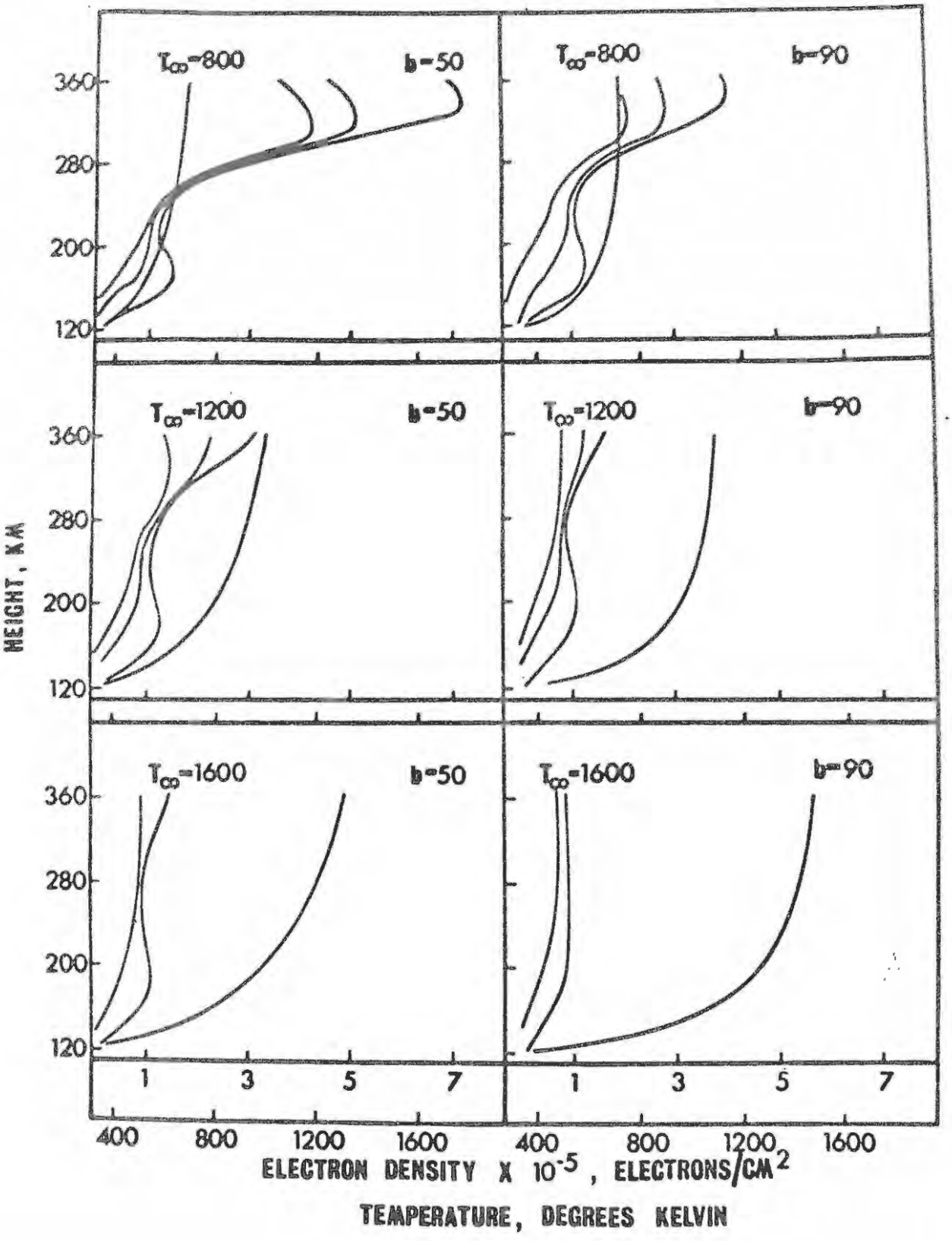
T_∞=800
b=50
T_∞=800
b=90
T_∞=1200
b=50
T_∞=1200
b=90
T_∞=1600
b=50
T_∞=1600
b=90
360
280
200
120
HEIGHT, KM
1
3
5
7
400
800
1200
1600
ELECTRON DENSITY X 10^{-5}, ELECTRONS/CM^2
TEMPERATURE, DEGREES KELVIN

TABLE 17

T= 800. B= 90.0 SECCHI= 1.0000 E= 3.00E-14 GAM= 4.0E-12 FAC= 1.00 ALPHA= 6.0E-08 DIP ANGLE= 63.13 DEGREES DELTA H= 4.00

HT	TEMP	Z-O	H-O	N(O)	N(O2)	N(N2)	O	REAC RATE	N	BET	Q	DIFSN	LOSS
120	355	0.00	19	7.60E+10	1.20E+11	5.80E+11	2.11E+08	4.00E-12	8.18E+03	2.82E+00	4	0	4
128	448	.36	24	4.19E+10	4.61E+10	2.44E+11	4.30E+08	4.00E-12	2.88E+04	2.82E+00	49	0	49
136	509	.66	28	2.72E+10	2.22E+10	1.26E+11	7.05E+08	4.00E-12	5.53E+04	1.39E+00	183	0	183
144	552	.93	30	1.91E+10	1.18E+10	7.25E+10	1.04E+09	4.00E-12	8.25E+04	7.65E-01	406	0	406
152	584	1.18	32	1.40E+10	6.77E+09	4.39E+10	1.46E+09	4.00E-12	1.05E+05	4.46E-01	660	0	660
160	609	1.42	33	1.06E+10	4.01E+09	2.76E+10	1.98E+09	4.00E-12	1.21E+05	2.71E-01	862	0	862
168	628	1.66	35	8.14E+09	2.44E+09	1.78E+10	2.62E+09	4.00E-12	1.29E+05	1.69E-01	968	0	968
176	644	1.88	36	6.34E+09	1.51E+09	1.17E+10	3.41E+09	4.00E-12	1.32E+05	1.07E-01	981	0	981
184	657	2.10	36	4.99E+09	9.60E+08	7.83E+09	4.38E+09	4.00E-12	1.31E+05	6.97E-02	928	0	928
192	669	2.32	37	3.96E+09	6.14E+08	5.29E+09	5.57E+09	4.00E-12	1.27E+05	4.57E-02	838	0	838
200	678	2.53	38	3.16E+09	3.97E+08	3.60E+09	7.07E+09	4.00E-12	1.23E+05	3.03E-02	734	0	734
208	686	2.73	38	2.53E+09	2.58E+08	2.47E+09	8.80E+09	4.00E-12	1.19E+05	2.02E-02	630	0	630
216	694	2.94	39	2.04E+09	1.69E+08	1.71E+09	1.09E+10	4.00E-12	1.15E+05	1.36E-02	533	0	533
224	700	3.14	39	1.65E+09	1.12E+08	1.18E+09	1.36E+10	4.00E-12	1.13E+05	9.24E-03	447	0	447
232	705	3.34	40	1.34E+09	7.46E+07	8.30E+08	1.68E+10	4.00E-12	1.13E+05	6.30E-03	373	0	373
240	711	3.54	40	1.09E+09	4.98E+07	5.82E+08	2.07E+10	4.00E-12	1.16E+05	4.32E-03	310	0	310
248	715	3.74	40	8.93E+08	3.34E+07	4.10E+08	2.55E+10	4.00E-12	1.21E+05	2.97E-03	257	0	257
256	719	3.93	41	7.30E+08	2.25E+07	2.89E+08	3.12E+10	4.00E-12	1.30E+05	2.05E-03	212	0	212
264	723	4.13	41	5.99E+08	1.52E+07	2.05E+08	3.82E+10	4.00E-12	1.43E+05	1.43E-03	176	0	176
272	726	4.32	41	4.92E+08	1.03E+07	1.46E+08	4.67E+10	4.00E-12	1.61E+05	9.97E-04	145	0	145
280	729	4.51	42	4.05E+08	7.00E+06	1.04E+08	5.68E+10	4.00E-12	1.83E+05	6.97E-04	120	0	120
288	732	4.70	42	3.33E+08	4.77E+06	7.45E+07	6.91E+10	4.00E-12	2.11E+05	4.89E-04	99	0	99
296	735	4.89	42	2.75E+08	3.26E+06	5.33E+07	8.39E+10	4.00E-12	2.45E+05	3.44E-04	82	0	82
304	737	5.07	42	2.27E+08	2.23E+06	3.83E+07	1.01E+11	4.00E-12	2.85E+05	2.42E-04	68	0	68
312	739	5.26	43	1.88E+08	1.53E+06	2.75E+07	1.23E+11	4.00E-12	3.33E+05	1.71E-04	56	0	56
320	741	5.45	43	1.56E+08	1.05E+06	1.98E+07	1.48E+11	4.00E-12	3.71E+05	1.21E-04	47	-2	45
328	743	5.63	43	1.29E+08	7.30E+05	1.43E+07	1.79E+11	4.00E-12	3.94E+05	8.66E-05	39	-5	34
336	745	5.81	43	1.08E+08	5.05E+05	1.03E+07	2.16E+11	4.00E-12	4.06E+05	6.17E-05	32	-7	25
344	747	6.00	43	8.94E+07	3.49E+05	7.53E+06	2.60E+11	4.00E-12	4.09E+05	4.41E-05	27	-9	18
352	749	6.18	44	7.44E+07	2.42E+05	5.46E+06	3.13E+11	4.00E-12	4.05E+05	3.15E-05	22	-9	12
360	750	6.36	44	6.19E+07	1.68E+05	3.97E+06	3.77E+11	4.00E-12	3.97E+05	2.26E-05	18	-9	8

TABLE 18

T_∞=1200. B= 50.0 SECCHI= 1.0000 E= -1.00E-13 GAM= 4.0E-12 FAC= 1.00 ALPHA= 6.0E-08 DIP ANGLE= 63.13 DEGREES DELTA H= 4.00

HT	TEMP	Z-O	H-O	N(O)	N(O2)	N(N2)	D	REAC RATE	N	BET	Q	DIFSN	LOSS
120	355	0.00	19	7.60E+10	1.20E+11	5.80E+11	2.11E+08	4.00E-12	8.18E+03	7.12E+00	4	0	4
128	441	.36	24	4.23E+10	4.64E+10	2.45E+11	4.22E+08	4.00E-12	2.94E+04	2.84E+00	52	0	52
136	512	.66	28	2.69E+10	2.18E+10	1.23E+11	7.15E+08	4.00E-12	5.59E+04	1.37E+00	187	0	187
144	570	.93	31	1.85E+10	1.14E+10	6.99E+10	1.09E+09	4.00E-12	8.14E+04	7.38E-01	395	0	395
152	620	1.17	34	1.33E+10	6.50E+09	4.21E+10	1.58E+09	4.00E-12	1.01E+05	4.28E-01	612	0	612
160	662	1.40	36	1.00E+10	3.88E+09	2.66E+10	2.19E+09	4.00E-12	1.15E+05	2.61E-01	773	0	773
168	696	1.61	38	7.68E+09	2.41E+09	1.74E+10	2.93E+09	4.00E-12	1.21E+05	1.66E-01	854	0	854
176	730	1.81	40	6.01E+09	1.54E+09	1.17E+10	3.83E+09	4.00E-12	1.23E+05	1.08E-01	863	0	863
184	758	2.00	42	4.77E+09	1.01E+09	8.08E+09	4.91E+09	4.00E-12	1.22E+05	7.28E-02	823	0	823
192	783	2.19	43	3.84E+09	6.78E+08	5.65E+09	6.20E+09	4.00E-12	1.20E+05	4.97E-02	756	0	756
200	805	2.37	45	3.12E+09	4.61E+08	4.02E+09	7.74E+09	4.00E-12	1.16E+05	3.45E-02	678	0	678
208	825	2.54	46	2.56E+09	3.17E+08	2.89E+09	9.55E+09	4.00E-12	1.12E+05	2.42E-02	598	0	598
216	843	2.71	47	2.11E+09	2.21E+08	2.10E+09	1.16E+10	4.00E-12	1.09E+05	1.72E-02	522	0	522
224	860	2.88	48	1.76E+09	1.55E+08	1.54E+09	1.42E+10	4.00E-12	1.06E+05	1.24E-02	452	0	452
232	875	3.04	49	1.47E+09	1.10E+08	1.14E+09	1.71E+10	4.00E-12	1.05E+05	8.99E-03	390	0	390
240	888	3.20	50	1.23E+09	7.92E+07	8.50E+08	2.05E+10	4.00E-12	1.04E+05	6.57E-03	336	0	336
248	901	3.35	51	1.04E+09	5.71E+07	6.37E+08	2.45E+10	4.00E-12	1.05E+05	4.83E-03	289	0	289
256	912	3.51	52	8.80E+08	4.14E+07	4.80E+08	2.92E+10	4.00E-12	1.07E+05	3.57E-03	248	0	248
264	923	3.66	53	7.47E+08	3.02E+07	3.63E+08	3.46E+10	4.00E-12	1.12E+05	2.66E-03	213	0	213
272	933	3.81	53	6.36E+08	2.21E+07	2.76E+08	4.09E+10	4.00E-12	1.18E+05	1.99E-03	184	0	184
280	942	3.96	54	5.43E+08	1.63E+07	2.11E+08	4.81E+10	4.00E-12	1.26E+05	1.49E-03	158	0	158
288	951	4.10	54	4.65E+08	1.20E+07	1.62E+08	5.65E+10	4.00E-12	1.37E+05	1.13E-03	136	0	136
296	959	4.25	55	3.99E+08	8.96E+06	1.24E+08	6.61E+10	4.00E-12	1.50E+05	8.58E-04	117	0	117
304	967	4.39	56	3.43E+08	6.67E+06	9.64E+07	7.72E+10	4.00E-12	1.66E+05	6.52E-04	101	0	101
312	974	4.53	56	2.95E+08	4.99E+06	7.47E+07	8.99E+10	4.00E-12	1.84E+05	4.98E-04	88	0	88
320	980	4.67	57	2.55E+08	3.74E+06	5.80E+07	1.04E+11	4.00E-12	2.05E+05	3.81E-04	76	0	76
328	987	4.81	57	2.20E+08	2.81E+06	4.51E+07	1.21E+11	4.00E-12	2.29E+05	2.93E-04	66	0	66
336	993	4.95	58	1.91E+08	2.12E+06	3.52E+07	1.40E+11	4.00E-12	2.57E+05	2.26E-04	57	0	57
344	998	5.09	58	1.65E+08	1.60E+06	2.76E+07	1.62E+11	4.00E-12	2.80E+05	1.74E-04	49	-1	48
352	1004	5.22	59	1.43E+08	1.21E+06	2.16E+07	1.87E+11	4.00E-12	2.96E+05	1.35E-04	43	-3	39
360	1009	5.36	59	1.25E+08	9.26E+05	1.70E+07	2.16E+11	4.00E-12	3.07E+05	1.05E-04	37	-5	31

TABLE 19

T_∞ = 1200. B= 90.0 SECCHI= 1.0000 E=1.00E-13 GAM= 4.0E-12 FAC= 1.00 ALPHA= 6.0E-08 DIP ANGLE= 63.13 DEGREES DELTA H= 4.00

HT	TEMP	Z-O	H-O	N(O)	N(O2)	N(N2)	D	REAC RATE	N	BET	Q	DIFSN	LOSS
120	355	0.00	19	7.60E+10	1.20E+11	5.80E+11	2.11E+08	4.00E-12	8.18E+03	7.12E+00	4	0	4
128	532	.32	29	3.65E+10	4.15E+10	2.17E+11	5.39E+08	4.00E-12	2.39E+04	2.53E+00	34	0	34
136	648	.57	35	2.34E+10	2.09E+10	1.16E+11	9.25E+08	4.00E-12	4.07E+04	1.30E+00	99	0	99
144	730	.78	40	1.69E+10	1.22E+10	7.17E+10	1.36E+09	4.00E-12	5.71E+04	7.76E-01	194	0	194
152	791	.97	43	1.29E+10	7.71E+09	4.75E+10	1.85E+09	4.00E-12	7.22E+04	4.99E-01	310	0	310
160	837	1.14	46	1.02E+10	5.12E+09	3.29E+10	2.41E+09	4.00E-12	8.50E+04	3.36E-01	427	0	427
168	875	1.31	48	8.27E+09	3.50E+09	2.35E+10	3.04E+09	4.00E-12	9.49E+04	2.34E-01	528	0	528
176	905	1.47	50	6.81E+09	2.45E+09	1.71E+10	3.76E+10	4.00E-12	1.01E+05	1.66E-01	601	0	601
184	930	1.63	52	5.67E+09	1.75E+09	1.27E+10	4.58E+09	4.00E-12	1.06E+05	1.20E-01	643	0	643
192	951	1.78	53	4.76E+09	1.26E+09	9.52E+09	5.52E+09	4.00E-12	1.08E+05	8.87E-02	657	0	657
200	969	1.93	54	4.03E+09	9.22E+08	7.21E+09	6.58E+09	4.00E-12	1.09E+05	6.57E-02	648	0	648
208	985	2.07	55	3.43E+09	6.79E+08	5.50E+09	7.79E+09	4.00E-12	1.08E+05	4.92E-02	622	0	622
216	998	2.21	56	2.93E+09	5.03E+08	4.23E+09	9.18E+09	4.00E-12	1.06E+05	3.70E-02	585	0	585
224	1010	2.36	57	2.52E+09	3.75E+08	3.26E+09	1.07E+10	4.00E-12	1.05E+05	2.81E-02	542	0	542
232	1021	2.49	58	2.17E+09	2.81E+08	2.53E+09	1.25E+10	4.00E-12	1.03E+05	2.14E-02	496	0	496
240	1031	2.63	58	1.87E+09	2.12E+08	1.97E+09	1.46E+10	4.00E-12	1.01E+05	1.63E-02	450	0	450
248	1039	2.77	59	1.62E+09	1.60E+08	1.54E+09	1.69E+10	4.00E-12	9.99E+04	1.26E-02	405	0	405
256	1047	2.90	59	1.41E+09	1.21E+08	1.21E+09	1.95E+10	4.00E-12	9.87E+04	9.73E-03	363	0	363
264	1054	3.03	60	1.22E+09	9.28E+07	9.55E+08	2.25E+10	4.00E-12	9.82E+04	7.53E-03	325	0	325
272	1060	3.16	61	1.06E+09	7.09E+07	7.54E+08	2.59E+10	4.00E-12	9.84E+04	5.85E-03	289	0	289
280	1066	3.30	61	9.32E+08	5.43E+07	5.97E+08	2.98E+10	4.00E-12	9.94E+04	4.56E-03	257	0	257
288	1071	3.42	61	8.15E+08	4.16E+07	4.73E+08	3.42E+10	4.00E-12	1.01E+05	3.56E-03	228	0	228
296	1076	3.55	62	7.13E+08	3.20E+07	3.76E+08	3.92E+10	4.00E-12	1.04E+05	2.78E-03	202	0	202
304	1081	3.68	62	6.25E+08	2.47E+07	2.99E+08	4.48E+10	4.00E-12	1.09E+05	2.18E-03	178	0	178
312	1085	3.81	63	5.48E+08	1.91E+07	2.38E+08	5.12E+10	4.00E-12	1.15E+05	1.72E-03	158	0	158
320	1089	3.93	63	4.81E+08	1.48E+07	1.90E+08	5.84E+10	4.00E-12	1.22E+05	1.35E-03	140	0	140
328	1093	4.06	63	4.23E+08	1.14E+07	1.52E+08	6.65E+10	4.00E-12	1.31E+05	1.07E-03	123	0	123
336	1096	4.18	64	3.72E+08	8.91E+06	1.22E+08	7.57E+10	4.00E-12	1.42E+05	8.46E-04	109	0	109
344	1100	4.31	64	3.28E+08	6.93E+06	9.81E+07	8.61E+10	4.00E-12	1.52E+05	6.70E-04	96	-2	95
352	1103	4.43	65	2.89E+08	5.40E+06	7.88E+07	9.79E+10	4.00E-12	1.58E+05	5.31E-04	85	-5	80
360	1106	4.55	65	2.55E+08	4.21E+06	6.34E+07	1.11E+11	4.00E-12	1.63E+05	4.22E-04	75	-9	66

TABLE 20

T_∞= 1600. B= 50.0 SECCHI= 1.0000 E= -1.00E-13 GAM= 4.0E-12 FAC= 1.00 ALPHA= 6.0E-08 DIP ANGLE= 63.13 DEGREES DELTA H= 4.00

HT	TEMP	Z-O	H-O	N(O)	N(O2)	N(N2)	D	REAC RATE	N	BET	Q	DIFSN	LOSS
120	355	0.00	19	7.60E+10	1.20E+11	5.80E+11	2.11E+08	4.00E-12	8.18E+03	7.12E+00	4	0	4
128	482	.34	26	3.94E+10	4.39E+10	2.31E+11	4.74E+08	4.00E-12	2.68E+04	2.68E+00	43	0	43
136	586	.61	32	2.47E+10	2.10E+10	1.18E+11	8.34E+08	4.00E-12	4.73E+04	1.31E+00	134	0	134
144	672	.84	37	1.71E+10	1.15E+10	6.91E+10	1.28E+09	4.00E-12	6.62E+04	7.39E-01	262	0	262
152	745	1.05	41	1.25E+10	6.95E+09	4.37E+10	1.84E+09	4.00E-12	8.19E+04	4.53E-01	398	0	398
160	807	1.23	44	9.68E+09	4.43E+09	2.91E+10	2.50E+09	4.00E-12	9.35E+04	2.93E-01	515	0	515
168	861	1.41	48	7.64E+09	2.94E+09	2.02E+10	3.27E+09	4.00E-12	1.01E+05	1.98E-01	597	0	597
176	908	1.57	50	6.16E+09	2.02E+09	1.44E+10	4.16E+09	4.00E-12	1.05E+05	1.38E-01	640	0	640
184	949	1.72	53	5.05E+09	1.42E+09	1.05E+10	5.19E+09	4.00E-12	1.07E+05	9.90E-02	652	0	652
192	986	1.87	55	4.20E+09	1.01E+09	7.85E+09	6.37E+09	4.00E-12	1.07E+05	7.21E-02	639	0	639
200	1019	2.01	57	3.52E+09	7.42E+08	5.92E+09	7.71E+09	4.00E-12	1.06E+05	5.34E-02	610	0	610
208	1048	2.15	59	2.98E+09	5.48E+08	4.53E+09	9.23E+09	4.00E-12	1.05E+05	4.00E-02	572	0	572
216	1075	2.28	60	2.55E+09	4.09E+08	3.49E+09	1.09E+10	4.00E-12	1.02E+05	3.03E-02	528	0	528
224	1099	2.41	62	2.19E+09	3.09E+08	2.72E+09	1.29E+10	4.00E-12	1.00E-05	2.32E-02	484	0	484
232	1121	2.54	63	1.89E+09	2.35E+08	2.13E+09	1.50E+10	4.00E-12	9.87E+04	1.79E-02	440	0	440
240	1141	2.66	65	1.64E+09	1.80E+08	1.69E+09	1.75E+10	4.00E-12	9.69E+04	1.39E-02	398	0	398
248	1159	2.78	66	1.43E+09	1.38E+08	1.34E+09	2.03E+10	4.00E-12	9.55E+04	1.09E-02	359	0	359
256	1176	2.90	67	1.25E+09	1.07E+09	1.07E+09	2.33E+10	4.00E-12	9.45E+04	8.60E-03	322	0	322
264	1192	3.02	68	1.09E+09	8.39E+07	8.62E+08	2.68E+10	4.00E-12	9.40E+04	6.80E-03	290	0	290
272	1207	3.14	69	9.64E+08	6.57E+07	6.95E+08	3.07E+10	4.00E-12	9.41E+04	5.41E-03	260	0	260
280	1221	3.25	70	8.50E+08	5.17E+07	5.62E+08	3.50E+10	4.00E-12	9.49E+04	4.32E-03	233	0	233
288	1233	3.36	71	7.52E+08	4.08E+07	4.57E+08	3.98E+10	4.00E-12	9.65E+04	3.46E-03	209	0	209
296	1245	3.48	72	6.66E+08	3.23E+07	3.72E+08	4.51E+10	4.00E-12	9.89E+04	2.78E-03	187	0	187
304	1256	3.59	73	5.91E+08	2.57E+07	3.04E+08	5.11E+10	4.00E-12	1.02E+05	2.24E-03	168	0	168
312	1267	3.70	73	5.26E+08	2.05E+07	2.49E+08	5.77E+10	4.00E-12	1.06E+05	1.81E-03	150	0	150
320	1277	3.80	74	4.68E+08	1.64E+07	2.04E+08	6.50E+10	4.00E-12	1.11E+05	1.47E-03	135	0	135
328	1286	3.91	75	4.18E+08	1.31E+07	1.68E+08	7.31E+10	4.00E-12	1.18E+05	1.20E-03	121	0	121
336	1295	4.02	75	3.73E+08	1.05E+07	1.39E+08	8.21E+10	4.00E-12	1.25E+05	9.80E-04	109	0	109
344	1303	4.12	76	3.34E+08	8.52E+08	1.15E+08	9.21E+10	4.00E-12	1.32E+05	8.01E-04	98	-1	96
352	1311	4.22	77	2.99E+08	6.88E+06	9.53E+07	1.03E+11	4.00E-12	1.37E+05	6.56E-04	88	-4	83
360	1318	4.33	77	2.68E+08	5.56E+06	7.91E+07	1.15E+11	4.00E-12	1.41E+5	5.93E-04	79	-7	71

were required to produce the observed storm variations. The curves for $T_\infty = 1600^\circ K$ show clearly the ionospheric G condition, typical of disturbed conditions when the F_2 electron density lies either below or very close to that of the F_1 layer.

An interesting feature is the appearance of a valley between the F_1 and F_2 layers. It was found that the valley disappeared when α became equal to $9 \times 10^{-8} cm^3/sec$. The results of these calculations have not been displayed, as the main features are essentially the same as those given. Decreasing α made the valley even more pronounced.

The results obtained here appear to be directly contradictory to those of Somayajulu (1966) who found that for typical storm increases in T of about $400^\circ K$ (Jacchia, 1959, 1960, 1963; Groves, 1961; Jacchia and Slowey, 1962, 1963), one could not account for the observed variations in electron density if β is independent of T. The approach he used was considerably simpler than that adopted here.

There is one aspect of the profiles shown here that is inconsistent with observation. The temperature values given in the CIRA (1965) model atmospheres for the period in question show that T_∞ should be of the order of $1400^\circ K$ at midday, $1000^\circ K$ at midnight and $1200^\circ K$ in the morning. Typical quiet and disturbed day profiles are shown in Figure 33 for Halley Bay and Sanae for 0700 hours in summer, when $\frac{\partial I}{\partial t} \approx 0$ for those stations. It is clear that for these values of T_∞ and I_∞, the computed values of N_{max} are far too low. This phenomenon can be attrib-

106/.....

FIGURE 32.

calculated electron density profiles for γ dependent on T for various values of T_∞ , b and E. The three curves in each block, from left to right, are for E = 0, -5×10^{-14} and -1×10^{-13} ergs. In cases where only two curves are shown, the one for E = 0 has been omitted.

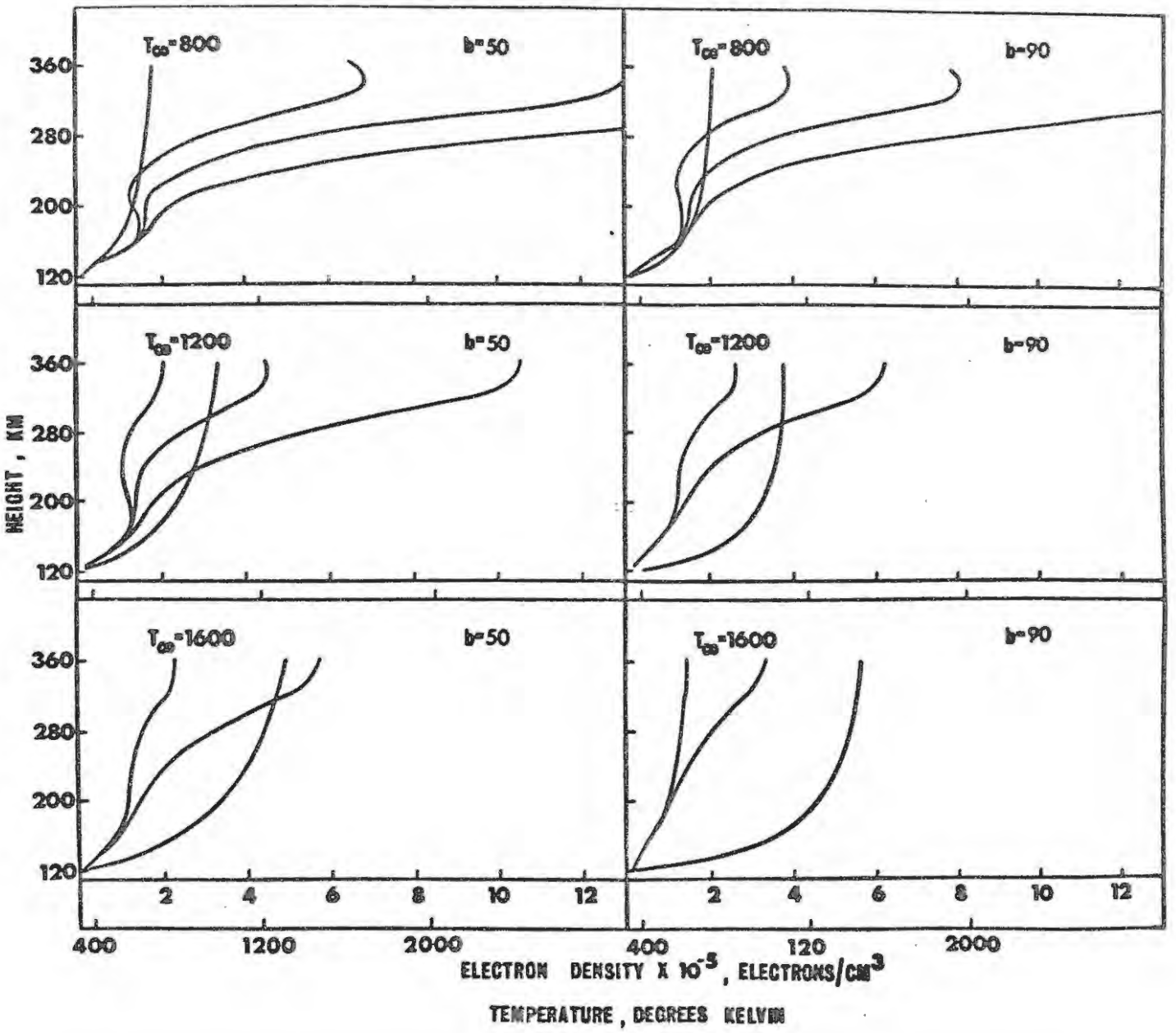
T_∞=800
b=50
T_∞=800
b=90
T_∞=1200
b=50
T_∞=1200
b=90
T_∞=1600
b=50
T_∞=1600
b=90
360
280
200
120
HEIGHT, KM
2
4
6
8
10
12
400
1200
2000
400
120
2000
ELECTRON DENSITY X 10^{-5}, ELECTRONS/CM^3
TEMPERATURE, DEGREES KELVIN

uted to the fact that the values of β shown in Tables 17 to 20 are too high. This view is supported by the results of Ratcliffe et al. (1956), Van Zandt et al. (1960) and Norton et al. (1964). However, the values for γ_1 and γ_2 used in the calculation have been accepted as correct (Donahue, 1966) and a change cannot be justified.

However, Donahue had suggested that a decrease rather than an increase in γ with increase in T would be more consistent with his deductions. During the trial calculations, it was discovered that for certain values of E, γ does in fact decrease with temperature when equation (32) is used. Figure 32 shows the results obtained when this possibility was investigated. The three curves shown in each block represent (from left to right) E = 0, -5×10^{-14} and -1×10^{-13} ergs for $\chi = 0$. (In cases where only 2 curves are shown, the one for E = 0 has been omitted.) The case where E = 0 represents $\gamma \propto T^{\frac{1}{2}}$. The values of β corresponding to these values of E and the values of T_∞ and b shown, are given in Tables 21 and 22. These tables show that (i) for $E \leq -1 \times 10^{-13}$ ergs, γ always decreases with temperature; (ii) for $E \geq -5 \times 10^{-14}$ ergs, γ decreases with temperature in the height range 120 to 140 km and then increases for $T_\infty \geq 1200^\circ$K and $b \geq 90$ km. The values of β obtained in case (i) are of the same order of magnitude as those of Ratcliffe et al. (1956) and Van Zandt et al. (1960). Furthermore, the N(h) profiles obtained using this approach bear a much better resemblance to the observed curves for $T_\infty \gtrsim 1200^\circ$K and for the values

107/.....

FIGURE 33.

Typical observed quiet and disturbed day N(h) profiles at Sanae and Halley Bay at 0700 hours in summer.

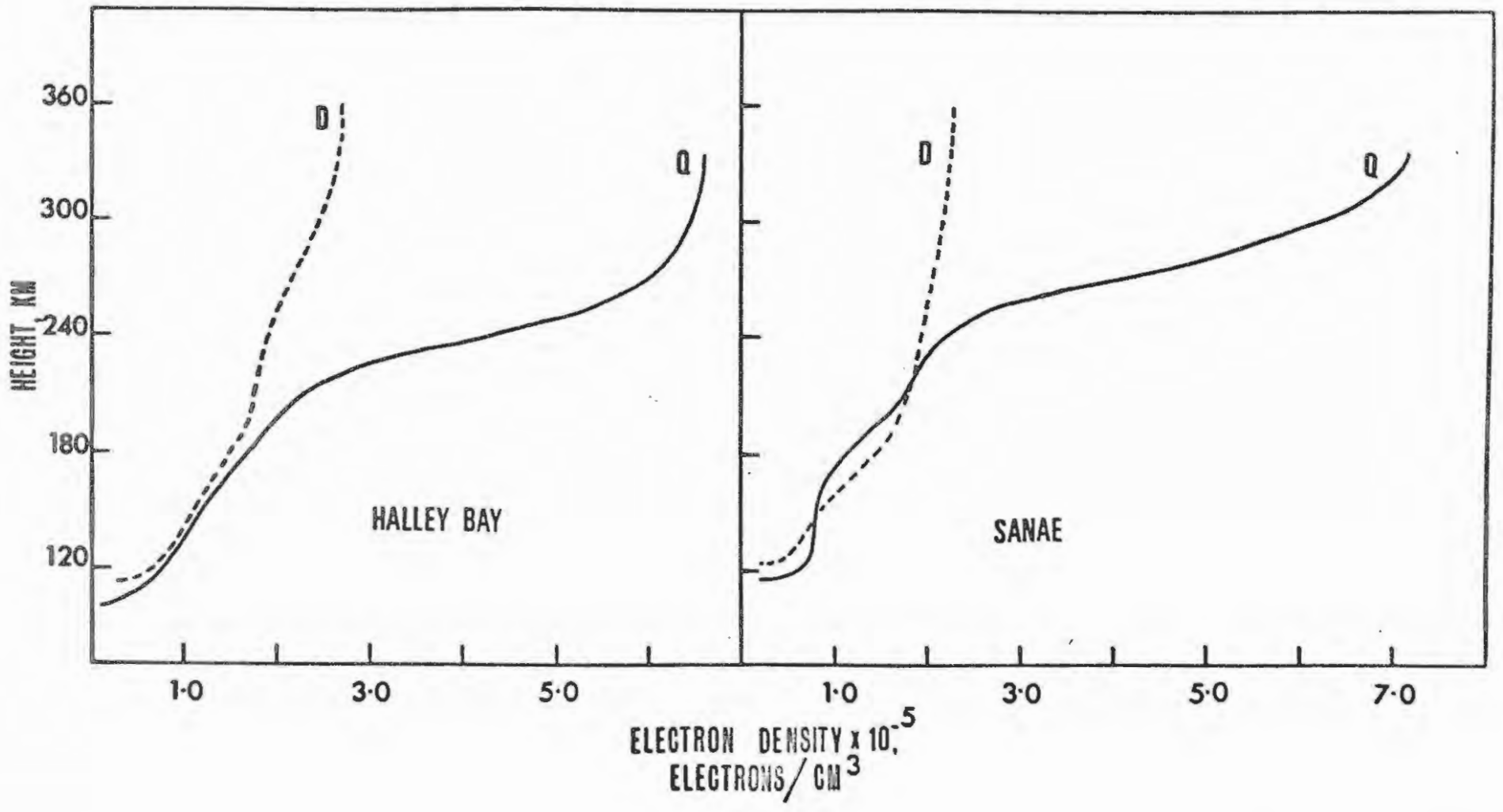
360
300
240
180
120
HEIGHT, KM
D
Q
HALLEY BAY
SANAE
1·0
3·0
5·0
7·0
ELECTRON DENSITY x 10^-5
ELECTRONS / CM^3

TABLE 21.

REACTION RATE IS X 10^{12}, E IS X 10^{13}.

	A=800 B=50 E=-1.0			A=800 B=90 E=-1.0			A=1200B=50 E=-1.0			A=1200B=90 E=-1.0			A=1600B=50 E=-1.0			A=1600B=90 E=-1.0		
HT	TEMP	REAC RATE	BET	TEMP	REAC RATE	BET	TEMP	REAC RATE	BET	TEMP	REAC RATE	BET	TEMP	REAC RATE	BET	TEMP	REAC RATE	BET
120	355	2.99	1.73E+00	355	2.99	1.73E+00	355	2.99	1.73E+00	355	2.99	1.73E+00	355	2.99	1.73E+00	355	2.99	1.73E+00
128	400	2.52	6.60E-01	448	2.19	5.36E-01	441	2.23	5.50E-01	532	1.85	4.04E-01	482	2.03	4.71E-01	617	1.65	3.27E-01
136	437	2.25	2.95E-01	509	1.93	2.44E-01	512	1.92	2.39E-01	648	1.60	1.87E-01	586	1.71	2.03E-01	788	1.45	1.56E-01
144	468	2.09	1.46E-01	552	1.79	1.30E-01	570	1.75	1.22E-01	730	1.50	1.07E-01	672	1.57	1.08E-01	908	1.38	9.57E-02
152	494	1.98	7.78E-02	584	1.72	7.58E-02	620	1.65	6.96E-02	791	1.45	6.89E-02	745	1.48	6.51E-02	997	1.34	6.52E-02
160	516	1.90	4.34E-02	609	1.67	4.63E-02	662	1.58	4.22E-02	837	1.41	4.67E-02	807	1.43	4.19E-02	1066	1.32	4.71E-02
168	536	1.84	2.51E-02	628	1.63	2.92E-02	698	1.53	2.68E-02	875	1.39	3.28E-02	861	1.40	2.84E-02	1121	1.31	3.53E-02
176	552	1.79	1.49E-02	644	1.61	1.89E-02	730	1.50	1.76E-02	905	1.38	2.37E-02	908	1.38	1.99E-02	1165	1.31	2.71E-02
184	567	1.76	9.14E-03	657	1.59	1.24E-02	758	1.47	1.19E-02	930	1.37	1.74E-02	949	1.36	1.44E-02	1202	1.30	2.12E-02
192	580	1.73	5.68E-03	669	1.57	8.34E-03	783	1.45	8.24E-03	951	1.36	1.29E-02	986	1.35	1.06E-02	1233	1.30	1.68E-02
200	592	1.70	3.59E-03	678	1.56	5.63E-03	805	1.44	5.79E-03	969	1.35	9.79E-03	1019	1.34	7.95E-03	1260	1.30	1.34E-02
208	602	1.68	2.30E-03	686	1.55	3.84E-03	825	1.42	4.12E-03	985	1.35	7.44E-03	1048	1.33	6.04E-03	1283	1.30	1.08E-02
216	612	1.66	1.48E-03	694	1.54	2.64E-03	843	1.41	2.97E-03	998	1.34	5.79E-03	1075	1.32	4.64E-03	1303	1.29	8.82E-03
224	620	1.65	9.74E-04	700	1.53	1.82E-03	860	1.40	2.17E-03	1010	1.34	4.39E-03	1099	1.32	3.60E-03	1321	1.29	7.20E-03
232	628	1.63	6.42E-04	705	1.53	1.27E-03	875	1.39	1.59E-03	1021	1.34	3.40E-03	1121	1.31	2.82E-03	1336	1.29	5.91E-03
240	636	1.62	4.27E-04	711	1.52	8.88E-04	888	1.39	1.18E-03	1031	1.33	2.64E-03	1141	1.31	2.22E-03	1351	1.29	4.87E-03
248	642	1.61	2.86E-04	715	1.51	6.23E-04	901	1.38	8.82E-04	1039	1.33	2.06E-03	1159	1.31	1.76E-03	1363	1.29	4.02E-03
256	648	1.60	1.92E-04	719	1.51	4.39E-04	912	1.37	6.62E-04	1047	1.33	1.62E-03	1176	1.31	1.40E-03	1375	1.29	3.33E-03
264	654	1.59	1.30E-04	723	1.51	3.10E-04	923	1.37	5.00E-04	1054	1.33	1.27E-03	1192	1.30	1.12E-03	1385	1.29	2.77E-03
272	659	1.58	8.90E-05	726	1.50	2.20E-04	933	1.37	3.79E-04	1060	1.33	1.00E-03	1207	1.30	9.08E-04	1394	1.29	2.31E-03
280	664	1.58	6.09E-05	729	1.50	1.56E-04	942	1.36	2.89E-04	1066	1.32	7.93E-04	1221	1.30	7.31E-04	1403	1.29	1.93E-03
288	669	1.57	4.19E-05	732	1.50	1.11E-04	951	1.36	2.21E-04	1071	1.32	6.29E-04	1233	1.30	5.96E-04	1411	1.29	1.61E-03
296	673	1.57	2.89E-05	735	1.49	8.00E-05	959	1.36	1.69E-04	1076	1.32	4.99E-04	1245	1.30	4.85E-04	1418	1.29	1.35E-03
304	677	1.56	2.00E-05	737	1.49	5.73E-05	967	1.35	1.30E-04	1081	1.32	3.97E-04	1256	1.30	3.96E-04	1425	1.29	1.13E-03
312	681	1.56	1.39E-05	739	1.49	4.12E-05	974	1.35	1.01E-04	1085	1.32	3.16E-04	1267	1.30	3.24E-04	1431	1.29	9.57E-04
320	684	1.55	9.73E-06	741	1.49	2.96E-05	980	1.35	7.85E-05	1089	1.32	2.52E-04	1277	1.30	2.66E-04	1437	1.29	8.06E-04
328	687	1.55	6.81E-06	743	1.49	2.14E-05	987	1.35	6.10E-05	1093	1.32	2.02E-04	1286	1.30	2.19E-04	1443	1.29	6.80E-04
336	691	1.54	4.78E-06	745	1.48	1.53E-05	993	1.34	4.76E-05	1096	1.32	1.61E-04	1295	1.29	1.80E-04	1448	1.29	5.74E-04
344	694	1.54	3.36E-06	747	1.48	1.12E-05	998	1.34	3.72E-05	1100	1.32	1.29E-04	1303	1.29	1.49E-04	1452	1.29	4.85E-04
352	696	1.54	2.37E-06	749	1.48	8.12E-06	1004	1.34	2.91E-05	1103	1.32	1.04E-04	1311	1.29	1.23E-04	1457	1.29	4.11E-04
360	699	1.53	1.68E-06	750	1.48	5.90E-06	1009	1.34	2.28E-05	1106	1.32	8.38E-05	1318	1.29	1.02E-04	1461	1.29	3.48E-04

TABLE 22.

REACTION RATE IS X 10^{12}, E IS X 10^{13}.

	A=800 B=90 E=-5.0			A=1200B=50 E=-5.0			A=1200B=90 E=-5.0			A=1600B=50 E=-5.0		
HT	TEMP	REAC RATE	BET	TEMP	REAC RATE	BET	TEMP	REAC RATE	BET	TEMP	REAC RATE	BET
120	355	3.60	2.09E+00	355	3.60	2.09E+00	355	3.60	2.09E+00	355	3.60	2.09E+00
128	448	3.27	8.00E-01	441	3.29	8.10E-01	532	3.14	6.84E-01	482	3.21	7.44E-01
136	509	3.17	4.01E-01	512	3.16	3.94E-01	648	3.07	3.58E-01	586	3.10	3.67E-01
144	552	3.12	2.26E-01	570	3.11	2.17E-01	730	3.06	2.19E-01	672	3.06	2.12E-01
152	584	3.10	1.36E-01	620	3.08	1.29E-01	791	3.06	1.45E-01	745	3.06	1.33E-01
160	609	3.08	8.54E-02	662	3.07	8.17E-02	837	3.07	1.01E-01	807	3.07	8.96E-02
168	628	3.08	5.50E-02	698	3.06	5.34E-02	875	3.08	7.26E-02	861	3.08	6.24E-02
176	644	3.07	3.61E-02	730	3.06	3.59E-02	905	3.09	5.31E-02	908	3.10	4.48E-02
184	657	3.07	2.40E-02	758	3.06	2.47E-02	930	3.10	3.95E-02	949	3.11	3.28E-02
192	669	3.06	1.62E-02	783	3.06	1.73E-02	951	3.11	2.97E-02	986	3.13	2.45E-02
200	678	3.06	1.10E-02	805	3.07	1.23E-02	969	3.12	2.25E-02	1019	3.14	1.86E-02
208	686	3.06	7.58E-03	825	3.07	8.90E-03	985	3.13	1.72E-02	1048	3.15	1.43E-02
216	694	3.06	5.24E-03	843	3.08	6.48E-03	998	3.13	1.32E-02	1075	3.17	1.10E-02
224	700	3.06	3.64E-03	860	3.08	4.76E-03	1010	3.14	1.02E-02	1099	3.18	8.67E-03
232	705	3.06	2.54E-03	875	3.08	3.52E-03	1021	3.14	7.98E-03	1121	3.19	6.83E-03
240	711	3.06	1.78E-03	888	3.09	2.63E-03	1031	3.15	6.22E-03	1141	3.20	5.41E-03
248	715	3.06	1.25E-03	901	3.09	1.97E-03	1039	3.15	4.87E-03	1159	3.21	4.31E-03
256	719	3.06	8.88E-04	912	3.10	1.49E-03	1047	3.15	3.83E-03	1176	3.22	3.46E-03
264	723	3.06	6.29E-04	923	3.10	1.13E-03	1054	3.16	3.02E-03	1192	3.23	2.78E-03
272	726	3.06	4.47E-04	933	3.10	8.61E-04	1060	3.16	2.38E-03	1207	3.23	2.25E-03
280	729	3.06	3.19E-04	942	3.11	6.58E-04	1066	3.16	1.89E-03	1221	3.24	1.82E-03
288	732	3.06	2.28E-04	951	3.11	5.05E-04	1071	3.16	1.50E-03	1233	3.25	1.48E-03
296	735	3.06	1.63E-04	959	3.11	3.89E-04	1076	3.17	1.19E-03	1245	3.25	1.21E-03
304	737	3.06	1.17E-04	967	3.12	3.01E-04	1081	3.17	9.50E-04	1256	3.26	9.93E-04
312	739	3.06	8.45E-05	974	3.12	2.33E-04	1085	3.17	7.58E-04	1267	3.27	8.15E-04
320	741	3.06	6.09E-05	980	3.12	1.81E-04	1089	3.17	6.06E-04	1277	3.27	6.71E-04
328	743	3.06	4.40E-05	987	3.13	1.41E-04	1093	3.17	4.85E-04	1286	3.28	5.53E-04
336	745	3.06	3.18E-05	993	3.13	1.10E-04	1096	3.18	3.89E-04	1295	3.28	4.57E-04
344	747	3.06	2.30E-05	998	3.13	8.65E-05	1100	3.18	3.12E-04	1303	3.29	3.78E-04
352	749	3.06	1.67E-05	1004	3.13	6.79E-05	1103	3.18	2.51E-04	1311	3.29	3.14E-04
360	750	3.06	1.21E-05	1009	3.14	5.34E-05	1106	3.18	2.02E-04	1318	3.30	2.61E-04

of I_{∞} given in Table 16. In fact it was possible to find values for T_{∞} and b which gave reasonably good fits to observed N(h) profiles. A typical example is shown in Figure 34. $T_{\infty} = 1200^{\circ}K$ and b = 90 km, and the observed profile represents a typical evening quiet day profile at Sanae. The very high values of N_{max} in Figure 32 for $T_{\infty} = 800^{\circ}K$ can be attributed to the fact that these conditions apply to sunspot minimum when I_{∞} is lower than that used here.

Again it is obvious that these profiles are highly sensitive to temperature change. An increase of $150^{\circ}K$ at heights of 150 km without any corresponding change in T_{∞} reduces N_{max} by a factor of about 1.5.

The figures for the diffusion rate shown in Tables 17 to 20 show that this only becomes important near the peak of the layer, where it determines the height of N_{max}. Comparison of the values for diffusion shown in Table 17 where $T_{\infty} = 800^{\circ}K$, with those in Table 20 where $T_{\infty} = 1600^{\circ}K$, shows that the rate of diffusion is practically insensitive to large changes in temperature. Hence the height of N_{max} is also rather insensitive to increases in T, requiring increases of the order of $800^{\circ}K$ in T to produce a noticeable change. It seems likely, however, that since the layer tends toward the ionospheric G condition when T is increased from $1200^{\circ}K$ to $1600^{\circ}K$, that the virtual height of the layer may increase considerably. This would be even more pronounced in cases where there is a valley between the F_1 and F_2 layers.

The main temperature effect revealed by the present investigation is an increase in the thickness of the F_2 layer and a decrease in $N_{max}F_2$.

108/.....

FIGURE 34.

Observed and calculated N(h) profiles for 1700 hours at Sanae where the Watanabe and Hinteregger (1962) values of I_{∞} and CIRA values of T_{∞} have been used.

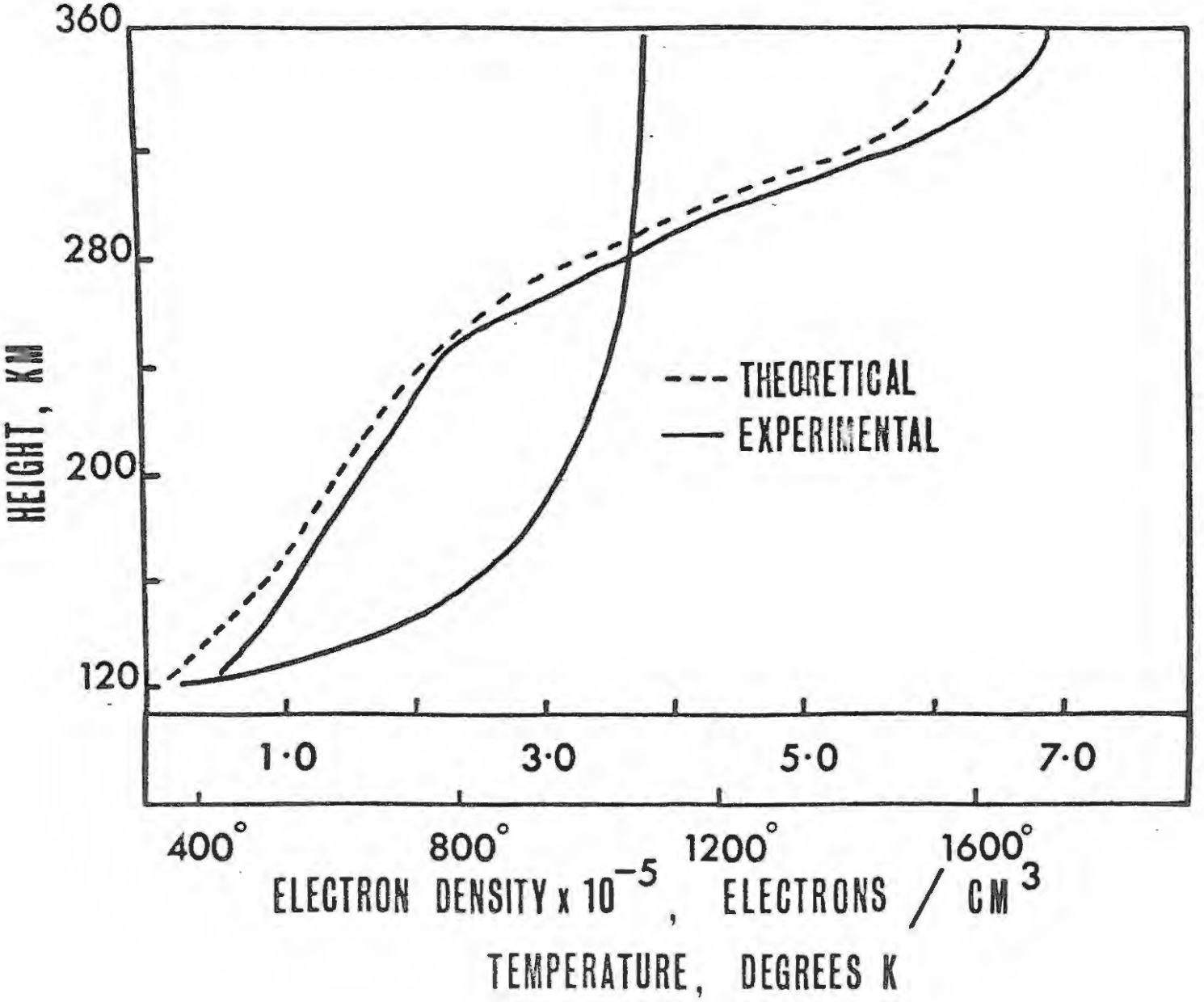
360
280
200
120
HEIGHT, KM
--- THEORETICAL
—— EXPERIMENTAL
1·0
3·0
5·0
7·0
400°
800°
1200°
1600°
ELECTRON DENSITY x 10⁻⁵, ELECTRONS / CM³
TEMPERATURE, DEGREES K

The fact that small changes in T at heights of about 150km produce a noticeable decrease in N_{max}, without affecting the F_1 region, suggests that the heating takes place mainly near this height. In this event the particles involved should have energies of the order of 1 - 10 kev. (Rees, 1963). It seems possible therefore that the flux of electrons with $E \geq 40$ kev, is probably responsible for the D region enhanced ionization, and that the main heating flux consists of lower energy particles which vary in intensity in the same way in space and time.

7.4 Factors Responsible for the Decrease in Electron Density.

7.4.1. The Diffusion Rate.

The results given in Tables 17 to 20 show that the diffusion rate is of the order of 10 electrons/cm^3/sec. Therefore diffusion only becomes important when production and loss are of comparable magnitude. Consider the cases where (1) $T_\infty = 800^\circ K$, b = 90 km and (2) $T_\infty = 1600^\circ K$ and b = 50 km. In case (1) diffusion becomes increasingly important at heights above 320 km, as the production and loss rates are small at these heights for values of T shown. In case (2), however, both production and loss have increased considerably due to upward expansion of the atmosphere. Diffusion on the other hand is smaller, as the diffusion coefficient is inversely proportional to $n_A^{(o)}$ which increases more rapidly than $T^{\frac{1}{2}}$ at heights above 300 km. For example at 320 km $n_A^{(o)}$ increases by a factor of 3 from case (1) to case (2) whereas $T^{\frac{1}{2}}$ only increases by a

109/.....

factor of 1.3. Thus the shape of the layer is controlled largely by production and loss at high temperatures. It was found that even when the diffusion coefficient was increased by a factor of 2, the production and loss terms were still dominant. Therefore it was decided to abandon the original aim of a detailed investigation of the effect of changes in the diffusion coefficient on the F region electron density distribution.

7.4.2. The Loss Rate.

The results given in Table 21 show that γ (labelled REAC RATE) is most sensitive to temperature in the region T = 300°K to 400°K. For example,(1); γ decreases from 4 X 10^{-12}* at 300°K to 2.5 X 10^{-12} cm^3/sec at 400°K. The decrease from 700°K to 1400°K is much smaller, viz. 1.5 X 10^{-12} to 1.3 X 10^{-12} cm^3/sec. (2); consider cases (1) and (2) of the previous section again. At 320 km $n(N_2)$ increases by a factor of approximately 10 from case (1) to (2). This results in an increase of an order of magnitude in the attachment coefficient β, as $\beta = \gamma n(N_2)$. The diffusion coefficient, on the other hand, decreases by a factor of 2. Therefore it is not the temperature dependence of the reaction rate that is responsible for the sensitivity of β to temperature, but rather the temperature dependence of the number densities.

* See Section 6.6. In the actual calculations γ was taken to be 4.0 X 10^{-12} cm^3/sec. (Donahue, 1966) and not 3.0 X 10^{-12} cm^3/sec. as given in equation 31 at 300°K.

110/.....

It is evident that similar results could be obtained for N if γ were made a constant and about 3.5 to 4 times lower than the currently accepted laboratory tested value. It is therefore concluded that either γ is dependent on T in a way similar to that presented here, or that it is a constant with a value 3 to 4 times lower than the currently accepted one.

The main conclusion drawn is that the temperature dependence of neither the diffusion coefficient nor the reaction rate is vital to the explanation of the observed variations in electron density that occur during MID's. It is evident that the changes in q and L with increase in T are due to change in atmospheric composition with expansion of the neutral gases.

7.4.3. The Production Rate.

The conclusions drawn above can be most readily demonstrated with the production rate in which the only temperature dependent quantities are the number densities. Figure 35 shows production rate profiles for a variety of values of T_∞ and b for $\chi = 45^\circ$, 60°, 75° and 80°. The rows illustrate the dependence of q on T for constant values of b and the columns for constant values of T_∞.

These curves show that as T increases, the height of maximum production (hq_{max}) increases and the maximum production rate decreases. For example, if we consider cases (1) and (2) of Section 7.4.1 again, at a height of 320 km q increases from 47 to 135 electrons/cm^3/sec.

111/.....

FIGURE 35.

This illustrates the effect of temperature change on the production rate for χ = 45°, 60°, 75° and 80°. The last line of the horizontal label should read '....IN ELECTRONS PER CC PER SECOND...' a represents T_∞.

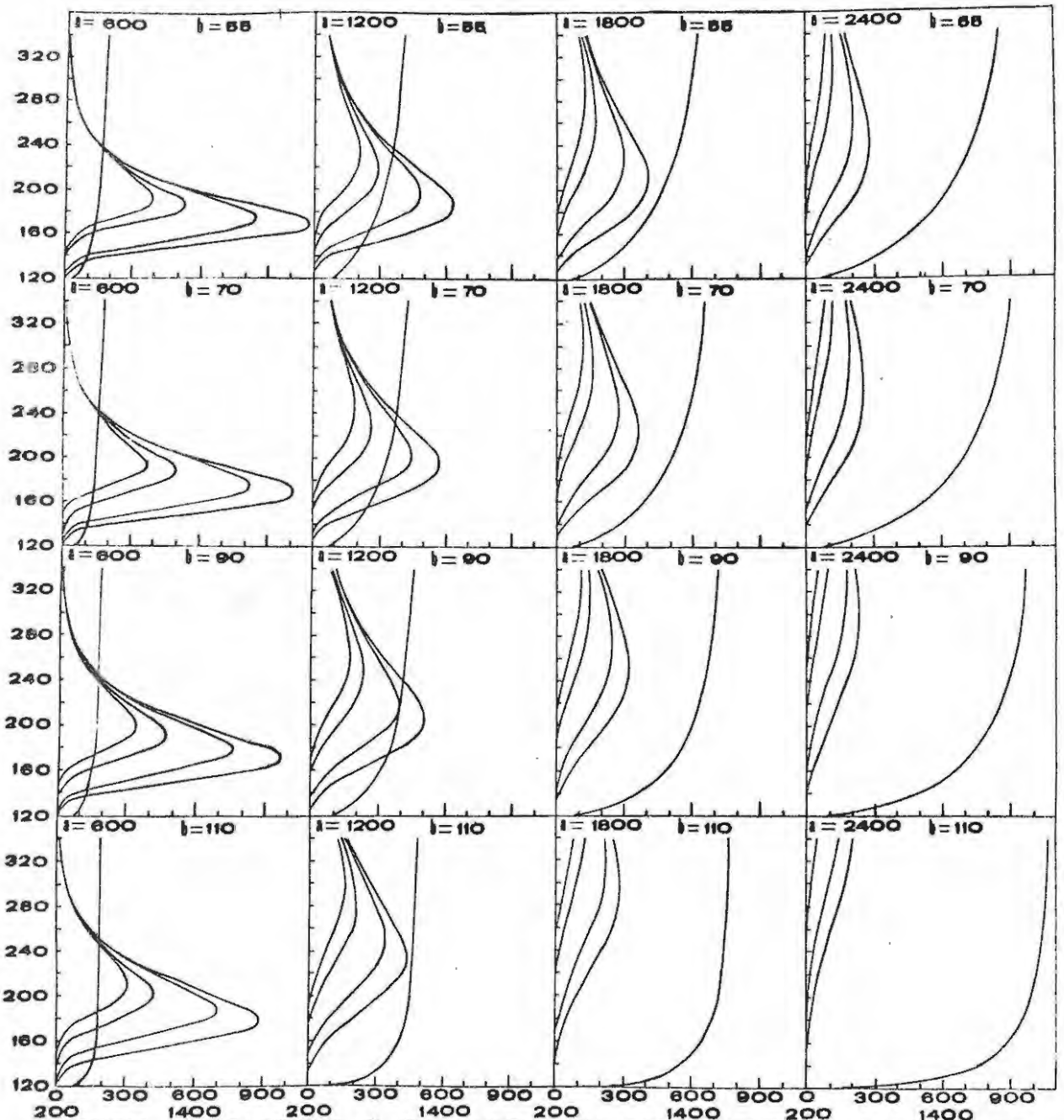

VERTICAL SCALE: HEIGHT IN KMS. HORIZONTAL SCALE: UPPER, PRODUCTION RATE IN ELECTRONS PER CC PER SECOND. LOWER, TEMPERATURE IN DEGREES KELVIN.

This increase in the production rate with temperature must be due to change in atmospheric composition, as the number densities are the only temperature dependent terms in equation (2). This is obviously due to redistribution of the gas with expansion over a more widespread area. Therefore, the result is an overall increase in production at altitudes above hq_{max} and a decrease below this height. The magnitude of the changes involved make it certain that the temperature dependence of q must have a profound effect on the resulting electron density distribution.

7.5 Case (2) of Section 6.7.

It was found that no significant changes occurred when the calculations were repeated using the alternative expression for the diffusion rate in Section 6.7. The approach was abandoned after trial calculations, as the involved equations only complicated the analysis further without yielding significant results.

7.6 The Effect of a Vertical Drift Velocity on the Electron Density Distribution.

An analysis has been started in which the effects of a vertical drift velocity on the electron density distribution are investigated. As a preliminary assesment, a rather arbitrary expression given by Yonezawa (1958) was used to represent the vertical drift of electrons,

$$V = V_o \exp \frac{m(z - z_o)}{H} \qquad (90)$$

where m is a parameter.

The preliminary results obtained indicated that an upward drift

112/.....

increased both N_{max} and $h(N_{max})$ and vice versa, as was found by Yonezawa. It was possible to find values for V_o and m in equation (90) which gave a much better fit near the peak of the curves shown in Figure 34. These results, however, have not been taken seriously, but constitute the beginning of another avenue of research.

7.7 Conclusions.

It has been shown that temperature changes have a remarkable effect on the electron density distribution in the F region of the ionosphere. It is certain from this analysis that changes in T of about 200°K at heights of about 150 km can easily account for the typical decreases in f_oF_2 observed during MID's. Whether energy required to produce increases in temperature of this magnitude could be supplied by electron influx is uncertain at present. It has been established that an i.d. always occurs when the p.e.f. is equal to or exceeds 2.3×10^4 electrons/cm^2/sec. This suggests that the energy input from electron influx must be large enough to cause the disturbances. If their energies are about 50 kev, the energy influx is about 2×10^{-3} ergs/cm^2/sec, which is about 0.005 of that from the UV flux (Watanabe and Hinteregger, 1962). Therefore, it is difficult to understand how such a large effect could be produced by such a small increase in the total energy flux. This is a problem which will have to be investigated in the future.

It has also been shown that it is unlikely that either diffusion or the temperature dependence of the reaction rate are responsible for

113/.....

the observed decreases in f_0F_2. The evidence strongly indicates that the variations in f_0F_2 are due to changes in atmospheric composition because of the temperature dependence of the number densities. This dependence is most evident in the loss and production rates, making these the dominant factors controlling the behaviour of the ionosphere. The results also suggest that either the accepted value for γ is too high or that γ must decrease with temperature.

7.8 Future Work.

Work to be done in the immediate future will involve inclusion of a corpuscular source of ionization in the production rate and an estimation of the heat input and temperature rise to be expected from typical observed p.e.f. intensities. This will be done using an approach based on that of Gledhill and van Rooyen (1963) and Rees (1963) for comparison with results of the type discussed above. Attention will also be given to resolving the present uncertainty in the reaction rate.

An attempt will then be made to calculate the diurnal and seasonal variations of f_0F_2 at locations along the L shells investigated in Part 1.

The main objective of the research will be to explain the day-time longitudinal variations of f_0F_2 observed along L shells of the outer radiation belt. Particular emphasis will be laid on estimating the reliability of CRPL data in regions far removed from ionospheric stations, with the view of producing better charts for radio prediction services. It is hoped that facilities will be available for the experimental confirmation of these calculations.

APPENDIX 1.

FORTRAN LISTING

```
*FANDK0806
C      PRECIPITATED AND TRAPPED ELECTRON FLUX AT L= 2, 3 AND 4
       DIMENSION LONGN(180),KUT(360),LSUM(360),IB(180),IA(360),LOST(360)
       DIMENSION CUT(360)
   627 FORMAT(I2)
   623 FORMAT(I4,F4.1,F5.3)
   625 FORMAT(I2)
   638 FORMAT(45H PRECIPITATED AND TRAPPED PROTON FLUX AT L=,F3.0///)
    99 FORMAT(62H SOUTHERN HEMISPHERE  NORTHERN HEMISPHERE PRECIPITATED
       TRAPPED/52H  LONG  PITCH ANGLE  LONG  PITCH ANGLE  N-H  S-H)
    87 FORMAT(3X,I4,5XF5.1,7XI4,5X,F5.1,3X,F5.2,2X,F5.2,2X,F7.2)
       READ 625, KKK
       DO 190 IJJ=1,KKK
       READ 627,IDG
   624 FORMAT(45H PRECIPITATED AND TRAPPED ELECTRON FLUX AT L=,F3.0///)
       K=18
       M=1
       DO 111 N=1,10
       READ 79,(LONGN(J),J=M,K)
       M=K+1
   111 K=K+18
       M=1
       K=14
       DO 211 N=1,25
```

115/.....

```
      READ 901,(CUT(J),J=M,K)
      M=K+1
  211 K=K+14
  901 FORMAT (14F5.3)
  902 FORMAT (10F5.3)
      READ 902,(CUT(J),J=351,360)
      READ 623,LONGS,EL,B100
   79 FORMAT (1814)
      IF(IDG)639,639,640
  639 PRINT 624,EL
      GO TO 641
  640 PRINT 638,EL
  641 PRINT 99
      LX=900
      I=1
      DO 900 J=1,360
      IF(CUT(J)-100)746,746,747
  746 KUT(J)=900
      CUT(J)=900
      GO TO 900
  747 CUT(J)=1800.*ATAN(SQRT(B100/CUT(J))/SQRT(1.-B100/CUT(J)))/3.1416
      KUT(J)=CUT(J)
      BCUT=KUT(J)
      IF(CUT(J)-(BCUT+0.5))900,900,812
  812 KUT(J)=KUT(J)+1
  900 CONTINUE
      DO 360 J=2,360,2
      IF(KUT(J)-KUT(J-1))8,360,360
    8 MB=KUT(J)
```

116/.....

```
      KUT(J)=KUT(J-1)
      IB(I)=J
      KUT(J-1)=MB
      I=I+1
  360 CONTINUE
      IGA=I-1
      LOST(1)=KUT(1)
      LSUM(1)=LX-KUT(1)
      MAX=KUT(1)
      LA=1
      DO 180 J=2,360
      IF(KUT(J)-KUT(J-1))1,1,2
    1 LSUM(J)=LX-KUT(J)+LSUM(J-1)
      LOST(J)=KUT(J)
      GO TO 170
    2 IF(KUT(J)-MAX)12,14,14
   14 MAX=KUT(J)
      LA=J
      LSUM(J)=(LX-KUT(J))*J
      GO TO 1000
   12 IF(KUT(J)-KUT(J-2))500,500,21
  500 LSUM(J)=LSUM(J-2)+(LX-KUT(J))*2
      GO TO 1000
   21 K=1
      DO 4 I=LA,J,2
      IF(KUT(J)-KUT(I))3,3,4
    3 IA(K)=I
      K=K+1
    4 CONTINUE
```

117/.....

```
      N=IA(K-2)
      LSUM(J)=LSUM(N)+(LX-KUT(J)*(J-N)
 1000 LOST(J)=LSUM(J-1)+LX-LSUM(J)
  170 CONTINUE
  180 CONTINUE
      DO 86 I=1,IGA
      J=B(I)
      MB=LOST(J)
      LOST(J)=LOST(J-1)
   86 LOST(J-1)=MB
      DO 190 J=2,360,2
      K=J/2
      L=J-1
      IF(IDG)628,628,629
  628 LONGS=LONGS+2
      IF(LONGS-360)311,212,311
  629 LONGS=LONGS-2
      IF(LONGS)311,331,311
  331 LONGS=360
      GO TO 311
  212 LONGS=0
  311 CONTINUE
      CCUT=LOST(J)
      BLOST=CUT(J)/10.
      CCUT=CCUT/900.
      CUTT=LOST(J-1)
      ALOST=CUT(J-1)/10.
      CUTT=CUTT/900.
      SUM=LSUM(J)
```

118/.....

```
      SUM=SUM/900.
      PRINT 87,LONGS,ALOST,LONG(K),BLOST,CCUT,CUTT,SUM
  190 CONTINUE
      END
```

---oo0oo---

* APPENDIX 2 *

PRECIPITATED AND TRAPPED ELECTRON FLUX AT L = 2 PRECIPITATED AND TRAPPED PROTON FLUX AT L = 2

SH = SOUTHERN HEMISPHERE
NH = NORTHERN HEMISPHERE
CPA = CRITICAL PITCH ANGLE
PEF = PRECIPITATED ELECTRON FLUX
TEF = TRAPPED ELECTRON FLUX

SH LONG	SH CPA	SH PEF	NH LONG	NH CPA	NH PEF	TEF	SH LONG	SH CPA	SH PEF	NH LONG	NH CPA	NH PEF	TEF
352	90.0	1.41	327	53.0	.59	0.00	358	90.0	1.40	358	53.2	.59	0.00
354	90.0	1.40	329	53.1	.59	0.00	356	90.0	1.40	355	53.2	.59	0.00
356	90.0	1.40	331	53.2	.59	0.00	354	90.0	1.40	352	53.1	.59	0.00
358	90.0	1.40	333	53.2	.59	0.00	352	90.0	1.41	350	53.0	.59	0.00
0	86.5	1.33	335	53.3	.59	.07	350	86.5	1.33	347	52.9	.58	.07
2	85.1	1.30	338	53.4	.59	.18	348	85.1	1.30	344	52.9	.58	.18
4	83.1	1.25	340	53.4	.59	.33	346	84.0	1.28	342	52.7	.58	.31
6	82.3	1.23	342	53.4	.59	.50	344	82.3	1.24	340	52.5	.58	.48
8	81.0	1.20	344	53.5	.59	.70	342	80.4	1.20	338	52.4	.58	.69
10	80.4	1.19	347	53.4	.59	.91	340	78.7	1.17	335	52.2	.58	.94
12	79.2	1.16	350	53.4	.59	1.15	338	77.3	1.14	333	5.19	.57	1.22
14	77.8	1.13	352	53.4	.59	1.42	336	75.7	1.10	331	51.9	.57	1.54
16	76.5	1.11	355	53.3	.59	1.72	334	74.3	1.07	329	51.7	.57	1.88
18	75.7	1.09	358	53.2	.59	2.03	332	73.0	1.05	327	51.5	.57	2.26
20	75.0	1.07	360	53.1	.59	2.37	330	71.8	1.02	325	51.5	.57	2.66
22	74.0	1.05	2	52.9	.58	2.72	328	71.0	1.00	323	51.4	.57	3.08
24	73.0	1.03	4	52.9	.58	3.10	326	69.7	.98	321	51.2	.57	3.53
26	72.4	1.02	8	52.6	.58	3.49	324	68.8	.96	319	51.2	.56	4.00
28	71.5	1.00	10	52.4	.58	3.90	322	67.9	.94	318	51.1	.56	4.49
30	71.0	.99	12	52.4	.58	4.32	320	67.0	.92	316	51.0	.56	5.00
32	70.2	.98	15	52.2	.58	4.75	318	66.2	.90	314	50.9	.56	5.53
34	69.7	.97	17	52.0	.57	5.20	316	65.3	.88	313	50.8	.56	6.08
36	68.8	.95	20	51.9	.57	5.67	314	64.4	.86	312	50.6	.56	6.65
38	68.1	.94	22	51.7	.57	6.16	312	63.5	.85	310	50.5	.56	7.23
40	67.5	.92	24	51.5	.57	6.66	310	62.9	.83	309	50.5	.56	7.83
42	66.6	.91	27	51.4	.57	7.18	308	62.1	.82	308	50.3	.56	8.45
44	65.7	.89	30	51.1	.56	7.72	306	61.5	.81	307	50.2	.55	9.08
46	64.9	.88	32	50.7	.56	8.27	304	61.0	.79	306	50.1	.55	9.73
48	64.1	.86	35	50.2	.55	8.85	302	60.3	.78	305	50.0	.55	10.39
50	63.1	.84	37	50.0	.55	9.44	300	59.6	.76	403	50.0	.55	11.06
52	62.3	.83	40	49.6	.55	10.06	298	59.1	.75	304	49.9	.55	11.75
54	61.4	.81	42	49.4	.54	10.70	296	58.6	.74	303	49.7	.55	12.45
56	60.7	.80	43	49.3	.54	11.35	294	58.2	.74	302	49.7	.55	13.15

119/.....

SH LONG	SH CPA	SH PEF	NH LONG	NH CPA	NH PEF	TEF	SH LONG	SH CPA	SH PEF	NH LONG	NH CPA	NH PEF	TEF
58	59.9	.78	45	49.1	.54	12.02	292	57.9	.73	301	49.6	.55	13.86
60	59.2	.77	47	48.9	.54	12.70	290	57.4	.72	300	49.6	.55	14.59
62	58.2	.75	50	48.4	.53	13.40	288	57.1	.71	299	49.5	.55	15.32
64	57.3	.73	52	48.1	.53	14.13	286	56.7	.71	298	49.3	.54	16.06
66	56.3	.72	53	48.0	.53	14.88	284	56.2	.70	297	49.2	.54	16.80
68	55.5	.70	55	47.8	.53	15.64	282	55.9	.69	296	49.1	.54	17.56
70	54.5	.68	57	47.5	.52	16.43	280	55.5	.68	296	49.0	.54	18.33
72	53.6	.66	59	47.3	.52	17.24	278	55.2	.68	295	48.9	.54	19.10
74	52.8	.65	61	47.0	.52	18.07	276	54.8	.67	294	48.8	.54	19.88
76	52.0	.63	63	46.7	.52	18.91	274	54.4	.66	293	48.7	.54	20.68
78	51.3	.62	65	46.6	.51	19.77	272	54.0	.66	292	48.5	.54	21.47
80	50.7	.61	68	46.3	.51	20.64	270	53.7	.65	292	48.5	.53	22.28
82	50.1	.60	70	46.1	.51	21.52	268	53.5	.65	291	48.4	.53	23.09
84	49.6	.59	72	46.0	.51	22.42	266	53.0	.64	290	48.3	.54	23.91
86	49.2	.58	74	45.8	.50	23.33	264	52.6	.63	289	48.3	.53	24.74
88	48.7	.57	77	45.6	.50	24.24	262	52.4	.62	288	48.2	.53	25.57
90	48.2	.56	80	45.4	.50	25.17	260	52.0	.62	287	48.1	.53	26.42
92	47.8	.55	82	45.2	.50	26.11	258	51.8	.61	286	48.0	.52	27.26
94	47.3	.55	84	45.1	.50	27.06	256	51.5	.61	285	47.8	.53	28.12
96	47.0	.54	87	44.8	.49	28.01	254	51.2	.60	284	47.8	.53	28.98
98	46.7	.54	90	44.7	.49	28.97	252	50.8	.60	282	47.6	.53	29.85
100	46.4	.53	93	44.6	.49	29.94	250	50.6	.59	281	47.6	.52	30.72
102	46.1	.53	96	44.5	.49	30.91	248	50.3	.59	280	47.6	.52	31.60
104	45.8	.52	99	44.4	.49	31.89	246	50.1	.58	279	47.5	.52	32.49
106	45.6	.52	102	44.4	.49	32.88	244	49.8	.58	278	47.5	.52	33.38
108	45.3	.51	104	44.3	.49	33.87	242	49.6	.57	277	47.5	.52	34.28
110	45.2	.51	107	44.4	.49	34.86	240	49.4	.57	276	47.5	.52	35.18
112	45.0	.50	110	44.4	.49	35.86	238	49.3	.56	274	47.5	.52	36.08
114	44.8	.50	113	44.5	.49	36.87	236	49.1	.56	272	47.5	.52	36.99
116	44.6	.49	116	44.6	.49	37.87	234	48.9	.55	271	47.5	.52	37.90
118	44.6	.49	118	44.7	.50	38.88	232	48.7	.55	270	47.5	.52	38.82
120	44.5	.49	121	44.9	.51	39.87	230	48.5	.55	268	47.6	.52	39.74
122	44.4	.49	124	45.1	.53	40.84	228	47.7	.53	267	47.6	.53	40.68
124	44.4	.49	126	45.4	.54	41.80	226	47.5	.52	265	47.7	.53	41.62
126	44.3	.49	128	45.6	.58	42.72	224	47.3	.52	264	47.8	.53	42.55
128	44.3	.49	131	46.0	.60	43.62	222	47.3	.52	263	47.8	.54	43.48
130	44.3	.49	133	46.3	.62	44.51	220	47.8	.53	261	48.0	.54	44.41
132	44.3	.49	135	46.6	.64	45.37	218	47.6	.53	260	48.1	.55	45.33
134	44.4	.49	138	46.9	.70	46.17	216	47.6	.52	258	48.3	.57	46.23
136	44.4	.49	140	47.2	.64	47.03	214	47.5	.52	256	48.4	.56	47.14
138	44.5	.49	143	47.6	.75	47.78	212	47.5	.52	255	48.6	.58	48.02
140	44.5	.49	146	47.9	.72	48.56	210	47.4	.52	254	48.7	.60	48.89
142	44.6	.49	149	48.3	.80	49.26	208	47.3	.52	252	48.9	.61	49.75
144	44.6	.49	152	48.7	.89	49.88	206	47.3	.52	251	49.1	.59	50.62
146	44.7	.49	154	49.1	.78	50.59	204	47.2	.52	249	49.3	.64	51.46
148	44.8	.49	157	49.4	.80	51.29	202	47.2	.52	248	49.4	.61	52.32
150	44.9	.50	159	49.6	.81	51.97	200	47.1	.52	246	49.6	.71	53.08
152	45.1	.50	162	50.0	.83	52.64	198	47.0	.52	244	49.8	.68	53.88
154	45.2	.50	166	50.5	1.01	53.12	196	47.0	.52	242	50.0	.64	54.71
156	45.3	.50	169	51.0	1.04	53.57	194	46.9	.52	240	50.1	.70	55.48
158	45.4	.50	172	51.3	.98	54.08	192	46.8	.52	238	50.3	.71	56.24
160	45.5	.50	175	51.6	.91	54.66	190	46.7	.52	236	50.5	.66	57.06
162	45.6	.50	178	51.9	.83	55.32	188	46.6	.51	234	50.7	.74	57.80
164	45.7	.50	180	52.0	.84	55.97	186	46.6	.51	232	50.8	.68	58.60

120/.....

SH LONG	SH CPA	SH PEF	NH LONG	NH CPA	NH PEF	TEF	SH LONGN	SH CPA	SH PEF	NH LONG	NH CPA	NH PEF	TEF
166	45.8	.50	183	52.1	.75	56.71	184	46.5	.51	230	50.9	.76	59.32
168	45.8	.51	186	52.2	.65	57.55	182	46.4	.51	228	51.1	.69	60.10
170	45.9	.51	189	52.1	.64	58.39	180	46.3	.51	226	51.2	.70	60.88
172	46.0	.51	192	52.0	.64	59.23	178	46.2	.51	224	51.3	.79	61.57
174	46.1	.51	195	51.7	.63	60.08	176	46.2	.51	222	51.5	.71	62.34
176	46.2	.51	198	51.5	.63	60.93	174	46.1	.51	220	51.7	.91	62.92
178	46.2	.51	201	51.3	.62	61.79	172	46.0	.51	217	52.0	.93	63.47
180	46.3	.51	203	51.2	.62	62.65	170	45.9	.51	215	52.1	.74	64.21
182	46.4	.51	206	51.1	.61	63.52	168	45.8	.51	212	52.2	.65	65.05
184	46.5	.51	208	50.9	.61	64.38	166	45.8	.50	210	52.1	.65	65.89
186	46.6	.51	210	50.8	.61	65.26	164	45.7	.50	208	52.0	.65	66.74
188	46.6	.51	212	50.7	.60	66.13	162	45.6	.50	206	51.9	.64	67.58
190	46.7	.52	215	50.5	.60	67.01	160	45.5	.50	203	51.6	.64	68.43
192	46.8	.52	217	50.3	.59	67.89	158	45.4	.50	201	51.3	.63	69.29
194	46.9	.52	220	50.1	.59	68.77	156	45.3	.50	198	51.0	.62	70.16
196	47.0	.52	222	50.0	.58	69.66	154	45.2	.50	195	50.5	.61	71.04
198	47.0	.52	224	49.8	.58	70.55	152	45.1	.50	192	50.0	.61	71.92
200	47.1	.52	226	49.6	.58	71.45	150	44.9	.50	189	49.6	.60	72.82
202	47.2	.52	228	49.4	.57	72.35	148	44.8	.49	186	49.4	.59	73.72
204	47.2	.52	230	49.3	.57	73.25	146	44.7	.49	183	49.1	.59	74.63
206	47.3	.52	232	49.1	.56	74.16	144	44.6	.49	180	48.7	.58	75.55
208	47.3	.52	234	48.9	.56	75.07	142	44.6	.49	178	48.3	.57	76.47
210	47.4	.52	236	48.7	.55	75.99	140	44.5	.49	175	47.9	.56	77.41
212	47.5	.52	238	48.6	.55	76.91	138	44.5	.49	172	47.6	.56	78.35
214	47.5	.52	240	48.4	.54	77.83	136	44.4	.49	169	47.2	.55	79.30
216	47.6	.52	242	48.3	.54	78.76	134	44.4	.49	166	46.9	.55	80.26
218	47.6	.53	244	48.1	.53	79.69	132	44.3	.49	162	46.6	.54	81.22
220	47.8	.53	246	48.0	.53	80.62	130	44.3	.49	159	46.3	.53	82.19
222	47.3	.52	248	47.8	.53	81.56	128	44.3	.49	157	46.0	.52	83.17
224	47.3	.52	249	47.8	.53	82.50	126	44.3	.49	154	45.6	.52	84.16
226	47.5	.52	251	47.7	.53	83.44	124	44.4	.49	152	45.4	.51	85.15
228	47.7	.53	252	47.6	.53	84.37	122	44.4	.49	149	45.1	.51	86.14
230	48.5	.65	254	47.6	.52	85.19	120	44.5	.49	146	44.9	.50	87.14
232	48.7	.60	255	47.5	.52	86.06	118	44.6	.49	143	44.7	.50	88.15
234	48.9	.58	256	47.5	.52	86.95	116	44.6	.49	140	44.6	.49	89.16
236	49.1	.62	258	47.5	.52	87.80	114	44.8	.50	138	44.5	.49	90.16
238	49.3	.63	260	47.5	.52	88.63	112	45.0	.53	135	44.4	.49	91.13
240	49.4	.61	261	47.5	.52	89.49	110	45.2	.53	133	44.4	.49	92.10
242	49.6	.71	263	47.5	.52	90.25	108	45.3	.53	131	44.3	.49	93.08
244	49.8	.67	264	47.5	.52	91.05	106	45.6	.56	128	44.4	.49	94.02
246	50.1	.75	265	47.5	.52	91.77	104	45.8	.59	126	44.4	.49	94.93
248	50.3	.71	267	47.6	.52	92.53	102	46.1	.61	124	44.5	.49	95.82
250	50.6	.79	268	47.6	.52	93.20	100	46.4	.63	121	44.6	.49	96.69
252	50.8	.74	270	47.6	.53	93.93	98	46.7	.61	118	44.7	.49	97.58
254	51.2	.84	271	47.8	.53	94.56	96	47.0	.66	116	44.8	.49	98.41
256	51.5	.86	272	47.8	.53	95.16	94	47.3	.73	113	45.1	.50	99.18
258	51.8	.89	274	48.0	.53	95.73	92	47.8	.75	110	45.2	.50	99.92
260	52.0	.91	276	48.1	.53	96.29	90	48.2	.84	107	45.4	.50	100.57
262	52.4	1.14	277	48.2	.53	96.61	88	48.7	.81	104	45.6	.50	101.24
264	52.6	1.26	278	48.3	.53	96.81	86	49.2	.90	102	45.8	.50	101.83
266	53.0	1.49	279	48.3	.53	96.78	84	49.6	.94	99	46.0	.51	102.37
268	53.5	1.51	280	48.4	.53	96.73	82	50.1	.98	96	46.1	.51	102.88
270	53.7	1.31	281	48.5	.53	96.88	80	50.7	1.01	93	46.3	.51	103.34
272	54.0	1.32	282	48.5	.54	97.01	78	51.3	1.22	90	46.6	.51	103.60

121/.....

SH LONG	SH CPA	SH PEF	NH LONG	NH CPA	NH PEF	TEF	SH LONG	SH CPA	SH PEF	NH LONG	NH CPA	NH PEF	TEF
274	54.4	1.34	284	48.7	.54	97.12	76	52.0	1.28	87	46.7	.52	103.79
276	54.8	1.58	285	48.8	.54	96.99	74	52.8	2.00	84	47.0	.52	103.27
278	55.2	1.60	286	48.9	.54	96.84	72	53.6	2.38	82	47.3	.52	102.36
280	55.5	1.38	287	49.0	.54	96.91	70	54.5	2.69	80	47.5	.52	101.14
282	55.9	1.64	288	49.1	.54	96.72	68	55.5	3.01	77	47.8	.53	99.80
284	56.2	1.66	289	49.2	.54	96.50	66	56.3	2.87	74	48.0	.53	98.19
286	56.7	1.93	290	49.3	.54	96.02	64	57.3	2.95	72	48.1	.53	96.70
288	57.1	1.45	291	49.5	.55	96.01	62	58.2	3.29	70	48.4	.53	94.87
290	57.4	1.72	292	49.6	.55	95.74	60	59.2	3.39	68	48.9	.54	92.93
292	57.9	1.74	292	49.6	.55	95.44	58	59.9	2.39	65	49.1	.54	91.99
294	58.2	1.76	293	49.7	.55	95.12	56	60.7	2.97	63	49.3	.54	90.46
296	58.6	1.52	294	49.7	.55	95.04	54	61.4	2.75	61	49.4	.54	89.16
298	59.1	2.07	295	49.9	.55	94.41	52	62.3	3.37	59	49.6	.55	87.24
300	59.6	2.09	296	50.0	.55	93.76	50	63.1	3.14	57	50.0	.55	85.54
302	60.3	2.67	296	50.0	.55	92.53	48	64.1	3.78	55	50.2	.55	83.20
304	61.0	2.71	297	50.1	.55	91.25	46	64.9	3.55	53	50.7	.56	81.08
306	61.5	2.48	298	50.2	.55	90.21	44	65.7	3.00	52	51.1	.56	79.51
308	62.1	2.51	299	50.3	.56	89.14	42	66.6	3.96	50	51.4	.57	76.97
310	62.9	3.13	300	50.5	.56	87.44	40	67.5	3.40	47	51.5	.57	74.99
312	63.5	2.59	301	50.5	.56	86.29	38	68.1	3.14	45	51.7	.57	73.28
314	64.4	3.22	302	50.6	.56	84.50	36	68.8	2.85	43	51.9	.57	71.84
316	65.3	3.57	303	50.8	.56	82.36	34	69.7	4.19	42	52.0	.57	69.07
318	66.2	3.94	304	50.9	.56	79.86	32	70.2	2.61	40	52.2	.58	67.87
320	67.0	3.38	304	51.0	.56	77.90	30	71.0	3.62	37	52.4	.58	65.66
322	67.9	3.43	305	51.1	.56	75.90	28	71.5	2.67	35	52.4	.58	64.40
324	68.8	3.81	306	51.2	.56	73.51	26	72.4	4.05	32	52.6	.58	61.76
326	69.7	4.20	307	51.2	.57	70.74	24	73.0	3.07	30	52.9	.58	60.10
328	71.0	5.27	308	51.4	.57	66.90	22	74.0	4.15	27	52.9	.58	57.35
330	71.8	3.69	309	51.5	.57	64.62	20	75.0	4.55	24	53.1	.59	54.20
332	73.0	5.11	310	51.5	.57	60.93	18	75.7	3.90	22	53.2	.59	51.71
334	74.3	5.21	312	51.7	.57	57.14	16	76.5	3.95	20	53.3	.59	49.16
336	75.7	6.35	313	51.9	.57	52.21	14	77.8	5.43	17	53.4	.59	45.13
338	77.3	6.84	314	51.9	.57	46.78	12	79.2	6.61	15	53.4	.59	39.92
340	78.7	6.23	316	52.2	.58	41.97	10	80.4	5.22	12	53.4	.59	36.10
342	80.4	7.05	318	52.4	.58	36.32	8	81.0	3.43	10	53.5	.59	34.08
344	82.3	8.70	319	52.5	.58	29.04	6	82.3	6.46	8	53.4	.59	29.02
346	84.0	7.72	321	52.7	.58	22.73	4	83.1	4.27	4	53.4	.59	26.15
348	85.1	5.51	323	52.9	.58	18.63	2	85.1	8.92	2	53.4	.59	18.63
350	86.5	6.74	325	52.9	.58	13.29	360	86.5	6.74	360	53.3	.59	13.29

PRECIPITATED AND TRAPPED ELECTRON FLUX AT L = 3

18	90.0	1.35	348	58.0	.64	0.00
20	90.0	1.35	350	58.1	.64	0.00
22	90.0	1.35	352	57.9	.64	0.00
24	90.0	1.35	354	57.8	.64	0.00
26	90.0	1.35	356	57.7	.64	0.00
28	86.8	1.28	358	57.6	.64	.07
30	84.5	1.24	360	57.5	.64	.19
32	83.7	1.22	2	57.5	.64	.33
34	82.9	1.20	5	57.4	.63	.48
36	81.1	1.16	8	57.3	.63	.68
38	79.6	1.13	12	57.2	.63	.91

PRECIPITATED AND TRAPPED PROTON FLUX AT L = 3

356	90.0	1.35	356	57.7	.64	0.00
354	90.0	1.35	354	57.8	.64	0.00
352	90.0	1.35	352	57.9	.64	0.00
350	90.0	1.35	350	58.1	.64	0.00
348	90.0	1.35	348	58.0	.64	0.00
346	86.8	1.28	347	57.9	.64	.07
344	85.5	1.25	345	57.9	.64	.17
342	85.5	1.25	344	57.9	.64	.27
340	83.7	1.21	342	57.8	.64	.41
338	82.9	1.20	340	57.7	.64	.56
336	82.3	1.18	339	57.6	.64	.73

122/.....

SH LONG	SH CPA	SH PEF	NH LONG	NH CPA	NH PEF	TEF
40	78.3	1.10	14	57.1	.63	1.17
42	77.2	1.08	17	56.9	.63	1.45
44	75.8	1.05	20	56.6	.62	1.77
46	74.6	1.03	22	56.4	.62	2.11
48	73.4	1.00	25	56.1	.62	2.48
50	71.9	.97	28	56.0	.62	2.88
52	70.3	.94	30	55.7	.61	3.31
54	68.9	.91	32	55.4	.61	3.78
56	67.6	.89	35	54.9	.61	4.28
58	66.2	.86	37	54.7	.60	4.81
60	65.2	.84	40	54.3	.60	5.36
62	64.0	.82	42	54.0	.60	5.93
64	62.8	.79	45	53.7	.59	6.54
66	61.6	.77	47	53.4	.59	7.16
68	60.5	.75	50	53.0	.58	7.82
70	59.5	.73	53	52.6	.58	8.49
72	58.5	.72	56	52.3	.58	9.19
74	57.6	.70	58	52.0	.57	9.91
76	56.9	.68	60	51.8	.57	10.64
78	56.1	.67	63	51.5	.57	11.40
80	55.4	.66	66	51.2	.57	12.16
82	54.9	.65	68	51.0	.56	12.94
84	54.1	.64	70	50.7	.56	13.74
86	53.5	.62	72	50.6	.56	14.55
88	53.0	.61	75	50.3	.56	15.37
90	52.5	.61	78	50.2	.55	16.20
92	52.0	.60	81	50.0	.55	17.04
94	51.6	.59	84	49.8	.55	17.89
96	51.2	.58	86	49.8	.55	18.75
98	50.8	.57	89	49.7	.55	19.62
100	50.5	.57	92	49.7	.55	20.50
102	50.2	.56	94	49.7	.55	21.38
104	49.8	.55	97	49.7	.55	22.28
106	49.4	.55	100	49.7	.55	23.17
108	49.1	.54	103	49.7	.55	24.07
110	48.8	.54	106	49.7	.56	24.96
112	48.6	.54	109	49.8	.56	25.85
114	48.4	.53	112	49.8	.58	26.73
116	48.2	.53	115	49.9	.58	27.61
118	48.0	.53	118	50.0	.57	28.50
120	47.9	.53	121	50.1	.59	29.36
122	47.8	.53	123	50.2	.62	30.20
124	47.7	.53	126	50.3	.58	31.09
126	47.6	.53	129	50.3	.61	31.94
128	47.6	.52	131	50.4	.62	32.79
130	47.6	.52	134	50.5	.62	33.63
132	47.6	.52	137	50.7	.67	34.43
134	47.6	.52	140	51.0	.72	35.18
136	47.6	.52	144	51.4	.74	35.91
138	47.6	.53	147	51.7	.81	36.57
140	47.7	.53	150	52.0	.78	37.26
142	47.7	.53	153	52.5	.85	37.87
144	47.7	.53	157	53.0	.94	38.39
146	47.8	.53	161	53.3	.84	39.01

SH LONG	SH CPA	SH PEF	NH LONG	NH CPA	NH PEF	TEF
334	80.1	1.14	337	57.5	.64	.95
332	78.7	1.11	336	57.4	.63	1.20
330	77.5	1.08	334	57.3	.63	1.48
328	75.8	1.04	332	57.2	.63	1.79
326	74.6	1.02	331	57.1	.63	2.14
324	73.4	1.00	329	56.9	.63	2.50
322	72.4	.98	328	56.8	.63	2.89
320	71.4	.95	327	56.7	.63	3.30
318	70.3	.93	325	56.5	.62	3.74
316	69.5	.91	324	56.4	.62	4.19
314	68.5	.89	323	56.3	.62	4.67
312	67.7	.88	322	56.1	.62	5.16
310	67.2	.87	320	55.9	.62	5.67
308	66.7	.86	318	55.7	.61	6.19
306	66.0	.85	317	55.6	.61	6.72
304	65.4	.83	316	55.5	.61	7.26
302	64.6	.82	315	55.3	.61	7.83
300	64.0	.81	313	55.0	.61	8.40
298	63.7	.80	312	54.9	.61	8.98
296	63.0	.79	311	54.8	.60	9.58
294	62.6	.78	309	54.5	.60	10.19
292	62.1	.77	308	54.4	.60	10.81
290	61.7	.77	307	54.1	.60	11.43
288	61.4	.76	305	53.9	.59	12.07
286	60.9	.75	304	53.7	.59	12.72
284	60.6	.75	303	53.7	.59	13.37
282	60.4	.74	302	53.6	.59	14.02
280	60.1	.74	301	53.4	.59	14.69
278	59.8	.73	300	53.3	.59	15.36
276	59.6	.73	299	53.2	.59	16.03
274	59.4	.73	298	53.1	.59	16.71
272	59.1	.72	297	52.9	.58	17.40
270	58.8	.71	297	52.9	.58	18.09
268	58.4	.71	296	52.8	.58	18.79
266	58.2	.71	295	52.7	.58	19.49
264	58.0	.70	294	52.6	.58	20.20
262	57.7	.70	293	52.5	.58	20.92
260	57.4	.69	292	52.4	.58	21.64
258	57.3	.69	291	52.3	.58	22.37
256	57.0	.68	291	52.3	.58	23.10
254	56.7	.68	290	52.1	.58	23.84
252	56.5	.67	289	52.0	.67	24.58
250	56.2	.67	289	52.0	.57	25.33
248	56.0	.66	288	51.9	.57	26.09
246	55.8	.66	287	51.8	.57	26.85
244	55.5	.66	286	51.7	.57	27.61
242	55.3	.65	284	51.6	.57	28.38
240	55.1	.65	284	51.6	.57	29.16
238	54.9	.64	283	51.5	.57	29.94
236	54.6	.64	282	51.4	.57	30.72
234	54.4	.63	281	51.4	.57	31.51
232	54.2	.63	280	51.2	.57	32.31
230	54.0	.63	279	51.2	.56	33.11
228	53.8	.63	278	51.0	.56	33.91

123/.....

SH LONG	SH CPA	SH PEF	NH LONG	NH CPA	NH PEF	TEF
148	47.8	.53	164	53.5	.85	39.62
150	47.9	.53	168	53.9	.87	40.21
152	47.9	.53	171	54.1	.89	40.79
154	48.0	.53	175	54.4	.91	41.34
156	48.0	.53	178	54.5	.75	42.05
158	48.1	.53	181	54.5	.67	42.84
160	48.1	.53	185	54.5	.67	43.62
162	48.2	.53	188	54.5	.67	44.41
164	48.3	.53	191	54.4	.67	45.20
166	48.4	.53	194	54.3	.66	45.99
168	48.5	.54	197	54.2	.66	46.78
170	48.6	.54	199	54.0	.66	47.58
172	48.7	.54	202	54.0	.65	48.38
174	48.8	.54	204	53.8	.65	49.18
176	48.9	.54	206	53.7	.65	49.99
178	49.0	.54	209	53.7	.64	50.80
180	49.1	.54	212	53.5	.64	51.60
182	49.2	.54	214	53.4	.63	52.42
184	49.4	.54	216	53.2	.63	53.23
186	49.4	.55	218	53.1	.63	54.05
188	49.5	.55	220	53.0	.62	54.87
190	49.6	.55	222	52.8	.62	55.70
192	49.6	.55	224	52.6	.61	56.53
194	49.7	.55	227	52.3	.61	57.36
196	49.7	.55	229	52.0	.60	58.20
198	49.8	.55	231	51.8	.59	59.05
200	49.8	.55	233	51.6	.59	59.91
202	49.9	.55	235	51.4	.58	60.76
204	50.0	.55	237	51.2	.58	61.63
206	50.0	.55	239	51.0	.57	62.49
208	50.2	.55	240	50.9	.57	63.36
210	50.2	.55	242	50.8	.57	64.23
212	50.3	.55	242	50.7	.57	65.10
214	50.3	.56	246	50.6	.56	65.98
216	50.4	.56	247	50.5	.56	66.85
218	50.5	.56	249	50.5	.56	67.73
220	50.5	.56	250	50.5	.56	68.60
222	50.7	.57	252	50.5	.56	69.47
224	50.7	.57	253	50.5	.56	70.33
226	50.8	.56	255	50.5	.56	71.20
228	50.9	.61	256	50.4	.56	72.03
230	51.0	.60	258	50.4	.56	72.86
232	51.2	.60	260	50.4	.56	73.70
234	51.4	.64	261	50.4	.56	74.49
236	51.6	.66	263	50.4	.56	75.27
238	51.7	.67	264	50.4	.56	76.03
240	52.0	.68	266	50.5	.56	76.78
242	52.2	.69	267	50.5	.56	77.52
244	52.3	.70	269	50.5	.56	78.25
246	52.5	.72	270	50.5	.56	78.97
248	52.8	.73	271	50.6	.56	79.67
250	53.0	.74	273	50.7	.56	80.36
252	53.1	.76	275	50.8	.56	81.04
254	53.4	.77	276	50.9	.56	81.70

SH LONG	SH CPA	SH PEF	NH LONG	NH CPA	NM PEF	TEF
226	53.6	.62	277	51.0	.56	34.72
224	53.4	.62	276	50.9	.56	35.53
222	53.1	.61	275	50.8	.56	36.35
220	53.0	.61	273	50.7	.56	37.17
218	52.8	.61	271	50.6	.56	38.00
216	52.5	.60	270	50.5	.56	38.83
214	52.3	.60	269	50.5	.56	39.66
212	52.2	.59	267	50.5	.56	40.50
210	52.0	.59	266	50.5	.56	41.35
208	51.7	.59	264	50.4	.56	42.20
206	51.6	.58	263	50.4	.56	43.05
204	51.4	.58	261	50.4	.56	43.91
202	51.2	.57	260	50.4	.56	44.77
200	51.0	.57	258	50.4	.56	45.64
198	50.9	.57	252	50.4	.56	46.50
196	50.8	.56	255	50.5	.56	47.37
194	50.7	.56	253	50.5	.56	48.24
192	50.7	.56	252	50.5	.56	49.12
190	50.5	.56	250	50.5	.56	49.99
188	50.5	.56	249	50.5	.56	50.87
186	50.4	.56	247	50.5	.56	51.74
184	50.3	.56	246	50.6	.56	52.62
182	50.3	.55	242	50.7	.59	53.47
180	50.2	.55	242	50.8	.57	54.34
178	50.2	.55	240	50.9	.61	55.17
176	50.0	.55	239	51.0	.57	56.04
174	50.0	.55	237	51.2	.63	56.84
172	49.9	.55	235	51.4	.65	57.63
170	49.8	.55	233	51.66	.66	58.41
168	49.8	.55	132	51.8	.68	59.18
166	49.7	.55	229	52.0	.74	59.88
164	49.7	.55	227	52.3	.77	60.55
162	49.6	.55	224	52.6	.79	61.21
160	49.6	.55	222	52.8	.75	61.90
158	49.5	.55	220	53.0	.69	62.66
156	49.4	.55	218	53.1	.77	63.34
154	49.4	.54	216	53.2	.71	64.08
152	49.2	.54	214	53.4	.71	64.81
150	49.1	.54	212	53.5	.80	65.46
148	49.0	.54	209	53.7	.73	66.18
146	48.9	.54	206	53.7	.74	65.89
144	48.8	.54	204	53.8	.74	67.60
142	48.7	.54	202	54.0	.75	68.31
140	48.6	.54	199	54.0	.76	69.00
138	48.5	.54	197	54.2	.87	69.59
136	48.4	.53	194	54.3	.66	70.39
134	48.3	.53	191	54.4	.89	70.96
132	48.2	.53	188	54.5	.79	71.63
130	48.1	.53	185	54.5	.67	72.42
128	48.1	.53	181	54.5	.67	73.20
126	48.0	.53	178	54.5	.67	73.99
124	48.0	.53	175	54.4	.67	74.78
122	47.9	.53	171	54.1	.67	75.57
120	47.9	.53	168	53.9	.66	76.38

124/.....

SH LONG	SH CPA	SH PEF	NH LONG	NH CPA	NH PEF	TEF	SH LONG	SH CPA	SH PEF	NH LONG	NH CPA	NH PEF	TEF
256	53.6	.78	277	51.0	.56	82.34	118	47.8	.53	164	53.5	.65	77.18
258	53.8	.89	278	51.0	.56	82.88	116	47.8	.53	161	53.3	.65	78.00
260	54.0	.72	279	51.2	.56	83.58	114	47.7	.53	157	53.0	.64	78.82
262	54.2	.94	280	51.2	.57	84.07	112	47.7	.53	153	52.5	.63	79.66
264	54.4	.74	281	51.4	.57	84.75	110	47.7	.53	150	52.0	.62	80.50
266	54.6	1.07	282	51.4	.57	85.11	108	47.6	.53	147	51.7	.62	81.35
268	54.9	1.05	283	51.5	.57	85.48	106	47.6	.52	144	51.4	.61	82.20
270	55.1	1.06	284	51.6	.57	85.84	104	47.6	.52	140	51.0	.60	83.07
272	55.3	1.07	285	51.6	.57	86.19	102	47.6	.52	137	50.7	.60	83.94
274	55.5	1.30	286	51.7	.57	86.31	100	47.6	.52	134	50.5	.59	84.82
276	55.8	1.09	287	51.8	.57	86.64	98	47.6	.52	131	50.4	.59	85.69
278	56.0	1.10	288	51.9	.57	86.95	96	47.6	.53	129	50.3	.59	86.57
280	56.2	1.34	289	52.0	.57	87.03	94	47.7	.53	126	50.3	.58	87.46
282	56.5	1.35	289	52.0	.57	87.09	92	47.8	.53	123	50.2	.58	88.34
284	56.7	.90	290	52.1	.58	87.60	90	47.9	.53	121	50.1	.58	89.22
286	57.0	1.38	291	52.3	.58	87.64	88	48.0	.53	118	50.0	.57	90.11
288	57.3	1.39	291	52.3	.58	87.66	86	48.2	.53	115	49.9	.57	91.00
290	57.4	1.17	292	52.4	.58	87.91	84	48.4	.53	112	49.8	.57	91.89
292	57.7	1.42	293	52.5	.58	87.90	82	48.6	.54	109	49.8	.56	92.79
294	58.0	1.43	294	52.6	.58	87.88	80	48.8	.54	106	49.7	.56	93.68
296	58.2	1.20	295	52.7	.58	88.09	78	49.1	.54	103	49.7	.55	94.58
298	58.4	1.21	296	52.8	.58	88.29	76	49.4	.55	100	49.7	.55	95.47
300	58.8	1.47	297	52.9	.58	88.23	74	49.8	.55	97	49.7	.55	96.36
302	59.1	1.49	297	52.9	.58	88.15	72	50.2	.62	94	49.7	.55	97.18
304	59.4	1.50	298	53.1	.59	88.05	70	50.5	.64	92	49.7	.55	97.98
306	59.6	1.51	299	53.2	.59	87.94	68	50.8	.72	89	49.7	.55	98.71
308	59.8	1.26	300	53.3	.59	88.08	66	51.2	.75	86	49.8	.55	99.40
310	60.1	1.27	301	53.4	.59	88.22	64	51.6	.77	84	49.8	.55	100.07
312	60.4	1.82	302	53.6	.59	87.80	62	52.0	.80	81	50.0	.55	100.71
314	60.6	1.29	303	53.7	.59	87.90	60	52.5	.89	78	50.2	.55	101.26
316	60.9	1.30	304	53.7	.59	88.00	58	53.0	.85	75	50.3	.56	101.84
318	61.4	2.15	305	53.9	.59	87.24	56	53.5	1.02	72	50.6	.56	102.26
320	61.7	1.89	307	54.1	.60	86.75	54	54.1	1.07	70	50.7	.56	102.62
322	62.1	1.91	308	54.4	.60	86.23	52	54.9	1.57	68	51.0	.56	102.48
324	62.6	2.22	309	54.5	.60	85.40	50	55.4	1.93	66	51.2	.57	101.98
326	63.0	1.95	311	54.8	.60	84.84	48	56.1	2.21	63	51.5	.57	101.19
328	63.7	2.86	312	54.9	.61	83.37	46	56.9	2.28	60	51.8	.57	100.33
330	64.0	1.69	313	55.0	.61	83.06	44	57.6	2.59	58	52.0	.57	99.16
332	64.6	2.62	315	55.3	.61	81.82	42	58.5	2.93	56	52.3	.58	97.64
334	65.4	2.95	316	55.5	.61	80.25	40	59.5	3.30	53	52.6	.58	95.74
336	66.0	2.99	317	55.6	.61	78.63	38	60.5	3.42	50	53.0	.58	93.73
338	66.7	2.72	318	55.7	.61	77.28	36	61.6	3.83	47	53.4	.59	91.30
340	67.2	2.75	320	55.9	.62	75.91	34	62.8	3.94	45	53.7	.59	88.76
342	67.7	2.46	322	56.1	.62	74.82	32	64.0	4.63	42	54.0	.60	85.53
344	68.5	3.13	323	56.3	.62	73.06	30	65.2	4.46	40	54.3	.60	82.46
346	69.5	4.15	324	56.4	.62	70.28	28	66.2	3.62	37	54.7	.60	80.23
348	70.3	3.87	325	56.5	.62	67.77	26	67.6	5.27	35	54.9	.61	76.35
350	71.4	4.60	327	56.7	.63	64.54	24	68.9	5.08	32	55.4	.61	72.65
352	72.4	4.32	328	56.8	.63	61.59	22	70.3	5.83	30	55.7	.61	68.20
354	73.4	4.37	329	56.9	.63	58.58	20	71.9	6.28	28	56.0	.62	63.29
356	74.6	4.78	331	57.1	.63	55.15	18	73.4	6.06	25	56.1	.62	58.60
358	75.8	5.20	332	57.2	.63	51.31	16	74.6	4.79	22	56.4	.62	55.18
0	77.5	7.41	334	57.3	.63	45.26	14	75.8	5.21	20	56.6	.62	51.34
2	78.7	5.38	336	57.4	.63	41.23	12	77.2	5.99	17	56.9	.63	46.70

125/.....

SH LONG	SH CPA	SH PEF	NH LONG	NH CPA	NH PEF	TEF
4	80.1	5.82	337	57.5	.64	36.76
6	82.3	9.23	339	57.6	.64	28.89
8	82.9	3.78	340	57.7	.64	26.46
10	83.7	3.83	342	57.8	.64	23.99
12	85.5	8.07	344	57.9	.64	17.27
14	85.5	1.25	345	57.9	.64	17.37
16	86.8	6.28	347	57.9	.64	12.44

PRECIPITATED AND TRAPPED ELECTRON FLUX AT L = 4

30	89.7	1.28	351	64.2	.71	0.00
32	89.0	1.26	353	64.2	.71	.02
34	88.2	1.24	356	64.1	.71	.06
36	87.3	1.22	358	64.0	.71	.12
38	85.9	1.19	360	64.0	.71	.22
40	85.0	1.18	4	63.8	.70	.33
42	83.7	1.15	7	63.7	.70	.47
44	82.3	1.12	9	63.5	.70	.64
46	80.6	1.08	12	63.3	.70	.85
48	78.3	1.03	14	63.2	.70	1.11
50	77.6	1.02	17	62.8	.69	1.38
52	76.2	.99	20	62.6	.69	1.69
54	75.0	.97	22	62.3	.69	2.02
56	73.5	.94	25	62.0	.68	2.39
58	72.0	.91	28	61.7	.68	2.79
60	70.8	.89	31	61.3	.68	3.22
62	69.5	.86	33	61.0	.67	3.67
64	68.2	.84	36	60.6	.67	4.16
66	67.8	.83	39	60.2	.66	4.65
68	65.8	.80	42	59.5	.66	5.19
70	64.6	.78	45	58.6	.65	5.75
72	63.7	.77	47	57.9	.64	6.34
74	62.8	.76	50	57.2	.63	6.94
76	62.0	.74	53	56.8	.63	7.56
78	61.2	.73	56	56.6	.62	8.20
80	60.6	.72	59	56.4	.62	8.86
82	59.8	.70	62	56.3	.62	9.53
84	59.2	.69	65	56.2	.62	10.21
86	58.5	.67	68	56.2	.62	10.91
88	57.9	.66	71	56.2	.62	11.62
90	57.3	.64	74	56.2	.62	12.35
92	56.5	.63	77	56.2	.62	13.10
94	55.4	.61	80	56.2	.63	13.85
96	54.2	.60	83	56.2	.64	14.60
98	53.5	.59	86	56.2	.65	15.35
100	53.5	.59	90	56.2	.65	16.10
102	53.5	.59	93	56.2	.65	16.85
104	53.5	.59	96	56.2	.65	17.60
106	53.5	.59	99	56.2	.65	18.35
108	53.5	.59	102	56.2	.65	19.10
110	53.3	.59	106	56.2	.65	19.86
112	53.1	.59	109	56.2	.65	20.61
114	52.7	.58	112	56.2	.66	21.36

SH LONG	SH CPA	SH PEF	NH LONG	NH CPA	NH PEF	TEF
10	78.3	5.36	14	57.1	.63	42.70
8	79.6	5.80	12	57.2	.63	38.26
6	81.1	6.25	8	57.3	.63	33.37
4	82.9	8.18	5	57.4	.63	26.54
2	83.7	3.83	2	57.5	.64	24.07
360	84.5	4.64	360	57.5	.64	20.79
358	86.8	9.70	358	57.6	.64	12.44

PRECIPITATED AND TRAPPED ELECTRON FLUX AT L = 4

116	52.3	.58	116	56.2	.66	22.11
118	52.0	.57	119	56.2	.67	22.86
120	51.9	.57	122	56.2	.67	23.61
122	51.9	.57	126	56.2	.67	24.36
124	51.8	.57	129	56.2	.67	25.11
126	51.8	.57	133	56.2	.67	25.86
128	51.8	.57	136	56.2	.67	26.62
130	51.8	.57	140	56.2	.67	27.37
132	51.7	.57	143	56.5	.80	27.98
134	51.7	.57	146	56.7	.77	28.63
136	51.7	.57	150	57.1	.89	29.17
138	51.7	.57	154	57.6	.96	29.62
140	51.7	.57	158	58.3	1.11	29.93
142	51.8	.57	161	58.6	.90	30.45
144	51.8	.57	165	58.4	.72	31.15
146	51.9	.57	168	58.2	.71	31.86
148	51.9	.57	172	58.2	.71	32.56
150	52.0	.57	175	58.5	.73	33.25
152	52.1	.57	179	59.0	1.03	33.63
154	52.2	.58	183	58.9	.72	34.32
156	52.3	.58	187	58.8	.72	35.02
158	52.4	.58	190	58.8	.72	35.71
160	52.4	.58	193	58.9	.73	36.40
162	52.5	.58	196	59.1	.82	36.99
164	52.5	.58	200	59.1	.73	37.68
166	52.6	.58	203	58.9	.72	38.37
168	52.7	.58	206	58.7	.71	39.06
170	52.8	.58	210	58.4	.71	39.77
172	52.8	.58	213	58.1	.70	40.48
174	52.9	.58	216	57.8	.69	41.19
176	52.9	.58	220	57.3	.68	41.92
178	53.0	.58	221	57.2	.68	42.65
180	53.2	.59	222	57.0	.67	43.38
182	53.2	.59	224	56.8	.67	44.12
184	53.3	.59	226	56.5	.66	44.86
186	53.3	.59	228	56.3	.65	45.61
188	53.4	.59	231	56.2	.65	46.36
190	53.5	.59	233	56.2	.65	47.11
192	53.6	.59	235	56.2	.65	47.86
194	53.7	.59	237	56.2	.65	48.62
196	53.8	.59	239	56.2	.65	49.37
198	54.0	.60	241	56.2	.64	50.12
200	54.2	.60	243	56.2	.64	50.87

126/.....

SH LONG	SH CPA	SH PEF	NH LONG	NH CPA	NH PEF	TEF
204	54.3	.60	247	56.2	.64	52.37
206	54.4	.60	249	56.2	.64	53.12
208	54.4	.60	250	56.2	.64	53.87
210	54.5	.60	252	56.2	.64	54.62
212	54.5	.60	254	56.2	.64	55.38
214	54.5	.60	256	56.2	.64	56.13
216	54.5	.60	257	56.2	.64	56.88
218	54.5	.60	259	56.2	.64	57.63
220	54.5	.60	260	56.2	.64	58.38
222	54.6	.60	262	56.2	.64	59.13
224	54.7	.60	263	56.2	.64	59.88
226	54.8	.60	265	56.2	.64	60.63
228	54.9	.61	266	56.2	.63	61.38
230	55.1	.61	267	56.2	.63	62.14
232	55.3	.61	269	56.2	.63	62.89
234	55.6	.61	270	56.2	.63	63.64
236	55.9	.62	271	56.2	.62	64.39
238	56.2	.62	272	56.2	.62	65.14
240	56.4	.74	274	56.2	.62	65.77
242	56.5	.69	275	56.2	.62	66.45
244	56.7	.76	276	56.2	.62	67.06
246	56.7	.63	277	56.2	.62	67.80
248	56.6	.63	278	56.2	.62	68.54
250	56.8	.71	279	56.2	.62	69.20
252	57.1	.88	280	56.2	.62	69.70
254	57.6	1.08	281	56.2	.62	69.99
256	58.2	1.21	282	56.2	.62	70.15
258	58.6	1.06	282	56.2	.62	70.46
260	58.7	.78	283	56.2	.62	71.06
262	58.9	.89	284	56.2	.62	71.54
264	59.0	.79	285	56.3	.62	72.12
266	59.2	1.00	285	56.3	.62	72.50
268	59.4	1.10	286	56.3	.62	72.77
270	59.5	.90	287	56.4	.62	73.24
272	59.7	1.11	287	56.4	.62	73.49
274	59.8	.91	288	56.5	.62	73.95
276	60.0	1.13	289	56.5	.62	74.19
278	60.1	.92	289	56.5	.62	74.64
280	60.3	1.15	290	56.6	.62	74.86
282	60.5	1.15	291	56.7	.63	75.07
284	60.7	1.17	291	56.7	.63	75.27
286	60.8	.94	292	56.8	.63	75.69
288	60.9	.95	292	56.8	.63	76.10
290	61.2	1.42	292	56.9	.63	76.04
292	61.5	1.44	293	56.9	.63	75.96
294	61.7	1.21	293	57.0	.63	76.11
296	62.0	1.47	294	57.0	.63	76.01
298	62.4	1.74	294	57.0	.63	75.63
300	62.7	1.50	294	57.0	.63	75.49
302	62.9	1.26	294	57.1	.63	75.59
304	63.1	1.27	295	57.2	.63	75.68
306	63.3	1.28	296	57.3	.63	75.76
308	63.8	2.08	296	57.3	.63	75.04
310	63.8	.78	297	57.4	.63	75.62
312	64.0	1.31	297	57.4	.63	75.66
314	64.3	1.59	298	57.5	.63	75.43
316	64.5	1.33	299	57.6	.64	75.45
318	64.8	1.62	299	57.7	.64	75.19
320	65.1	1.63	300	57.9	.64	74.91
322	65.5	1.93	301	58.0	.64	74.33
324	65.8	1.66	301	58.0	.64	74.02
326	66.1	1.68	302	58.2	.64	73.69
328	66.3	1.40	303	58.3	.64	73.64
330	66.8	2.29	304	58.5	.65	72.70
332	67.2	2.01	305	58.7	.65	72.04
334	67.5	1.73	306	58.9	.65	71.65
336	68.0	2.34	307	59.0	.65	70.64
338	68.3	1.76	308	59.3	.65	70.22
340	68.7	2.09	309	59.4	.66	69.46
342	69.1	2.10	310	59.6	.66	68.69
344	69.5	2.12	312	60.0	.66	67.90
346	70.0	2.46	313	60.2	.66	66.77
348	70.2	1.52	314	60.5	.67	66.58
350	71.0	3.46	315	60.6	.67	64.43
352	71.6	2.86	317	61.0	.67	62.90
354	72.3	3.22	318	61.2	.68	61.00
356	73.0	3.25	320	61.5	.68	59.06
358	74.0	2.20	321	61.7	.68	56.07
0	74.5	2.65	323	62.0	.68	54.72
2	75.3	3.70	324	62.2	.69	52.32
4	76.3	4.44	326	62.5	.69	49.18
6	77.2	4.15	328	62.7	.69	46.32
8	77.4	1.72	329	62.8	.69	45.90
10	79.4	8.19	331	63.0	.70	39.01
12	80.5	5.04	333	63.3	.70	35.26
14	81.9	6.21	335	63.5	.70	30.34
16	83.4	6.67	337	63.7	.70	24.96
18	85.0	7.14	339	63.8	.70	19.10
20	86.5	6.89	341	63.9	.71	13.50
22	87.9	6.60	343	64.0	.71	8.18
24	89.0	5.53	345	64.1	.71	3.94
26	89.8	4.43	347	64.2	.71	.79
28	90.0	2.08	349	64.2	.71	0.00

127/.....

PRECIPITATED AND TRAPPED ELECTRON FLUX AT L = 1.5

SH LONG	SH CPA	SH PEF	NH LONG	NH CPA	NH PEF	TEF
332	90.0	1.40	318	53.6	.59	0.00
334	90.0	1.40	320	53.6	.59	0.00
336	90.0	1.40	321	53.6	.59	0.00
338	90.0	1.40	323	53.6	.59	0.00
340	90.0	1.40	325	53.6	.59	0.00
342	90.0	1.40	326	53.6	.59	0.00
344	84.9	1.29	327	53.5	.59	.11
346	82.9	1.24	329	53.4	.59	.26
348	81.3	1.21	331	53.3	.59	.46
350	80.0	1.18	333	53.2	.59	.68
352	78.8	1.16	334	53.1	.59	.93
354	77.3	1.12	336	52.9	.58	1.21
356	76.0	1.10	338	52.7	.58	1.52
358	75.2	1.08	340	52.6	.58	1.85
0	73.7	1.05	342	52.4	.58	2.21
2	72.7	1.03	344	52.2	.58	2.60
4	72.0	1.02	346	52.0	.57	2.99
6	71.1	1.00	348	51.9	.57	3.41
8	70.0	.98	350	51.7	.57	3.86
10	69.5	.97	351	51.6	.57	4.31
12	68.7	.95	353	51.4	.57	4.78
14	68.0	.94	354	51.2	.57	5.27
16	67.5	.93	356	51.0	.56	5.77
18	66.6	.91	358	50.9	.56	6.29
20	66.2	.90	1	50.7	.56	6.82
22	65.8	.90	5	50.6	.56	7.35
24	65.2	.88	10	50.4	.56	7.90
26	64.8	.88	14	50.2	.55	8.46
28	64.4	.87	16	50.1	.55	9.03
30	64.2	.87	19	49.8	.55	9.60
32	63.7	.86	21	49.6	.55	10.19
34	63.3	.85	24	49.4	.54	10.78
36	62.9	.85	26	49.2	.54	11.38
38	62.6	.84	28	48.9	.54	11.99
40	62.3	.84	30	48.7	.54	12.60
42	61.9	.83	32	48.4	.53	13.23
44	61.5	.83	34	48.2	.53	13.86
46	61.1	.82	36	48.0	.53	14.50
48	60.7	.81	38	47.8	.53	15.15
50	60.2	.81	40	47.6	.53	15.81
52	59.7	.79	43	47.4	.52	16.48
54	59.1	.79	45	47.2	.52	17.17
56	58.3	.77	47	47.0	.52	17.87
58	57.8	.76	49	46.8	.52	18.59
60	57.0	.75	52	46.7	.51	19.32
62	56.2	.73	54	46.5	.51	20.07
64	55.4	.71	56	46.3	.51	20.83
66	54.6	.70	58	46.1	.51	21.62
68	53.8	.68	60	45.9	.51	22.42
70	53.0	.66	62	45.7	.50	23.25
72	52.3	.65	63	45.5	.50	24.08
74	51.6	.64	65	45.3	.50	24.94

PRECIPITATED AND TRAPPED PROTON FLUX AT L = 1.5

SH LONG	SH CPA	SH PEF	NH LONG	NH CPA	NH PEF	TEF
330	90.0	1.40	299	53.6	.59	0.00
328	90.0	1.40	298	53.6	.59	0.00
326	90.0	1.40	296	53.6	.59	0.00
324	90.0	1.40	295	53.6	.59	0.00
322	90.0	1.40	294	53.6	.59	0.00
320	90.0	1.40	293	53.6	.59	0.00
318	84.9	1.29	292	53.5	.59	.11
316	82.9	1.24	291	53.5	.59	.26
314	81.3	1.21	290	53.5	.59	.46
312	79.4	1.17	289	53.4	.59	.69
310	78.3	1.14	288	53.4	.59	.95
308	76.8	1.11	287	53.3	.59	1.24
306	76.0	1.09	285	53.2	.59	1.56
304	74.4	1.06	284	53.0	.58	1.90
302	73.0	1.03	283	52.9	.58	2.28
300	71.7	1.00	282	52.8	.58	2.68
298	70.5	.98	281	52.6	.58	3.12
296	69.5	.96	280	52.4	.58	3.57
294	68.5	.94	278	52.4	.58	4.05
292	67.1	.91	276	52.2	.58	4.56
290	66.0	.88	275	52.0	.57	5.09
288	65.2	.87	274	51.7	.57	5.64
286	64.4	.85	273	51.5	.57	6.21
284	63.7	.84	271	51.2	.57	6.80
282	62.9	.83	270	50.9	.56	7.40
280	62.3	.82	268	50.6	.56	8.01
278	61.6	.81	267	50.2	.55	8.64
276	61.0	.79	265	50.0	.55	9.28
274	60.2	.78	264	49.8	.55	9.94
272	59.7	.77	262	49.5	.55	10.62
270	59.1	.76	260	49.3	.54	11.30
268	58.6	.75	259	49.2	.54	12.00
266	58.2	.74	257	49.0	.54	12.71
264	57.8	.74	255	48.9	.54	13.42
262	57.3	.73	254	48.8	.54	14.15
260	56.8	.72	252	48.7	.54	14.86
258	56.3	.71	250	48.7	.54	15.63
256	55.9	.70	248	48.6	.54	16.39
254	55.4	.69	246	48.5	.54	17.16
252	54.9	.68	244	48.4	.53	17.94
250	54.5	.67	242	48.4	.53	18.72
248	54.0	.66	240	48.4	.53	19.52
246	53.6	.65	238	48.5	.54	20.33
244	53.1	.64	235	48.5	.54	21.15
242	52.6	.63	233	48.6	.54	21.98
240	52.3	.62	230	48.6	.54	22.82
238	51.9	.61	228	48.7	.54	23.66
236	51.6	.60	226	48.8	.54	24.52
234	51.2	.59	223	48.9	.54	25.38
232	51.0	.58	221	49.0	.54	26.24
230	50.7	.58	219	49.1	.54	27.12
228	50.6	.57	217	49.2	.54	27.99

128/.....

SH LONG	SH CPA	SH PEF	NH LONG	NH CPA	NH PEF	TEF
76	51.0	.63	67	45.2	.50	25.80
78	50.6	.62	69	44.9	.50	26.68
80	49.8	.60	71	44.7	.49	27.57
82	49.2	.59	73	44.6	.49	28.48
84	48.5	.58	75	44.4	.49	29.40
86	48.0	.57	77	44.3	.49	30.33
88	47.6	.56	79	44.2	.56	31.27
90	47.1	.55	81	44.1	.49	32.22
92	46.7	.55	84	44.0	.48	33.18
94	46.3	.54	86	43.9	.48	34.15
96	46.1	.54	89	43.8	.48	35.12
98	45.7	.53	91	43.7	.48	36.11
100	45.5	.52	94	43.7	.48	37.09
102	45.3	.52	97	43.7	.48	38.09
104	45.1	.51	99	43.7	.48	39.08
106	44.9	.51	101	43.7	.48	40.08
108	44.8	.50	103	43.8	.48	41.09
110	44.7	.50	106	43.9	.48	42.09
112	44.6	.50	108	44.0	.48	43.10
114	44.5	.49	110	44.1	.49	44.11
116	44.4	.49	112	44.2	.49	45.13
118	44.3	.49	114	44.4	.49	46.14
120	44.2	.50	116	44.5	.50	47.14
122	44.2	.49	119	44.7	.52	48.12
124	44.1	.49	121	44.9	.54	49.08
126	44.1	.49	124	45.2	.55	50.03
128	44.1	.49	126	45.4	.60	50.94
130	44.1	.49	128	45.6	.55	51.89
132	44.1	.49	130	45.9	.63	52.76
134	44.1	.49	132	46.1	.65	53.62
136	44.1	.49	134	46.3	.63	54.50
138	44.1	.49	137	46.5	.64	55.36
140	44.1	.49	140	46.8	.65	56.22
142	44.2	.49	143	47.0	.66	57.07
144	44.2	.49	146	47.3	.73	57.84
146	44.4	.49	149	47.6	.81	58.53
148	44.5	.49	152	48.0	.77	59.26
150	44.6	.49	154	48.3	.86	59.90
152	44.7	.49	156	48.7	.80	60.60
154	44.8	.49	158	49.1	.90	61.20
156	44.9	.50	160	49.5	1.01	61.69
158	45.1	.50	162	50.0	1.04	62.14
160	45.2	.50	164	50.4	.88	62.76
162	45.3	.50	166	50.9	1.08	63.16
164	45.4	.50	169	51.4	1.12	63.54
166	45.5	.50	171	51.7	1.04	63.98
168	45.6	.50	173	52.1	.96	64.51
170	45.7	.50	176	52.3	.86	65.14
172	45.9	.51	178	52.6	1.10	65.52
174	46.0	.51	180	52.9	1.00	66.00
176	46.7	.52	182	53.1	.77	66.70
178	46.8	.52	184	53.3	.90	67.28
180	46.3	.51	186	53.4	.79	67.97
182	46.5	.51	189	53.5	.79	68.66

SH LONG	SH CPA	SH PEF	NH LONG	NH CPA	NH PEF	TEF
226	50.4	.57	214	49.5	.55	28.87
224	50.2	.56	211	49.6	.55	29.76
222	49.9	.55	209	49.8	.55	30.64
220	49.7	.55	206	50.0	.56	31.53
218	49.5	.55	204	50.2	.57	32.41
216	49.2	.54	202	50.4	.59	33.27
214	49.1	.54	199	50.6	.60	34.12
212	48.9	.54	196	50.7	.62	34.96
210	48.8	.54	194	50.9	.61	35.80
208	48.7	.54	192	51.1	.67	36.59
206	48.5	.54	189	51.3	.66	37.38
204	48.4	.53	186	51.5	.64	38.21
202	48.2	.53	184	51.6	.68	38.98
200	48.1	.53	182	51.8	.69	39.75
198	48.0	.53	180	52.0	.66	40.55
196	47.9	.53	178	52.2	.72	41.30
194	47.8	.53	176	52.4	.73	42.04
192	47.7	.53	173	52.4	.69	42.82
190	47.6	.52	171	52.6	.75	43.53
188	47.5	.52	169	52.8	.76	44.24
186	47.4	.52	166	52.9	.71	45.00
184	47.3	.52	164	53.0	.65	45.82
182	47.2	.52	162	53.1	.72	46.57
180	47.0	.52	160	53.2	.73	47.32
178	47.0	.52	158	53.3	.73	48.06
176	46.8	.52	156	53.4	.74	48.80
174	46.7	.52	154	53.4	.66	49.61
172	46.6	.51	152	53.4	.66	50.43
170	46.5	.51	149	53.5	.75	51.16
168	46.3	.51	146	53.4	.67	51.97
166	46.8	.52	143	53.3	.66	52.78
164	46.7	.52	140	53.1	.66	53.60
162	46.0	.51	137	52.9	.66	54.43
160	45.9	.51	134	52.6	.66	55.26
158	45.7	.50	132	52.3	.65	56.09
156	45.6	.50	130	52.1	.65	56.94
154	45.5	.50	128	51.7	.64	57.78
152	45.4	.50	126	51.4	.63	58.64
150	45.3	.50	124	50.9	.62	59.51
148	45.2	.50	121	50.4	.61	60.39
146	45.1	.50	119	50.0	.61	61.28
144	44.9	.50	116	49.5	.60	62.18
142	44.8	.49	114	49.1	.59	63.08
140	44.7	.49	112	48.7	.58	64.00
138	44.6	.49	110	48.3	.58	64.93
136	44.5	.49	108	48.0	.57	65.86
134	44.4	.49	106	47.6	.56	66.80
132	44.2	.49	103	47.3	.55	67.75
130	44.2	.49	101	47.0	.55	68.70
128	44.1	.49	99	46.8	.54	69.66
126	44.1	.49	97	46.5	.54	70.63
124	44.1	.49	94	46.3	.54	71.60
122	44.1	.49	91	46.1	.53	72.57
120	44.1	.49	89	45.9	.53	73.55

129/.....

SH LONG	SH CPA	SH PEF	NH LONG	NH CPA	NH PEF	TEF
184	46.6	.51	192	53.4	.66	69.47
186	46.7	.52	194	53.4	.66	70.28
188	46.8	.52	196	53.4	.66	71.10
190	47.0	.52	199	53.3	.66	71.91
192	47.0	.52	202	53.2	.66	72.73
194	47.2	.52	204	53.1	.65	73.55
196	47.3	.52	206	53.0	.65	74.37
198	47.4	.52	209	52.9	.65	75.20
200	47.5	.52	211	52.8	.64	76.02
202	47.6	.52	214	52.6	.64	76.85
204	47.7	.53	217	52.4	.63	77.68
206	47.8	.53	219	52.4	.63	78.52
208	47.9	.53	221	52.2	.62	79.36
210	48.0	.53	223	52.0	.62	80.20
212	48.1	.53	226	51.8	.61	81.05
214	48.2	.53	228	51.6	.61	81.90
216	48.4	.53	230	51.5	.60	82.76
218	48.5	.54	233	51.3	.60	83.61
220	48.7	.54	235	51.1	.59	84.48
222	48.8	.54	238	50.9	.58	85.34
224	48.9	.54	240	50.7	.58	86.22
226	49.1	.54	242	50.6	.57	87.09
228	49.2	.54	244	50.4	.57	87.97
230	49.5	.55	246	50.2	.55	88.86
232	49.7	.55	248	50.0	.56	89.74
234	49.9	.55	250	49.8	.55	90.63
236	50.2	.57	252	49.6	.55	91.51
238	50.4	.58	254	49.5	.55	92.37
240	50.6	.60	255	49.2	.54	93.22
242	50.7	.61	257	49.1	.54	94.06
244	51.0	.63	259	49.0	.54	94.88
246	51.2	.67	260	48.9	.54	95.65
248	51.6	.70	262	48.8	.54	96.41
250	51.9	.77	264	48.7	.54	97.09
252	52.3	.76	265	48.6	.54	97.79
254	52.6	.76	267	48.6	.54	98.40
256	53.1	.88	268	48.5	.54	98.97
258	53.6	1.16	270	48.5	.54	99.27
260	54.0	1.51	271	48.4	.53	99.22
262	54.5	1.75	273	48.4	.53	98.93
264	54.9	1.55	274	48.4	.53	98.83
266	55.4	2.02	275	48.5	.54	98.27
268	55.9	1.60	276	48.6	.54	98.12
270	56.3	1.85	278	48.7	.54	97.72
272	56.8	1.88	280	48.7	.54	97.29
274	57.3	1.67	281	48.8	.54	97.07
276	57.8	1.94	282	48.9	.54	96.58
278	58.2	1.72	283	49.0	.54	96.31
280	58.6	1.74	284	49.2	.54	96.02
282	59.1	2.27	285	49.3	.54	95.20
284	59.7	2.05	287	49.5	.55	94.59
286	60.2	2.34	288	49.8	.55	93.69
288	61.0	2.65	289	50.0	.55	92.48
290	61.6	2.71	290	50.2	.55	91.21

SH LONG	SH CPA	SH PEF	NH LONG	NH CPA	NH PEF	TEF
118	44.1	.49	86	45.6	.52	74.54
116	44.1	.49	84	45.4	.52	75.53
114	44.1	.49	81	45.2	.51	76.52
112	44.1	.49	79	44.9	.50	77.52
110	44.2	.49	77	44.7	.50	78.53
108	44.2	.49	75	44.5	.50	79.54
106	44.3	.49	73	44.4	.49	80.55
104	44.4	.49	71	44.2	.49	81.56
102	44.5	.50	69	44.1	.49	82.57
100	44.6	.50	67	44.0	.48	83.57
98	44.7	.51	65	43.9	.48	84.57
96	44.8	.52	63	43.8	.48	85.56
94	44.9	.54	62	43.7	.48	86.52
92	45.1	.56	60	43.7	.48	87.47
90	45.3	.54	58	43.7	.48	88.44
88	45.5	.61	56	43.7	.48	89.34
86	45.7	.60	54	43.7	.48	90.25
84	46.1	.69	52	43.8	.48	91.06
82	46.3	.63	49	43.9	.48	91.94
80	46.7	.75	47	44.0	.48	92.70
78	47.1	.78	45	44.1	.49	93.43
76	47.6	.81	43	44.2	.49	94.12
74	48.0	.91	40	44.3	.49	94.72
72	48.5	.94	38	44.4	.49	95.28
70	49.2	1.06	36	44.6	.49	95.72
68	49.8	1.10	34	44.7	.49	96.12
66	50.6	1.33	32	44.9	.50	96.28
64	51.0	1.00	30	45.2	.50	96.78
62	51.6	1.33	28	45.3	.50	96.94
60	52.3	1.28	26	45.5	.50	97.14
58	53.0	1.45	24	45.7	.50	97.18
56	53.8	1.92	21	45.9	.51	96.75
54	54.6	2.42	19	46.1	.51	95.82
52	55.4	2.71	16	46.3	.51	94.59
50	56.2	2.55	14	46.5	.51	93.52
48	57.0	2.61	10	46.7	.51	92.38
46	57.8	2.44	5	46.8	.52	91.42
44	58.3	2.24	1	47.0	.52	90.65
42	59.1	2.79	358	47.2	.52	89.33
40	59.7	2.07	356	47.4	.52	88.72
38	60.2	2.37	354	47.6	.53	87.82
36	60.7	1.87	353	48.2	.53	87.42
34	61.1	2.16	351	48.0	.53	86.72
32	61.5	1.64	350	48.2	.53	86.54
30	61.9	2.21	348	48.4	.53	85.79
28	62.3	1.67	346	48.7	.54	85.57
26	62.6	1.98	344	48.6	.54	85.05
24	62.9	1.70	342	49.2	.54	84.80
22	63.3	1.72	340	49.4	.54	84.52
20	63.7	2.02	338	49.6	.55	83.94
18	64.2	2.64	336	49.8	.55	82.74
16	64.4	1.17	334	50.1	.55	83.01
14	64.8	2.09	333	50.2	.55	82.36
12	65.2	2.10	331	50.4	.56	81.70

130/.....

SH LONG	SH CPA	SH PEF	NH LONG	NH CPA	NH PEF	TEF	SH LONG	SH CPA	SH PEF	NH LONG	NH CPA	NH PEF	TEF
292	62.3	2.48	291	50.6	.56	90.16	10	65.8	2.75	329	50.6	.56	80.38
294	62.9	2.81	292	50.9	.56	88.78	8	66.2	2.15	327	50.7	.56	79.66
296	63.7	2.87	293	51.2	.57	87.34	6	66.6	2.49	326	51.0	.56	78.60
298	64.4	2.93	294	51.5	.57	85.83	4	67.5	3.80	325	51.0	.56	76.23
300	65.2	3.30	295	51.7	.57	83.96	2	68.0	2.23	323	51.2	.57	75.43
302	66.0	3.36	296	52.0	.57	82.02	360	68.7	3.56	321	51.4	.57	73.30
304	67.1	4.38	298	52.2	.58	79.05	358	69.5	3.27	320	51.6	.57	71.45
306	68.5	5.45	299	52.4	.58	75.02	356	70.0	2.64	318	51.7	.57	70.23
308	69.5	4.24	300	52.4	.58	72.19	354	71.1	5.04	317	51.9	.57	66.60
310	70.5	4.66	301	52.6	.58	68.94	352	72.0	4.09	315	52.0	.57	63.94
312	71.7	5.07	303	52.8	.58	65.28	350	72.7	3.10	314	52.2	.58	62.25
314	73.0	5.16	305	52.9	.58	61.52	348	73.7	4.53	312	52.4	.58	59.13
316	74.4	5.96	306	53.0	.58	56.97	346	75.2	6.37	310	52.6	.58	54.18
318	76.0	6.76	307	53.2	.59	51.61	344	76.0	3.94	308	52.7	.58	51.64
320	76.8	4.35	308	53.3	.59	48.66	342	77.3	5.81	307	52.9	.58	47.24
322	78.3	6.24	310	53.4	.59	43.83	340	78.8	7.00	306	53.1	.59	41.64
324	79.4	5.21	312	53.4	.59	40.02	338	80.0	5.25	305	53.2	.59	37.79
326	81.3	8.29	314	53.5	.59	33.13	336	81.3	6.06	303	53.3	.59	33.13
328	82.9	7.29	315	53.5	.59	27.24	334	82.9	7.29	301	53.4	.59	27.24
330	84.9	9.32	317	53.5	.59	19.33	332	84.9	9.32	300	53.5	.59	19.33

APPENDIX 3.

Calculation of Northern Hemisphere Values of P.E.F.

(the injected flux (Torr, 1965))

To estimate a median value for x/in the northern hemisphere, an average value of the fraction of x precipitated (Pa) in that hemisphere was calculated for each shell from all the p.e.f. results given in Appendix 2. If M is the median value of p.e.f. calculated from all the satellite observations made on a given shell, x was calculated from $Pax = M$ or $x = \frac{M}{Pa}$. Having obtained a value for x, the actual median value of flux precipitated in each longitudinal section could be calculated using the fraction of x precipitated (Appendix 2) for that particular section. Having obtained a value for x by means of the above method, values of p.e.f. in the southern hemisphere could be calculated using the approach described in Section 2.6.

131/.....

APPENDIX 4.

$$z = \int_{h_o}^{h} \frac{dh}{H} \qquad (4.1)$$

where $H = \frac{kT}{mg}$ (4.2)

$$T = T_\infty - \frac{k'}{h - b} \qquad (4.3)$$

$$k' = (T_\infty - T_o)(h_o - b) \qquad (4.4)$$

$$g = g_o\left(\frac{h_o + R_E}{h + R_E}\right)^2 \qquad (4.5)$$

$$\therefore \quad z = \frac{mg_o}{k}(h_o + R_E)^2 \int_{h_o}^{h} \frac{dh}{(h + R_E)^2\left(T_\infty - \frac{k'}{(h - b)}\right)} \qquad (4.6)$$

$$= a\int_{h_o}^{h} \frac{(h - b)dh}{(h + R_E)^2(T_\infty h - d)} \qquad (4.7)$$

where $a = \frac{mg_o}{k}(h_o + R_E)^2$ (4.8)

$$d = k' + T_\infty b \qquad (4.9)$$

This can be evaluated by standard forms:

$$\int \frac{dx}{(a + bx)^2(a' + b'x)} = \frac{1}{(ab' - a'b)}\left[\frac{1}{(a + bx)} + \frac{b'}{(ab' - a'b)} \ln\left(\frac{a' + b'x}{a + bx}\right)\right]$$

and

$$\int \frac{x\,dx}{(a + bx)^2(a' + b'x)} = \frac{-a}{b(ab' - a'b)(a + bx)} - \frac{a'}{(ab' - a'b)^2} \ln\left(\frac{a' + b'x}{a + bx}\right)$$

132/.....

$$\therefore a\int_{h_o}^{h} \frac{(h-b)\,dh}{(h+R_E)^2(T_\infty h-d)} = a\left[\frac{-b}{T_\infty R_E+d}\left(\frac{1}{h+R_E}+\frac{T_\infty}{T_\infty R_E+d}\ln\left(\frac{T_\infty h-d}{h+R_E}\right)\right)-\frac{R_E}{(T_\infty R_E+d)(h+R_E)}+\frac{d}{(T_\infty R_E+d)^2}\ln\left(\frac{T_\infty h-d}{h+R_E}\right)\right]_{h_o}^{h}$$

$$= a\left[\frac{d-T_\infty b}{(T_\infty R_E+d)^2}\ln\left(\frac{T_\infty h-d}{h+R_E}\right)-\frac{(b+R_E)}{(T_\infty R_E+d)(h+R_E)}\right]_{h_o}^{h}$$

$$\therefore z = \frac{A}{h+R_E} + B\ln\left(\frac{T_\infty h-d}{h+R_E}\right) - C \qquad (4.10)$$

$$\text{where } A = \frac{-a(b+R_E)}{(T_\infty R_E+d)} \qquad (4.11)$$

$$B = \frac{a(d-T_\infty b)}{(T_\infty R_E+d)^2} \qquad (4.12)$$

$$C = \frac{A}{h_o+R_E} + B\ln\left(\frac{T_\infty h_o-d}{h_o+R_E}\right) \qquad (4.13)$$

133/.....

APPENDIX 5.

$$V = -D \sin^2 I \left[\frac{1}{N} \frac{\partial N}{\partial h} + \frac{1}{T} \frac{\partial T}{\partial h} + \frac{\mathcal{M}}{H} \right] \tag{5.1}$$

$$\therefore \frac{\partial (NV)}{\partial h} = - \sin^2 I \left\{ \left[N \frac{\partial D}{\partial h} + D \frac{\partial N}{\partial h} \right] \left[\frac{1}{N} \frac{\partial N}{\partial h} + \frac{1}{T} \frac{\partial T}{\partial h} + \frac{\mathcal{M}}{H} \right] + DN \left[\frac{-1}{N^2} \left(\frac{\partial N}{\partial h} \right)^2 + \frac{1}{N} \frac{\partial^2 N}{\partial h^2} - \frac{1}{T^2} \left(\frac{\partial T}{\partial h} \right)^2 + \frac{1}{T} \frac{\partial^2 T}{\partial h^2} - \frac{\mathcal{M}}{H^2} \frac{\partial H}{\partial h} + \frac{1}{Hdh} \right] \right\} \tag{5.2}$$

$$= -D \sin^2 I \left\{ \frac{\partial^2 N}{\partial h^2} + \frac{\partial N}{\partial h} \left[\frac{1}{T} \frac{\partial T}{\partial h} + \frac{\mathcal{M}}{H} + \frac{1}{D} \frac{\partial D}{\partial h} \right] + \frac{N}{T} \left[\frac{1}{D} \frac{\partial D}{\partial h} \left(\frac{\partial T}{\partial h} + \frac{\mathcal{M} T}{H} \right) + \frac{\partial^2 T}{\partial h^2} - \frac{1}{T} \left(\frac{\partial T}{\partial h} \right)^2 - \frac{\mathcal{M} T}{H^2} \frac{\partial H}{\partial h} + \frac{T}{H} \frac{\partial \mathcal{M}}{\partial H} \right] \right\} \tag{5.3}$$

where:

a) Case (1): $$D = \frac{bT^{\frac{1}{2}}}{n} \qquad (n = n(0)) \tag{5.4}$$

(1) $$\frac{\partial D}{\partial h} = b \left[\frac{1}{2nT^{\frac{1}{2}}} \frac{\partial T}{\partial h} + T^{\frac{1}{2}} \left(\frac{-1}{n^2} \frac{\partial n}{\partial h} \right) \right] \tag{5.5}$$

Since $$n = \frac{n_o T_o e^{-z(0)}}{T} \tag{5.6}$$

$$\frac{\partial n}{\partial h} = \frac{n_o T_o}{T^2} \left(-Te^{-z(0)} \frac{\partial z(0)}{\partial h} - e^{-z(0)} \frac{\partial T}{\partial h} \right) \tag{5.7}$$

$$= -n \left(\frac{1}{H(0)} + \frac{1}{T} \frac{\partial T}{\partial h} \right) \tag{5.8}$$

where we have used the fact that $\frac{\partial z}{\partial h} = \frac{1}{H}$

Therefore substituting equation (5.8) into (5.5)

134/.....

$$\frac{\partial D}{\partial h} = D\left[\frac{3}{2T}\frac{\partial T}{\partial h} + \frac{1}{H(0)}\right] \tag{5.9}$$

where H(0) is the scale height of atomic oxygen.

(2) $$T = T_\infty - \frac{(T_\infty - T_o)(h_o - b)}{(h - b)} \tag{5.10}$$

$$\frac{\partial T}{\partial h} = \frac{(T_\infty - T_o)(h_o - b)}{(h - b)^2} \tag{5.11}$$

and $$\frac{\partial^2 T}{\partial h^2} = -2\frac{(T_\infty - T_o)(h_o - b)}{(h - b)^3} \tag{5.12}$$

(3) $$\frac{dH}{dh} = \frac{k}{m(0)}\frac{\partial}{\partial h}\left(\frac{T}{g}\right) \tag{5.13}$$

$$= \frac{k}{mg}\left(\frac{\partial T}{\partial h} - \frac{T}{g}\frac{dg}{dh}\right) \tag{5.14}$$

where $$g = g_o\left(\frac{h_o + R_E}{h + R_E}\right)^2 \tag{5.15}$$

and $$\frac{\partial g}{\partial h} = \frac{-2g}{(h + R_E)} \tag{5.16}$$

(4) $$\mu = \tfrac{1}{2} \quad \text{and} \quad \frac{\partial \mu}{\partial h} = 0 \tag{5.17}$$

b) Case (2):

(1) $$D = \frac{bT^{\frac{1}{2}}}{\Sigma n_i} \tag{5.18}$$

$$b = \frac{3}{8\sigma^2}\left(\frac{k}{2\pi}\right)^{\frac{1}{2}}\left(m\right)^{\frac{1}{2}}$$

where $$m = m(0) + \frac{\Sigma m_i n_i}{\Sigma n_i} \tag{5.19}$$

$$m(0)\,\frac{\Sigma m_i n_i}{\Sigma n_i}$$

135/.....

$$= \frac{\Sigma n_i}{\Sigma m_i n_i} - \frac{1}{m(0)} \qquad (5.20)$$

where m(0) is the mass of atomic oxygen and subscript i refers to summation over the three atmospheric constituents.

$$\frac{\partial D}{\partial h} = \frac{\partial}{\partial h}\left(bT^{\frac{1}{2}}\right)\frac{1}{\Sigma n_i} + bT^{\frac{1}{2}}\frac{\partial}{\partial h}\left(\frac{1}{\Sigma n_i}\right) \qquad (5.21)$$

$$\frac{\partial}{\partial h}(bT^{\frac{1}{2}}) = T^{\frac{1}{2}}\frac{\partial b}{\partial h} + \frac{b}{2}T^{-\frac{1}{2}}\frac{\partial T}{\partial h} \qquad (5.22)$$

$$\frac{\partial b}{\partial h} = \left[\frac{3}{8\sigma^2}\left(\frac{k}{2\pi}\right)^{\frac{1}{2}}\right]\frac{1}{2}m^{-\frac{1}{2}}\frac{\partial m}{\partial h} \qquad (5.23)$$

$$\frac{\partial m}{\partial h} = \frac{\partial}{\partial h}\left(\frac{\Sigma n_i}{\Sigma m_i n_i}\right) \qquad (5.24)$$

$$= \frac{1}{\Sigma m_i n_i}\left[-\Sigma\left\{n_i\left(\frac{1}{T}\frac{\partial T}{\partial h} + \frac{1}{H_i}\right)\right\} + \left(\Sigma n_i\right)\left\{\frac{\Sigma\left\{m_i n_i\left(\frac{1}{T}\frac{\partial T}{\partial h} + \frac{1}{H_i}\right)\right\}}{(\Sigma m_i n_i)^2}\right\}\right] \qquad (5.25)$$

using equation (5.8).

Therefore $$\frac{\partial m}{\partial h} = \frac{1}{\Sigma n_i m_i}\left[\frac{\Sigma n_i \Sigma \frac{m_i n_i}{H_i}}{\Sigma m_i n_i} - \Sigma\frac{n_i}{H_i}\right] \qquad (5.26)$$

Using equations (5.26), (5.23), (5.22) and (5.21)

$$\frac{\partial D}{\partial h} = D\left[\frac{1}{2bm^{\frac{1}{2}}}\frac{\Sigma n_i \Sigma m_i n_i/H_i}{(\Sigma m_i n_i)^2} + \Sigma n_i/H_i\left(\frac{1}{\Sigma n_i} - \frac{1}{2bm^{\frac{1}{2}}\Sigma n_i m_i}\right) + \frac{3}{2T}\frac{\partial T}{\partial h}\right] \qquad (5.27)$$

(2) $$H = \frac{kT}{m_a g} \qquad (5.28)$$

where $$m_a = \frac{\Sigma m_i n_i}{\Sigma n_i} \qquad (5.29)$$

136/.....

Therefore $$\frac{\partial H}{\partial h} = k\left[\frac{1}{m_a}\frac{\partial}{\partial h}\left(\frac{T}{g}\right) + \frac{T}{g}\frac{\partial}{\partial h}\left(\frac{1}{m_a}\right)\right] \qquad (5.30)$$

$$\frac{\partial}{\partial h}\left(\frac{1}{m_a}\right) = -\frac{1}{m_a^2}\frac{\partial m_a}{\partial h} \qquad (5.31)$$

where $\frac{\partial m_a}{\partial h} = \frac{\partial m}{\partial h}$ given by equation (5.26) and

$$\frac{\partial}{\partial h}\left(\frac{T}{g}\right) = \frac{1}{g}\left(\frac{\partial T}{\partial h} - \frac{T}{g}\frac{\partial g}{\partial h}\right)$$

$$\mu = \frac{m(0)}{2m_a} \qquad (5.32)$$

$$\frac{\partial \mu}{\partial h} = \frac{m(0)}{2}\frac{\partial m_a}{\partial h}$$

137/.....

APPENDIX 6.

VALUES OF CONSTANTS USED IN THE CALCULATIONS:

$g_o = 946.69$ cm/sec^2.

$k = 1.38 \times 10^{-16}$ ergs/deg. K.

$m(N2) = 4.64 \times 10^{-23}$ gms.

$m(O2) = 5.31 \times 10^{-23}$ gms.

$m(O) = 2.65 \times 10^{-23}$ gms.

$n_o(N2) = 5.80 \times 10^{11}$ molecules/cm^3.

$n_o(O2) = 1.20 \times 10^{11}$ molecules/cm^3.

$n_o(O) = 7.60 \times 10^{10}$ molecules/cm^3.

$T_o = 355^{\circ}$K.

$h_o = 120$ km.

$\sigma = 2.0 \times 10^{-8}$ cm.

$\gamma_2 = 4.0 \times 10^{-11}$ cm^3/sec.

$\gamma_1 = 4.0 \times 10^{-12}$ cm^3/sec.

$\alpha = 6.0 \times 10^{-8}$ sec^{-1}. cm^3.

138/.....

APPENDIX 7

FORTRAN LISTING

```
C     NUMERICAL SOLUTION OF THE IONOSPHERIC CONTINUITY EQUATION

      DIMENSION IAA(116),ANE(31),EN(3),ANS(31),ANT(31)
      DIMENSION EM(3),UIN(09),S(27),Z(3),END(3),HI(3),AA(4),BB(4),CC(4)
  101 FORMAT (3E11.4,3E8.1,E9.2/8E9.2/9E8.1/9E8.1/9E8.1/F7.4/F7.4/F7.4)
 7343 FORMAT(E8.1)
  131 FORMAT (8E9.2/8E9.2/8E9.2/8E9.2/E9.2)
 1972 FORMAT(E9.2,F6.3,2E10.3,F6.0,F5.0,E9.2)
 9103 FORMAT(25(/))
 2316 FORMAT(E10.3,E9.2,2F5.0,F6.1)
 5612 FORMAT(11(/))
 4964 FORMAT(E8.1,F5.0)
  102 FORMAT(14,15,F5.2,F5.0,9E9.2,3F6.0)
  103 FORMAT (3H A=,F6.0,3H B=,F6.1,8H SECCHI=,F7.4,3H E=,E9.2,7H  GAM=
     1,E8.1,6H  FAC=,F5.2,15H  VERTICAL VEL=,F6.1,4H EM=,F6.3,7H ALPHA=
     2E8.1)
  109 FORMAT (40X,10HDIP ANGLE=F6.2,19H DEGREES   DELTA H=F5.2)
  104 FORMAT(56H  HT TEMP  Z-O  H-O    N(O)    N(O2)    N(N2)       O
     162HREAC RATE   EXPT    THEOR     BET    Q/BET      Q  DIFSN  LOSS)
 1397 FORMAT(313)
      READ 131,(ANE(J),J=1,8),(ANE(J),J=9,16),(ANE(J),J=17,24),(ANE(J),J
     1=25,31)
 7332 READ 101,(EM(L),L=1,3),(END(L),L=1,3),UIN(1),(UIN(L),L=2,9),(S(L),
     1L=1,9),(S(L),L=10,18),(S(L),L=19,27),SECHI,HJ,DIP
 8174 READ 1972,ALPHA,FAC,EMM,VEL,A,DELA,E
      READ 2316,DELE,GAM,BO,B300,DELB
      READ 1397,MEI,MA2,MB3
      READ 4964,DDN,TOPP
 7111 FORMAT(F5.2)
      READ 7111,CORR
      READ 7343, GAMO2
      DIFFHT=(360.-TOPP)*1.E5
      DO 6177 J=1,9
 6177 UIN(J)=UIN(J)*CORR
      CONBO=BO
      CONA=A
      DO 2000 KE1=1,MEI
      E=E+DELE
      A=CONA
      DO 2000 KA2=1,MA2
      A=A+DELA
      BO=CONBO
      B300=BO
      DO 2000 KB3=1,MB3
      BO=BO+DELB
      B300=B300+DELB
      III=1
      PRINT 103,A,BO,SECHI,E,GAM,FAC,VEL,EMM,ALPHA
      PRINT 109,DIP,HJ
      PRINT 104
      CONDIP=DIP
      CONHJ=HJ
      HO=1.2E7
      H=112.E5
```

139/.....

```
      RE=6.3783E8
      K66=0
      TO=355.
      DIP=(SINF(DIP*3.1415927/180.))**2
      B300=B300*1.0E5
      BO=BO*1.0E5
      B1=(B300-BO)/3.0E7
      TOP=TOPP/HJ
      QDD=0.
      QD=0
      IIG=8./HJ
      HJ=HJ*1.0E5
      IPR=1
      K=31
      AA(1)=.5
      AA(2)=1.-SQRTF(.5)
      AA(3)=1.+SQRTF(.5)
      AA(4)=1./6.
      BB(1)=2.
      BB(2)=1.
      BB(3)=1.
      BB(4)=2.
      CC(1)=.5
      CC(2)=AA(2)
      CC(3)=AA(3)
      CC(4)=.5
      B=B1*H+BO
      AK=(A-TO)*(HO*(1.-B1)-BO)
      B1D=1.-B1
      BD=(TO-A)*(B1D*HO-BO)-A*BO
      AD=A*B1D
      K67=0
      IMAX=TOP+(DIFFHT*1.E-5-120.)/8.+1.
      DO 1 I=1,IMAX
  507 IF(III)1001,1001,506
 1001 IF(K67)1136,1136,1137
 1136 IF(SENSE SWITCH 1)4965,4963
 4963 DQH=0
      DO 5729 N8=1,3
 5729 HI(N8)=HI(N8)*1.E5
      DO 821 N=1,9
      M=3*N
      SNIM1=S(M-2)*EN(1)/EM(1)
      SNIM2=S(M-1)*EN(2)/EM(2)
      SNIM3=S(M)*EN(3)/EM(3)
      SNIM4=SNIM1+SNIM2+SNIM3
      SNIM5=SNIM1/HI(1)+SNIM2/HI(2)+SNIM3/HI(3)
      DTEXP1=SNIM4*(DTG-DT/GRAV)-SNIM5*T/GRAV
      DEXP=EXPF(-(SNIM1+SNIM2+SNIM3)*T*1.38044E-16*SECHI/GRAV)
      DEXP2=+SECHI*1.38044E-16*DEXP*DTEXP1
  821 DQH=DQH-UIN(N)*EN(3)*(DEXP2+DEXP*(1./HI(3)+DT/T))
      IF(SENSE SWITCH 2)7330,7331
 7330 DBET=-(GAM*EN(1)*(DT/T+1./HI(1))+GAM02*EN(2)*(DT/T+1./HI(2)))
      GO TO 7628
 7331 DBET=BET*((E/(T*T*1.38044E-16)-.5/T)*DT-1./HI(1))
 7628 DQBET=(DQH*BET-Q*DBET)/(2.*BET**2)
      DNFN=2./SQRTF(1.+4.*BET**2/(ALPHA*Q))*(2.*BET*DBET/Q-(BET/Q)**2*DQ
     1H)/ALPHA
      DN=ANS(K+1)
      DDN=DQBET*DN*2.*BET/Q+.5*Q/BET*DNFN
 4965 IPR=1
```

140/.....

```
      DN=ANS(K+1)
      K67=1
      K66=1
      GO TO 1137
  506 IF(H-DIFFHT)1152,1300,1300
 1152 H=H+8.E5
      K123=1
      GO TO 40
 1300 111=0
      GO TO 507
 1137 K123=4
   40 DO 20 J=1,K123
      IF(111)151,1269,151
 1269 H=H+HJ/4.
  151 T=A-AK/(H-B)
      DT=AK*(1.-B1)/(H-B)**2
      DO 2 L=1,3
      AKAP=EM(L)*946.69*6.4983E8**2/1.38044E-16
      GRAV=946.69*((RE+HO)/(RE+H))**2
      H1(L)=1.38044E-16*T/(EM(L)*GRAV)
      A1=-AKAP*(B1D*RE+BO)/(RE*AD-BD)
      B1=-AKAP*(B1D*BD+AD*BO)/(RE*AD-BD)**2
      CONS=A1/(RE+HO)+B1*LOGF((BD+AD*HO)/(RE+HO))
      Z(L)=A1/(RE+H)+B1*LOGF((BD+AD*H)/(RE+H))-CONS
      DZ=1./H1(L)
    2 EN(L)=355.*ENO(L)*EXPF(-Z(L))/T
      Q=0
      DO 5 N=1,9
      M=3*N
    5 Q=Q+U1N(N)*EN(3)*EXPF(-(S(M-2)*EN(1)/EM(1)+S(M-1)*EN(2)/EM(2)+S(M)
     1*EN(3)/EM(3))*T*1.38044E-16*((H+6.3783E8)/6.4983E8)**2*SECH1/946.6
     29)
      C1=3.0E16*SQRTF(1.38044E-16/6.2831854)/32.
      IF(SENSE SWITCH 2)7327,7328
 7327 BET=GAM*EN(1)+GAMO2*EN(2)
      GAMA=GAM
      GO TO 7329
 7328 GAMA=(GAM*EXPF(E/(1.38044E-16*300.))/SQRTF(300.))*SQRTF(T)*EXPF(-E
     1/(1.38044E-16*T))
      BET=GAMA*EN(1)
 7329 D=C1*SQRTF(T/EM(3))*FAC/EN(3)
      DGRAV=-2.*GRAV/(H+RE)
      DTG=(DT*GRAV-T*DGRAV)/GRAV**2
  991 ANS(K)=(Q/(2.*BET))*(1.+SQRTF(1.+4.*BET**2/(ALPHA*Q)))
      GONE=ALPHA*BET*ANS(K)**2/(ALPHA*ANS(K)+BET)
      BETD=GONE/ANS(K)
      IF(111)990,990,600
  990 DD=D*(1.5*DT/T+1./H1(3))
      R=DT/T+.5/H1(3)+DD/D
      DDT=-2.*AK*(1.-B1)**2/(H-B)**3
      DH13=1.38044E-16/EM(3)*DTG
      GDASH=(DDT-DT**2/T-.5*T/H1(3)**2*DH13+DD/D*(DT+.5*T/H1(3)))/T
      OLD=DDN
      OLDDN=DN
 1969 G=GDASH+BETD/(D*DIP)
      W=Q/(D*DIP)
      DDDN=-R*DDN-G*DN+W
      DIFF1=-DIP*D*(DDDN+DDN*R+DN*G)+BETD*DN-VEL*DDN
      DDK=DDDN
      DDN=DDN+HJ*AA(J)*(DDK-BB(J)*QDD)
      DK=DDN
```

141/. ....

```
      DN=DN+HJ*AA(J)*(DK-BB(J)*QD)
      IF(ABSF((ANS(K)-DN)/DN)-.1)1968,1968,1967
 1967 BETD=ALPHA*BET*DN/(ALPHA*DN+BET)
      ANS(K)=DN
      DN=OLDDN
      DDN=DLD
      GO TO 1969
 1968 QDD=QDD+3.*AA(J)*(DDK-BB(J)*QDD)-CC(J)*DDK
   20 QD=QD+3.*AA(J)*(DK-BB(J)*QD)-CC(J)*DK
      IF(IPR-11G)1,9,9
    9 IH=H*1.E-5
      ANS(K)=DN
      QB=Q/BET
      GONE=BETD*DN
      GO TO 716
  600 QB=SQRTF(Q/ALPHA)
      DIFF1=0
      IH=H*1.E-5
  716 ANT(K)=T
      IT=T
      HI(1)=HI(1)*1.E-5
      HI(2)=HI(2)*1.E-5
      HI(3)=HI(3)*1.E-5
      I10=111+1
      GO TO (717,718),I10
  717 SUM=Q-DIFF1-GONE
      GO TO 994
  718 SUM=Q-GONE
  994 PRINT 102,IH,IT,Z(3),HI(3),EN(3),EN(2),EN(1),D,GAMA,ANE(K),ANS(K),
     1BET,QB,Q,DIFF1,GONE
      K=K-1
      IF(111)500,500,1
  500 IPR=0
    1 IPR=IPR+1
  110 FORMAT (I4,99A1,17A1)
      PRINT 9103
      DO 10 I=1,116
   10 IAA(I)=0
      DO 11 I=1,31
      IT=ANT(I)
      CHK=ANT(I)/20.
      JCHK=CHK
      JCHK=JCHK*20+10
      IF(IT-JCHK)21,22,22
   21 IT=(IT-340)/20+1
      GO TO 23
   22 IT=(IT-340)/20+2
   23 IAA(IT)=0300
      CHK=ANE(I)/1.0E3
      IE=CHK
      CHK=ANE(I)/1.0E4
      JCHK=CHK
      JCHK=JCHK*10+5
      IF(IE-JCHK)24,25,25
   24 IE=IE/10+1
      GO TO 26
   25 IE=IE/10+2
   26 IAA(IE)=1400
      CHK=ANS(I)/1.0E3
      I2=CHK
      CHK=ANS(I)/1.0E4
```

142/.....

```
      JCHK=CHK
      JCHK=JCHK*10+5
      IF(I2-JCHK)12,13,13
   12 I2=I2/10+1
      GO TO 3719
   13 I2=I2/10+2
 3719 IF(I2)1926,1926,1928
 1926 I2=2
      GO TO 14
 1928 IF(116-I2)1929,14,14
 1929 I2=116
   14 IF(I2-IE)27,28,27
   27 IAA(I2)=1000
      GO TO 29
   28 IAA(I2)=7000
   29 JHA=360-8*(I-1)
      PRINT 110,JHA,(IAA(J),J=1,116)
      IAA(IT)=0
      IAA(IE)=0
   11 IAA(I2)=0
  112 FORMAT (104X,16H1111111111111111/14X,106H111111111122222222223333
     13333344444444445555555555666666666677777777778888888888999999999990
     1000000000111111)
  113 FORMAT (4X,116H.................................................
     1.............................................................)
  114 FORMAT (4X,116H01234567890123456789012345678901234567890123456789 0
     11234567890123456789012345678901234567890123456789012345678901 2345)
  115 FORMAT (70X,2H-5/50X,20HELECTRON DENSITY *10//)
  116 FORMAT (37X,83H111111111111111111111111111111111111111111111111112
     1222222222222222222222222222222)
  117 FORMAT (4X,116H3334444455555666667777788888999990000011111 22222333
     133444445555566666777778888899999000001111122222333334444455555666/
     24X,116H46802468024680246802468024680246802468024680246802468024680
     324680246802468024680246802468024680246802468024680246802468024)
  118 FORMAT (4X,116H000000000000000000000000000000000000000000000000000
     10000000000000000000000000000000000000000000000000000000000000000)
  119 FORMAT (44X,29HTEMPERATURE IN DEGREES KELVIN////)
      PRINT 112
      PRINT 113
      PRINT 114
      PRINT 115
      PRINT 116
      PRINT 117
      PRINT 118
      PRINT 119
      PRINT 5612
      DIP=CONDIP
      HJ=CONHJ
      B0=B0*1.E-5
      B300=B300*1.E-5
 2000 CONTINUE
      IF(SENSE SWITCH 3)8174,8175
 8175 IF(SENSE SWITCH 4)7350,7332
 7350 CONTINUE
      END
```

143/.....

REFERENCES

(1960), Akasofu, S. I., J. Atmos. Terr. Phys., 18, 160.

(1952), Appleton, E. V. and W. R. Piggott, J. Atmos. Terr. Phys., 2, 236.

(1965), Armstrong, T. J., J. Geophys. Res., 70, 2077.

(1957), Bailey, D. K., J. Geophys. Res., 62, 431.

(1959), Bailey, D. K., Proc. Inst. Rad. Eng., 47, 255.

(1964), Baker, D.C. and J. A. Gledhill, COSPAR Conference, Florence.

(1960), Bates, D.R. and M. Nicolet, J. Atmos. Terr. Phys., 18, 15.

(1960), Bellchambers, W. H. and W. R. Piggott, Proc. Roy. Soc., 256, 200.

(1962), Bowhill, S. A., J. Atmos. Terr. Phys., 24, 503.

(1962), Bowles, K. L., US - NBS Rept., 7633.

(1961), Brown, R. R., T. R. Hartz, B. Landmark, H. Leinbach and H. Ortner, J. Geophys. Res., 66, 1035.

(1961), Brown, R.R. and R. S. Weir, Arkiv. för Geophys., 3, 523.

(1956), Byram, E. T., T. A. Chubb and H. Friedman, J. Geophys. Res., 61, 251.

(1961), Campbell, W. H. and H. Leinbach, J. Geophys. Res., 66, 25.

(1962), Carpenter, D. L., J. Geophys. Res., 67, 135.

(1966), Chandra, S. and S. Rangaswamy, J. Geophys. Res., 71, 217.

(1957), Chapman, S., Smithsonian Contribution Astrophys., 2, No. 1.

(1960), Chapman, J. H., Canad. J. Phys., 38, 1195.

(1960), Chapman, S. and T. G. Cowling, The Mathematical Theory of Non-Uniform Gases, Cambridge Univ. Press.

(1960), Chubb, T.A., H. Friedman, R. W. Kreplin, R. L. Blake and A. E.

144/.....

Unzicker, 10th International Astrophysics Symposium, Liége, p. 11.

(1960b), Chubb, T. A., H. Friedman and R. W. Kreplin, 10th International Astrophysics Symposium, Liége, p.26.

(1961), Cladis, J. B. and A. J. Dessler, J. Geophys. Res., 66, 343.

(1965), Cospar International Reference Atmosphere (CIRA), North - Holland Publishing Company, Amsterdam.

(1962), Cole, K. D., Aust. J. Phys., 15, 223.

(1961), Collins, C., D. H. Jelly and A. G. Matthews, Canad. J. Phys. 39, 35.

(1959), Coroniti, S. G. and R. Penndorf, J. Geophys. Res., 64, 5.

(1960), Dalgarno, A. and D. Parkinson, J. Atmos. Terr. Phys., 18, 335.

(1958a), Dalgarno, A., J. Atmos. Terr. Phys., 12, 219.

(1958b), Dalgarno, A., Phil. Trans. Roy. Soc., 250, 426.

(1961), Dalgarno, A., Ann. Geophys., 17, 16.

(1964), Dalgarno, A., J. Atmos. Terr. Phys., 26, 939.

(1935), Dellinger, J. H., Science, 82, 351.

(1937), Dellinger, J. H., J. Res. Natl. Bur. Standards, 19, 111.

(1959), Dessler, A. J., J. Geophys. Res., 64, 397.

(1950), Dieminger, W. and R. H. Geisweid, J. Atmos. Terr. Phys., 1, 42.

(1956), Dodson, H. W., E. R. Hedeman and R. R. McMath, Ap. J. Supp., 2, 241.

(1966), Donahue, T. M., Panet. Space Sci., 14, 33.

(1965), Fehsenfeld, F. C., A. L. Schmeltekopf and E. E. Ferguson, Planet. Space Sci., 13, 219.

(1964), Frank, L. A., J. A. Van Allen and H. K. Hills, J. Geophys. Res.,

145/.....

69, 2171.

(1965), Frank, L. A., J. Geophys. Res., 70, 3533.

(1958), Friedman, H, T. A. Chubb, J. E. Kupperian Jr., J. R. Kreplin and J. C. Lindsay, Ann. de Geophys., 14, 232.

(1963), Friedman, H., Proc. Int. Conf. The Ionosphere, Inst. Phys. and Phys. Soc., London, p. 3.

(1960), Garriott, O. K., J. Geophys. Res., 65, 1139.

(1963), Garriott, O. K. and H. Rishbeth, Planet. Space Sci., 11, 591.

(1965), Geisler, J. E. and S. A. Bowhill, Aeronomy Report No. 5, Aeronomy Lab. Univ. of Ill.

(1962), Ginsburg, V. L., L. V. Kurnosova, V. I. Logachev, L. A. Razorenov, I. A. Sirotkin and M. I. Fradkin, Planet. Space Sci., 9, 848.

(1962), Gledhill, J. A. and H. O. van Rooyen, Nature, 196, 973.

(1963), Gledhill, J. A. and H. O. van Rooyen, Proc. 5th Int. Symp. Space Technol. and Sci., Tokyo, p. 1003.

(1965), Gledhill, J. A. and D. G. Torr, Space Research 6.

(1967), Gledhill, J. A., D. G. Torr and M. R. Torr, J. Geophys. Res., 72,209.

(1960), Gliddon, J. E. C. and P. C. Kendall, J. Geophys. Res., 65, 2279.

(1961), Groves, G. V., Rep. Univ. College, London.

(1961), Hakura, Y. and T. Goh, Rep. Ionos. Space Res. Japan, 15, 235.

(1962a), Harris, J. and W. Priester, J. Atmos. Terr. Phys., 19, 286.

(1962b), Harris, J. and W. Priester, NASA Tech Note TND - 1444.

(1958), Heppner, J. P. and L. H. Meredith, J. Geophys. Res., 63, 51.

146/.....

(1960), Hill, G. E., J. Geophys. Res., 65, 3183.

(1955), Hirono, M., Rep. Ionos. Res. Japan, 9, 95.

(1960), Hinteregger, H. E., GRD Tech Note 39, AFCRL-TN-60 485.

(1961), Hinteregger, H. E., J. Geophys. Res., 66, 2367.

(1962), Hinteregger, H. E. and J. Watanabe, J. Geophys. Res., 67, 3373.

(1959), Hirsh, A. J., J. Atmos. Terr. Phys., 17, 86.

(1961), Hughes, M., Physical Chemistry, Pergamon Press, London, 2nd Edition.

(1959), Jacchia, L. G., Nature, 183, 1662.

(1960), Jacchia, L. G., J. Geophys. Res., 65, 2775.

(1961), Jacchia, L. G., Space Research, 2, 747.

(1963), Jacchia, L. G., Space Research, 3, 3.

(1962), Jacchia, L. G. and J.Slowey, Smithsonian Astrophys. Obs. Spec. Rept. 84.

(1963), Jacchia, L. G. and J. Slowey, Smithsonian Astrophys. Obs. Spec. Rept. 125.

(1962), Jelly, D. H., J. Phys. Soc. Japan, 17, Suppl. A-1, 122.

(1964), Kallman-Bijl, H. K. and W. L. Sibley, Space Research, 4, 279.

(1959), Knecht, R. W., J. Geophys. Res., 64, 1243.

(1962), Knecht, R. W. and R. E. McDuffie, J. Phys. Soc. Japan, 17, Suppl. A-1, 280.

(1953), Lewis, R. P. and D. H. McIntosh, J. Atmos. Terr. Phys., 3, 186.

(1960), Leinbach, H. and G. C. Reid, Monograph No. 7, IUGG, 145.

(1963a), Lincoln, J. Virginia, J. Geophys. Res., 68, 1156.

147/.....

(1963b), Lincoln, J. Virginia, J. Geophys. Res., 68, 1767.

(1963c), Lincoln, J. Virginia, J. Geophys. Res., 68, 2339.

(1963d), Lincoln, J. Virginia, J. Geophys. Res., 68, 3302.

(1963e), Lincoln, J. Virginia, J. Geophys. Res., 68, 3725.

(1963f), Lincoln, J. Virginia, J. Geophys. Res., 68, 4361.

(1955), Maeda, K., Rep. Ionos. Res. Japan, 9. 71.

(1965), Maeda, K., J. Atmos. Terr, Phys., 27, 259.

(1953), Martyn, D. F., Proc. Roy. Soc., A218, 1.

(1953), Matsushita, S., J. Geomag. Geoelect., 5, 109.

(1959), Matsushita, S., J. Geophys. Res., 64, 305.

(1961), Matsushita, S., J. Geophys. Res., 66, 3958.

(1963), Matuura, N., J. Rad. Res. Lab. Japan, 10, 1.

(1964), McDiarmid, I. B. and J. R. Burrows, Can J. Phys., 42, 1135.

(1960), McIlwain, C. E., J. Geophys. Res., 65, 2727.

(1953), Meek, J. H., J. Geophys. Res., 58, 445.

(1930), Mögel, H., Telefunken - Zeitung, 11, 14.

(1954), Nagata, T., Rep. Ionos. Res. Japan, 8, 39.

(1961), Nicolet, M., Planet. Space Sci., 5, 1.

(1963), Nicolet, M. and W. Swider, Planet. Space Sci., 11, 1459.

(1963), Nisbet, J. S. and T. P. Quinn, J. Geophys. Res., 68, 1031.

(1964), Norton, R. B. and T. E. Van Zandt, J. Atmos. Terr. Phys., 26, 1047.

(1952), Obayashi, T., Rep. Ionos. Res. Japan, 6, 79.

(1954), Obayashi, T., Rep. Ionos. Res. Japan, 8, 135.

(1959), Obayashi, T., Rep. Ionos. Res. Japan, 13, 201.

148/.....

(1961), Obayashi, T., J. Geomag. Geoelect., 13, 26.

(1964), O'Brien, B. J., J. Geophys. Res., 60, 13.

(1962), Piggott, W. R. and A. H. Shapley. Antarctic Research Monograph, American Geophys. Union, 7, 111.

(1956), Ratcliffe, J. A., Spec. Suppl. to J. Atmos. Terr. Phys., 6, 1.

(1963), Rees, M. H., Planet. Space Sci., 11, 1209.

(1959), Reid, G. C. and C. Collins, J. Atmos. Terr. Phys., 14, 63.

(1961), Reid, G. C., J. Geophys. Res., 66, 4071.

(1960 , Rishbeth, H. and O. W. Barron, J. Atmos. Terr. Phys., 18, 234.

(1963), Rishbeth, H., Planet. Space Sci., 11, 31.

(1964), Rishbeth, H., J. Atmos. Terr. Phys., 26, 657.

(1964), Rishbeth, H. and O. K. Garriott, NASA Tech. Rept. No. 8, SU-SEL-64-111.

(1965), Roederer,J. and J. Welch, NASA Rept.,X - 640 - 65, 149.

(1960), Romanelli, M. J., Mathematical Methods For Digital Computers, Ed. A. Ralston and H. S. Wilf, Publisher: John Wiley.

(1959), Rothwell, P., J. Geophys. Res., 64, 2026.

(1956), Sato, T., J. Geomag. Geoelect., 8, 129.

(1957), Sato, T., J. Geomag. Geoelect., 9, 1.

(1959), Sato, T. and K. Maeda, Proc. Inst. Rad. Eng., 47, 232.

(1963), Seward, F. D. and J. N. Kornblum, Univ. of Calif. Rept., UCRL-6693-ED.

(1958), Shapley, A. H. and R. W. Knecht, US-NBS Rept., No. 5596.

149/.....

(1957), Shapley, A. H. and R. W. Knecht, Inst. Rad. Eng. Trans., AP 5, 326.

(1965), Sharp, G. W., W. L. Imhof and R. G. Johnson, COSPAR Conference, Buenos Aires.

(1957), Shimazaki, T. J., J. Rad. Res. Lab. Japan, 4, 309.

(1953), Sinno, K., Rep. Ionos. Res. Japan, 7, 7.

(1954), Sinno, K., Rep. Ionos. Res. Japan, 8, 127.

(1955), Sinno, K., Rep. Ionos. Res. Japan, 9, 166.

(1964), Somayajulu, Y. V., Penn. State Univ., Sci.Rept. No. 226.

(1966), Somayajulu, Y. V., Penn. State Univ., Sci. Rept. No. 270.

(1963), Swider, W. Jr., Penn. State Univ., Sci. Rept. No. 201.

(1965), Swider, W., J. Geophys. Res., 70, 4859.

(1966), Thomas, L. and F. H. Venables, J. Atmos. Terr. Phys., 28, 599.

(1964), Torr, M. R., Honours Project, Rhodes Univ.

(1965), Torr, M. R., M.Sc. Thesis, Rhodes Univ.

(1967), Torr, M. R. and D. G. Torr, J. Geophys. Res., Submitted for publication.

(1951), Tousey, R., K. Watanabe and J. D. Purcell, Phys. Rev., 83, 792.

(1958), Tousey, R., See Rishbeth, H. and O. K. Garriott, NASA Tech. Rept., No. 8, SU-SEL-64-111, p. 81.

(1961), Tousey, R., J. Opt. Soc. Am., 51, 384.

(1960), Van Zandt, T. E., R. B. Norton and G. H. Stonehocker, J. Geophys. Res., 65, 2003.

(1962), Vernov, S. I., I. A. Savenko, P. I. Shavrin and N . F. Pisarenko, Planet. Space Sci., 9, 861.

150/.....

(1959), Violet, J. and W. A. Rense, Astrophys. J., 130, 954.

(1963), Warwick, C.S., Radio Astronomical and Satellite Studies of the Atmosphere, Ed. J. Aarons, North-Holland Publishing Company - Amsterdam, p457.

(1958), Watanabe, K., Advances in Geophys., Academic Press, New York. p155.

(1960), Watanabe, K., Tech. Rept. 60-3-N, Geophys. Coorporation Am., Bedford Massachusetts.

(1962), Watanabe, K. and H. E. Hinteregger, J. Geophys. Res., 67, 999.

(1956), Weissler, G. L., Handbuch der Physik, Springer-Verlag, Berlin, p304.

(1965), Williams, D. J. and J. W. Kohl, Space Research 6.

(1962), Winckler, J. R., J. Geophys. Res., 67, 371.

(1962), Wright, J.W., J. Res. Natl. Bur. of Standards, 66D, 3, 297.

(1963), Wright, J. W., J. Geophys. Res., 68, 4379.

(1961), Yeh, K. C. and G. W. Swenson, J. Geophys. Res., 66, 1061.

(1956), Yonezawa, T., J. Radio Res. Labs., 3, 1.

(1958), Yonezawa, T., J. Radio Res. Labs., 5, 165.

(1963), Yonezawa, T., Proc. Conf. The Ionosphere, Inst. Phys. and Phys. Soc., London, p128.